



# DEVELOPING A DECISION SUPPORT SYSTEM FOR WATER USE AND WATER-USE EFFICIENCY OF IRRIGATED CROPS IN THE INKOMATI-USUTHU WATER MANAGEMENT AREA

Report to the  
**Water Research Commission**

and

**Inkomati-Usuthu Water Management Area**

prepared by

**S DZIKITI<sup>1</sup>, P DANGARE<sup>1</sup>, GP NEL<sup>1</sup>, JN MASANGANISE<sup>1,5</sup>,  
E KAPANGAZIWIRI<sup>3,6</sup>, A KLEINERT<sup>1</sup>, PJ CRONJE<sup>1,4</sup>, SJE MIDGLEY<sup>1,7</sup>,  
P RAATH<sup>1,4</sup>, EZ MASHIMBYE<sup>2</sup>, Z NTSHIDI<sup>6</sup>**

<sup>1</sup> Department of Horticultural Science, Stellenbosch University

<sup>2</sup> Department of Geography and Environmental Studies, Stellenbosch University

<sup>3</sup> Institute for Water Studies, University of the Western Cape

<sup>4</sup> Citrus Research International

<sup>5</sup> Department of Physics and Engineering, Bindura University of Science and Technology, Zimbabwe

<sup>6</sup> Council for Scientific and Industrial Research

Corresponding author: Sebinasi Dzikiti, e-mail: [sdzikiti@sun.ac.za](mailto:sdzikiti@sun.ac.za)

**WRC Report No. 3129/1/24**  
**ISBN 978-0-6392-0606-6**

**April 2024**



**Obtainable from**

Water Research Commission  
Bloukrans Building, Lynnwood Bridge Office Park  
4 Daventry Street  
Lynnwood Manor  
PRETORIA

[orders@wrc.org.za](mailto:orders@wrc.org.za) download from [www.wrc.org.za](http://www.wrc.org.za)

The publication of this report emanates from a project entitled: ***Developing a decision support system for water use and water-use efficiency of irrigated crops in the Inkomati-Usuthu Water Management Area*** (WRC Project No. C2020/2023-00399).

**DISCLAIMER**

This report has been reviewed by the Water Research Commission (WRC) and approved for publication. Approval does not signify that the contents necessarily reflect the views and policies of the WRC, nor does mention of trade names or commercial products constitute endorsement or recommendation for use.

**Published in the Republic of South Africa**

**© Water Research Commission**

## EXECUTIVE SUMMARY

### Motivation

Key economic activities in the Inkomati-Usuthu Water Management Area (IUWMA), e.g. agriculture, forestry, mining, and eco-tourism are inextricably tied to the health of the catchment's river systems (Simpson *et al.*, 2019). Yet in most parts of the catchment the demand for water already exceeds supply. The situation is likely to worsen in future as competition for the limited resources heightens. Threats to the catchment's water supply arise from the growing population, the increasing frequency and severity of droughts due to climate change (Maponya *et al.*, 2013; Singels and Jones, 2018), invasive alien plants that consume large quantities of water (Le Maitre *et al.*, 2005; Dzikiti *et al.*, 2013; Dzikiti *et al.*, 2016), and the degradation of water quality mostly by mining and agricultural return flows (Rogers and Luton, 2016). So, there is need for accurate information and tools for the effective, efficient, and sustainable management of the water resources in line with the Catchment's Management Strategy. This is critical for water-intensive sectors such as irrigated agriculture that uses up to 57% of the catchment's surface water (Simpson *et al.*, 2019).

The IUWMA has a proactive approach to water management aimed at implementing the provisions of the National Water Act, Act 36 of 1998. For example, following the recent completion of the Validation and Verification of Lawful Water Use in the catchment, there are plans to implement Water Allocation Reforms in the entire catchment. This is essential to address water over/under-allocation issues and to promote equitable and sustainable use of the resource. For informed decision-making, the catchment has embraced state-of-the-art management technologies such as the HydroNet ([www.hydronet.co.za](http://www.hydronet.co.za)) platform. This platform enhances the catchment's capability to better manage its resources. However, for accurate and reliable assessments there is need for local validation, especially of the remote sensing-based eLeaf product used by HydroNet to estimate crop water use with actual measurements (Jarmain *et al.*, 2009).

The Water Research Commission (WRC), in collaboration with grower associations, has over the years initiated and funded research to quantify the actual water use of selected crops in the IUWMA. These studies aimed to generate critical baseline information to improve irrigation scheduling and for water allocation planning. Crops investigated include citrus (Gush and Taylor, 2014; Vahrmeijer and Taylor., 2018), macadamia nuts (Gush and Taylor, 2014; Taylor *et al.*, 2021), maize and sugarcane (Olivier and Singels, 2003; Jarmain *et al.*, 2014), among others.

Despite these efforts, there are still many important crops with significant irrigation allocations in the IUWMA whose water requirements are not known. Examples include mango, banana, litchi, pecan nuts, tobacco, cotton, tea, etc. Given that farmers tend to over-irrigate when they do not have access to reliable water use data (Volschenk *et al.*, 2003), there is need to update the database of actual measured crop water use in the catchment. These data can be used for several purposes. Firstly, crop coefficients can be derived for irrigation

scheduling, irrigation system designs, and for water allocation planning. Secondly, water use estimating tools, e.g. eLeaf currently in use in the IUWMA can be validated with the data. Thirdly, new decision support systems (DSS) can be developed using these (and historical) data to improve the accuracy of crop water use estimates. This was the intention of the current study.

The study sought to address the following questions:

- 1) How do the water use patterns of major irrigated crops vary in the IUWMA?
- 2) What are the main drivers of water use and how do these affect fruit yield and quality?
- 3) How do the biophysical and economic water productivity of the different irrigated crops vary within the IUWMA?
- 4) Can these data be used to develop an accurate DSS that can assist with compliance monitoring and enforcement activities within IUWMA?

To answer these questions, this study first collected detailed data from irrigated crops (mango, grapefruit, banana and litchi) whose water use is not known thereby filling an important information gap. The data collected from this and from previous studies was used to develop a Decision Support System (DSS) (Fig. 1) for estimating the crop water requirements, yield and water use efficiency in all quaternary catchments thus adding another tool to the IUWMA toolbox.

## **AIMS AND OBJECTIVES**

### **Overall aim**

The overall aim was to determine the water use and yield of banana, mango, litchis, sugarcane, and citrus from planting to full-bearing age in selected climatic zones and specific soils.

### **Specific objectives**

The specific objectives were:

- 1) To expand the current database of crop water use data in the WMA to include selected key irrigated crops namely banana, mango, litchis, sugarcane, and citrus.
- 2) To use this data and that collected in previous studies to develop a DSS for estimating water use efficiency of, and water allocation to, crops in the WMA.

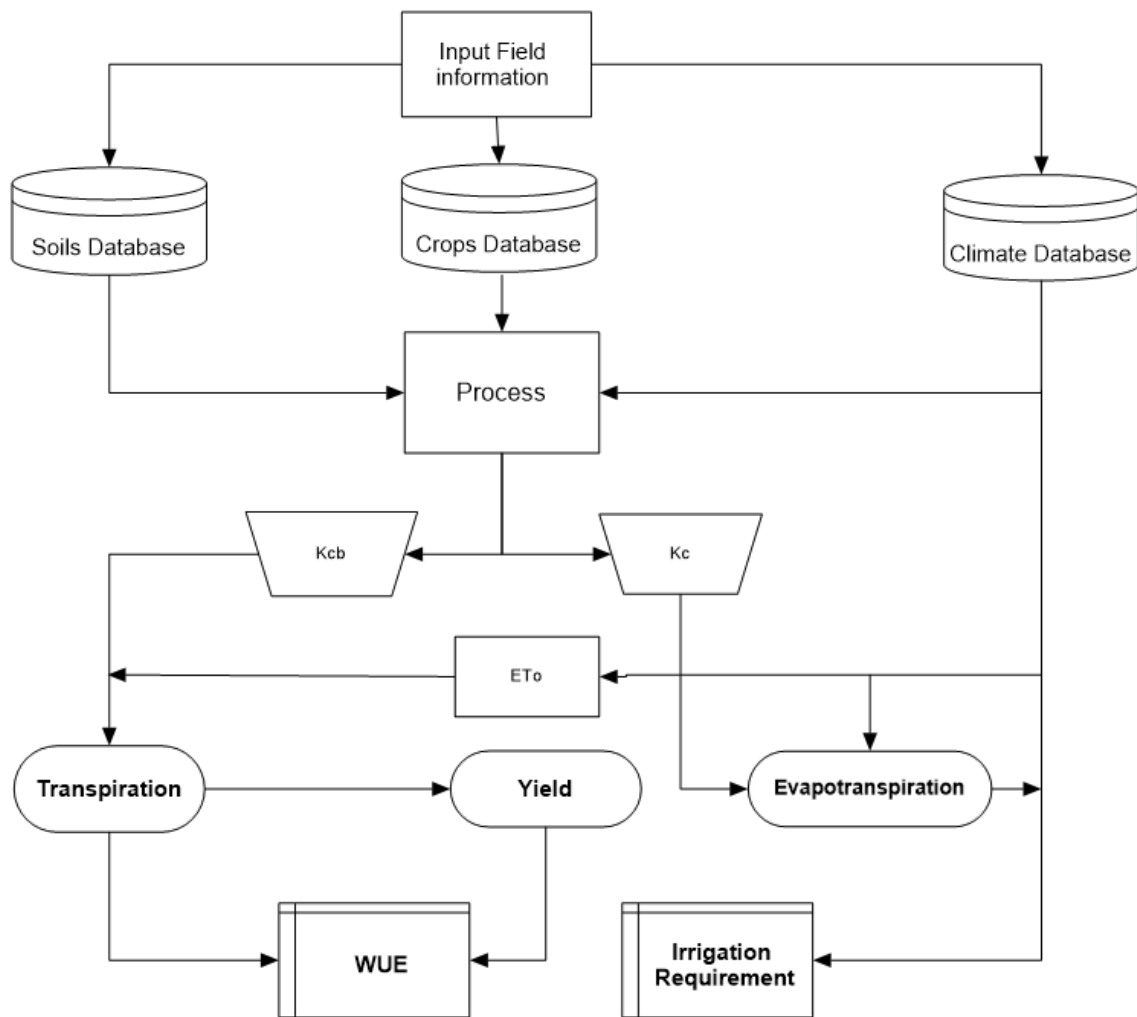


Figure 1: Schematic representation of the DSS for water use and water use efficiency of selected subtropical crops.

## MATERIALS AND METHODS

Data were collected for the period July 2020 to February 2024 in mango, litchi, grapefruit, banana orchards and a sugarcane plantation. The mango, litchi, grapefruit and sugarcane study sites were at Riverside Farm in Malelane, while the banana orchard was in Komatipoort. Data collection in the mango, litchi and grapefruit orchards were done over two growing seasons to account for the variability in climatic and management conditions. The banana data were collected over one full season while the sugarcane data were collected over five months.

Tree transpiration data were measured using the heat ratio method of monitoring sap flow on at least four instrumented trees per site. This method gave hourly transpiration measurements over the duration of the study. Use of the thermal dissipation probes to

measure the sap flow of banana crops was not successful due to the complex tissue structure of the stems. The evapotranspiration component was measured in the mango, litchi and grapefruit orchards using the open path eddy covariance method while the surface renewal technique was deployed in banana and sugarcane fields. Volumetric soil water was monitored in the rootzone using time domain reflectometer probes. Irrigation volumes, orchard microclimate, canopy size, fruit growth, tree water status, leaf photosynthesis, etc. were also measured during specific seasons.

Two models were developed and tested to extrapolate the water use data to other orchards. The first model was a dual source water use model wherein orchard evapotranspiration (ET<sub>c</sub>) was partitioned into a tree transpiration and orchard floor evaporation component. Orchard ET<sub>c</sub> was calculated as the algebraic sum of these two fluxes. This model enabled estimates of orchard water use to be obtained for trees with various canopy cover from planting to full-bearing age. The second model is an extension of the FAO 56 model which is an adapted version of the Allen and Pereira (A&P 2009) method. This model estimated the crop coefficients from readily available data, something that can directly benefit the users, especially irrigation farmers.

## **RESULTS AND DISCUSSION**

Leaf gas exchange measurements for mango, litchi and grapefruit all showed that these species have low maximum photosynthetic ( $< 5 \mu\text{mol}/\text{m}^2/\text{s}$ ) and transpiration rates due to very strict stomatal regulation of gas exchange. Peak stomatal conductance was also low, generally less than 2.0 mm/s compared to close to 10 mm/s for unstressed apple trees, for example. Planting distance varied widely per crop type. For example, grapefruit orchards had a tree density of about 476 trees/ha, followed by mango with 303 and litchi with only 70 trees per ha. The wider tree spacings led to larger trees and higher transpiration rates per tree. For example, peak transpiration of the litchi trees approached 200 litres/tree/d, followed by mango at about 62 litres/tree/d and then grapefruit at around 23 litres/tree/d. However, expressing the annual water use in equivalent depth units, the litchi orchard had the least annual transpiration of around 335 mm, followed by grapefruit at 437 mm and lastly mango at 601 mm. The results are summarized in Table I.

According to the original A&P approach, the stomatal sensitivity of a given crop is referenced to the leaf resistance of an annual crop, generally around 100 s/m and this has not worked well for tree crops. However, given the differences in the aerodynamic properties of annual crops and tree crops, we replaced the 100 s/m with  $\alpha$  and solved for this parameter

using the measured data for all the other variables as detailed in Mobe *et al.* (2020). A small subset of the data was used when the trees were at full canopy cover, and well-watered. Typical values of  $\alpha$  were 37 s/m for grapefruit, 26 s/m for litchi and around 21 s/m for mango. Using these parameters to calculate the crop coefficients led to transpiration and evapotranspiration values that were close to the measured values.

The estimated annual total evapotranspiration for the litchi orchard was about 960 mm which was about 65% higher than the measured transpiration (335 mm). Water input into the orchard, i.e. rainfall (558) plus irrigation (437) giving a total of 995 mm almost matched the modelled annual ETc. These values, however, suggest very high non-beneficial water losses through orchard floor evaporation which can be reduced, e.g. by using drip, mulching, or scheduling the irrigation more precisely. The crop coefficients for the litchi orchard fluctuated between 0.70 and 0.91. The water use efficiency (Yield/ETc) of the litchi orchard was very low at about 0.85 kg of fruit per m<sup>3</sup> of water used. Estimates of the economic water productivity (Rands per m<sup>3</sup>) are shown in Table I, but these are based on retail prices of litchis found online. So, they may not be as accurate as we would have wished.

The mango orchard on the other hand had an annual total ETc of about 887 mm which was about 32% higher than the transpiration (601 mm). Annual total irrigation was about 456 mm and 558 mm of rainfall (giving total application of 1 014 mm). The crop coefficient for the mango orchard was in the range 0.62 and 0.86 depending on season. The water use efficiency was about 5.01 kg of fruit per m<sup>3</sup> of water used. Annual total ETc of the grapefruit was high at about 1069 mm, about 59% higher than the transpiration. The orchard received massive irrigation at about 997 mm per year for unclear reasons. The water use efficiency of the grapefruit was about 3.52 kg/m<sup>3</sup>.

The measured data, including that of other crops which were not part of the current study namely macadamia and two citrus cultivars were used to develop the decision support system (DSS). At the heart of the DSS are three databases namely for climate, soils, and crop parameters. Fifty years of daily climate data were used with a weather station located at the centroid of each quaternary catchment in IUWMA. Crops that are currently included in the DSS are mango, litchi, grapefruit, citrus (bahianinha navel and Washington navel), and macadamia. The DSS uses simple readily available data as inputs such as site coordinates, crop type, average vegetation height, fractional vegetation cover, soil type, irrigation system, and cover crop status. The DSS produces outputs at the monthly and annual time scales for; i) actual transpiration, ii) actual evapotranspiration, iii) irrigation requirements, iv) maximum potential yield, and v) water use efficiency. The simulations are run per quaternary catchment.

Table I. Summary of the water use and water use efficiency (water productivity) of the most commonly irrigated crops in the IUWMA. Crops preceded by the letter “a” were studied in this project; those marked “b” were included in previous studies. Sources of the economic water productivity data are indicated by the references marked “x” to “dd”.

Crop type	Cultivar	Age (yr)	Number of plants per ha	Peak LAI	Irrigation system	Transpiration (mm/yr.)	Evapotranspiration (mm/yr.)	Irrigation (mm/yr.)	Yield (t/ha)	Water Use Efficiency (kg/m <sup>3</sup> )	Economic Water Productivity (R/m <sup>3</sup> )
<sup>a</sup> Mango	Tommy Atkins	32	303	3.7	Microsprinkler	601	887	456	44.5	5.01	116 <sup>x</sup>
<sup>a</sup> Litchi	Mauritius	53	70	3.9	Microsprinkler	335	960	437	8.1	0.85	51 <sup>y</sup>
<sup>a</sup> Grapefruit	Star Ruby	14	476	3.5	Microsprinkler	437	1069	997?	37.6	3.52	88 <sup>z</sup>
<sup>a</sup> Sugarcane	N53	-	-	-	Drip	-	1266	-	60.0	4.74	-
<sup>a</sup> Banana	William Cavendish	-	-	-	Microsprinkler	-	965	-	40.0	4.15	125 <sup>aa</sup>
<sup>b</sup> Macadamia	Beaumont	11	312	-	Drip	340	-	164	6.0	1.94	118 <sup>bb</sup>
<sup>b</sup> Citrus	Various types	-	-	-	-	-	539-953	-	-	3.9-14.4 <sup>dd</sup>	
<sup>b</sup> Avocado	Hass	5	357	-	Drip	678	1071	113	-	1.62	41 <sup>cc</sup>

<sup>x</sup> [www.evergreenspta.co.zw](http://www.evergreenspta.co.zw) (accessed on 31 March 2024)

<sup>y</sup> [www.vanzylfresh.co.za/products/lychee-500g?variant=37189926944934](http://www.vanzylfresh.co.za/products/lychee-500g?variant=37189926944934) (accessed on 31 March 2024)

<sup>z</sup> [www.checkers.co.za/](http://www.checkers.co.za/) (accessed on 31 March 2024)

<sup>aa</sup>Taylor NJ., Mazhawu E., Clulow A., Midgley SJE., Roets N., Smit T., Annandale JG. 2021a. Water use of avocado orchards, Volume 1. WRC report.

<sup>cc</sup>Taylor NJ., Smit T., Smit A., Clulow A., Midgley SJE., Dlamini K., Annandale JG. 2021b. Water use of macadamia orchards, Volume 2. WRC report.

<sup>dd</sup>Vahrmeijer TJ., Taylor NJ. 2018. Quantifying citrus water use and water stress at orchard level. WRC Report TT772/2/18.

## NEW KNOWLEDGE AND INNOVATION

New knowledge generated includes:

- Accurate quantitative information on the water use of irrigated crops and how it is partitioned between beneficial and non-beneficial uses under current irrigation management;
- Accurate crop coefficients for subtropical tree crops which are currently not readily available;
- A decision support system that can be used for water allocation planning.

Some aspects of this study have been published or are under review by international journals as follows:

1. Dangare P, Nel GP, Sawunyama T, Cronje PJ, Dziki S (in press). Measurement and Modelling of Water Use of Litchi (*Litchi sinensis*) under subtropical conditions. *Acta Horticulturae*.
2. Nel GP, P. Dangare, A. Kleinert, S Dziki (3<sup>rd</sup> round of review). Estimating crop coefficients and water use of a full-bearing mango orchard in north-eastern South Africa using the fraction of vegetation cover and a dual source evapotranspiration model. *Scientiae Horticulturae journal*.

## CONCLUSIONS

This study reports on detailed data collection on the water use characteristics of selected subtropical tree crops. A range of quantitative techniques are used to understand the soil-plant-atmosphere interactions in the orchards with data collected at the leaf scaled up to whole orchard level. Our data suggests that tree crops like mango, litchi, and citrus have conservative water use rates. Large water losses from orchards are a result of evaporation from the orchard floor rather than from transpiration. For this reason, practices such as mulching, use of drip irrigation and optimal irrigation scheduling should be encouraged to reduce non-beneficial water losses. The measured and historical data (for some crops) were used to develop a DSS that can potentially be used to support the implementation of planned activities in the IUWMA such as water allocation reforms.

## **RECOMMENDATIONS FOR FUTURE RESEARCH**

These are as follows:

- 1) The improved protocol for deriving crop coefficients of irrigated tree crops still needs to be tested widely in a range of orchards and growing conditions;
- 2) The DSS itself also needs to be validated even with current environmental, water use and yield data especially to test water use-yield functions;
- 3) More irrigated crops should be included in the DSS, e.g. avocados, pecans, vegetables, etc.
- 4) The DSS can be adapted to use remote sensing inputs to provide spatial information;
- 5) There is need for training of potential users (i.e. farmers, catchment managers, irrigators, etc.) on how to use the DSS.

## **EXTENT TO WHICH CONTRACT OBJECTIVES HAVE BEEN MET**

The terms of reference of this project were largely met, and in some instances exceeded. The first goal of the study was to collect water use and water use efficiency data from mango, litchi, grapefruit, banana, and sugarcane crops to expand the database of measured water used data in the study area. This goal has been met although there was limited time for sugarcane due to the short duration of the project owing to delays in the start of the project due to Covid-19. In most other crop types, data were collected over at least two growing seasons thereby capturing, to some degree, the year-to-year variations in growing conditions. The second goal was to develop a Decision Support System for estimating water use and water use efficiency. This goal was also achieved using data collected in this project and in the previous studies on macadamia nuts and different citrus cultivars. The DSS has features such as farm boundaries and it uses 50 years of daily weather data to calculate the crop water use. Another novel aspect of the DSS is the protocol for calculating the crop coefficients using readily available data such as average crop height, fractional vegetation cover, soil type, wetted soil fraction, etc. as inputs. This potentially extends the functionality of the DSS to a tool for routine irrigation scheduling using its crop coefficients functionality. This indeed exceeds what was stipulated in the terms of reference. In addition, the DSS can be used as a basic teaching aid demonstrating basic concepts in crop water requirements, irrigation scheduling, the potential contribution of cover crops to orchard water use, etc. A decision still needs to be made on who will host the DSS beyond the life of the project as most online platforms charge a substantial fee.

## ACKNOWLEDGEMENTS

We acknowledge the Water Research Commission (WRC) and the Inkomati-Usuthu Water Management Area (IUWMA) for initiating and funding this study. We are sincerely grateful to Riverside Farm in Malelane and Welgelegen Farm in Komatipoort for allowing us to work in their productive orchards. We thank Mr Dean van Heerden and other managers at Riverside farm for their assistance with many aspects of the project including providing orchard information, charging, and changing batteries for the equipment, changing memory cards, etc. We also thank Mr Vivian White for assistance with downloading the data.

Lastly, we acknowledge inputs from the following reference group members, their support was invaluable:

Prof NS Mpandeli	:	Water Research Commission (Chairman)
Dr L Nhamo	:	Water Research Commission (Co-Chairman)
Dr SN Hlophe-Ginindza	:	Water Research Commission
Dr J Mehl	:	South African Subtropical Growers' Association
Dr N Murovhi	:	Agricultural Research Council
Prof A van Niekerk	:	Stellenbosch University
Dr NJ Taylor	:	University of Pretoria
Dr Nwabisa Masekwana	:	Agricultural Research Council
Prof. A Ramoelo	:	University of Pretoria
Dr Tendai Sawunyama	:	Inkomati-Usuthu Catchment Management Agency
Mr Andre Botha	:	South African Subtropical Growers' Association
Prof Sue Walker	:	Agricultural Research Council

This page was intentionally left blank

## TABLE OF CONTENTS

EXECUTIVE SUMMARY .....	iii
ACKNOWLEDGEMENTS .....	xi
List of Abbreviations and Acronyms .....	xxviii
List of Symbols .....	xxix
CHAPTER 1: GENERAL INTRODUCTION.....	1
1.1. Research Background .....	1
1.2. Aims and Objectives .....	4
CHAPTER 2: KNOWLEDGE REVIEW.....	5
2.1. Major Irrigated Crops Grown in the IUWMA.....	5
2.2. The Sub-Tropical Fruit and Sugarcane Industries .....	7
2.2.1. Banana Industry.....	7
2.2.1.1. Extent of the banana industry in the IUWMA.....	7
2.2.1.2. Irrigation types and irrigation scheduling in banana orchards.....	9
2.2.1.3. Water related challenges and priorities for the banana industry .....	10
2.2.2. Mango Industry .....	11
2.2.2.1. Extent of the mango industry in the IUWMA.....	11
2.2.2.2. Irrigation types and irrigation scheduling in mango orchards.....	12
2.2.2.3. Water related challenges and priorities for the mango industry .....	13
2.2.3. Litchi Industry.....	13
2.2.3.1. Extent of the litchi industry in the IUWMA .....	13
2.2.3.2. Irrigation types and irrigation scheduling in litchi orchards .....	14
2.2.3.3. Water related challenges and priorities for the litchi industry .....	15
2.2.4. Sugarcane Industry.....	15
2.2.4.1. Extent of the sugarcane industry in the IUWMA.....	15
2.2.4.2. Irrigation types and irrigation scheduling in sugarcane fields.....	17
2.2.4.3. Water related challenges and priorities for the sugarcane industry .....	18
2.3. Water Requirements of Selected Fruit Tree Crops in the IUWMA: A Review .....	20
2.3.1. Banana .....	20
2.3.2. Citrus .....	21
2.3.3. Avocados.....	23

2.3.4.	Macadamia Nuts .....	23
2.3.5.	Sugarcane .....	24
2.4.	Climate Change and Expected Impacts in the IUWMA .....	25
2.4.1.	Historical/Current Climate of the IUWMA .....	25
2.4.2.	Observed Trends in the Climate of the IUWMA.....	25
2.4.3.	Climate Change Projections for the IUWMA.....	26
2.4.3.1.	Narrative 1: A hot and dry future .....	26
2.4.3.2.	Narrative 2: A warmer future with increased rainfall.....	26
2.4.4.	Impacts of Climate Change on Water Resources of the IUWMA.....	26
2.5.	Water Resources and Management in the IUWMA .....	33
2.5.1.	Description of the Hydrology of the Study Area.....	33
2.5.2.	Water Allocation Practices and Relevant Legislation.....	34
2.5.3.	Water Management Priorities to Improve Water Allocation and Efficiencies...	35
2.5.4.	Current Tools for Water Resource Management in the IUWMA .....	36
CHAPTER 3: DETERMINING WATER USE OF MATURE MANGO ORCHARDS UNDER SUBTROPICAL CONDITIONS .....		37
3.1.	Summary .....	37
3.2.	Introduction .....	38
3.3.	Materials and Methods.....	39
3.3.1.	Soil Characteristics and Irrigation for the Mango Orchard .....	42
3.3.2.	Rootzone Soil Water Content.....	48
3.3.3.	Orchard Microclimate.....	49
3.3.4.	Canopy Temperature and Radiation Interception.....	50
3.3.5.	Transpiration Measurements .....	51
3.3.6.	Actual Evapotranspiration .....	55
3.3.7.	Ecophysiological Measurements.....	56
3.3.8.	Water Productivity.....	58
3.3.9.	Modelling mango orchard water use .....	59
3.4.	Results and Discussion.....	61
3.4.1.	Climatic Conditions .....	61

3.4.2.	Rootzone Soil Moisture Dynamics and Canopy Growth .....	64
3.4.3.	Stomatal responses to environmental variables .....	67
3.4.4.	Daily and seasonal trends in measured water use .....	70
3.4.5.	Seasonal trends in modelled water use and crop coefficients for mango orchards .....	74
3.4.6.	Discussion .....	79
3.4.7.	Tree water status .....	81
3.5.	Conclusion .....	83
CHAPTER 4: WATER USE OF MATURE LITCHI ORCHARDS UNDER SUBTROPICAL CONDITIONS .....		85
4.1.	Summary .....	85
4.2.	Introduction .....	86
4.3.	Materials and Methods .....	88
4.3.1	Study Site and Plant Material .....	88
4.3.2	Soil Water Content and Irrigation Measurements .....	89
4.3.3	Transpiration Measurements in the Litchi Orchard .....	91
4.3.4	Plant Stress and Radiation Interception Measurements .....	92
4.3.5	Modelling Water Use of Litchi Orchards .....	94
4.3.5.1	Modelling Leaf Stomatal Conductance .....	94
4.3.5.2	Calculation of Basal Crop Factors ( <i>K<sub>cb</sub></i> ) .....	95
4.3.5.3	Statistical Analysis .....	97
4.4.	Results and Discussion .....	97
4.4.1	Leaf Area Index and Soil Moisture Dynamics .....	97
4.4.2	Leaf Gas Exchange and Transpiration Dynamics of Litchi Trees .....	100
4.4.3	Litchi Orchard Evapotranspiration .....	106
4.4.4	Modelling Crop Coefficients and Water Use of a Litchi Orchard .....	108
4.4.4.1	Stomatal Conductance .....	108
4.4.4.2	Estimating the Basal Crop Coefficients ( <i>K<sub>cb</sub></i> ) and Orchard Transpiration .... .....	110
4.5.	Conclusion .....	115

CHAPTER 5: WATER USE OF MATURE GRAPEFRUIT ORCHARDS UNDER SUBTROPICAL CONDITIONS .....	116
5.1. Summary .....	116
5.2. Materials and Methods.....	117
5.2.1 Plant material.....	117
5.2.2 Soil Water Content, Growth, and Water Use Measurements.....	118
5.2.3 Leaf Gas Exchange and Plant Water Status .....	121
5.3. Results and Discussion.....	122
5.3.1 Seasonal Tree Growth .....	122
5.3.2 Soil Water Content, Irrigation, and Leaf Gas Exchange .....	123
5.3.3 Water Use of Grapefruit Orchards and its Drivers .....	125
5.4. Conclusions .....	133
CHAPTER 6: WATER USE OF A BANANA ORCHARD UNDER SUBTROPICAL CONDITIONS .....	134
6.1. Summary .....	134
6.2. Introduction .....	134
6.3. Materials and Methods.....	136
6.3.1 Description of the study site and plant material .....	136
6.3.2 Data collection .....	136
6.3.2.1 Orchard microclimate.....	136
6.3.2.2 Eddy covariance and surface renewal measurements.....	137
6.3.2.3 Transpiration measurements .....	139
6.3.2.4 Irrigation .....	139
6.3.2.5 Evapotranspiration .....	139
6.3.2.6 Data processing.....	140
6.3.2.7 Statistical analysis .....	142
6.4. Results.....	142
6.4.1 Microclimate.....	142
6.4.2 Energy balance for the banana orchard .....	144
6.4.3 Calibration of surface renewal.....	148

6.4.4	Sensible and latent heat fluxes derived from measurements of surface renewal .....	150
6.4.5	Evapotranspiration estimates.....	152
6.4.6	Transpiration measurements .....	155
6.5.	Discussion .....	159
6.6.	Conclusions .....	162
CHAPTER 7: WATER USE OF A SUGARCANE PLANTATION UNDER SUBTROPICAL CONDITIONS.....		163
7.1.	Summary .....	163
7.2.	Introduction.....	164
7.3.	Materials and Methods.....	165
7.3.1	Study Site and Plant Material.....	165
7.3.2	Soil water content and irrigation measurements.....	166
7.3.3	Actual Evapotranspiration .....	167
7.3.4	Modelling sugarcane plantation water use .....	170
7.4.	Results and Discussion.....	170
7.4.1	Soil Moisture Dynamics .....	170
7.4.2	Climatic drivers of evapotranspiration .....	171
7.4.3	Calibration and validation of SR method .....	173
7.4.4	Sugarcane plantation crop coefficients and modelled evapotranspiration ....	173
7.5.	Conclusion.....	176
CHAPTER 8: DEVELOPMENT AND TESTING OF A DECISION SUPPORT SYSTEM FOR WATER USE AND WATER USE EFFICIENCY OF IRRIGATED TREE CROPS.....		177
8.1.	Summary .....	177
8.2	Scientific basis behind the DSS .....	177
8.3	Description of the DSS.....	179
8.4	Outputs from the DSS.....	184
CHAPTER 9: CONCLUSIONS AND RECOMMENDATIONS.....		187
9.1.	Conclusions .....	187
9.2	Recommendations.....	189

REFERENCES .....	190
APPENDICES .....	199
Appendix 1. Capacity Building .....	199
Appendix 2. Summary of crop growth stages used in the DSS. ....	200
Appendix 3. Typical soil water characteristics for different soils (FAO 56). ....	201

## LIST OF FIGURES

Figure 1.1: Map of catchments in the Mpumalanga province showing the Inkomati-Usuthu catchments. ....	2
Figure 2.1: Banana production areas (ha) in South Africa in 2010. (Source: DAFF, 2011).....	8
Figure 2.2: Total production and gross value of bananas in South Africa from 1985/86 until 2017/18 (Source of data: DAFF, 2019). ....	8
Figure 2.3: Mango plantings by production area (Subtrop, 2020).....	12
Figure 2.4: Litchi plantings by production area (Subtrop, 2020).....	14
Figure 2.5: Map of sugarcane production areas of South Africa. Source: <a href="https://sasa.org.za/the-sugar-industry-at-a-glance/">https://sasa.org.za/the-sugar-industry-at-a-glance/</a> .....	16
Figure 2.6: Total production and gross value of sugarcane in South Africa from 1985/86 until 2018/19 (Source of data: DAFF, 2019, using data supplied by SASA).....	17
Figure 2.7: Areas under sugarcane production (shaded areas), important rivers and water quality sampling points (identified by triangles) in the Crocodile and Komati-Lomati River catchments. Source: Van der Laan et al. (2012) .....	20
Figure 2.8: Range of potential impacts of climate change on the mean annual catchment runoff for secondary catchments for the period 2040 to 2050 due to the Unconstrained Emissions (UCE) scenario relative to the base scenario. The northern part of the W4 catchment and the X1 catchment (last two catchments on the X-axis) are within the IUWMA. Source: DEA, 2013a. ....	29
Figure 2.9: Median impact of climate change on the average annual catchment runoff for the period 2040-2050 relative to the base scenario average for 1990-2000 for all secondary catchments in South Africa derived from a Hybrid Frequency Distribution (HFD) analysis of all possible global circulation model (GCM) outputs (+6000 scenarios) for the unconstrained emissions scenario (UCE). The northern part of the W4 catchment and the X1, X2, X3 and X4 catchments (indicated roughly by the red circle) are within the IUWMA. Source: DEA, 2013a. ....	30
Figure 2.10: Average annual water demand (top) for the 19 WMAs for the period 2040 to 2050 and the estimated proportion of demand that can be supplied under the base scenario (symbols) and models representing the minimum, 25th, median, 75th percentile and maximum impact under the unconstrained emissions scenario (UCE) for different sectors. In each plot the symbol represents the percentage of the average annual demand that can be supplied under the base scenario in each WMA while the box plots show the median and the inter-quartile range and the bars show the maximum and minimum model results. Source: DEA, 2013a.....	31
Figure 2.11: Source: Schulze and Kunz (2010) – figure taken from DEA (2013b) .....	33

Figure 3.1: The ‘Tommy Atkins’ mango orchard at Riverside farm. ....	40
Figure 3.2: The two profile pits made in the mango orchard to study the soil characteristics. The following soil form were classified in the field profile MA was a Inhoek and Profile MB was a Glenrosa. ....	42
Figure 3.3: A Sandy loam.....	45
Figure 3.4: Sandy clay loam.....	45
Figure 3.5: Water flow meter monitoring the irrigation volumes in the mango orchard.....	48
Figure 3.6: Placement of moisture probes to measure the volumetric soil water content in the mango orchard.....	49
Figure 3.7: (a) Automatic weather station installed to monitor the basic weather variables at Riverside Farm, (b) Measuring light interception by the mango canopy using line quantum sensors. ....	50
Figure 3.8: Stem size distribution for 25 randomly selected trees with varying circumferences. The four red highlighted trees are trees selected for instrumentation with sap flow sensors.	54
Figure 3.9: Tree box with four HRM probes. The insert shows an HRM probe, with two thermocouples installed at the top and bottom and a heater installed in the middle. ....	54
Figure 3.10: The eddy covariance flux tower used to measure orchard evapotranspiration (ET <sub>c</sub> ) and the surface energy balance components. ....	56
Figure 3.11: Infrared gas analyser measuring leaf photosynthesis, transpiration, and stomatal conductance of a mango tree in Malelane.....	58
Figure 3.12: Schematic representation of the Shuttleworth and Wallace model (after Shuttleworth and Wallace, 1985). ....	60
Figure 3.13: Daily weather conditions at Riverside farm in Malelane from September 2021 to August 2022 representing (a) the daily solar radiation, (b) maximum and minimum temperatures, (c) vapour pressure deficit of the air, and (d) rainfall.....	63
Figure 3.14: The dynamic volumetric soil moisture content in response to irrigation and rainfall events at various depths in a mature full-bearing mango orchard for 2021/22. A) The response of volumetric water content in the tree row reflecting irrigation and rainfall. and B) represents the non-irrigated inter-row area responding to rainfall only. Where 200 mm, 500 mm and 1000 mm is the depth at which the probes were installed in the soil profile. $\theta_{FC}$ is the field water capacity of the soil and $\theta_{PVP}$ is the permanent wilting point of the crop.....	65
Figure 3.15: Typical seasonal variations in the leaf area index of the mango orchard during the 2021/2022 season. Where I) Indicates when pruning occurred. Measurements were conducted on 06 September 2021, 14 November 2021, 07 February 2022 and 09 July 2022. ....	66

Figure 3.16: Response of  $A_{max}$  to increasing (A)  $T_{leaf}$  (N= 338) and (B)  $VPD_{leaf}$  (N= 338), (C) the response of  $g_s$  to  $VPD_{leaf}$  (N= 338) and (D) the response of  $A_{max}$  to  $g_s$  (N= 338). (E) Representative responses of  $A$  to intercellular  $CO_2$  concentration ( $C_i$ ) showing the method used to calculate stomatal limitations ( $I = (AII-AI)/AI$ ) as outlined by Long and Bernacchi (2003) of Three experimental trees (N = 99) measured on 2022/02/23 and 2022/07/21. (F) Response of  $A$  to PAR in fully sun-exposed leaves of four trees (N = 126) measured on 2022/02/23 and 2022/07/21. Means followed by the same letter are not significantly different ( $p = 0.05$ ) as analysed using repeated measures ANOVA. Data from figures A-F were pooled data obtained from several measurement campaign. .... 69

Figure 3.17: (a) Daily reference evapotranspiration; and (b) average daily transpiration of a mango tree from 01 August 2021 to 20 July 2022. .... 70

Figure 3.18: Effect of various environmental drivers on transpiration by mango trees which include (a) daily solar radiation, (b) vapour pressure deficit of the air, (c)  $E_{to}$  and (d) soil water deficit. .... 72

Figure 3.19: Relationship between the whole orchard transpiration, actual evapotranspiration and reference evapotranspiration from March to July 2022. .... 73

Figure 3.20: Effect of the atmospheric evaporative demand on the actual evapotranspiration of the mango orchard. .... 73

Figure 3.21: Comparison between the measured and dual source (S&W) modelled: (a) orchard transpiration, (b) actual evapotranspiration, and; (c) orchard floor evaporation. .... 76

Figure 3.22: Seasonal changes in: (a) the actual and modelled weekly basal crop coefficients, (b) actual and modelled weekly single crop coefficients for the mature mango orchard in comparison with the FAO four stage crop coefficients.  $K_{cb}$  FAO and  $K_c$  FAO depict the basal and single crop coefficients from the four stage FAO approach,  $K_{cb}$  A&P,  $K_c$  A&P depict the basal and single crop coefficients from the Allen and Pereira method,  $K_{cb}$  mod and  $K_c$  mod represents the basal and single crop coefficients modelled by the dual source model. .... 78

Figure 3.23: Cumulative seasonal fluxes of reference evapotranspiration, modelled evapotranspiration, actual transpiration, and water application (irrigation plus rainfall) from January to December 2022. .... 79

Figure 3.24: (a) Dendrometer measuring hourly growth of the mango. (b) Typical growth curve for a Tommy Atkins mango fruit. .... 81

Figure 3.25: (a) Volumetric soil water content and midday canopy-air temperature, and (b) stem diameter variation and micro-tensiometer xylem tension as indicators of water status. .... 83

Figure 4.1: Orthomosaic of the litchi orchard created by drone images over the litchi orchard. .... 88

Figure 4.2: Soil Moisture probes installed at 30 cm, 60 cm and 120 cm horizontally below the ground in the profile pit.....	90
Figure 4.3: Heat Ratio Method setup on a litchi tree with multiple stems.....	92
Figure 4.4: Setup of the infrared (IR) thermometer used to continuously measure canopy temperature of litchi trees.....	93
Figure 4.5: Leaf area index of the litchi orchard over the study period.....	98
Figure 4.6: Seasonal dynamics in the soil water content in the rootzone of the litchi trees representing (a) the within and (b) between row positions.....	99
Figure 4.7: Diurnal photosynthesis and stomatal conductance for a litchi tree.....	100
Figure 4.8: Diurnal course of the stem/ xylem water potential and leaf photosynthesis for a litchi tree.....	101
Figure 4.9: Seasonal variation of the measured stomatal conductance for the litchi trees at midday.....	101
Figure 4.10: Daily (a) reference evapotranspiration and (b) single litchi tree transpiration (in L/d) in Malelane.....	102
Figure 4.11: Seasonal transpiration dynamics of the mature litchi orchard in comparison with the reference evapotranspiration.....	103
Figure 4.12: Effect of (a) solar radiation, (b) VPD and (c) reference evapotranspiration on the transpiration of a litchi orchard.....	104
Figure 4.13: Effect of (a) the daily total solar radiation and, (b) VPD on the basal crop coefficient for litchi orchards.....	105
Figure 4.14: Weekly basal crop coefficients for a mature litchi orchard in Malelane.....	106
Figure 4.15: Effect of (a) solar radiation, (b) VPD, (c) ETo, and (d) soil water content on ETc.....	107
Figure 4.16: Relationship between modelled and measured stomatal conductance for Litchi trees over selected days during the growing season.....	109
Figure 4.17: Jarvis modelled stomatal conductance monthly averages for the litchi trees over the course of the growing season.....	110
Figure 4.18: Relationship between monthly average stomatal conductance and (a) reference evapotranspiration, (b) solar radiation, (c) vapour pressure deficit of the air.....	111
Figure 4.19: Comparison between measured monthly transpiration and modelled tree transpiration using, (a) Allen and Pereira (2009, A&P) method using measured stomatal conductance, (b) Modified Allen and Pereira (2009, A&P) method using Jarvis (1976) derived stomatal conductance and a resistance parameter, (c) Modified Allen and Pereira (2009, A&P) method using measured stomatal conductance and a resistance parameter for the litchi tree.....	113

Figure 4.20: Seasonal changes in the crop coefficients for a mature litchi orchard at Malelane, Mpumalanga Province. ....	114
Figure 5.1: Location of the 'grapefruit' orchard at Riverside farm.....	118
Figure 5.2: Illustration of the setup for the monitoring transpiration using the heat ratio method (HRM) sap flow technique.....	119
Figure 5.3: Eddy covariance system measuring evapotranspiration in the grapefruit orchard. ....	120
Figure 5.4: Measuring the leaf gas exchange with the Li 6800 in a mature grapefruit orchard. ....	121
Figure 5.5: Leaf area index for the grapefruit orchard in Malelane from December 2021 to June 2023.....	122
Figure 5.6: Measured soil water content in the root zone of the grapefruit orchard, (a) within tree row and (b) between tree rows for the period October 2021 to October 2023. ....	123
Figure 5.7: Diurnal variation of the measured photosynthesis rate and stomatal conductance for the grapefruit tree on a sunny day.....	124
Figure 5.8: Diurnal variation of the measured photosynthesis rate and stem water potential for the grapefruit tree on a sunny day.....	125
Figure 5.9: Measured grapefruit transpiration and reference evapotranspiration from December 2021 to September 2023. ....	126
Figure 5.10: Effect of various environmental drivers on transpiration by grapefruit trees which include, 2(a) solar radiation, 2(b) vapour pressure deficit, 2(c) reference evapotranspiration, and 2(d) soil moisture deficit for the period November 2021 to September 2023.....	127
Figure 5.11: Measured monthly basal coefficient and modelled basal coefficients for the grapefruit tree using a modified Allen and Pereira (2009, A&P) method which includes measured stomatal conductance. ....	128
Figure 5.12: Relationship between measured monthly transpiration and modelled transpiration for the grapefruit using the modified Allen and Pereira (2009, A&P) method which includes measured stomatal conductance and a minimum leaf resistance of 200 s/m. ....	128
Figure 5.13: Comparison between measured monthly transpiration and modelled transpiration for the grapefruit using the modified Allen and Pereira (2009, A&P) method which includes measured stomatal conductance and a minimum leaf resistance of 1000 s/m. ....	129
Figure 5.14: Seasonal dynamics in the measured transpiration and modelled ET <sub>c</sub> for the grapefruit orchard. The blue circles depict the measured ET <sub>c</sub> .....	130
Figure 5.15: Water balance of the grapefruit orchard from January to December 2022 (a) with irrigation and rainfall presented separately, and (b) with irrigation and rainfall combined. .	132

Figure 6.1: Diurnal variations of half-hourly sensible heat flux ( $HEC$ ), latent heat flux ( $LEEC$ ), net radiation ( $Rn$ ) and soil heat flux ( $G$ ). .....	144
Figure 6.2: Diurnal variations of half-hourly values of the consumed energy flux ( $H + LE$ ) and the available energy flux ( $Rn - G$ ) derived from EC measurements of $H$ and $LE$ .....	145
Figure 6.3: Energy balance closure for the banana orchard based on EC measurements of $H$ and $LE$ using (a) data for stable and unstable conditions and (b) data for unstable conditions only.....	146
Figure 6.4: Regression lines for calibrating surface renewal using eddy covariance. The lines were generated using SR measurements from (a) TC1 and a time lag of 0.4 s; (b) TC1 and a time lag of 0.8 s; (c) TC2 and a time lag of 0.4 s and (d) TC2 and a time lag of 0.8 s. The slope of each line is the $\alpha$ value. ....	149
Figure 6.5: Diurnal variations of half-hourly sensible heat flux estimated using a time lag of 0.4 s ( $HSRr = 0.4$ ), sensible heat flux estimated using a time lag of 0.8 s ( $HSRr = 0.8$ ), net radiation ( $Rn$ ), soil heat flux ( $G$ ), latent heat flux estimated using a time lag of 0.4 s ( $LESr = 0.4$ ) and latent heat flux estimated using a time lag of 0.8 s ( $LESr = 0.8$ ).....	150
Figure 6.6: Diurnal variations of hourly sensible heat flux estimated using a time lag of 0.4 s ( $HSRr = 0.4$ ), sensible heat flux estimated using a time lag of 0.8 s ( $HSRr = 0.8$ ), net radiation ( $Rn$ ), soil heat flux ( $G$ ), latent heat flux estimated using a time lag of 0.4 s ( $LESr = 0.4$ ), latent heat flux estimated using a time lag of 0.8 s ( $LESr = 0.8$ ) on a day (a) with irrigation and (b) without irrigation.....	151
Figure 6.7: Diurnal variations of actual evapotranspiration derived from surface renewal using a time lag of 0.4 s ( $ETSRr = 0.4$ ), using a time lag of 0.8 s ( $ETSRr = 0.8$ ) and daily evapotranspiration derived from the crop coefficient method ( $ETKc$ ).....	152
Figure 6.8: Dependence of actual evapotranspiration derived from surface renewal ( $ETSR$ ) on (a) reference evapotranspiration ( $ETo$ ); (b) vapour pressure deficit (VPD) and (c) solar radiation ( $Rs$ ). ....	153
Figure 6.9: An example of Baseline user interface window showing (a; b; c) abnormal trend of $dTmax$ values and (d) normal trend of $dTmax$ values. ....	156
Figure 6.10: Diurnal variations of hourly sap flow ( $F$ ) determined by four TDPs and the photosynthetically active radiation (PAR) during 3 consecutive days. ....	157
Figure 6.11: Relationship between sap flow ( $F$ ) and (a) reference evapotranspiration ( $ETo$ ); (b) vapour pressure deficit (VPD) and (c) solar radiation ( $Rs$ ). ....	158
Figure 6.12: Time series for daily transpiration and irrigation during the study period.....	159
Figure 7.1: Sugarcane field at Riverside farm, Malelane. ....	165

Figure 7.2: Soil Moisture probes installed at 30 and 60 cm horizontally below the ground in the profile pit. ....	166
Figure 7.3: Surface renewal setup for measuring the sugarcane field evapotranspiration. ....	168
Figure 7.4: Calibration of the surface renewal method using the open path eddy covariance system. ....	169
Figure 7.5: Measured volumetric soil moisture content and irrigation in the sugarcane plantation. ....	171
Figure 7.6: Climate drivers of sugarcane plantation evapotranspiration showing, (a) solar radiation, (b) vapour pressure deficit and (c) reference evapotranspiration. ....	172
Figure 7.7: Validation of the surface renewal sensible heat flux calibration. ....	173
Figure 7.8: Comparison between measured evapotranspiration using surface renewal method and modelled evapotranspiration using Priestley-Taylor model. ....	174
Figure 7.9: Monthly sugarcane crop coefficients. ....	175
Figure 7.10: Modelled monthly total evapotranspiration. ....	175
Figure 8.1: Schematic representation of the DSS for water use and water use efficiency of selected subtropical crops. ....	179
Figure 8.2: Landing page of the DSS. Area bounded in red is the IUWMA. ....	181
Figure 8.3: Location of interest (a) on the landing page, and; (b) after zooming to the site of interest. The blue lines depict farm boundaries. ....	182
Figure 8.4: Input form to be populated. ....	183
Figure 8.5: Long-term monthly total water use and rainfall for a litchi orchard. ....	185
Figure 8.6: Cumulative total water use by a litchi orchard and rainfall ....	186
Figure 8.7: Two monthly irrigation requirement for a litchi orchard. ....	186

## LIST OF TABLES

Table 2.1: The 20 largest irrigated crops in the IUWMA (South African areas) in decreasing order of area (hectares) under irrigation. Analysis based on the WARMS database downloaded on 15 September 2015.....	6
Table 2.2: Types of impacts linked to climate variability in Mpumalanga (Source: DEA & GIZ, 2015a). .....	28
Table 3.1: Characteristics of the mango orchard at Riverside Farm.....	41
Table 3.2: Soil topography description data and the associated parent material. ....	44
Table 3.3: Soil profile diagnostic horizons and properties.....	44
Table 3.4: Profile information showing the physical properties of each profile's different horizon.....	44
Table 3.5: Chemical soil properties: organic carbon percentages, soil pH in KCl. electrical conductivity, exchangeable basic. KCl exchangeable acidity, extractable P.% bases saturation, exchangeable % Na, CEC and ECEC. ....	46
Table 3.6: Details of the sap flow probe installations for the mango trees. ....	53
Table 3.7: Parameter values for the dual source evapotranspiration model and optimised parameters for Allen and Pereira Model for a mature mango orchard. ....	61
Table 3.8: Summary of the monthly weather conditions at Riverside farm from August 2021 to July 2022. ....	64
Table 3.9: Mean light-saturated net CO <sub>2</sub> assimilation rate ( $A_{max}$ ), stomatal conductance ( $g_s$ ), leaf-to-air vapour pressure deficit ( $VPD_{leaf}$ ), leaf temperature ( $T_{leaf}$ ), relative humidity (RH%) and solar radiation ( $R_s$ ), spot measurements conducted throughout the study period. N is the sample size. ....	68
Table 3.10: Comparison of the daily estimated $ET_c$ by the modified S&W model and by the FAO Allen and Pereira method for the period 03 March to 03 July 2022. ....	75
Table 3.11: Summary of the monthly water use, and crop coefficients estimated using the dual-source evapotranspiration model and from the fraction of vegetation cover (A&P) method. ....	77
Table 4.1: Characteristics of the litchi orchard at Riverside farm.....	89
Table 4.2: Typical soil classification analysis for the litchi orchard used in this study. EC = Electrical conductivity; WHC = Water holding capacity.....	91
Table 4.3: Specific dates when stomatal conductance measurements were taken on the litchi trees.....	93
Table 4.4: Parameter values for the Jarvis model applied to litchi. ....	95
Table 4.5: Monthly total water use summary for the litchi orchard. ....	108

Table 4.6: Measured monthly basal crop coefficient ( $K_{cb\_measured}$ ), modelled monthly basal crop coefficient ( $K_{cb\_modelled}$ ) and minimum unstressed canopy resistance ( $\alpha$ ).....	110
Table 4.7: Typical monthly crop coefficients for a mature litchi orchard.....	114
Table 5.1: Characteristics of the grapefruit orchard at Riverside Farm.	117
Table 5.2: Summary of heat pulse sap flow monitoring equipment installed in the citrus orchard at Riverside farm.....	120
Table 5.3: Monthly crop coefficients for the grapefruit orchard .....	130
Table 5.4: Monthly summary of the water use data from the grapefruit orchard in Malelane. ....	131
Table 6.1: Summary of daily rainfall (Rain); maximum ( $T_{max}$ ), minimum ( $T_{min}$ ) air temperature; solar radiation ( $R_s$ ); grass reference evapotranspiration ( $ET_o$ ); maximum ( $RH_{max}$ ), minimum ( $RH_{min}$ ) relative humidity and wind speed ( $U$ ) at the farm recorded from 31 May to 4 July 2022.....	143
Table 7.1: Typical monthly crop coefficients, reference evapotranspiration and evapotranspiration for sugarcane plantation in Malelane, Mpumalanga.....	176
Table 8.1: Typical outputs of water use and yield variables for a litchi orchard at IUWMA.....	184

## List of Abbreviations and Acronyms

A&P	Allen and Pereira
ANOVA	Analysis of Variance
AS	Faculty of AgriSciences
AWS	Automatic Weather Station
DWS	Department of Water and Sanitation
FAO	Food and Agriculture Organization of The United Nations
FP	Florigenic Promotor
HRM	Heat Ratio Method
IUWMA	Inkomati-Usuthu Water Management Area
LAI	Leaf Area Index
NMAE	Normalized Mean Absolute Error
NRMSE	Normalized Root Mean Square Error
NSE	Nash-Sutcliffe Efficiency
OPEC	Open Path Eddy Covariance
PPFD	Photosynthetic Photon Flux Density ( $\mu\text{mol}/\text{m}^2/\text{s}$ )
$R^2$	Coefficient of Determination
RAW	Readily Available Water (mm)
RH	Relative Humidity (%)
S&W	Shuttleworth and Wallace
SPAC	Soil-Plant-Atmosphere Continuum
TAW	Total Available Soil Water (mm)
US	Stellenbosch University
V&V	Validation and Verification of Lawful Water Use
VPD	Vapour Pressure Deficit (kPa)
WAR	Water Allocation Reforms
WP	Water Productivity ( $\text{kg}/\text{m}^3$ )
WRC	Water Research Commission
WUE	Water Use Efficiency ( $\text{kg}/\text{m}^3$ or $\text{kg}/\text{kg}$ )

## List of Symbols

$\alpha$	Fraction of sunlit canopy leaf area
$A$	Net carbon dioxide (CO <sub>2</sub> ) assimilation rate ( $\mu\text{mol}/\text{m}^2/\text{s}$ )
$A_{\text{max}}$	Maximum net carbon dioxide (CO <sub>2</sub> ) assimilation rate ( $\mu\text{mol}/\text{m}^2/\text{s}$ )
$A_{\text{area}}$	Surface area ( $\text{m}^2$ )
$b_1$	Minimum soil surface resistance (s/m)
$b_2$	Curvature of the soil water stress factor ( – )
$C_a$	Partial pressure of CO <sub>2</sub> (Pa) in ambient air
$C_i$	Internal CO <sub>2</sub> concentration ( $\mu\text{mol}/\text{mol}$ )
$C_p$	Specific heat capacity of air (J/kg/K)
$C_s$	Specific heat capacity of the sap (J/kg/°C)
$C_w$	Specific heat capacity of the wood matrix (J/kg/°C)
$d$	Zero plane displacement (m)
$E_{c \text{ max}}$	Maximum canopy transpiration (mm/d)
$E_{\text{so}}$	Potential evaporation from wet soil surface (mm/d)
$E_{\text{soil}}$	Evaporation from the orchard floor (mm/d)
$ET_c$	Crop evapotranspiration (mm/d)
$ET_o$	Reference evapotranspiration (mm/d)
$f_{\text{ceff}}$	Effective fraction of ground shaded near solar noon
$Fr$	Adjustment factor relative to stomatal control
$f_w$	Fraction of the orchard floor that is wetted by irrigation
$G$	Ground heat flux ( $\text{W}/\text{m}^2$ )
$g_a$	Aerodynamic conductance (m/s)
$g_c$	Canopy conductance (m/s)
$g_{\text{max}}$	Maximum stomatal conductance (m/s)
$g_s$	Stomatal conductance (m/s)
$h$	Plant height during the midseason period (m)
$U$	Sap flux density ( $\text{kg}/\text{m}^2/\text{s}$ )
$J_{\text{max}}$	Electron transport rate ( $\mu\text{mol}/\text{m}^2/\text{s}$ )
$k$	Hydraulic conductance ( $\text{mmol}/\text{m}^2/\text{s}/\text{MPa}$ )
$k$	von Karman's constant
$K_c$	Crop coefficient
$K_{c \text{ max}}$	Maximum crop coefficient
$K_{c \text{ min}}$	Minimum crop coefficient
$K_{cb}$	Basal crop coefficient

$K_{cb\ cover}$	Basal crop coefficient of understorey vegetation
$K_{cb\ full}$	Basal crop coefficients for fully grown orchard
$K_d$	Canopy density coefficient
$K_{e\ dry}$	Dry soil evaporation coefficient
$K_{e\ wet}$	Wet soil evaporation coefficient
$k_r$	Parameter for solar radiation stress factor (W/m)
$K_{soil}$	Soil water evaporation coefficient
$K_{vpd}$	Vapour pressure deficit stress factor (kPa)
$k_w$	Thermal diffusivity of green (fresh) wood ( $cm^2/s$ )
$M_L$	Parameter that simulates the physical limits imposed on water flux
$p$	The average fraction of total available soil water
$P_a$	Atmospheric pressure (Pa)
$R$	Solar irradiance
$r_b$	Boundary layer resistance (s/m)
$R_d$	Mitochondrial respiration rate ( $\mu mol/m^2/s$ )
$r_l$	Mean leaf resistance (s/m)
$R_n$	Net radiation ( $W/m^2$ or $MJ/m^2/day$ )
$R_{so}$	Solar radiation under clear sky conditions ( $MJ/m^2/day$ )
$T_{air}$	Air temperature at 2 m height ( $^{\circ}C$ )
$T_{leaf}$	Leaf surface temperature ( $^{\circ}C$ )
$T_{max}$	Maximum air temperature ( $^{\circ}C$ )
$T_{min}$	Minimum temperature ( $^{\circ}C$ )
$T_{opt}$	Optimal temperature for tree growth ( $^{\circ}C$ )
$t_w$	Average time between independent wetting events (days)
$u_2$	Wind speed at 2 m height (m/s)
$v_1$	Increase in temperature of upper thermocouple ( $^{\circ}C$ )
$v_2$	Increase in temperature of the lower thermocouple ( $^{\circ}C$ )
$V_c$	Corrected heat pulse velocity (cm/h)
$V_h$	Heat pulse velocity (cm/h)
$VPD_{leaf}$	Leaf-air vapour pressure deficit (kPa)
$V_s$	Sap velocity (cm/h)
$z_o$	Roughness length (m)
$Z_r$	Soil sample depth (m)
$\gamma$	Psychrometric constant (kPa/K)
$\Delta$	Slope of the saturation vapour pressure vs air temperature curve (kPa/K)
$\theta$	Volumetric soil water content ( $cm^3/cm^3$ )

$\theta_{FC}$	Volumetric soil water content at field capacity ( $\text{cm}^3/\text{cm}^3$ )
$\theta_{PWP}$	Volumetric soil water content at wilting point ( $\text{cm}^3/\text{cm}^3$ )
$\lambda$	Latent heat of vaporization (J/kg)
$\rho_a$	Density of dry air ( $\text{kg}/\text{m}^3$ )
$\rho_b$	Density of wood or soil ( $\text{g}/\text{cm}^3$ )
$\rho_w$	Density of water ( $\text{kg}/\text{m}^3$ )
$\Psi_{\text{leaf}}$	Leaf water potential (MPa)
$\Psi_{\text{soil}}$	Soil water potential (MPa)

This page was intentionally left blank

## CHAPTER 1: GENERAL INTRODUCTION

### 1.1. Research Background

Key economic activities in the Inkomati-Usuthu Water Management Area (IUWMA), e.g. agriculture, forestry, mining, and eco-tourism are inextricably tied to the health of the catchment's river systems (Simpson *et al.*, 2019). Yet in most parts of the catchment the demand for water already exceeds supply. The situation is likely to worsen in future as competition for the limited resources heightens. Threats to the catchment's water supply arise from several factors. These include the growing population, the increasing frequency and severity of droughts due to climate change (Maponya *et al.*, 2013; Singels and Jones, 2018), invasive alien plants that consume large quantities of water, and the degradation of water quality mostly by mining and agricultural return flows (Rogers and Luton, 2016). There is need for accurate information and tools for the effective, efficient, and sustainable management of water resources and to assist with the implementation of the Catchment's Water Management Strategy.

The IUWMA (Fig. 1.1) has a proactive approach to water management aimed at implementing the provisions of the National Water Act, Act 36 of 1998. For example, following the recent completion of the Validation and Verification of Lawful Water Use in the catchment, there are plans to implement Water Allocation Reforms (WAR) in the entire catchment. The aim of the reforms is to address water access issues, especially over-allocation issues to promote equitable and sustainable use of the resource. Historically, some users have had access to large amounts of water while others do not. This reduces the contribution of the latter group to job creation, poverty reduction, and to the development of the economy of the province. Currently, the catchment is using state-of-the-art water management technologies such as the HydroNet ([www.hydronet.co.za](http://www.hydronet.co.za)) platform. This platform enhances the catchment's capability to better manage its water resources combining remote sensing information and user defined inputs to make decisions. However, for accurate and reliable assessments there is need for local validation, especially of the remote sensing based eLeaf product used by HydroNet to estimate crop water use with actual measurements (Jarmain *et al.*, 2009; Dzikiti *et al.*, 2018a).

The Water Research Commission (WRC), in collaboration with various grower associations, has over the years initiated and funded research to quantify the water use of selected irrigated crops in the IUWMA. These studies, aimed to generate critical baseline information to improve irrigation scheduling and for water allocation planning. Crops

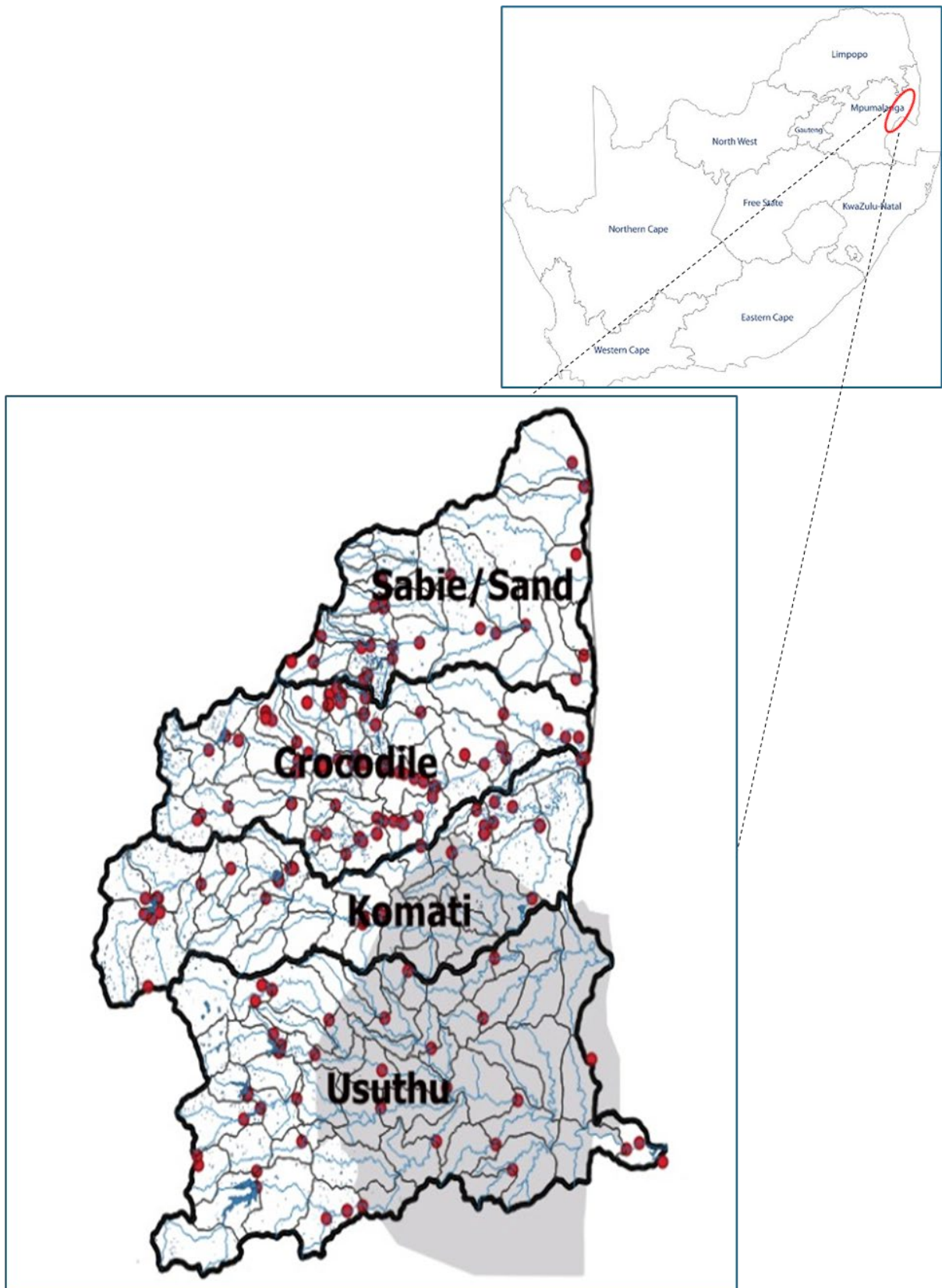


Figure 1.1: Map of catchments in the Mpumalanga province showing the Inkomati-Usuthu catchments.

investigated include citrus and macadamia nuts (Gush and Taylor, 2014; Ibraimo *et al.*, 2014), maize and sugarcane (Olivier and Singels, 2003; Jarman *et al.*, 2014), avocado and macadamia (Taylor and Clulow, 2022). The goals of some of the studies were to identify and quantify factors that affect orchard water use such as orchard age group (through canopy cover variations), cultivar, soils, microclimate, irrigation method, etc.

Despite these efforts, there are still many important crops with significant irrigation allocations whose water requirements are not known. Examples include mango, banana, litchis, pecan nuts, tobacco, cotton, tea, etc. While water use data has been collected in citrus orchards in IUWMA, this is grown over a range of microclimatic conditions and soils (Gush and Taylor, 2014; Taylor and Vahrmeijer, 2018). More data is therefore still needed to better understand the water requirements of some citrus cultivars and to improve irrigation efficiencies. Given that farmers tend to over-irrigate when they do not have access to reliable water use data and tools, (Volschenk *et al.*, 2003) there is need to update the database of actual measured crop water use in the catchment. These data can be used for several purposes. Firstly, crop coefficients can be derived for irrigation scheduling, irrigation system designs, and for water allocation planning. Secondly, water use estimating tools, e.g. eLeaf currently in use in the IUWMA can be validated with these data. Thirdly, new decision support systems (DSS) can be developed to complement existing ones using these (and historical) data to improve the accuracy of crop water use estimates. This is the intention of the present study.

The current research sought to address the following questions:

- 1) How do the water use patterns of irrigated mango, litchi, banana, and grapefruit vary in the IUWMA? What are the maximum unstressed water use levels?
- 2) What are the key drivers of water use and how do these affect yield?
- 3) How does the water productivity (kg of fruit per m<sup>3</sup> of water consumed) of these crops vary within the IUWMA?
- 4) Is it possible to improve the accuracy of crop water use estimates using DSS that uses readily available input data?
- 5) Can such a DSS assist with compliance monitoring and enforcement activities being planned in IUWMA?

To answer these questions, this study firstly collected detailed data from irrigated crops (mango, banana, grapefruit, litchi, and sugarcane) whose water use is either not known or it is very sketchy thereby filling an important information gap. The IUWMA has highly variable climatic and soil conditions, because of its varied topography. This exacerbates the field-to-

field variations in water use even for the same crop type. For this reason, strategically important irrigated crops with substantial irrigation allocation, e.g. citrus and sugarcane will be included focusing on microclimatic, soils, irrigation, and cultivar differences. It is our expectation that the DSS will be more accurate than the existing tools currently being used in the catchment given that it is based on actual measured data thus adding another tool to the IUWMA toolbox.

## **1.2. Aims and Objectives**

According to the project terms of reference, the aim of this study was to determine the water use, yield and quality of banana, mango, litchis, sugarcane, and citrus from planting to full-bearing age in selected climatic zones and specific soils. However, given the highly quantitative approach adopted in this study involving intensive measurements of the soil-plant-atmosphere interactions, data were collected from mature high yielding orchards under optimal management. The effect of canopy size from planting to full-bearing age were inferred through water use modelling. An important advantage of using modelling is that it provides a tool that allows the extrapolation of the study results to other orchards outside the study area.

Specific objectives of the study were to

- i) Expand the current database of crop water use data in the WMA to include selected key irrigated crops namely banana, mango, litchi, sugarcane, and citrus.
- ii) Use the measured data and that collected in previous studies to develop a Decision Support System (DSS) for estimating water use efficiency of, and water allocation to crops in the IUWMA.

## CHAPTER 2: KNOWLEDGE REVIEW

### 2.1. Major Irrigated Crops Grown in the IUWMA

Irrigated agriculture constitutes one of the main drivers of the economy in IUWMA. The agricultural sector contributes about 14.9% of the Gross Geographic Product (GGP) of the CMA, which was estimated at around R 9 billion per annum in 2012 (DWA, 2012). Agricultural production is highly dependent on irrigation, using around 33% of the allocated available water (IUWMA, 2018). The IUWMA is (apart from catchment areas situated in Eswatini) situated entirely within Mpumalanga Province, covering most of Ehlanzeni District Municipality (DM), the eastern regions of Gert Sibande DM, and a small eastern portion of the Nkangala DM (Fig. 1.1). The present study focused on one irrigated field crop (sugarcane) and the most prevalent irrigated subtropical fruit crops in the IUWMA namely citrus, banana, litchi, and grapefruit. Details on macadamia and avocado production can be found in Taylor *et al.* (2021a, b).

The diverse topography, climate, and soils of the IUWMA creates excellent production potential for a wide range of crops. The Lowveld region is particularly well suited to sugarcane, bananas, citrus, and other sub-tropical fruit crops, as well as tree nut species. In the hot Lowveld with a distinct dry season, crop yields and profitability are ensured through irrigation. Other major irrigated crops include maize, tomatoes, cotton, tea, tobacco, potatoes, summer and winter vegetable crops, and cut flowers; these are mainly grown in the cooler Highveld. Table 2.1 presents the 20 crop types with the highest irrigated area within the IUWMA (South Africa only), as captured by the WARMS database in September 2015. Sugarcane (mainly Komati and Crocodile River catchments), bananas (mainly the Sabie/Sand River catchment) and maize (Komati, Crocodile, Usuthu River catchments) together account for around 47% of the total area under irrigation. Cash crops, tomatoes, potatoes, vegetables, and soybeans together cover around 28% of the total irrigated area. Tree fruit and nut crops are grown intensively, requiring less area compared to the aforementioned crops, and account for around 10% of the total irrigated area. The top 20 irrigated crops together cover 85% of the total area for all irrigated crops (Table 2.1).

Table 2.1: The 20 largest irrigated crops in the IUWMA (South African areas) in decreasing order of area (hectares) under irrigation. Analysis based on the WARMS database downloaded on 15 September 2015.

No.	Crop	Hectares irrigated	% ha irrigated relative to all irrigated crops	% ha irrigated relative to top 20 crops	Tertiary catchments	Name of secondary catchment
1	Sugarcane	20,719	21.5	25.3	W51, X13, X14 X21, X22, X23, X24 X31	Usuthu Komati Crocodile Sabie/Sand
2	Bananas	13,393	13.9	16.4	X11, X13, X14 X22, X23, X24 X31, X32	Komati Crocodile Sabie/Sand
3	Maize	10,800	11.2	13.2	W51, W52, W53, W54 W55 X11, X12, X13, X14 X21, X22, X23, X24 X31, X32	Usuthu Komati Crocodile Sabie/Sand
4	Tomatoes	6,575	6.8	8.0	W51 X11, X12, X13 X22 X31	Usuthu Komati Crocodile Sabie/Sand
5	Cotton	6,227	6.5	7.6	X11, X12 X22	Komati Crocodile
6	Vegetables – summer	4,024	4.2	4.9	W51, W52, W53, W55, W56 X11, X12, X13, X14 X21, X22, X23, X24 X31, X32	Usuthu Komati Crocodile Sabie/Sand
7	Tea	4,000	4.2	4.9	X12	Komati
8	Macadamia nuts	2,887	3.0	3.5	X12 X21, X22, X23 X31	Komati Crocodile Sabie/Sand
9	Avocados	2,850	3.0	3.5	X11, X12 X21, X22 X31	Komati Crocodile Sabie/Sand
10	Potatoes	2,060	2.1	2.5	W51, W53, W55 X11, X12 X21, X22, X23 X31	Usuthu Komati Crocodile Sabie/Sand
11	Citrus	1,517	1.6	1.9	X11, X12, X13, X14 X21, X22, X23, X24 X31, X32	Komati Crocodile Sabie/Sand
12	Vegetables – winter	1,261	1.3	1.5	W51, W52, W53, W55, W56 X11 X22, X24 X31	Usuthu Komati Crocodile Sabie/Sand
13	Tobacco	1,134	1.2	1.4	X11 X21, X22, X23 X31	Komati Crocodile Sabie/Sand
14	Mangoes	980	1.0	1.2	X11, X13, X14 X22, X23, X24 X31, X32	Komati Crocodile Sabie/Sand
15	Beans	961	1.0	1.2	W55 X11, X12, X13 X21, X22 X31	Usuthu Komati Crocodile Sabie/Sand
16	Soya beans	786	0.8	1.0	W54, W55 X11, X12 X21	Usuthu Komati Crocodile
17	Pecan nuts	622	0.6	0.8	W51 X21, X22, X23 X31	Usuthu Crocodile Sabie/Sand
18	Litchies	374	0.4	0.5	X14 X22, X24 X31	Komati Crocodile Sabie/Sand
19	Guavas	324	0.3	0.4	X11 X21, X22	Komati Crocodile
20	Cut flowers	300	0.3	0.4	X11 X22 X31	Komati Crocodile Sabie/Sand

## **2.2. The Sub-Tropical Fruit and Sugarcane Industries**

Data collection in this study focused mostly on subtropical fruit tree crops (i.e. mango, litchi, banana, grapefruit) and sugarcane. For this reason, we will provide a summary of the extent of each industry in the IUWMA in the sections that follow.

### **2.2.1. Banana Industry**

#### **2.2.1.1. Extent of the banana industry in the IUWMA**

Bananas are grown under sub-tropical climatic conditions in South Africa although they are a tropical crop and are thus severely limited by climate and only suited to specific areas of the country (Lagerwall, undated). The largest production area in Mpumalanga is around Onderberg near Malelane, with around 36% of the national area under production (in 2010), followed by Kiepersol near Hazyview, with around 22% of the area under production (DAFF, 2011; Fig. 2.1). Thus, approximately 58% of the total land under banana cultivation was in the IUWMA in 2010. As reported above, banana production in the IUWMA in 2017 was around 147 000 tons. But this was a drought year, so current production levels are likely to be higher.

Total banana production in South Africa (DAFF, 2019) has not grown over the past 10 years (Fig. 2.2). There are many reasons for this, including growing competition from producers in other countries with more optimal climatic conditions and other favourable factors of production (e.g. land, labour; notably Mozambique). Other factors constraining the growth of the industry are disease pressure, drought, and water stress (the impact of the 2016-2017 drought is clearly seen in Fig. 2.2), no further availability of land suitable for banana production, and no further availability of water resources for irrigation.

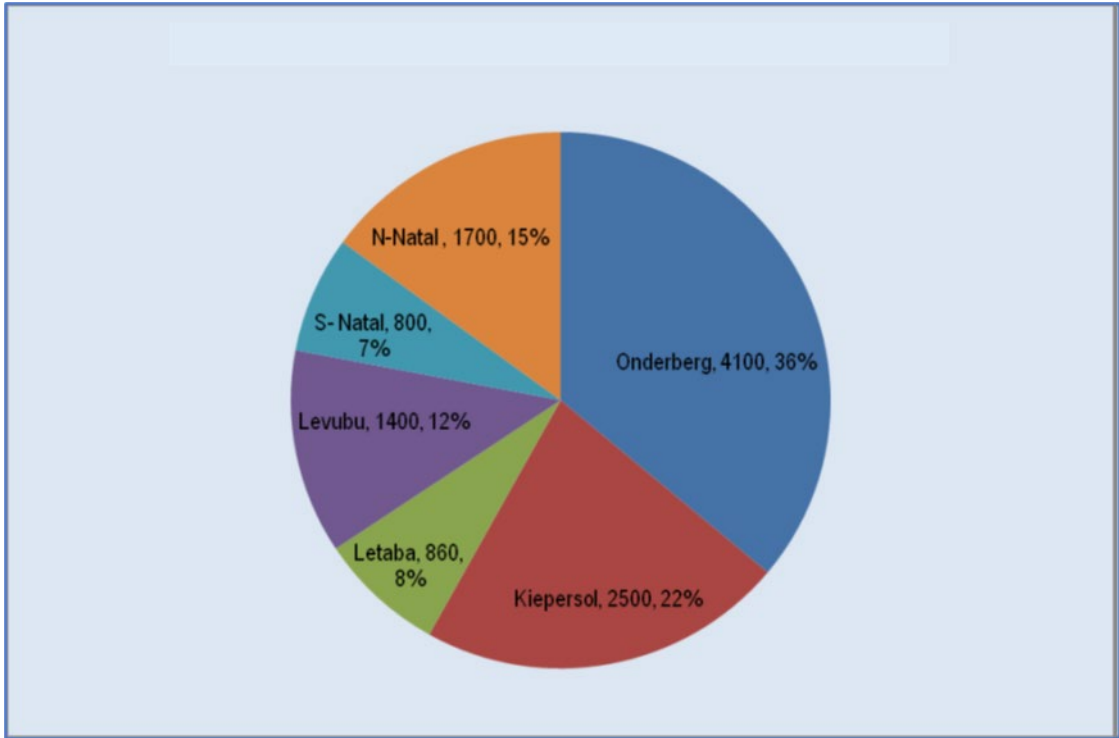


Figure 2.1: Banana production areas (ha) in South Africa in 2010. (Source: DAFF, 2011).

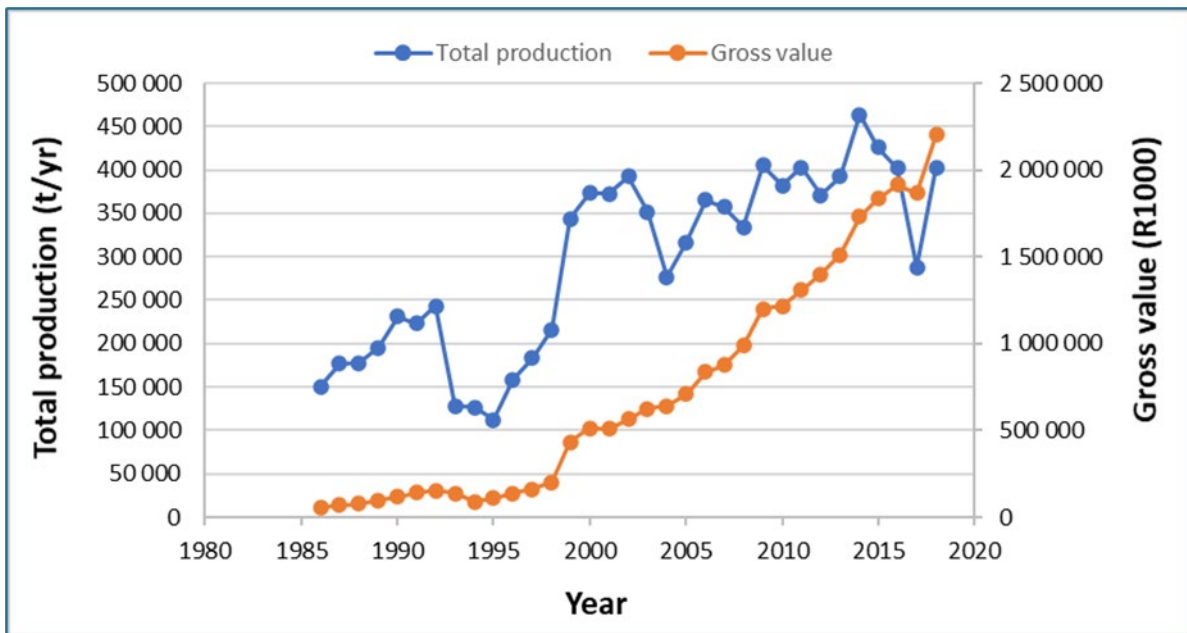


Figure 2.2: Total production and gross value of bananas in South Africa from 1985/86 until 2017/18 (Source of data: DAFF, 2019).

### 2.2.1.2. Irrigation types and irrigation scheduling in banana orchards

Water management for irrigated bananas under conditions of water scarcity has three major challenges, namely (i) minimising water losses, (ii) increasing the yield, and (iii) increasing the water productivity (Panigrahi *et al.*, 2021). The choice of irrigation system and scheduling must satisfy all three, whilst also factoring in other important agronomic considerations. Drip irrigation has been reported to be the most efficient with 95% application efficiency over other methods compared to micro irrigation (85%) and overhead sprinklers (60%) (Panigrahi *et al.*, 2021). The *centre pivot system* currently waters 74.3% of irrigated banana plantations in the IUWMA. This system is suitable for use over large areas (generally linked to large irrigation schemes) and is used on more than 10000 ha around the Komati River before it enters Mozambique. In this system, water losses to evaporation are higher than for drip and micro sprinkler systems. *Sprinkler systems* (dragline, hop-along, quick-coupling) make up 4.7% of irrigated area, spread across the main production areas. Only 18 ha (0.1% of irrigated area) is under flood irrigation (basin or furrow), and used only in Bushbuckridge (WARMS, 2015).

The high water-use efficiency under-tree micro sprinkler system or the drip irrigation system make them the best options for most situations. Drip irrigation conserves precious water resources since evaporation is significantly reduced. However, only 3.8% (507 ha) of current area under banana in the IUWMA uses drip irrigation. Drip is used around the Komati/Lomati Rivers (Onderberg area) and northern Bushbuckridge (WARMS, 2015). Banana growers sometimes use inexpensive disposable drip lines for the first 6 months after planting, which allows for targeted application to small plants rather than wasting scarce water resources on areas without roots initially. This system also minimises the need for weed control. The drawback of a drip system is that it cannot be used to create a spray to cool the plant down on very hot days. It can also lead to restricted root growth because of the limited volume of soil wetted compared to the micro sprinklers. If drip irrigation is applied under conditions of high evaporation, low rainfall and salt in the irrigation water, accumulation of salts at the boundary of wet and dry soil areas can occur to which banana plants are highly sensitive. Leaching then must be undertaken to avoid damage (FAO, 2020a).

Micro sprinkler systems are used in 17.1% (2 284 ha) of the current irrigated banana area, mainly around Kiepersol (WARMS, 2015). If drip irrigation is used for the first few months, this can be replaced with micro sprinklers as plants and their root systems become larger. Shelfhout (2013) recommended micro-jets delivering 3 to 4 mm/hour and not exceeding

7-8 mm/day gross application even in hot dry conditions, because banana plants cannot absorb and transpire water under very high evaporation rates. They will wilt temporarily regardless of irrigation above this threshold but can recover overnight with optimal irrigation. Irrigation of bananas best follows the strategy of "little and often" (ARC, 2008) owing to the shallow root system. Robinson and Alberts (1989) reported that approximately 40% of the total water loss in bananas in the Levubu region (Limpopo Province) was from the upper 100 mm of soil and 80% from the upper 300 mm, indicating a shallow extraction pattern for banana roots. The interval between irrigation has a pronounced effect on yields, with higher yields being achieved when intervals are kept short (FAO, 2020a). The optimal irrigation interval will depend on evaporative demand and the soil water holding capacity in the rooting depth. Under high evaporative conditions this will be up to three days. DAFF (2003) recommended an application of 20 mm of water every 3 days in summer and every 8 days in winter, for heavy loamy soils in South Africa. Crop coefficients can be used for banana irrigation scheduling (Allen *et al.*, 1998; FAO, 2020a).

The range of reported water productivity (sometimes still termed water use efficiency, WUE) of banana production is high. Research globally has estimated WUE at between 0.9 and 7.4 kg/m<sup>3</sup> (Panigrahi *et al.*, 2021) depending on climate, soil and irrigation system. FAO (2020a) give the general range at 2.5 to 4 kg/m<sup>3</sup> for the plant crop and 3.5 to 6 kg/m<sup>3</sup> for ratoon crops. This is based on an expected yield of 40-60 t/ha. WUE can be increased through soil management (to improve soil water holding capacity in the root zone) and irrigation practices that match water application rates to water crop demand, crop physiology, and soil capacity (Panigrahi *et al.*, 2021).

### **2.2.1.3. Water related challenges and priorities for the banana industry**

Increasing rainfall variability (possibly related to climate change, see section 4) and increasing competition for water resources in the IUWMA constrain the banana industry in this region, with little opportunity for expansion of plantations. Thus, the focus is on water-saving irrigation systems (minimising evaporative water losses and wetting of soil without banana roots), and irrigation scheduling to reduce drainage and runoff losses, and production technologies, thereby increasing the water productivity. The quality of surface water resources in certain parts of the IUWMA is a cause for great concern, according to the South African Mine Water Atlas (WRC, 2017). This report states that within the IUWMA, of the 61% of the quaternary catchments assessed, 24% of the catchment area includes stressed surface water resources that are under threat, 3% that require the precautionary approach to management

to maintain good condition, and 73% where the surface water resources do have capacity available to accept degrees of impact. The Komati sub-catchment, which has extensive irrigated banana plantations, is a catchment of particular concern (WRC, 2017), notably quaternary catchment X13K which has large areas of banana under centre pivot irrigation (WARMS, 2015), X14G (Lomati sub-catchment) and X23H (Crocodile sub-catchment). These QCs are classified as having a high threat.

## **2.2.2. Mango Industry**

### **2.2.2.1. Extent of the mango industry in the IUWMA**

The introduction of Florida (USA) cultivars has led to considerable growth in the local mango industry, which is approximately 50 years old. A 1995 tree census counted approximately 8 000 hectares comprising 3 million trees and total industry production of around 40 000 tonnes (Finnemore, 2000). Over the past 35 years the industry has grown significantly with total production of mangos for the 2018/2019 season reaching 93 869 tonnes. Of this total, 6 039 tonnes (6%) went to export markets, 5 956 tonnes (6%) to direct sales, 29 622 tonnes (32%) to national fresh produce markets, 15 547 tonnes (17%) went for juicing, 26 800 tonnes (29%) to achar, and the remaining 9 906 tonnes (11%) for drying ([www.mango.co.za](http://www.mango.co.za)). A 2020 tree census (Fig. 2.3) counted total plantings of 5 252 hectares of mango with Hoedspruit (44% – 2 325 ha), Letaba (1 128 ha – 22%) and Onderberg (785 ha – 15%) as the main production area (Subtrop, 2020). Despite the decrease in plantings over the time, total production has increased which is indicative of improved management and production practices. Other reasons for decrease in the area under mangoes are that growers have removed mangoes and planted different crops such as macadamias, avocados, and soft citrus. And very importantly, most growers top work old trees to new cultivars rather than plant new orchards, resulting in industry size remaining unchanged (Subtrop, 2020).

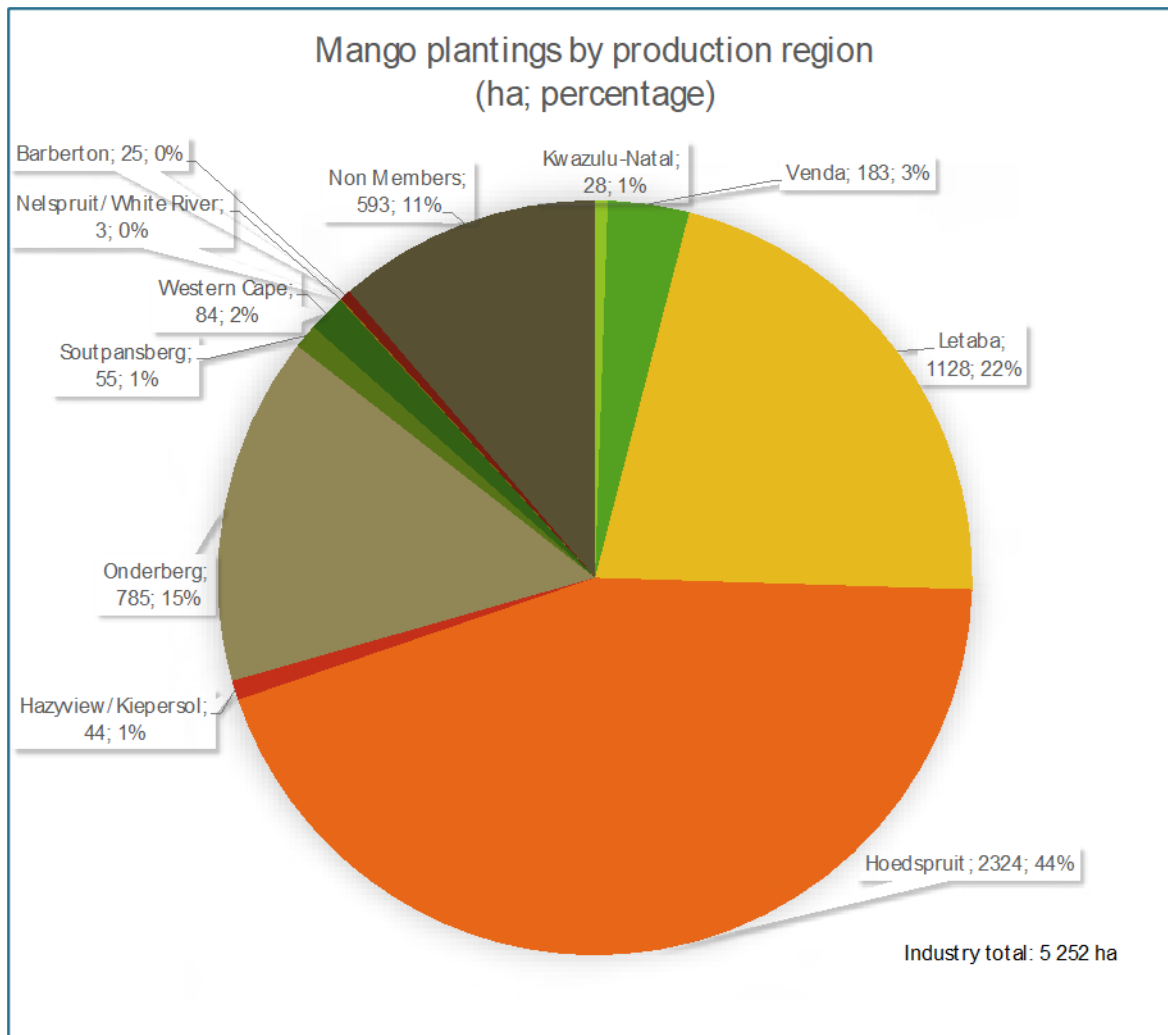


Figure 2.3: Mango plantings by production area (Subtrop, 2020)

### 2.2.2.2. Irrigation types and irrigation scheduling in mango orchards

The South African guideline for annual water use by a mature mango orchard range between 8 000 and 10 000 m<sup>3</sup>/ha (70% tree canopy coverage). Different areas and soil types will have an impact on the amount of water required. Daily water need also varies during the year with requirements of 20 m<sup>3</sup>/ha/month during winter and up to 44 m<sup>3</sup>/ha/month during summer months. Planting density will also have an impact on water need and use and the above values have been calculated at a planting density of 500 trees/ha (Botha, 2019). Predominantly drip and micro irrigation are used as the delivery options to mango orchards. Lack of water coupled with high energy and nitrogen costs in South Africa are necessitating the use of tools for more efficient water use. Irrigation scheduling is based on soil water measurement, which measures soil water directly to determine irrigation requirements, or a

soil water balance calculation where soil moisture status is estimated by calculating inputs (irrigation and precipitation) vs outputs (evaporation and run-off). The use of other measurements such as stomatal conductance, stem water potential, sap flow, and stem diameter variations have been investigated with varying degrees of success. Scheduling of irrigation according to the measurement of soil water availability in the different root zones appears to have had the most success in terms of mango production levels (Botha, 2019).

### **2.2.2.3. Water related challenges and priorities for the mango industry**

Mango is relatively resistant to drought conditions; however, fruit growth and development are severely inhibited by lack of sufficient water. For this reason, proper management of water during dry periods coinciding with fruit development is very important (Botha, 2019). During the first 42 days water supply is critical and drought during this phase leads to fruit dropping and reduced fruit mass (Botha, 2019). The cultivation of mangoes take place in tropical and sub-tropical areas throughout the world, as well as in some semi-arid regions. However, specific crop coefficients and fertiliser input needs for local conditions are still lacking (Levin *et al.*, 2018).

## **2.2.3. Litchi Industry**

### **2.2.3.1. Extent of the litchi industry in the IUWMA**

Litchi production in South Africa is still a relatively new industry when compared to China, for example (Begemann, 2014). The total plantings of litchi in 2012 was 1 731 hectares consisting of 344 500 trees with a total industry production of approximately 4 500 tonnes (Begemann, 2014). A 2020 tree census counted 1 549 ha of litchi plantings and coupled with total production of 4 434 tonnes litchis for the 2018/2019 season indicates that there has been no real measurable growth in this industry. Of this 4 434 tonnes total, 2 764 (62%) went to export markets, 546 tonnes (12%) direct sales, 93 tonnes (2%) bakkie sales, 1 302 tonnes (29%) to national fresh produce markets, and the remaining 368 tonnes (8%) went for processing ([www.litchisa.co.za](http://www.litchisa.co.za)). Mpumalanga represents 67% of the SA industry (1 034 ha) with Onderberg (Mpumalanga) as the largest production region in SA with 59% (907 ha) of total plantings. Limpopo contains 28% (441 ha) of plantings of which 23% (363 ha) are situated in Letaba. KwaZulu-Natal makes up 5% of the industry (73 ha) (Fig. 2.4) (Subtrop, 2020).

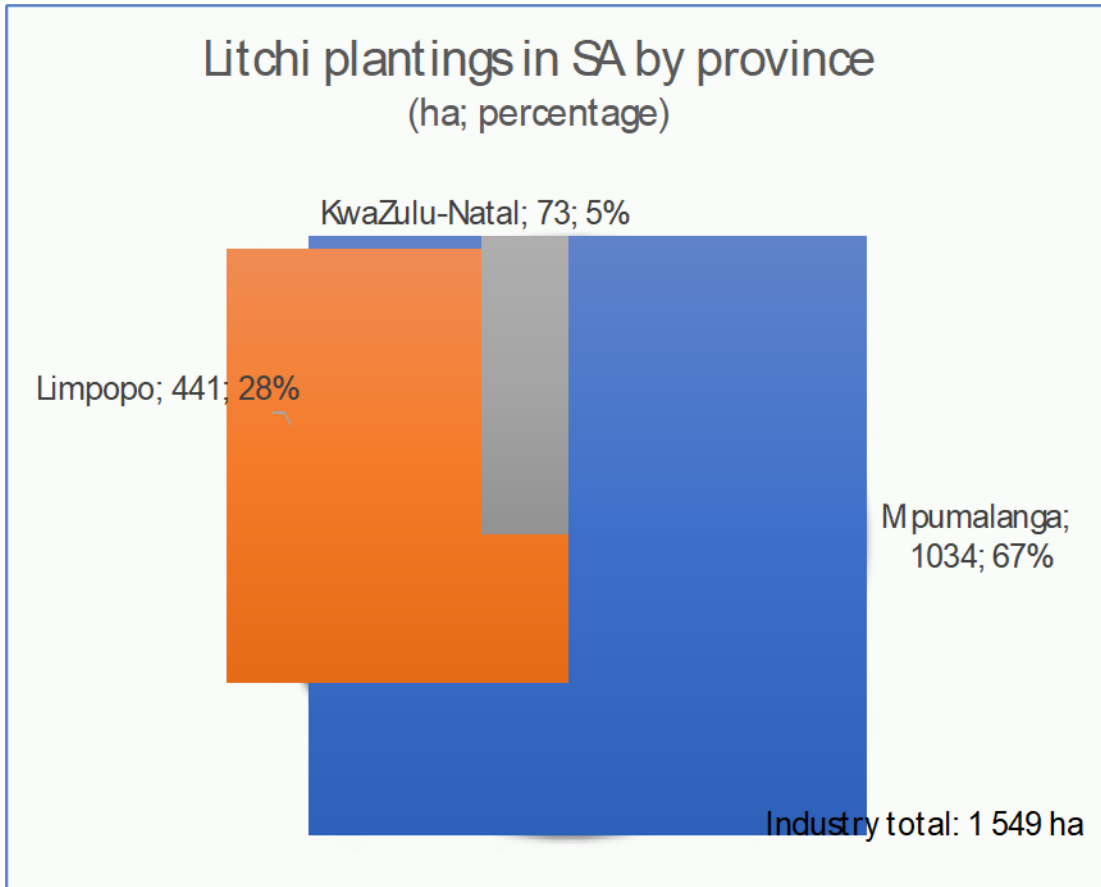


Figure 2.4: Litchi plantings by production area (Subtrop, 2020).

### 2.2.3.2. Irrigation types and irrigation scheduling in litchi orchards

The annual estimated water requirement for litchi trees in South Africa ranges between 9 000 and 11 000 m<sup>3</sup>/ha/annum for a mature orchard (70% of area covered by canopy). Daily water requirements vary during the year with monthly requirements ranging from 10 m<sup>3</sup>/ha in May to approximately 50 m<sup>3</sup>/ha in December. As for all crops, planting density has an impact on orchard water requirements and the above values have been calculated at a planting density of 167 trees/ha (Mostert, 2014). By 2014, less than 5% of litchi trees in South Africa were under dryland production conditions, approximately 80% are micro-irrigated and only around 10% were drip irrigated (Mostert, 2014). However, it has been pointed out that the litchi industry is in need of optimising its orchard practices (Begemann, 2014). Drip irrigation is considered the best system in terms of water, fertiliser, and labour input (Mostert, 2014). Irrigation scheduling is based on either soil matrix potential, measured using tensiometers, or soil water content, measured using capacitance probes (Mostert, 2014).

### **2.2.3.3. Water related challenges and priorities for the litchi industry**

Litchi trees are limited in their ability to withstand drought and heat stress in non-sub-tropical growing regions and therefore require optimal irrigation (Mostert, 2014). The most critical periods for water management of litchis is during; 1) postharvest to generate new flush as soon as possible after harvest, 2) time between flower induction and flower differentiation as water stress can enhance flower development, 3) time of flowering and fruit growth when adequate water supply is important for fruit set and size (Mostert, 2014). The total annual water requirements of orchards is the sum of effective rainfall together with irrigation. The contribution of rainfall should never be considered to be more than 40% effective, which implies that of 1000 mm rain, only 400 mm or 4 000 m<sup>3</sup>/ha can be taken into account (Mostert, 2014). The balance of water needs are then to be provided by irrigation, often in an already water scarce environment.

### **2.2.4. Sugarcane Industry**

#### **2.2.4.1. Extent of the sugarcane industry in the IUWMA**

Sugarcane can be grown in tropical and sub-tropical climates with a long, warm growing season, a high incidence of solar radiation, and adequate moisture, followed by a dry, sunny and fairly cool but frost-free ripening and harvesting period (FAO, 2020b). In South Africa, the crop is spread across two provinces, KwaZulu-Natal and Mpumalanga. Approximately 75% of the area of sugarcane plantations in the country is dryland and 25% is irrigated (SASA). Irrigation is found predominantly in Mpumalanga and northern KwaZulu-Natal, with the northern irrigated production areas including Pongola (northern KZN), and Malelane/Komati in the IUWMA (Mpumalanga Lowveld) (Fig. 2.5).

Sugarcane production (tons per annum) rose to a peak in 2001 and has since decreased by around 22% (Fig. 2.6). However, the gross value of the crop has continued to increase quite sharply since around 2009 due to a steep rise in the producer price. The reasons for the decline in production are varied but include the high variability of rainfall, with droughts in 1993-1995, 2010-2011, and 2014-2016. Rainfall has been very low in most of the production regions since November 2014 (SASA, 2020). The droughts affected both dryland production and irrigated production owing to water restrictions (Singels *et al.*, 2019).

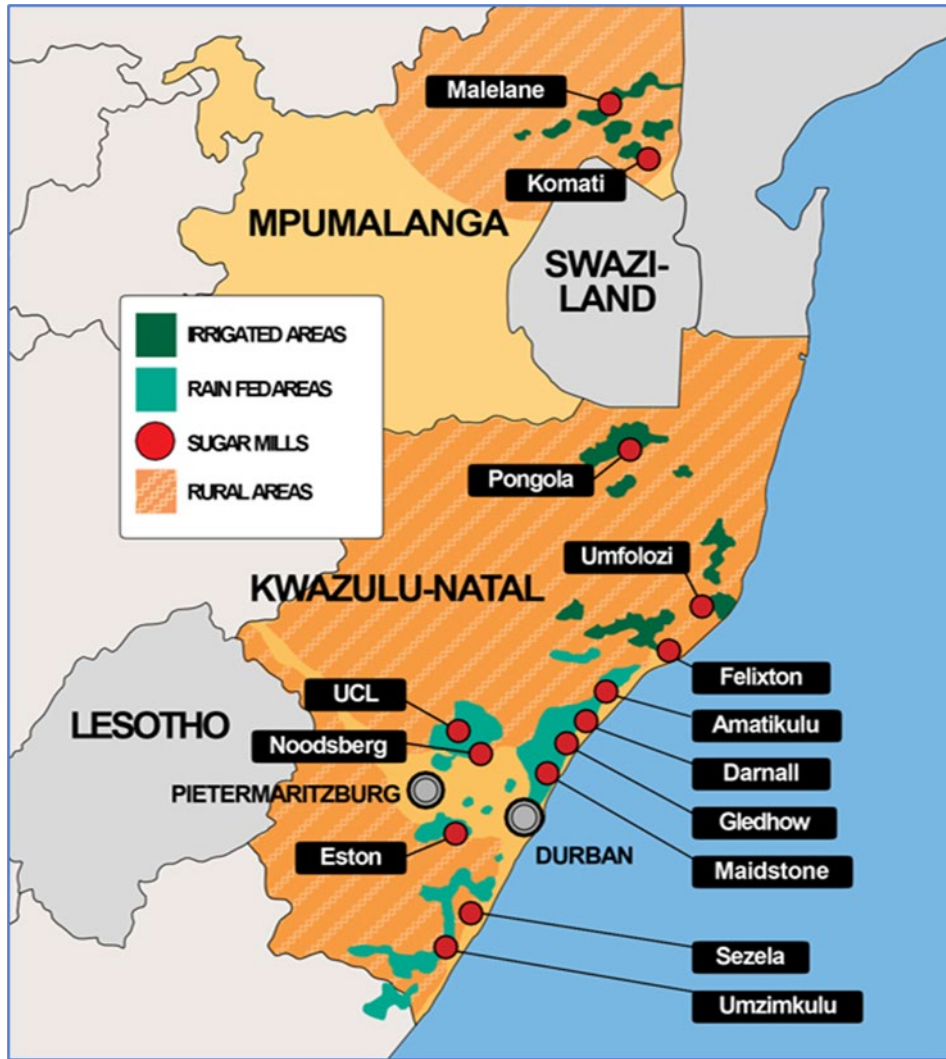


Figure 2.5: Map of sugarcane production areas of South Africa. Source: <https://sasa.org.za/the-sugar-industry-at-a-glance/>

Water restrictions reduced production in 2016/17 and 2017/18 with a recovery seen in 2018/19. In this year, the estimated production for Malelane and Komati comprised approximately 4 million tons, or 20.8% of the national figure.

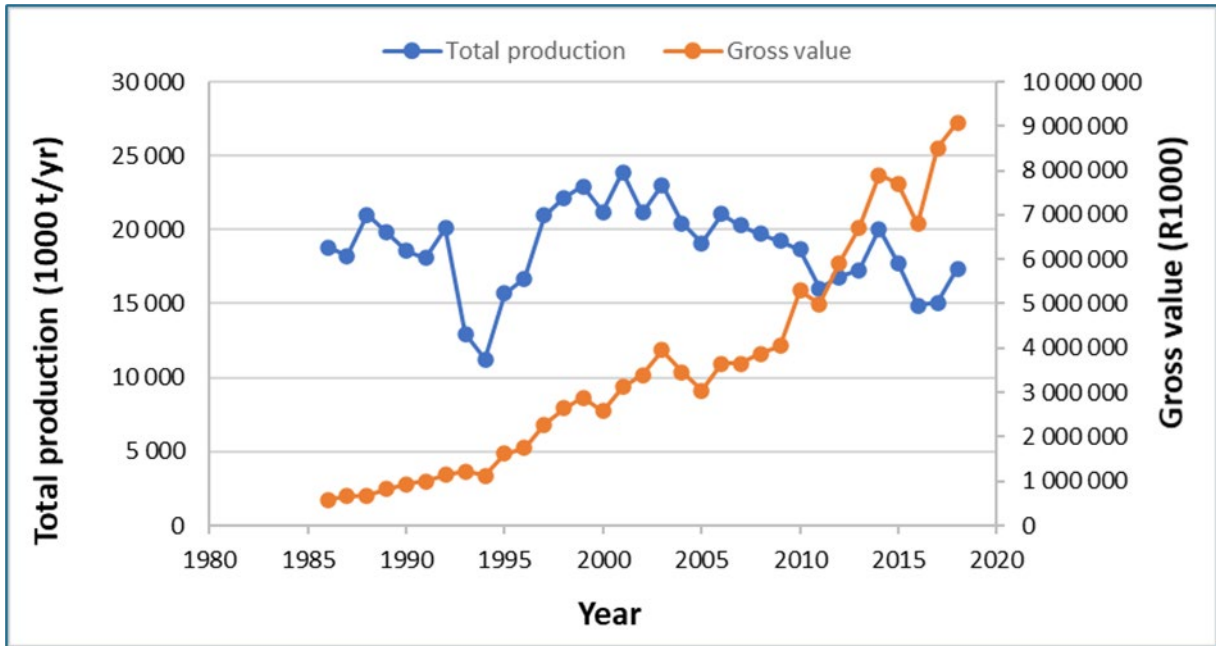


Figure 2.6: Total production and gross value of sugarcane in South Africa from 1985/86 until 2018/19 (Source of data: DAFF, 2019, using data supplied by SASA)

#### 2.2.4.2. Irrigation types and irrigation scheduling in sugarcane fields

As with bananas, water management of irrigated sugarcane in regions where water resources are under pressure demands a focus on minimising water losses, increasing the yield, and increasing the water productivity. Irrigation efficiencies are highest for drip and micro irrigation systems, and lower for overhead sprinkler systems including the centre pivot system. Irrigation systems for sugarcane in the IUWMA include centre pivot, sprinkler, and drip. Just over 10000 ha of sugarcane in the Komati River area (WARMS, 2015) is irrigated using the *centre pivot system* (49.3% of all irrigated sugarcane in the IUWMA). Other smaller plantations using this system are found in the Onderberg area on the Crocodile River, and in the Usuthu catchment, south-west of Piet Retief (WARMS, 2015). This system is often used for plantations serviced by large irrigation schemes but has higher losses of water to evaporation compared to drip or sprinkler systems. The *sprinkler system* is almost as widespread (9 543 ha, or 46.1% of all irrigated sugarcane), including both the dragline sprinkler system (4 401 ha), the quick-coupling sprinkler system (5 037 ha) and the permanent sprinkler system (105 ha) (WARMS, 2015).

Only 4.5% (935 ha) of irrigated sugarcane is under *drip irrigation*, mostly along the Komati/Lomati Rivers, as well as areas along the Crocodile River (WARMS, 2015). It is likely

that this system is primarily used to irrigate very young plantations. A very small area (30 ha) is classified by WARMS (2015) as being under *subsurface irrigation*. We assume that this is the same as the drip irrigation classification. The drip system has the lowest evaporative losses of all irrigation systems. Adetoro *et al.* (2020) modelled sub-surface drip (SSD) irrigation and centre pivot irrigation for the Malelane sugarcane production area and found that irrigation by SSD was substantially lower, by about 100 mm, when compared with centre pivot. This is because in the latter, some of the applied water is intercepted by the crop canopy cover and by the mulch cover (if applied) and is not available for uptake by the roots.

Irrigation scheduling strategies depend on the climate (and thus crop coefficients), soil, developmental stage, and rooting depth of the crop. During the emergence and establishment period, root systems are still small and the rate of water uptake is low, so that light and frequent irrigation is required. Any water stress should be avoided. In the early vegetative period, more frequent irrigation stimulates tillering. A lower frequency of irrigation with a higher application can be considered during the later vegetative (stem elongation) and yield formation periods since this can stimulate the growth of deeper roots, but this option depends on the soil type. Water deficits should still be avoided in these periods to avoid the development of short cane stems. During the ripening period, irrigation should be limited to extremely dry situations, and only for the surface layer. Irrigation intervals are extended or irrigation is stopped to avoid further vegetative growth, to allow the cane to dry, and to stimulate the conversion of sugars to recoverable sucrose.

Globally, the water productivity of sugarcane (80% moisture content) is estimated at 5 to 8 kg/m<sup>3</sup>, and for sucrose containing no moisture it is estimated at 0.6 to 1.0 kg/m<sup>3</sup>, both with the highest values for good ratoon crops in the subtropics (FAO, 2020b). Owing to the high cane yields achieved in the Lowveld region through excellent management, the (blue water) water productivity in this region has been estimated (using the MyCanesim model) at 16.9 kg/m<sup>3</sup> (centre pivot irrigation system, averaged for different soil types and with/without the use of mulch) and 19.8 kg/m<sup>3</sup>, (drip irrigation system, averaged for the same conditions) (Adetoro *et al.*, 2020). These values were reported in the article as blue water footprint (m<sup>3</sup>/ton) and have been converted for comparative purposes. The water productivity of the region can be further improved by greater use of drip irrigation systems, limiting evaporation through the use of mulch covers, and adjusting irrigation scheduling.

#### **2.2.4.3. Water related challenges and priorities for the sugarcane industry**

The recent prolonged droughts and changing rainfall patterns have had a major impact on the sugarcane industry (SASA, 2020). This requires attention to more efficient management of the available water resources through irrigation and production technologies (Singels *et al.*, 2019), water conservation and demand management, and good catchment stewardship and compliance to regulations (SASA, 2020). The industry has driven the development and application of sustainable management tools such as the Sustainable Sugarcane Farm Management System (SUSFARMS®).

As discussed above for banana production, surface water resources in parts of the IUWMA are under threat (WRC, 2017). Increasing demand for and use of water resources in the Crocodile and Komati-Lomati River sub-catchments has led to concerns about the deterioration in water quality and the implications for irrigated sugarcane production (van der Laan *et al.*, 2012). Water quality problems include salinity, sodicity, and nutrient enrichment, particularly of organic N and P fractions (van der Laan *et al.*, 2012; Fig. 2.7). According to the WRC (2017), these sub-catchments are affected in large parts. Irrigated sugarcane production areas (WARMS, 2015) classified as having a high threat to surface water resources include X13J, X13K and X13L (Komati sub-catchment), X14G (Lomati sub-catchment), and X23H, X24D and X24E (Crocodile sub-catchment).

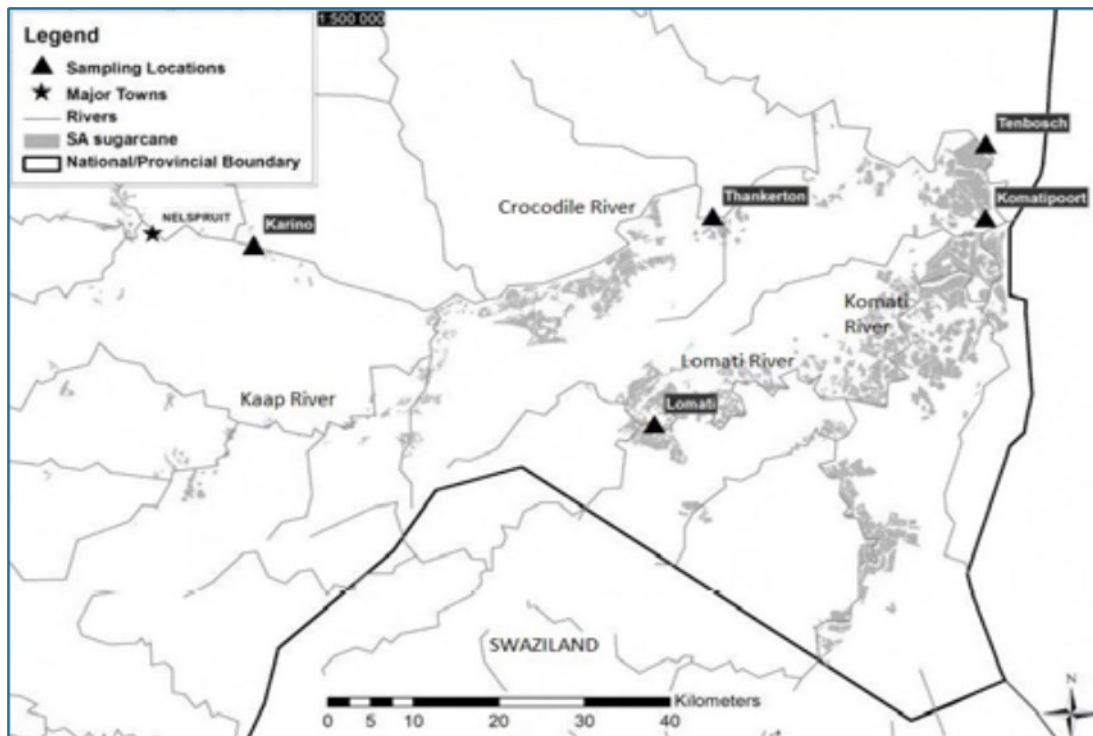


Figure 2.7: Areas under sugarcane production (shaded areas), important rivers and water quality sampling points (identified by triangles) in the Crocodile and Komati-Lomati River catchments. Source: Van der Laan *et al.* (2012)

## 2.3. Water Requirements of Selected Fruit Tree Crops in the IUWMA: A Review

### 2.3.1. Banana

The actual water use of bananas has not been measured under South African conditions. However, based on international literature, total water requirements of bananas are high, varying between approximately 1 200 mm in the humid tropics and 2 200 mm or more per year in the dry tropics (FAO, 2020a; Panigrahi *et al.*, 2021). For rain-fed production, average rainfall of 2 000 to 2 500 mm per year, well-distributed over the growing season, is required (Panigrahi *et al.*, 2021). This equates to around 20 000-25 000 m<sup>3</sup>/ha/year. Lagerwall (undated) indicated that an evenly distributed rainfall of 100 mm per month is the minimum requirement for rain-fed bananas in KwaZulu-Natal, whereas Panigrahi *et al.* (2021) report 138 mm per month under drip irrigation in semi-arid conditions. These figures also depend on the soil type. When rainfall does not contribute regularly to water availability in the soil, irrigation is essential. Banana plants have a shallow root system and do not tolerate dry periods. Production areas

in the IUWMA have a marked dry period and in most areas supplementary irrigation is essential for achieving high yields and excellent fruit quality demanded of commercial production. Greater yield responses to irrigation can be expected in drier years and in drier production areas (Queensland Government, 2004). Irrigation increases the area that can be planted to bananas, given suitable temperature regimes and soils.

Water deficits adversely affect banana crop growth and reduce potential yields (Panigrahi *et al.*, 2021). The response depends on the stage of plant development. In young, vegetatively growing plants, water deficits inhibit the rate of leaf development and result in a smaller plant, with negative impacts on flowering and fruiting, usually seen in smaller bunches (Queensland Government, 2004). During the period of fruit growth, water stress will reduce finger length and reduce fruit quality (poorly filled fingers and a shorter shelf life) but have less impact on bunch weight.

### **2.3.2. Citrus**

Based on the 2018 tree census, citrus was planted on about 6 985 ha in the entire Mpumalanga Province (Citrus Growers Association Report, 2020). More than 70% of the fruit is grown within the IUWMA in areas surrounding Nelspruit. In recent years, water use data were collected in 11 citrus orchards across South Africa (Gush and Taylor., 2014; Vahrmeijer and Taylor, 2018). But only one orchard, planted to the Midnight Valencia oranges was located in the IUWMA (IUWMA). A second orchard was also in the Mpumalanga province, but it was outside the IUWMA in Groblersdal. Given the substantial differences in growing conditions as a result of topographic, microclimatic, and soil variations within the IUWMA, there is need for more accurate actual measurements of water use in citrus orchards. Because access to water is a very divisive topic especially among irrigation farmers, it is critical that decision-making, e.g. around water allocation reforms, water re-allocations, water demand management, etc. in the catchment are based on the most accurate data.

Findings from the studies by both Gush and Taylor (2014) and also by Vahrmeijer and Taylor (2018) were rather unexpected. Contrary to expectations, the water use by the citrus orchards were quite low and they showed significant variations among cultivars, growing regions, soil type, canopy cover, irrigation system, etc. Citrus is a perennial evergreen crop, so high annual water use rates were expected, but this wasn't the case. The cultivars studied include the Midnight Valencia, Delta Valencia, Bahianinha navels, nadorcott mandarins, mostly in Citrusdal in the Western Cape, Groblersdal in Mpumalanga, and Letsitele in

Limpopo. Vahrmeijer and Taylor (2018) report an annual water use range between 139 mm for Valley Gold Mandarins and 953 mm for the Afourer Mandarins, which translates to 1 390 and 9 530 m<sup>3</sup>/ha/yr. However, it should be noted that while these water use values are based on transpiration (sap flow) measurements only, the actual orchard evapotranspiration is likely quite low since transpiration usually contributes the most to ET in fully grown orchards.

The annual total transpiration for the Midnight Valencias in Malelane were around 640 mm (average over two years), but the annual evapotranspiration (ET) was not reported. The crop water requirements (annual total ET) were estimated as 696 mm for the Rustenburg navels (Citrusdal), 732 mm for the Delta Valencia (Groblersdal), 994 mm for the Baianinha navel orchards (Groblersdal). These evapotranspiration values were obtained through modelling using data measured during short window periods per season lasting roughly one to two weeks using open path eddy covariance systems. Longer measurement campaigns with the eddy covariance systems were not possible due to the costs involved in running the system at remote sites and the high demand for the limited equipment. However, the modelled ET values in South African citrus orchards are quite similar to values reported elsewhere. For example, García Petillo and Castel, 2007 estimated the annual ET to be about 767 mm in a mature citrus orchard in Uruguay. Fares *et al.* (2008) reported much higher values of over 1 265 mm/yr in Florida USA. Therefore, there appears to be a wide range of water requirement values for citrus orchards necessitating further data collection to facilitate the development of an accurate decision support tool for the IUWMA catchment. Future research will need to address the water use dynamics of citrus orchards as influenced by the rootstock-scion combination. The rootstock, in addition to the cultivar type, also influences orchard water use as reported for apples (Muchena *et al.*, 2020). The South African studies suggest that the annual water use by mature citrus orchards, are in some cases lower than that used by deciduous fruit trees that have a shorter growing season such as apples as reported by Volschenk (2017); Dzikiti *et al.* (2018a, b); Gush *et al.* (2019); Mobe *et al.* (2020) and Ntshidi *et al.* (2020). Typical seasonal total evapotranspiration in mature well managed apple orchards in the Western ranges from 9 000 to 11 000 m<sup>3</sup>/ha, albeit for a shorter growing period from October to May, respectively. The low water use by citrus trees are a result of the very strong stomatal regulation of transpiration as widely reported in literature (Steppe *et al.*, 2006; Dzikiti *et al.*, 2007). However, the extent to which these low water consumption rates are incorporated in the current water management practices in IUWMA is unclear. Unlike the studies reported here, the current project will seek to measure the evapotranspiration in the citrus orchards over a full year growth cycle to reduce uncertainties in the ET data obtained through modelling.

### 2.3.3. Avocados

As of 2017, the area under avocados in Mpumalanga was around 2 922 ha with about 2 518 ha planted around the Nelspruit area. Data on the water use of avocados is very scarce besides the recent study by Taylor *et al.* (2021) co-funded by the WRC and the South African Avocado Growers Association (SAAGA). Unfortunately, none of these data were collected in IUWMA. The two sites used for the study were located in Howick, KwaZulu-Natal on the Hass cultivar grafted on a Dusa rootstock. The other water use monitoring study site was in Tzaneen also planted to the Hass cultivar on the Dusa rootstock.

The annual total evapotranspiration for the intermediate bearing and mature avocado orchards in KwaZulu-Natal, measured using open path eddy covariance systems were fairly high ranging from 975 to 1060 mm. This translates to crop water requirements between 9 750 and 10 600 m<sup>3</sup>/ha. These values are somewhat higher than those reported by Grismer (2014) at a coastal site in California. He reported annual total evapotranspiration estimates about 60% of the reference evapotranspiration (ET<sub>o</sub>) averaged over a twelve-year period and obtained using measurement techniques such as the Bowen ratio and soil water balance approaches. For the KwaZulu-Natal site, 60% of ET<sub>o</sub> translated to just under 700 mm per annum which is significantly lower than the eddy covariance measured values.

### 2.3.4. Macadamia Nuts

The first study to quantify the water requirements of macadamia nuts in the IUWMA was done at White River as reported by Ibraimo *et al.* (2014). Field measurements were conducted on a six-year-old, young bearing 'Beaumont' macadamia (*M. integrifolia* x *M. tetraphylla* hybrid) orchard planted in 2005 on a 'Beaumont' rootstock. This study was funded by the WRC (Project no WRC K5 1770/2/14) and the Department of Agriculture Forestry and Fisheries. However, given the rapid expansion of the macadamia industry and the growing threats posed by the increasing pressure on the limited water resources, the WRC subsequently partnered with the macadamia grower's association (South African Macadamia Growers Association). They commissioned a new four-year project (WRC K5 2552//4) with a broader scope. The project which started in April 2016 and ended in March 2021.

Because the present study was mostly interested in the maximum unstressed water use rates for licensing, compliance monitoring and enforcement, we focused this review only on the water use of mature full-bearing macadamia orchards. The annual total transpiration of

the macadamia orchards at White River as reported by Ibraimo *et al.* (2014) was about 465 mm/yr. This value is an average over two years, i.e. 2010/11 and 2011/12, respectively. As in the case of citrus, these transpiration rates are quite low for evergreen trees with a large leaf area index (> 3.0). Peak daily transpiration of the macadamia trees rarely exceeded 2.0 mm/d even on hot dry summer days. As with the case of citrus orchards, the modelled annual evapotranspiration, averaged over two years, was quite low at about 764 mm (or 7 640 m<sup>3</sup>/ha/yr.).

The low transpiration values in mature Beaumont macadamia nuts were confirmed by the recent data collected by Taylor *et al.* (2021a). They measured average annual transpiration rates of about 328 mm which were even lower than those reported by Ibraimo *et al.* (2014). The recent data were collected at Mayo Estate, about 30 km to the west of Nelspruit. Canopy cover of the macadamia trees in both studies were similar at about 60%. International literature on the water use of macadamia orchards is sparse. However, one study in Australia derived irrigation requirements for macadamia nuts ranging from about 210 to 770 mm per year (Carr, 2013).

### **2.3.5. Sugarcane**

Sugarcane water consumption is relatively high (Bastidas-Obando *et al.*, 2017). Approximately 800 mm of rainfall per annum or more is required for rain-fed sugarcane production in South Africa (SASA, 2020). Rainfall is particularly needed from December to March during the period of active crop growth and high evaporative demand. However, all sugarcane production in the IUWMA is under irrigation since the rainfall is not sufficient and/or not spread over the growing period as required, rainfall is highly variable from year to year, and evaporative demand is very high. For example, the mean annual rainfall at Malelane is about 600 mm (Adetoro *et al.*, 2020). The water requirement (ET) of sugarcane is estimated at around 1 500 to 2 500 mm per year, evenly distributed over the growing period (FAO, 2020b).

The sugarcane rooting depth varies depending on soil type and irrigation regime and can reach 5 m when water inputs are infrequent. However, active water uptake is usually limited to the surface zones (from the upper 1.2 m to 2.0 m) (FAO, 2020b). Under conditions of high evapotranspiration, up to 60% of the total plant available soil water can be used before negative impacts are seen on yield (Singels *et al.*, 2019). The developmental stage is important in influencing the response to water deficits. During the early vegetative growth

period, water deficit reduces tillering and tillers are smaller, with greater impacts on final yield than when deficit is experienced in later growth periods. During the period of stem elongation and yield formation, insufficient water leads to shorter stems, while during the latter part of stem elongation a severe water deficit can trigger premature crop ripening. The crop ripening period requires a low soil moisture content to reduce growth and stimulate sugar conversion; nevertheless, a serious water deficit can cause a reduction in sugar content (FAO, 2020b).

## **2.4. Climate Change and Expected Impacts in the IUWMA**

### **2.4.1. Historical/Current Climate of the IUWMA**

The Lowveld region of the IUWMA experiences a sub-tropical climate with hot summers and mild to cool winters (DEA, 2018). The Highveld region is more temperate and experiences cold winters with frost, and summers are warm. Mean annual rainfall is high towards the escarpment in the west and decreases towards the east. Rainfall occurs primarily in summer in the form of thunderstorms, but the escarpment receives rainfall throughout the year. Annual rainfall totals are around 400-1 000 mm over most of the IUWMA, reaching around 1 500 mm in the mountains of the escarpment.

### **2.4.2. Observed Trends in the Climate of the IUWMA**

The most recent national scientific summary assessment of climate trends across South Africa (DEA, 2018) concludes that there have been widespread and statistically significant temperature increases across South Africa over the last 50 years. Although there is a lack of weather stations with long term temperature records over Mpumalanga, the available data indicates that strong warming has possibly occurred over this province. The annual and seasonal averages of minimum and maximum temperature have increased nationally, and warm extremes show strong increasing trends, whilst cold nights are decreasing. Studies on historical trends in annual and extreme daily rainfall over South Africa indicate negative trends over the Lowveld region of Mpumalanga, although not statistically significant (DEA, 2018).

### **2.4.3. Climate Change Projections for the IUWMA**

Narratives of climate change were developed, based on the best available science, for each of South Africa's nine provinces (DEA, 2018). The following two narratives were presented for Mpumalanga Province. They arise from the high levels of uncertainty that exists for the projections for rainfall, with climate models indicating general drying in the long-term, while some models indicate possible slight wetting (see also DEA & GIZ, 2015a, 2015b).

#### **2.4.3.1. Narrative 1: A hot and dry future**

Mpumalanga may plausibly experience a climate future that is significantly hotter and drier compared to the present-day climate. Under low mitigation, temperature increases as large as 3°C may occur by 2040-2060, with associated drastic decreases in rainfall. Such a climate regime will also be associated with an increase in the frequency of occurrence of heat-wave days and high fire-danger days. Such a change towards a generally warmer and drier climate would pose significant threats to the forestry sector, due to the likelihood for more frequent forest fires occurring during more frequent periods of drought.

#### **2.4.3.2. Narrative 2: A warmer future with increased rainfall**

The main alternative narrative for Mpumalanga still implies significant increases in temperature, consistent with narrative 1. The main difference in this scenario is that rainfall totals increase under climate change, rather than to decrease. Such an increase may imply the more frequent occurrence of land-falling tropical lows over the lowveld regions, with potentially significant impacts on tourism and infrastructure in areas such as Kruger Park in the Lowveld region. Under such a scenario drought will not be such a major problem for the forestry sector as under narrative 1, but the increased occurrence of pests and pathogens affecting forestry and agriculture may well pose an alternative set of challenges.

### **2.4.4. Impacts of Climate Change on Water Resources of the IUWMA**

The climate change projections of greatest significance for the long-term water resources of the IUWMA are the increases in average and extreme temperatures, and the expected increase in rainfall variability, with an overall increase in heavy rainfall events (DEA & GIZ, 2015a, 2015b). These changes and their associated impacts are summarised in Table

2.2. The IUWMA is already water stressed and experiencing a decrease in water availability and water quality. Climate change projections suggest that water availability could be further reduced in future through changing rainfall patterns and increased evaporation, while the irrigation water demand is likely to be increased as temperatures rise and evapotranspiration increases (DWS, 2015; DEA, 2013a). Water quality could also be further decreased through the impacts of extreme rainfall and higher flooding incidences. However, it is likely that population and economic growth will increase domestic water demand and water demand for power generation, and this could have a greater impact on overall water needs and increasing competition between water users (DWS, 2015). Mining is also a significant water user and should water demand increase for both mining and agriculture, decisions will need to be made in the long-term regarding the optimal allocation of water resources to these two sectors (DEA, 2013a).

For the Long-Term Adaptation Scenarios (LTAS) Programme of the Department of Environmental Affairs, detailed hydrological modelling was conducted to estimate the change in mean annual catchment runoff for each secondary catchment of South Africa (Fig. 2.8). The range and spatial variation of potential impacts across the country is broad. For the IUWMA (parts of W4 and X1) there are both projected increases and decreases in runoff with no clear median signal (Fig. 2.9 and Fig. 2.10).

Table 2.2: Types of impacts linked to climate variability in Mpumalanga (Source: DEA & GIZ, 2015a).

Climate Variability	Type of Change	Impacts
Temperature Rise	Increased number of warm and very hot days, and increased daily maximum temperatures	<ul style="list-style-type: none"> <li>Increased evaporation impacting on the availability of surface water</li> <li>Soil degradation due to increased acidity, nutrient depletion, declining microbiological diversity, lower water retention, and increased runoff</li> <li>Positive or negative impacts on crops' growing seasons, yields, and growing range. Some crops – especially fruits – require a chill factor (a period of cold) in the winter to have a good harvest;</li> <li>Increased incidence of heat waves and associated health conditions for human and livestock health, such as heat stress. Heat especially impacts the health of the particularly old and young or those already suffering from other illness</li> <li>Increase in concentration and range of pests and pathogens that are human and livestock disease vectors (carriers), such as mosquitoes and ticks</li> </ul>
Change in Rainfall	Increased number of consecutive dry days	<ul style="list-style-type: none"> <li>Decreases in runoff and streamflow and an increased risk of drought, affecting crop production, food security, and rural livelihoods</li> <li>Reduced streamflow (a particular threat for communities dependent on surface water)</li> <li>Loss of soil moisture affecting crops and increased risk of soil erosion due to wind</li> <li>Increased risk of veld-fires and resultant threat to property, grazing, and crops</li> </ul>
	Increased number of wet days and/or increase in extreme (heavy) precipitation events	<ul style="list-style-type: none"> <li>Increased risk of floods and consequent damage to property, crops, and loss of life</li> <li>Water logging of soil which can affect crops</li> <li>Increased risk from water borne diseases, particularly after flood events</li> <li>Damage to bulk infrastructure such as irrigation systems</li> <li>Damage to property and crops from wind associated with violent storms</li> <li>Increase in lightning events which can damage crops and cause loss of life</li> </ul>
	Variability or change in the timing of precipitation	<ul style="list-style-type: none"> <li>Rain-fed agriculture, which relies on the timing of rains for planting and harvest, is particularly at risk</li> <li>Less predictability impacts on the management of water resources in catchments and large water infrastructure, with implications for water supply reliability</li> </ul>

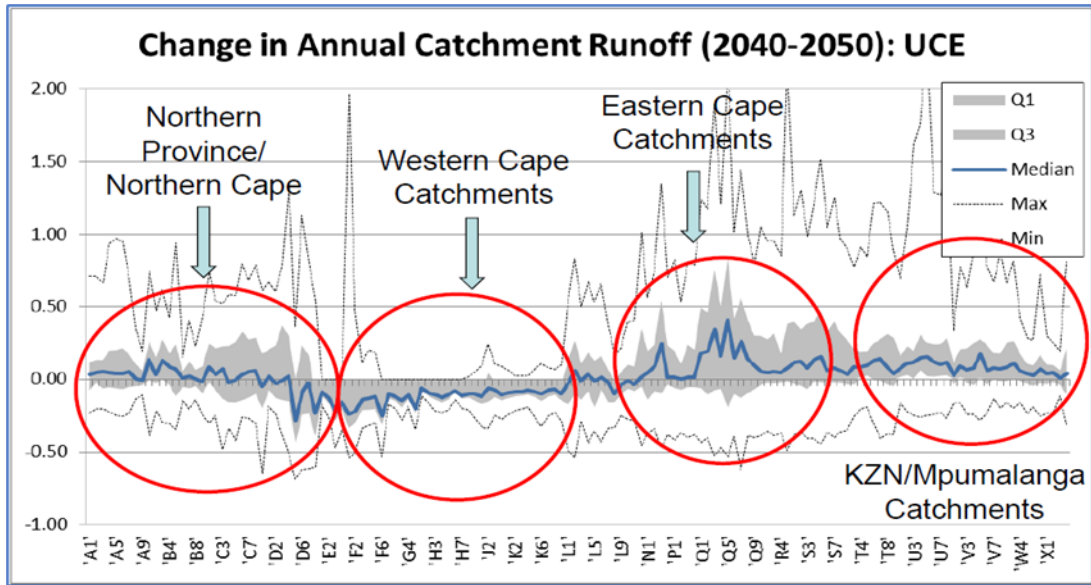


Figure 2.8: Range of potential impacts of climate change on the mean annual catchment runoff for secondary catchments for the period 2040 to 2050 due to the Unconstrained Emissions (UCE) scenario relative to the base scenario. The northern part of the W4 catchment and the X1 catchment (last two catchments on the X-axis) are within the IUWMA. Source: DEA, 2013a.

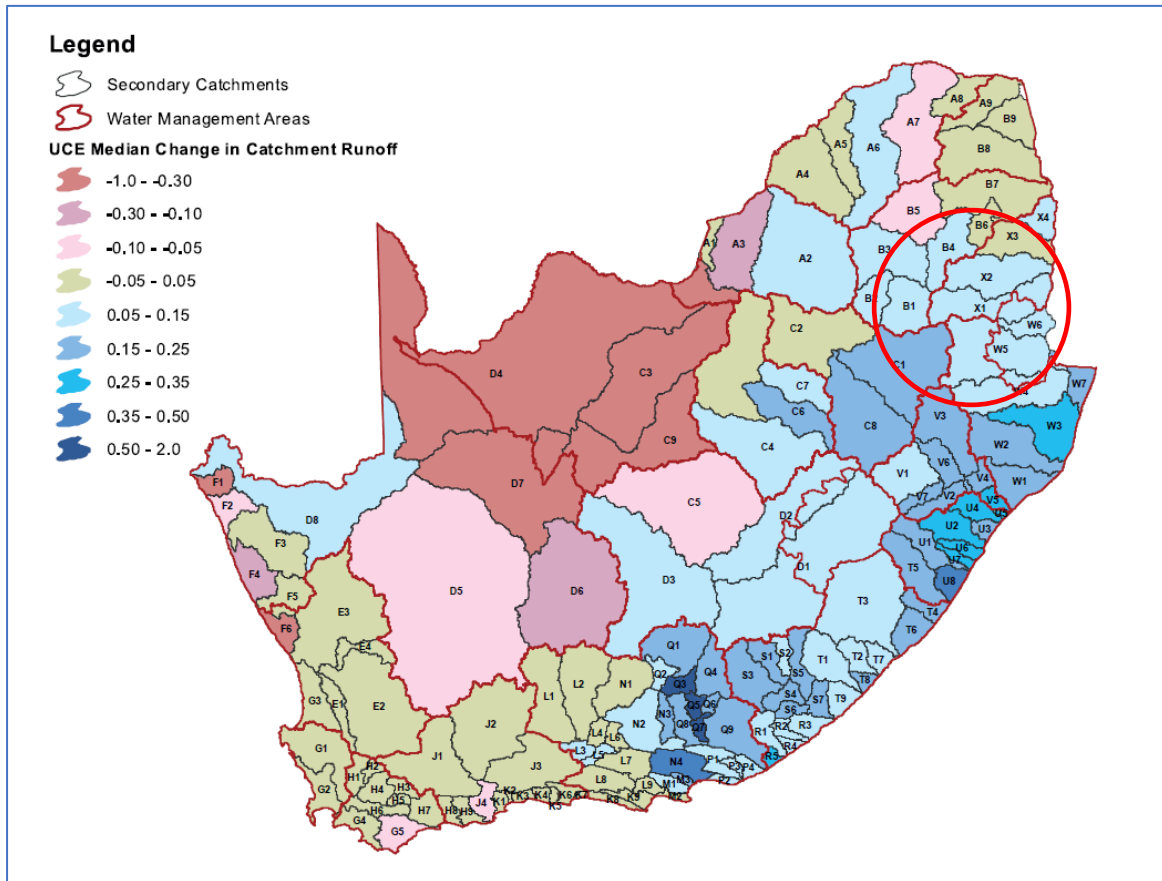


Figure 2.9: Median impact of climate change on the average annual catchment runoff for the period 2040-2050 relative to the base scenario average for 1990-2000 for all secondary catchments in South Africa derived from a Hybrid Frequency Distribution (HFD) analysis of all possible global circulation model (GCM) outputs (+6000 scenarios) for the unconstrained emissions scenario (UCE). The northern part of the W4 catchment and the X1, X2, X3 and X4 catchments (indicated roughly by the red circle) are within the IUWMA. Source: DEA, 2013a.

Modelled climate change impacts on the total average annual demand for the urban, bulk and irrigation sectors in each WMA by 2050 are presented in Fig. 2.10 (top). The other three figures in Fig. 2.10 show the proportion of this demand that can be supplied by 2050 for each of these sectors. WMA 5 is the previous Inkomati WMA, and WMA 6 is the previous Usuthu to Mhlatuze WMA.

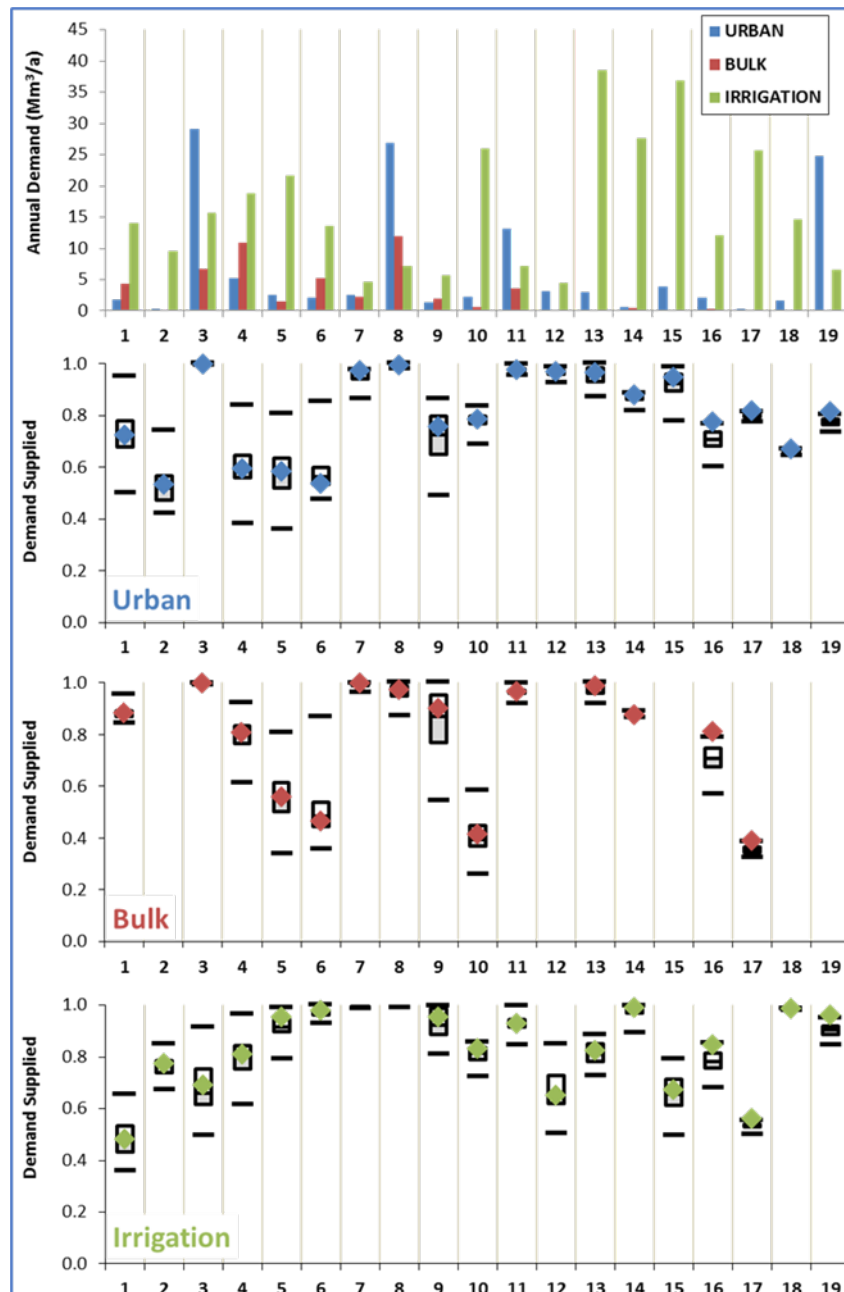


Figure 2.10: Average annual water demand (top) for the 19 WMAs for the period 2040 to 2050 and the estimated proportion of demand that can be supplied under the base scenario (symbols) and models representing the minimum, 25th, median, 75th percentile and maximum impact under the unconstrained emissions scenario (UCE) for different sectors. In each plot the symbol represents the percentage of the average annual demand that can be supplied under the base scenario in each WMA while the box plots show the median and the inter-quartile range and the bars show the maximum and minimum model results. Source: DEA, 2013a.

Demand for water in the Inkomati WMA is clearly dominated by the irrigation sector. In the Usuthu-Mhlatuze WMA the urban and bulk sectors comprise a larger proportion of water demand. Both WMAs are projected to be able to supply only 40-60% of demand (median) by mid-century for urban and bulk water, but more than 90% of demand for irrigation water

(bottom panel). The authors note that it was not intended as a detailed study of the potential impacts of climate change on the long-term yield and reliability of individual systems and that further detailed modelling of individual systems should be undertaken. The expected impact on the irrigated crop sector could be very significant, notwithstanding that rain-fed agriculture will likely be hardest hit. Changes to water allocations and water restrictions during times of multi-year drought will have deleterious impacts on yields and product quality of irrigated bananas, sugarcane, fruit tree crops and tree nut crops, the largest agricultural users of water in water stressed parts of the IUWMA. Other possible impacts include crop loss due to extreme weather conditions such as drought, floods, storms, and fires; and the spread of pests into new areas as temperatures become more favourable.

Only a few studies have been conducted to assess the impacts of climate change on sub-tropical fruit production in South Africa. Schulze and Schütte (2016a) modelled the projected changes in irrigated banana yield across South Africa from the present (1971-1990) into the intermediate future (2046-2065). The results suggest that irrigated banana yields could increase by around 10-20 t/ha and become suited to currently cooler inland regions based on expected temperature increases and reductions in frost risks. However, other factors such as soil types and availability of water are important in determining potential shifts in banana growing regions. The authors caution that water demands, whether for dryland or irrigated bananas, are projected to increase by 10-15% over this period.

A similar modelling study was conducted by Schulze and Schütte (2016b) for citrus fruit production. Projected future shifts in production areas for Navel and Valencia oranges, grapefruit and lemons were identified, showing both new areas and losses of existing areas depending on fruit species. However, only broad temperature criteria were used and future research should include other factors (humidity, hail risk, daily temperature thresholds, water availability, soil type). Sugarcane is also likely to become climatically suited to new inland areas under climate change projections (Fig. 2.11, left), and to show increased productivity (Fig. 2.11 right), even under the hotter/drier future scenarios (Schulze and Kunz, 2010). This study was only for dryland sugarcane, and further research is needed to assess the climate change impacts on irrigated sugarcane.

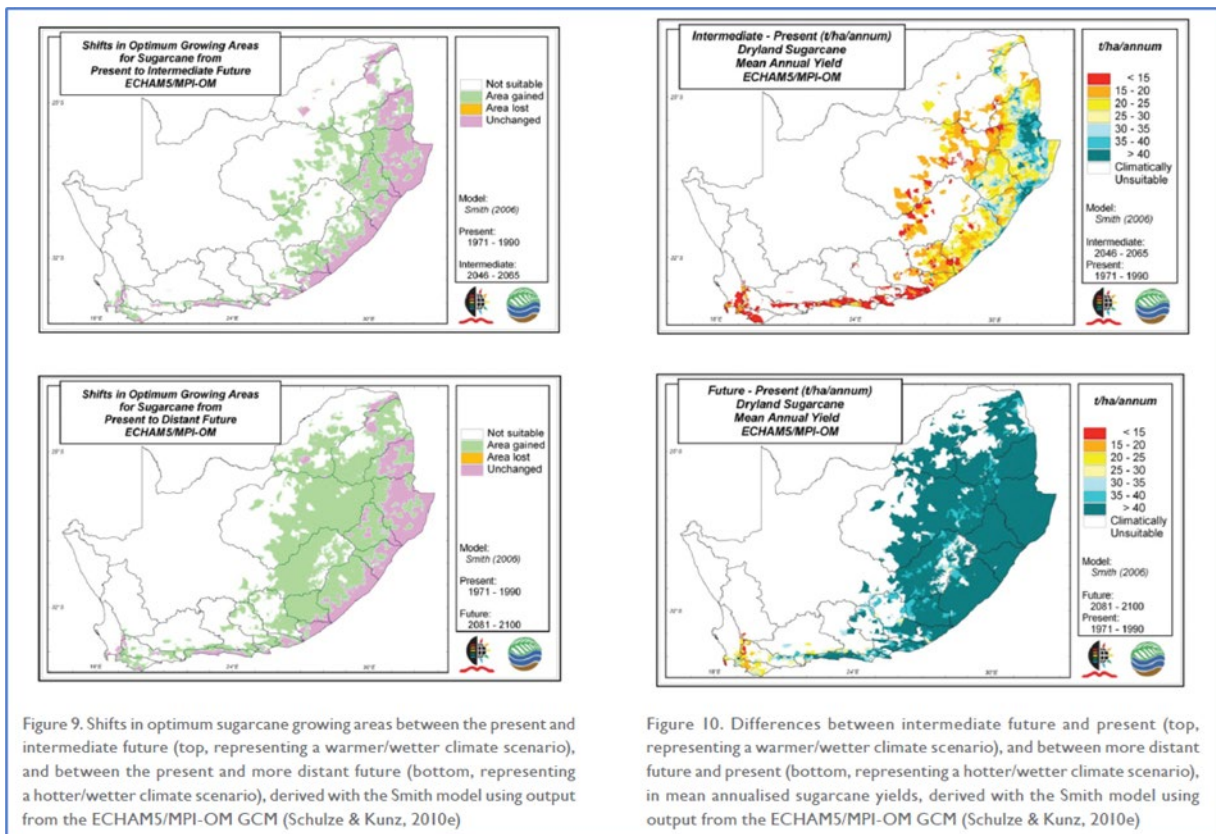


Figure 2.11: Source: Schulze and Kunz (2010) – figure taken from DEA (2013b)

For the IUWMA, the projected impacts of warming on sub-tropical fruit production could lead to greater productivity in currently cooler production regions such as the Escarpment and possibly allow for production in parts of the Highveld. In all areas, irrigation demand will increase. Thus, the irrigation sector and the IUWMA should monitor and assess the risks carefully, with due consideration of opportunities for adaptation. This could include long-term shifts of certain crops to areas with lower pressure on freshwater resources.

## 2.5. Water Resources and Management in the IUWMA

### 2.5.1. Description of the Hydrology of the Study Area

The IUWMA has four river drainage basins. These are the Usuthu (~ 7 780 km<sup>2</sup>), Komati (~ 8620 km<sup>2</sup>), Crocodile (~ 10 440 km<sup>2</sup>) and the Sabie-Sand (~ 9 300 km<sup>2</sup>). The Usuthu catchment is shared with eSwatini, while the Komati is shared with Mozambique, making the IUWMA a transboundary entity in physio-hydro-graphic extent (Fig. 1.1). This presents unique challenges with respect to the development, planning, and management of the water

resources as water sharing agreements with other downstream riparian states must be honoured before any developmental decisions could be made. From a demand perspective, it is prudent to note that water demand is naturally higher in the lower, drier, and hotter parts of the WMA where runoff quantities are also a relatively huge challenge. This implies that proper management of the available river flows is very important. IUWMA has thus installed a suite of 25 near-real-time rainfall gauges and 28 river-flow gauges to supplement any available monitoring stations operated by various government departments such as DWS and SAWS. The mean annual precipitation (MAP) of the IUWMA generally varies from around 1 330 mm/yr in the quaternary basin X31F in the westerly mountainous regions to around 460 mm/yr in the quaternary basin X33D in the low-lying eastern parts. This pattern of precipitation is occasioned by the Great Escarpment which divides the IUWMA into a western plateau and sub-tropical lowveld to the east. The mean annual class A evaporation of the IUWMA is about 1 900 mm/yr. This scenario gives a mean annual runoff ranging from 4.4 mm/yr for quaternaries X40B, X33D and X40D to 542.9 mm/yr for quaternary X31F.

### **2.5.2. Water Allocation Practices and Relevant Legislation**

The allocation of water for various, often competing uses in the IUWMA is not a straightforward process. However, this process, wherever it is necessary to allocate water resources for the social and economic development of any given area in South Africa, is based on the National Water Act of 1998 (NWA). The Act endeavours to ensure that South Africa's water resources are protected, used, developed, conserved, managed, and controlled in a sustainable and equitable manner, on benefit of all people. Any other allocation legislation draws its strength and mandate from this all-encompassing Act. The allocation of water resources in the IUWMA is thus guided by this Act. Redress for past injustices is an overarching objective and the NWA provides that water allocations are to be granted at the discretion of the relevant authorities, taking into account, *inter alia*, the need to transform and redress the results of past racial and gender discrimination. The major focus of the National Water Resource Strategy is equitable and sustainable access and use of water by all South Africans, whilst sustaining the water resource and ensuring that water is made available to previously disadvantaged groups. Catchment management agencies (CMAs) such as IUWMA and water user associations (WUAs) are platforms where local public and private interests can interact to shape the water allocation strategies.

However, these institutions apply to water resources that are entirely within South Africa's borders. For transboundary water courses, international and regional water protocols

take precedence. In practice each sovereign state has its own legislation and structures for water resources management, development, and allocation. In the case of the IUWMA, the national bodies through the relevant ministries or departments have a technical committee that sits to deliberate or discuss water resources developments and allocations for each country depending on their unique circumstances. The Tripartite Permanent Technical Committee (TPTC) Interim Agreement between the Republics of Mozambique as well as South Africa and the Kingdom of eSwatini is the relevant inter-governmental body formed for fostering co-operation on the Protection and Sustainable Utilisation of the water of the Incomati and Maputo Water Sources (TPTC, 2002). The deliberations are, as would be expected, guided by international and regional water laws and protocols such as the SADC Protocol on Shared Watercourses. These deliberations agree on the water allocation for each riparian state. Each country then uses its own legislation to allocate the resource within its boundaries. In South Africa the IUWMA is then bound by the allocated amounts, and the requirements of the National Water Strategy. The IUWMA is expected to have a catchment management strategy that is in line with the National Water Strategy to manage SA's share of the transboundary watercourses.

### **2.5.3. Water Management Priorities to Improve Water Allocation and Efficiencies**

More than twenty years after the promulgation of the National Water Act, previously disadvantaged and emerging farmers are still struggling to access water. Therefore, there is need for water allocation reforms for equitable distribution, not only in IUWMA, but throughout the country. For example, the recently concluded Verification and Validation of Lawful Water Use exercise, commissioned by the Department of Water and Sanitation is meant to be a starting point for water allocation reforms and redress. Details of the planned water allocation reforms in IUWMA are outlined in the Catchment Management Strategy. IUWMA has an online system to provide real-time insights on irrigation, and general, water use within specific areas. This is achieved using the remote sensing and GIS based HydroNET tool ([www.portal.hydronet.com](http://www.portal.hydronet.com)). However, South Africa faces a severe water shortage with the expectation being that water demand would exceed supply between 2025 and 2030. To regulate the amount of water being used for irrigation, South Africa introduced a water licensing mechanism in the National Water Act.

Auditing on compliance of water allocation is currently a major challenge for water managers in South Africa. For instance, IUWMA needs to monitor over 50 000 farmers spread

over an area of just over 36 000 km<sup>2</sup>. This makes it virtually impossible to monitor the use by farmers in a conventional way, naturally leading to non-compliance and unequal use of water resources.

#### **2.5.4. Current Tools for Water Resource Management in the IUWMA**

At the farm level, many of the farms schedule their irrigation with various tools. The methods range from digging profile pits, use of tensiometers to monitor the soil water potential, neutron probes and other soil moisture monitoring devices. In recent years the DFM probes have become the most popular irrigation scheduling tool used with the IrriCheck software ([www.irricheck.co.za](http://www.irricheck.co.za)). The IrriCheck system combines soil moisture measurements taken at different depths in the root zone of the plants with weather forecasts and real-time weather data to make irrigation scheduling decisions. The soil moisture probes determine volumetric soil water content in the soil and this is referenced to predetermined soil moisture depletion levels depending on soil type to determine the trigger points to initiate irrigation. The weather data is used to calculate the crop water requirements from the reference evapotranspiration and user defined crop coefficients. The entire system transmits the data either to the user's PC or smartphones (both Android and iOS). Several computer-based models have been developed in the sugarcane industry (Singels and Smit, 2006).

At the catchment level, the HydroNet system is being used for managing the water resources. The Water Auditing Control Room (HydroNET of the IUWMA) provides the management authority with a comprehensive monitoring tool that greatly enhances their effectiveness. For instance, the dashboards show the historical and current water use through irrigation by farmers based on satellite data from eLEAF. The water use is compared with the water allocations to identify farms with excessive water use. Such a tool has helped IUWMA to raise awareness among farmers by showing them their water use in comparison with their peers (<http://www.hydronet.com/product/waterauditing/>). In situations where every raindrop counts and needs to be made optimal use of for the management of the available water resources, this HydroNET tool provides access to almost all available weather information from the South African Weather Service, water use patterns, hydrological conditions, etc. to make well-informed, near real time management decisions of their water resources.

## CHAPTER 3: DETERMINING WATER USE OF MATURE MANGO ORCHARDS UNDER SUBTROPICAL CONDITIONS

### 3.1. Summary

For precise irrigation scheduling, irrigation system designs, and best on-farm water allocation planning, accurate information on actual orchard evapotranspiration and its components is essential. However, there is currently no reliable quantitative information on the water use of mature mango (*Mangifera indica* L.) orchards in South Africa. This lack of information may lead to poor use of the scarce water resources by causing inaccurate irrigation scheduling and water allocation decisions. This study sought to close this important knowledge gap by investigating how the water use varies with environmental factors under local South African conditions. The study focussed on the most widely planted 'Tommy Atkins' cultivar in a well-managed high yielding orchard. Environmental data collected over two growing seasons include orchard microclimate, volumetric soil water content in the root zone and in the work rows, and irrigation volumes. Actual tree transpiration was measured using the heat ratio method of monitoring sap flow while whole orchard evapotranspiration (ET<sub>c</sub>) was measured using an open path eddy covariance system at selected intervals. To explain the observed water use trends, leaf gas exchange data were collected seasonally using an infrared gas analyser while soil evaporation was monitored using microlysimeters. Results for the 2022 season showed that the daily orchard transpiration peaked at about 2.9 mm/d compared to ET<sub>c</sub> of ~ 4.3 mm/d in summer. The short grass reference evapotranspiration explained most of the variation in orchard transpiration ( $R^2 \sim 0.74$ ) compared to the solar radiation ( $R^2 \sim 0.64$ ) and the vapour pressure deficit of the air ( $R^2 \sim 0.45$ ). The estimated total annual evapotranspiration of the orchard was about 887 mm, with tree transpiration contributing about 601 mm. Total annual irrigation was 456 mm while rainfall contributed 558 mm. Net CO<sub>2</sub> assimilation peaked at less than 10  $\mu\text{mol}/\text{m}^2/\text{s}$  on typical clear days under well-watered conditions. Fruit yield under non-water-stressed conditions was 44.5 ton/ ha for the 2022 season amounting to an average yield of 147 kg/tree. Water productivity, defined as kg of fruit per m<sup>3</sup> of water consumed (ET<sub>c</sub>) was 5.01 kg/m<sup>3</sup>. Assuming a price per kg of R 23 for Tommy Atkins, the economic water productivity was about R 116 /m<sup>3</sup>. This study highlights the need to optimise irrigation for the sustainable use of water resources in this region given that actual water consumption in this specific orchard was far less than the total water input (rainfall plus irrigation).

### 3.2. Introduction

In dry countries like South Africa, commercial production of mango (*Mangifera Indica* L.) is often done under irrigation to improve yields and fruit quality (Mostert and Hoffmann, 1996; Lu., 2005). The major production area for mango in South Africa is the Inkomati-Usuthu Water Management Area (IUWMA), located in the northeastern parts of the country (Fig. 1.1). This region accounts for about 16% of the mangoes exported from South Africa. According to the Third National Water Resources Strategy for South Africa, water resources in this region are almost fully allocated due to the rising competition between irrigated agriculture and the growing population, increasing industrial and recreational activities, and the environment, among others (NWRS-3, 2022). This means that future expansion of irrigated agriculture can only be achieved by improving the efficiency of water use with the existing water allocations (Reinders *et al.*, 2013). The increasing frequency and severity of droughts in key fruit producing areas, related to climate change, exacerbates the water shortages thereby threatening the sustainability and growth of irrigated fruit production (Maponya and Mpandeli, 2016)

Effective management of water resources in orchards requires accurate quantitative information on the soil-plant-atmosphere interactions to determine the water requirements of the fruit trees (Volschenk *et al.*, 2003; Girona *et al.*, 2013; Gush and Taylor, 2014; Dzikiti *et al.*, 2018; Pereira *et al.*, 2021). Besides the studies by Mostert and Hoffmann (1996) in South Africa, Lu (2005) in Australia, and Wei *et al.* (2017) in China, few other studies have investigated, in detail, the water use dynamics in mango orchards. Little is also known about how the water use relates to yield quality and quantity. This paucity of information may lead to inaccurate management of scarce water resources, especially irrigation scheduling, and to poor water allocation decisions which may result in over or under irrigation. This has negative implications on both fruit yield and quality (Volschenk, 2017; Dzikiti *et al.*, 2018).

Orchard evapotranspiration is commonly determined using the soil water balance approach (Rallo *et al.*, 2017; Rallo *et al.*, 2014; Volschenk, 2017), micrometeorological techniques such as the eddy covariance (Gush and Taylor, 2014; Dzikiti *et al.*, 2017a), combining microlysimeter derived soil evaporation and transpiration (Bonachela *et al.*, 2001; Testi *et al.*, 2004), and using the surface energy balance method (Cammalleri *et al.*, 2010; Consoli and Papa, 2013; Consoli *et al.*, 2006; Dzikiti *et al.*, 2011). These methods are however, not suited for routine use in orchard water management. Instead, simple crop coefficients ( $K_c$ ) are widely used to estimate  $ET_c$  from reference evapotranspiration ( $ET_o$ ),

( $ET_c = K_c \times ET_o$ ), using the guidelines provided in FAO paper number 56 (Allen *et al.*, 1998). Whilst these have proven robust in a number of annual crops, they have been shown to be very site specific for perennial orchard crops where crop coefficients can vary according to variety, rootstock, tree spacing, canopy cover, microclimate and irrigation method (Naor *et al.* 2008). As a result, published  $K_c$  values can often result in poor estimates of water use for orchard crops. There is therefore a need for more mechanistic models which can provide reliable estimates of  $ET_c$  under a wide range of climatic conditions and management practices which can then be used to derive site specific  $K_c$  values for improved on-farm water resources management. These models require detailed data to calibrate and validate them. However, in cases where the soil water content falls below threshold values, plants experience water stress and  $K_c$  can be adjusted for the stress according to:

$$ET_c = (K_{cb} \times K_s + K_e \times K_r)ET_o \quad (mmd^{-1}) \quad (3.1)$$

where  $K_{cb}$  and  $K_e$  are the basal and soil evaporation coefficients,  $K_s$  and  $K_r$  are the transpiration and evaporation reduction coefficients described in detail by Allen *et al.* (1998) and Rallo *et al.* (2017). The FAO 56 has tabulated  $K_c$  values for major irrigated crops including mango. These values were derived under temperate subhumid climatic conditions (Paco *et al.*, 2019; Pereira *et al.*, 2020). However, there is a major challenge with their transferability to other growing regions given that the crop coefficients vary significantly between sites, with planting density, and management, among others (Mobe *et al.*, 2020; Pereira *et al.*, 2021). To solve the transferability of  $K_c$  problem, Allen and Periera (2009) developed an approach to estimate the crop coefficients from readily available data, effectively extending the FAO 56 paper. Given the need for accurate crop coefficients in orchard water management, the objectives of this study were firstly to quantify the evapotranspiration and its components in a mature high yielding mango orchard growing in a semi-arid environment. Secondly these data were used to investigate options to improve the accuracy of the crop coefficients for mango orchards under subtropical conditions. In the next chapters, models for estimating the crop coefficients will be explored.

### 3.3. Materials and Methods

For this study, data were collected in a mature mango (*Mangifera indica*) orchard, i.e. Block M11 at Riverside Farm (Fig. 3.1). The orchard was a high yielding mature “Tommy Atkins” orchard with an unknown rootstock (though suspected to be either Peach or Sabre). The “Tommy Atkins” cultivar was selected in consultation with the mango industry experts

because it is the most widely planted cultivar in the Mpumalanga Province and across South Africa, accounting for 56.6 and 20.0% respectively of the total planted area ([www.mango.co.za](http://www.mango.co.za)).



Figure 3.1: The 'Tommy Atkins' mango orchard at Riverside farm.

"Tommy Atkins" is an early cultivar, harvested in summer in December/January in South Africa. It produces large ovoid to slightly oblong-shaped fruit weighing between 450 and 700 g. The fruit has a strong blush skin colour which enhances its market potential (De Villiers and Joubert, 2008). The Tommy Atkins fruit has a good shelf life, and it is tolerant to black spot and anthracnose (De Villiers and Joubert, 2008). However, the fruit is susceptible to internal breakdown, jelly seed and stem-end rot (De Villiers and Joubert, 2008). Available historical records indicate that the orchard was established in 1984 making it currently approximately 37 years old when the study commenced in 2021. The tree spacing was 6 m x 5.5 m giving a tree density of 303 trees per ha. The orchard was large in spatial extent, being approximately 9.5 ha with a row orientation of 350° NNE as shown in Fig. 3.1. The terrain of the orchard was on a gentle north-south slope, less than 3 degrees. The trees were trained into an open vase system with an average height, canopy width and length of approximately 4.0, 3.5, and 6.0 metres, respectively. The tree shape was maintained by annual hand and machine pruning often done after harvest in December or January. Key attributes of the orchard are summarized in Table 3.1.

Table 3.1: Characteristics of the mango orchard at Riverside Farm.

ORCHARD CHARACTERISTICS	DESCRIPTION
Block name	M11
Cultivar	Tommy Atkins
Rootstock	Peach/Sabre
Planting date	1984
Plant density (no of trees per ha)	303
Orchard area	9.5 ha
Row orientation	North-South
GPS coordinates	S25°26'51.72"; E31° 33' 18,87"; 321 m asl
Soil texture	Sandy loam
Irrigation system	Microsprinkler
Irrigation delivery rate	50 L/h
Wetted diameter	1.5 m
Tree dimensions - Height - Canopy width - LAI (Tree & orchard)	4.0 m 3.5 m 2.99 ± 0.13 & 1.89 ± 0.28
Average yield	40 t/ha
Cover crop type and status	Indigenous Vlei Bristle Grass ( <i>Setaria incrasatta</i> )

Literature indicates that the rooting system of mango trees is vigorous and dense partly accounting for the apparent resistance of this crop to drought compared to other fruit species (Nel, 2024). The root system consists of a main taproot that penetrates the soil to depths of nearly 6 metres, with profuse and broad-spreading surface feeder roots (Siddiq *et al.*, 2017). The surface feeder roots are desiccation tolerant meaning they can regain full metabolic activity within 72 hours of rehydration after being exposed to severe soil water deficits (Sukonthasing *et al.*, 1991; Asami *et al.*, 2019). Anchor roots are also produced, reaching depths of 1.2 metres. They can spread quite far extending up to 7.5 metres from the main tree stem. In this study, profile pits were dug to establish the extent of the rooting system of the mango trees (Fig. 3.2) as detailed in the next section.

### 3.3.1. Soil Characteristics and Irrigation for the Mango Orchard

Water use by trees is driven by two main environmental factors. These include the available energy, which is provided by climatic factors. The second driver is the available soil moisture.

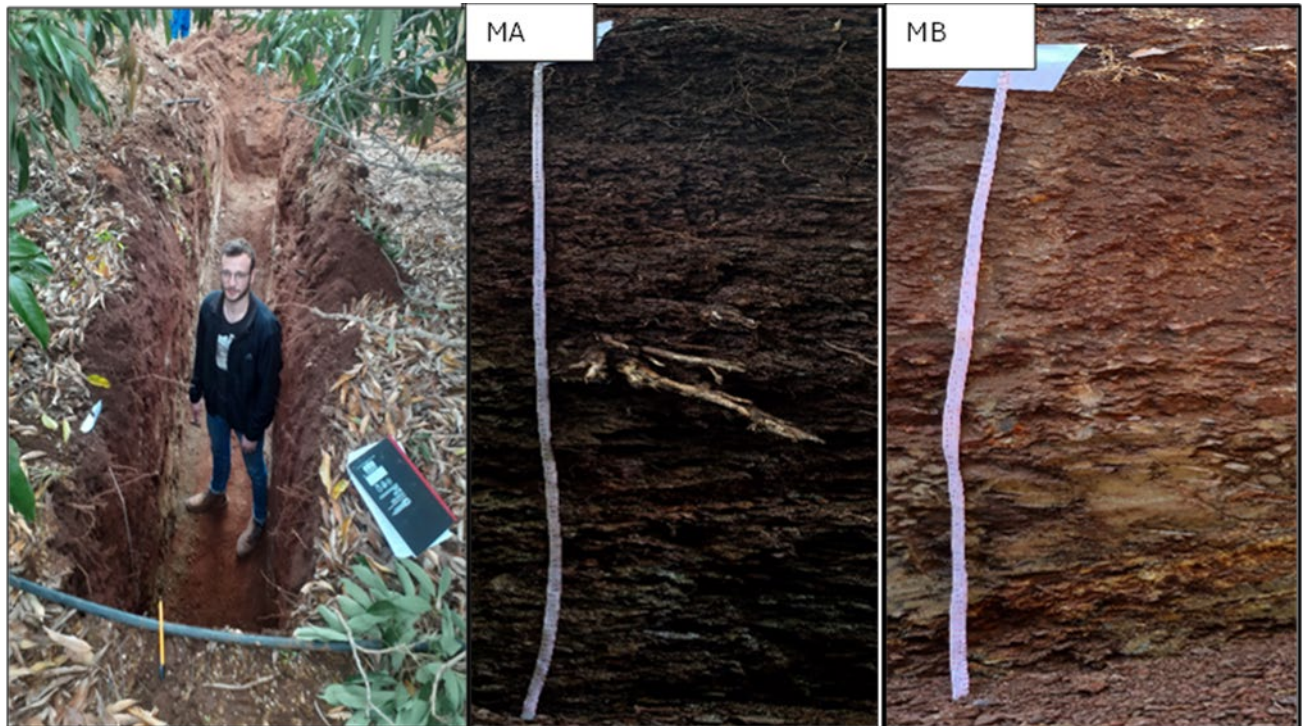


Figure 3.2: The two profile pits made in the mango orchard to study the soil characteristics. The following soil form were classified in the field profile MA was a Inhoek and Profile MB was a Glenrosa.

The available soil moisture is strongly influenced by the soil physical, and to some degree, chemical properties and Fig. 3.2 shows the soil characteristics at the study site. So, the soil characteristics are an integral part of the crop's water use directly influencing the amount of water available for absorption by the roots. The amount of water that is available for uptake is known as the available water-holding capacity (AWC) of the soil. The available water holding capacity (AWC) is the amount of water retained between field capacity (FC) and the permanent wilting point (PWP) in the soil. The FC and PWP are two distinct energy limits at which water is retained in the soil matrix, i.e. -1500 kPa for the PWP and -33 kPa for the FC, respectively (Smith and Browning, 1947). The AWC is affected by a wide range of soil physical and chemical characteristics. Therefore, a detailed soil analysis was conducted in this study by digging two 1.5-metre-deep profile pits one under the tree canopy and the second in the inter-row space (see Fig. 3.2). Each profile pit's visual features were recorded, and approximately one-kilogram soil samples were drawn by hand from each pit. The samples'

physical and chemical properties were then analysed by Labserve (Cape Town). Furthermore, using the Soil Classification, a Taxonomical System for South Africa (1991), the diagnostic horizon for the profile pits was generated, followed by the classification of the soils into soil form (Table 3.2). The diagnostic horizons and properties are shown in Table 3.3 while the soil physical properties are presented in Table 3.4.

The coarse fragment percentage of the Inhoek was moderate between 9% and 29% in the top 55 cm and lower 100 cm, with a sharp increase in the 55 to 100 cm area to 50%. The coarse fragments of the Glenrosa were very high throughout the profile, with a percentage between 50 and 65%. The texture of the soils fell into the loamy sand or sandy loam fractions (Texture Class triangle Fig. 3.3 and Fig. 3.4). The soils had very high sand percentages that never dropped below 50%, with a sharp increase above 75% which occurred in the lower depths. Therefore, the soils had good water infiltration into the profile, but crop rooting potential could be negatively affected (Mazaheri and Mahmoodabadi, 2012).

The soils had moderate clay and silt content between 9 and 27% throughout the profiles. Thus, the soils had moderate water retention ability and good drainage out of the soil profile (Lund, 1959). However, the sharp clay upsurge in the Glenrosa between 10 cm to 60 cm from 16% to 35% made it a luvisol horizon and, therefore, had a detrimental effect on water drainage out of the soil profiles. Using a high-frequency short irrigation pulse was recommended to improve water infiltration into the lower soil levels.

The A horizon of the Inhoek had a moderately high organic carbon (OC) percentage of 1.12%. compared to the subsoil horizons with an OC percentage below 0.60% (Table 3.5). The accumulation of OC in the topsoil of the Inhoek was due to the natural mulch layer formed under the canopy of the mango trees with additional irrigation for 37 years. These conditions promoted carbon absorption in the rhizosphere by stimulating root exudates and provided sufficient metabolic substrates for microorganism activity (Wang *et al.*, 2020). The OC percentages of 1.9% and 1.5% of the soils were significantly lower than 2.5% OC, therefore the OC% of the soils would not contribute to soil AWC (Olness and Archer, 2005).

Table 3.2: Soil topography description data and the associated parent material.

Profile Number and Soil Form	Latitude and Longitude	Terrain Unit	Aspect	Slope	Current Land Use	Parent Material
Inhoek (1)	-25.447924 31.5547226	Valley Bottom	North-West	2%	Mango Production	Colluvial Deposits
Glenrosa (2)	-25.448008 31.55482	Valley Bottom	North-West	2%	Inter-row	Colluvial Deposits

Table 3.3: Soil profile diagnostic horizons and properties

Profile Number and Soil Form	Horizon	Soil depth (cm)	Colour	Structure	Consistency	Mottles
Inhoek (1)	A	0-30	10R 2.5/2	weak fine massive	soft loose	few
	B1	30-55	10R 3/3	weak fine massive	soft loose	few
	B2	55-100	10R 3/2	Moderate medium sub angular blocky	slightly hard slightly firm	common
	B3	100+	10R 2.5/2	Weak medium platy	soft slightly firm	many
Glenrosa (2)	A	0-10	10R 2.5/2	weak fine massive	loose friable	none
	B1	10-60	10YR 2.5/4	weak medium massive	soft	few
	B2	60-140	10Y R3/3	Moderate coarse sub angular blocky	platy	few

Table 3.4: Profile information showing the physical properties of each profile's different horizon.

Profile Number and Soil Form	Horizon	Lab No.	Soil depth (cm)	Coarse Fragment % (v/v)			Fine Earth (%)		
							Sand	Silt	Clay
Inhoek (MA)	A	A22-02702	0-30		29	61	19	20	
	B1	A22-02703	30-55		27	61	15	24	
	B2	A22-02704	55-100		50	62	11	27	
	B3	A22-02705	100-150		9	80	11	9	
Glenrosa (MB)	A	A22-02706	0-10		50	61	23	16	
	B1	A22-02707	10-60		55	50	15	35	
	B2	A22-02708	60-140		65	76	11	13	

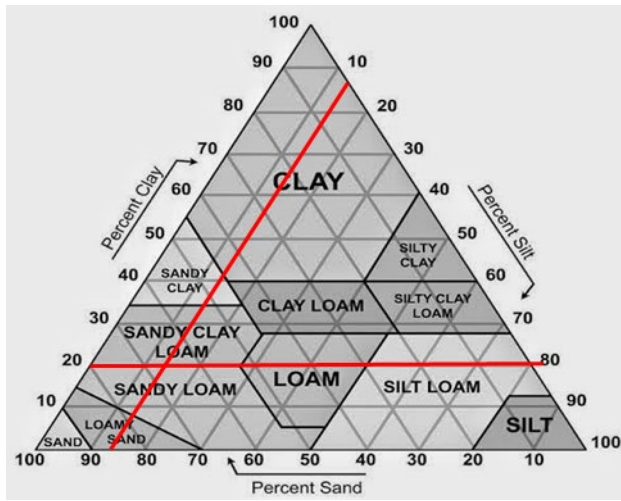


Figure 3.3: A Sandy loam

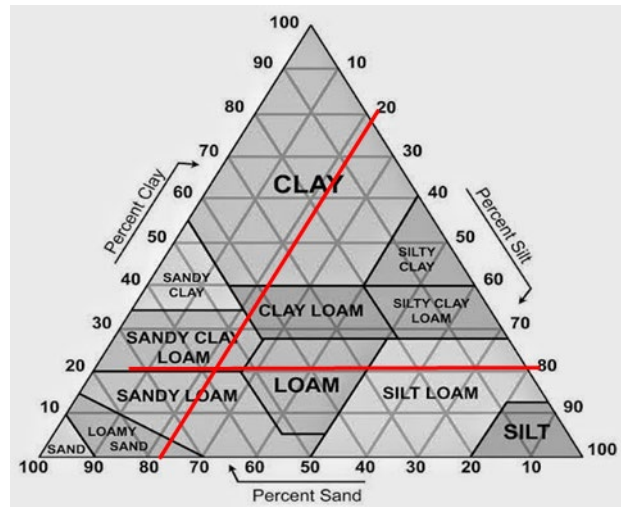


Figure 3.4: Sandy clay loam

Table 3.5: Chemical soil properties: organic carbon percentages, soil pH in KCl. electrical conductivity, exchangeable basic. KCl exchangeable acidity, extractable P.% bases saturation, exchangeable % Na, CEC and ECEC.

Profile Type and Number	Lab No	Organic Carbon (%)	Total OC in profile (%)	pH KCl	P (Ambic I) (mg/kg)	Acid Sat. (%)	Exchangeable %Na (ESP)	% Bases Saturation	EC (dS/M)	Exchangeable Basic Cations (cmolc/kg)					
										Na	K	Ca	Mg	CEC	ECEC
Inhoek (MA)	A22-02702	1.12		5.74	25.7	2.66	2.11	97.34	0.372	0.34	0.81	8.88	5.70	15.732	16.162
	A22-02703	0.47		5.12	3.8	3.04	2.43	96.96	0.39	0.51	0.29	10.03	9.72	20.557	21.202
	A22-02704	0.22	1.9	5.04	1.7	2.43	2.75	97.57	0.488	0.68	0.27	11.27	12.03	24.250	24.855
	A22-02705	0.09		5.04	1.1	2.44	2.31	97.56	0.627	0.49	0.21	8.59	11.53	20.822	21.342
Glenrosa (MB)	A22-02706	0.74		5.86	12.8	2.14	0.84	97.86	0.277	0.13	0.51	10.52	3.69	14.839	15.164
	A22-02707	0.6	1.5	5.21	4.2	2.98	0.87	97.02	0.305	0.17	0.27	11.32	6.94	18.697	19.272
	A22-02708	0.16		4.29	1.1	2.55	1.74	97.45	0.324	0.42	0.20	10.45	12.57	23.646	24.266

The soils had a suitable pH range between 5 and 6 to produce mangoes except for sample A22-02708 with a low pH of 4.29 (De Villiers and Joubert, 2008). The low pH of sample A22-02708 had the following adverse effects on nutrients available for plant uptake. Firstly, phosphorous became insoluble by binding with Al/Fe or absorbing to clays or oxides (McBride, 1994). Secondly, the ability of potassium (K) to absorb to CEC sites are limited by the presence of Al dominating the CEC sites. This is illustrated by the low K value of between 0.2 cmol<sub>c</sub>/kg in the sample (Table 3.4) (Bartlett and Riego, 1972). Lastly, at these low pH levels, the plant root hairs are damaged by toxic levels of manganese and aluminium preventing the plant's absorption of Ca, Mg and K (Alam *et al.*, 1999).

Furthermore, the extremely high calcium (Ca) and magnesium (Mg) concentrations are present in these soils ranging from 8.59 cmol<sub>c</sub>/kg to 11.32 cmol<sub>c</sub>/kg and 3.69 cmol<sub>c</sub>/kg to 12.57 cmol<sub>c</sub>/kg, respectively. At these levels, Ca and Mg can have a detrimental effect on the uptake of K, due to the competition that arises between the different cations. Furthermore, the K levels of all profiles' horizons are below the critical level of 80 mg/kg. Therefore, K applications are required (De Villiers and Joubert, 2008). The accumulation of Ca and Mg can be due to the parent material or is caused by the high acid saturation leading to the upsurge of protons (H<sup>+</sup>) present in the soils, and these protons exchange with Ca and Mg on mineral binding sites (McBride, 1994).

The Ambic I test was conducted to measure the total amount of available phosphorus (P) fixed in the soil. The minimum P requirement to produce mangoes is 20 mg/kg, and soil horizons below this threshold have a P deficiency (De Villiers and Joubert, 2008). The 25.7 mg/kg P in sample A22-02702 is the only horizon with adequate P content to produce mangoes. Furthermore, the rest of the soil horizons fall drastically below the minimum requirement of 20 mg/kg. The low available P in the lower soil horizons is due to the low soil pH between 4.29 and 5.21 at these acidic conditions. Fe oxides make P unavailable for plant uptake by binding strongly to labile phosphorus (McBride, 1994).

The electrical conductivity (EC) indicates the soil's nutrient availability and directly affects crops and soil microbial processes. The soils have a low EC value of 0.627 dS/M which is significantly lower than the critical value of 4 dS/M for sodic soils (Sparks, 2003). The soils have a high CEC and ECEC of above 11 cmol<sub>c</sub>/kg indicating that these soils consist of predominantly low activity and clays (e.g. Kaolinite and Illite) and require regular fertilisation to maintain high productivity (Bell *et al.*, 1966; McBride, 1994). The high ESP % of the soils are extremely low between 0.8 and 3% which is significantly lower than the 15% of brackish soils (McBride, 1994).

Orchard irrigation was applied by a single 50 L h<sup>-1</sup> micro-sprinklers per tree with a wetting diameter of 1.5 metres. Irrigation scheduling was done approximately once to twice a week using a DFM capacitance probe with the “IrriCheck” software. Irrigation volumes were monitored using inline water flow meters (Fig. 3.5).



Figure 3.5: Water flow meter monitoring the irrigation volumes in the mango orchard.

### 3.3.2. Rootzone Soil Water Content

The volumetric soil water content is being measured at several depths in the root zone using the CS616 soil moisture probes (Campbell Scientific, Utah, USA) as shown in Fig. 3.6. Three of the sensors are in the wetted zone at the depths of 30, 60 and 120 cm. The other three probes are in the tractor row also at the 30, 60 and 120 cm depths. Three additional

CS650 probes that measure the volumetric soil water content, electrical conductivity and the soil temperature were also installed.



Figure 3.6: Placement of moisture probes to measure the volumetric soil water content in the mango orchard.

### 3.3.3. Orchard Microclimate

Weather conditions in the study area were measured using an automatic weather station (Fig. 3.7a). The weather station was in an open area within 100 metres of the mango orchard. Ground cover around the station was covered by a short uniform grass surface. Solar radiation was measured using Campbell Scientific's Digital Thermopile Pyranometer (Model

CS320: Campbell Scientific, USA). The pyranometer was mounted facing northwards to avoid self-shading. The CS320 sensor measures radiation in the spectral range 385 to 2105 nm and it has a high measurement accuracy under both cloudy and clear sky conditions. Air temperature and relative humidity was measured using a digital probe (Model: CS215, Campbell Scientific Inc, Logan, UT, USA) installed at the standard 2.0 m height. Wind speed and direction was measured using a digital sonic anemometer (Model: ATMOS-22, METER Group, Pullman, WA, USA) mounted at a height of 2.0 m. Rainfall was monitored with a tipping bucket rain gauge (Model TE 525, Campbell Scientific, Utah, USA). All the sensors were connected to a CR1000 data logger (Campbell Scientific, Utah, USA) storing the data at hourly and daily intervals.

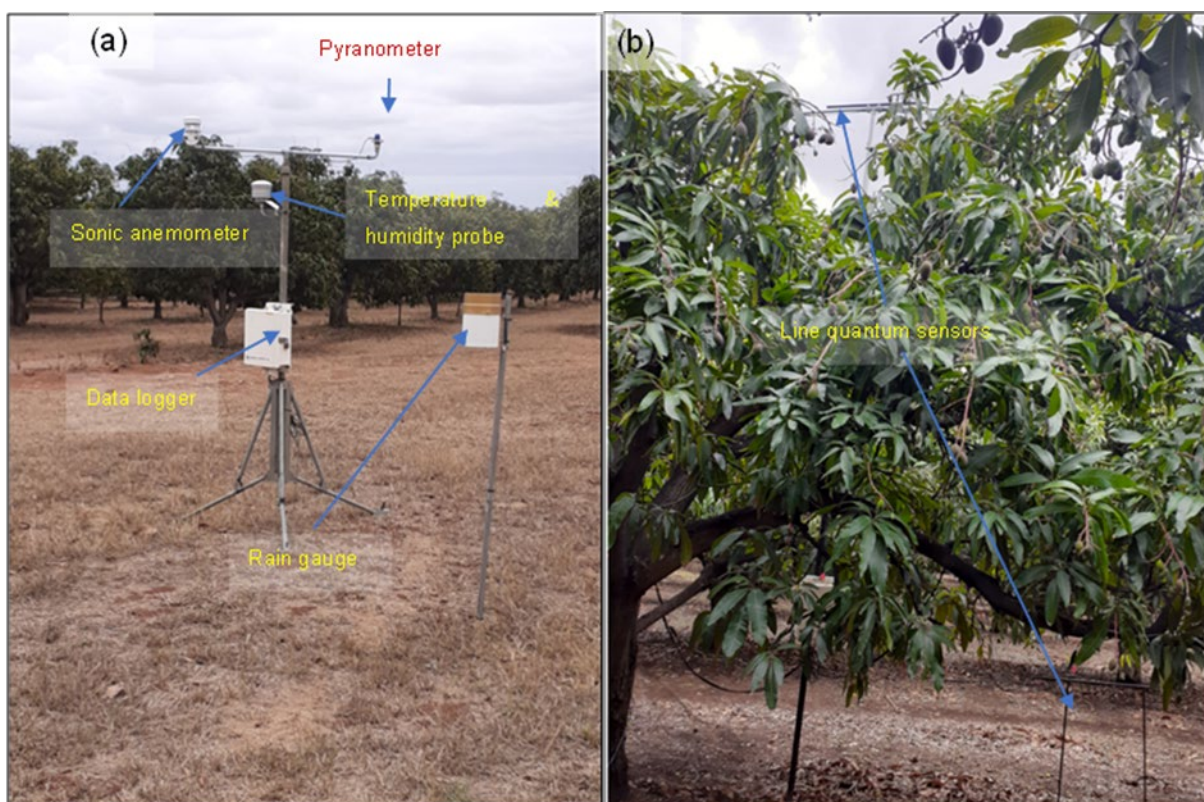


Figure 3.7: (a) Automatic weather station installed to monitor the basic weather variables at Riverside Farm, (b) Measuring light interception by the mango canopy using line quantum sensors.

### 3.3.4. Canopy Temperature and Radiation Interception

The canopy temperatures were measured using two Infrared thermometers (Model: SI-121-SS, Apogee UT, USA) (Fig. 3.7b). The data were measured hourly throughout the experiment. The Infrared thermometers were installed one metre above the canopy to measure an area of 0.33 m<sup>2</sup>. The Infrared thermometers data were compared to the automatic weather station's air temperature to identify periods of possible plant water stress (Blonquist *et al.*,

2009). The radiation intercepted by the canopy is critical for driving water use and other physiological processes. In this study the intercepted Photosynthetically Active Radiation (PAR) was measured using line quantum sensors (Model SQ110-apogee. Campbell Scientific. USA). One sensor was installed above and the other below the canopy about 0.75 m from the ground (Fig. 3.7b). The intercepted radiation (RI) was calculated as:

$$RI = 1 - \frac{\sum_{i=1}^{24} Q_i^*}{\sum_{i=1}^{24} Q_i} \quad (3.2)$$

where  $Q^*$  is the radiation measured under the canopy and  $Q$  is that measured at the top of the canopy. These line quantum sensors were supported on horizontal levelling fixtures aligned in a north-south orientation.

### 3.3.5. Transpiration Measurements

The heat ratio method (HRM) of the heat pulse velocity (HPV) sap flow technique (Burgess *et al.*, 2001) was used to monitor sap flow of four trees in the mango orchard. To install the sap flow sensors, a metal template with three precisely drilled holes aligned along the vertical axis of the trees and spaced at 5 mm apart was used to minimize errors due to probe misalignment (Ren *et al.*, 2017). Four HRM probe sets were installed per tree. Each probe set comprised a central heater that injected heat into the stems and two T-type thermocouples that measured the sapwood temperature at equal distances (about 0.5 cm) up and downstream of the heater. The four probe sets were installed in the four cardinal directions around the trees and at different depths into the sapwood to account for the radial and circumferential variations in the sap velocity (Wullschleger and King, 2000). The probe installation depths were 12, 20, 30, and 40 mm from the outer bark which was about 7 mm thick on average. The probes could not be installed at a larger depth because of the limitations in the reach of the brass sleeve (~ 40 mm) that house the heaters to spread the heat evenly into the wood. The stem diameter at the probe installation positions is shown in Table 3.6. The instrumented trees were selected to represent the range of stem sizes found in the orchard (Fig. 3.8).

The HRM system comprised a single thermally insulated tree box measuring about 35 cm x 25 cm x 10 cm which contained the electronics of the HRM system next to each instrumented tree (Fig. 3.9). Eight T-type thermocouple sensors and four heater probes, each about 1.5 m long were connected to the tree box which also housed a precision thermistor which gave the reference temperature for the thermocouples. Because the reference

temperature sensor was housed in the tree box and not in the datalogger (as in previous designs of the HRM system), this system therefore allowed long cable lengths to be used. In this study, the furthest tree was about 12 m from the datalogger, and this allowed for more representative sampling of the trees. The four tree boxes were connected to one datalogger (Model: CR1000, Campbell Scientific, Inc, Logan UT, USA) via a multiplexer (Model AM16/32B, Campbell Scientific, Inc., Logan UT, USA). The tree boxes and loggers were linked via a 25-core plain wire cable. Pulsing of the heat to the heaters, which lasted about 1 s was done via a control port on the datalogger. The electronics in each tree box were powered by a 7 Ah battery. The sap flow data were also collected at hourly intervals throughout the study period. The heat pulse velocity data were corrected for wounding due to sensor implantation according to the procedure by Burgess *et al.* (2001). Whole-tree transpiration (SF in litres per tree per day) for each instrumented tree were derived as the sum of the sap flows in four concentric rings in the sapwood with flow in each ring calculated as the product of the sap velocity ( $V_i$  in cm/h) at each probe depth and the sapwood area ( $A_i$ ) represented by that probe, i.e.

$$SF_i = \sum_{i=1}^4 A_i \times V_i \quad (3.3)$$

Orchard level transpiration in equivalent water depth units (T, in mm d<sup>-1</sup>) was calculated as the sum of the products of the sap flux density ( $U_i$ ) and the stand sapwood area index (SAI = m<sup>2</sup> of sapwood per m<sup>2</sup> of ground area) for trees in different stem diameter classes such that:

$$T_i = \sum_{i=1}^4 SAI_i \times U_i \quad (3.4)$$

Table 3.6: Details of the sap flow probe installations for the mango trees.

Tree #	Probe #	Tree dimensions		Insertion depths (mm)
		Circum. (cm)	Diam. (cm)	
1	1			12
	2	99.3	15.8	20
	3			30
	4			40
2	1			12
	2			20
	3	107.5	17.1	30
	4			40
3	1			12
	2			20
	3	112.3	17.9	30
	4			40
4	1			12
	2			20
	3	97.2	15.5	30
	4			40

The stem size distribution of 25 randomly selected mango trees is shown in Fig. 3.8. The trees marked in red are those that were selected for instrumentation with the sap flow sensors. Details of the installed sensors are shown in Fig. 3.9.

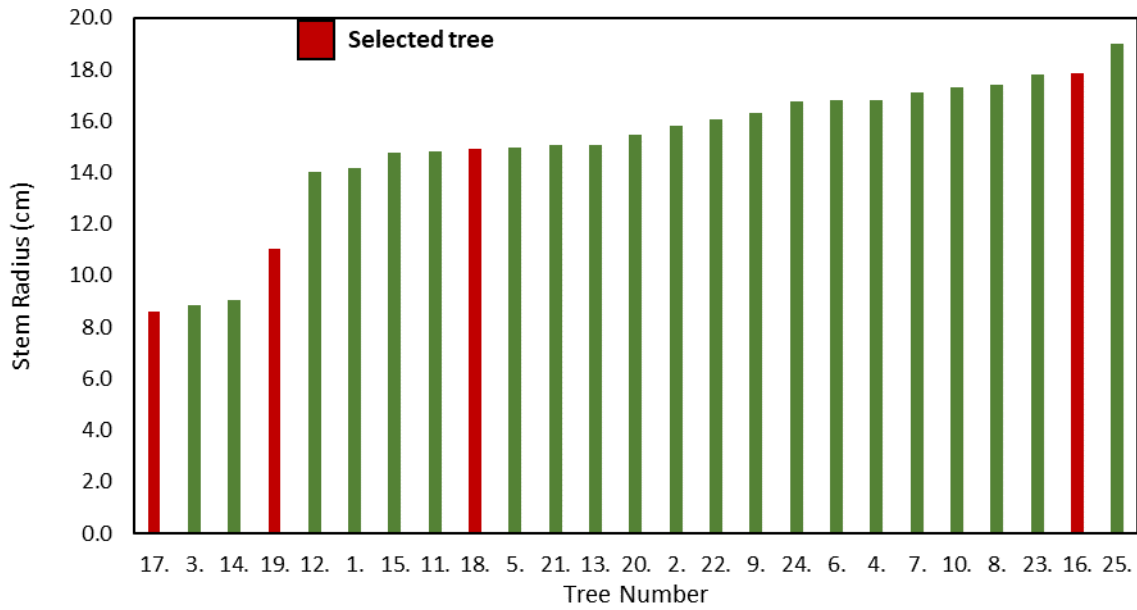


Figure 3.8: Stem size distribution for 25 randomly selected trees with varying circumferences. The four red highlighted trees are trees selected for instrumentation with sap flow sensors.



Figure 3.9: Tree box with four HRM probes. The insert shows an HRM probe, with two thermocouples installed at the top and bottom and a heater installed in the middle.

### 3.3.6. Actual Evapotranspiration

The actual evapotranspiration (ET<sub>c</sub>) from the mango orchard was quantified using the open-path eddy covariance (OPEC) system (Fig. 3.10). The OPEC method is the most accurate and most direct method that measures ET<sub>c</sub> from the vertical turbulent fluxes of water vapour and wind speed in the atmospheric boundary layer. It also measures atmospheric CO<sub>2</sub> exchange. However, this equipment is costly and in high demand. Therefore, it was deployed in the mango orchard from 03 April to 02 July 2022. Gap filling of the missing data was done using a dual source ET<sub>c</sub> model described in the next chapters. The extended open-path eddy covariance (OPEC) system measured the following variables: the net radiation (R<sub>n</sub>), sensible heat flux (H), latent heat flux (LE), and the soil heat flux (G). R<sub>n</sub> measurements were conducted using a single component net radiometer (Model: CNR1, Kipp & Zonen, Delft, The Netherlands), and the G was measured using soil heat flux plates (Model: Hukse Flux, Campbell Sci, Inc., Utah, USA). Soil averaging thermocouples measured the soil temperature above the soil heat flux plates to facilitate the correction of the soil heat flux data for the energy stored above the plates.

The data were collected every 10 Hz and averaged every 30 minutes. The high frequency data were corrected online using the EasyFlux program. Corrections were implemented for air density fluctuations according WPL approach, coordinate rotation, sensor time lags, etc. Corrections were also made for the lack of energy balance closure using the Bowen ratio method described by Cammalleri *et al.* (2010). The shortened surface energy balance equation for an extensive homogenous surface takes the form:

$$LE = R_n - G - H \quad (3.5)$$

Where LE (W/m<sup>2</sup>) is the latent heat flux (i.e. the energy equivalent of evapotranspiration), R<sub>n</sub> (W/m<sup>2</sup>) is the net radiation(W/m<sup>2</sup>), G (W/m<sup>2</sup>) is the soil heat flux and H (W/m<sup>2</sup>) is the sensible heat flux (energy used to warm the air). The Bowen ratio (β) is defined as:

$$\beta = \frac{H}{LE} \quad (3.6)$$

Substituting equation 3.22 into 3.21 and solving the equation for LE gives

$$LE = \frac{R_n - G}{1 + \beta} \quad (3.7)$$

This equation was used to calculate orchard ET corrected for the lack of surface energy balance closure.

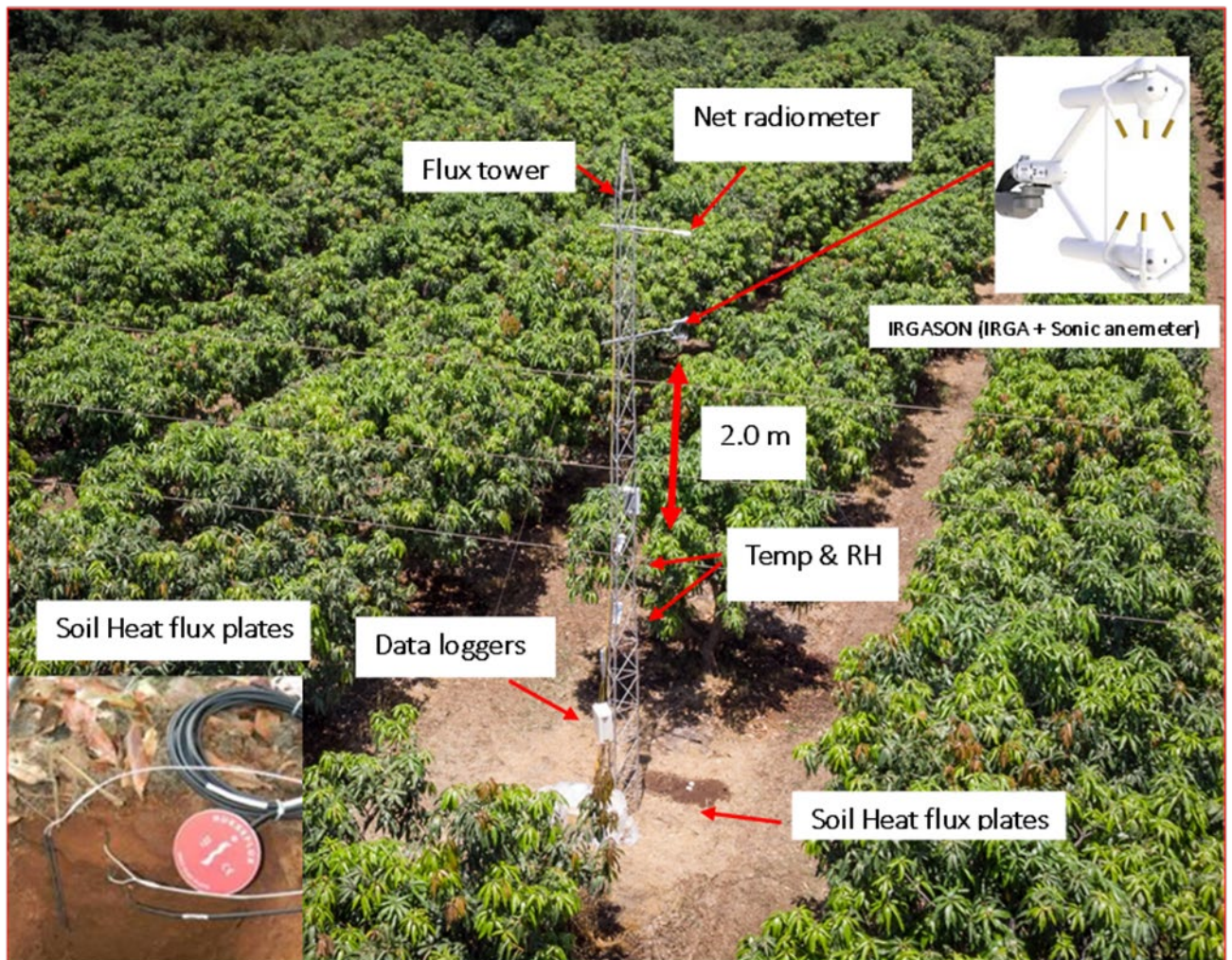


Figure 3.10: The eddy covariance flux tower used to measure orchard evapotranspiration (ET<sub>c</sub>) and the surface energy balance components.

### 3.3.7. Ecophysiological Measurements

To establish the water stress levels of the trees, leaf gas exchange measurements were conducted during four measurement campaigns from August 2021 to July 2022. Spot measurements were performed on four randomly selected leaves, two on the East and two on the West side of the tree. The selected leaves were fully mature, hardened-off, within two metres from the orchard surface and fully exposed to sunlight. Data collection was conducted from predawn to late afternoon using an infrared gas analyser (Model: LI-6400 XT photosynthesis system; Li-Cor, Nebraska, Lincoln, USA). The first diurnal measurements were on 12 November 2021. In subsequent campaigns, a more recent version of the infrared gas

analyser (Model: LI-6800 photosynthesis system; Li-Cor, Nebraska, Lincoln, USA) (Fig. 3.11) was used for the remainder of the trial on 27 February 2022 and 07 July 2022 when the LI-6400 XT developed technical problems.

The following leaf measurements were made: gas exchange parameters, net light-saturated CO<sub>2</sub> assimilation rate ( $A_{max}$ ), stomatal conductance ( $g_s$ ), and intercellular CO<sub>2</sub> concentration ( $C_i$ ), with measurements made when  $A$  stabilises (within 2 min after leaf insertion). Additionally, the photosynthetically active radiation (PAR) and leaf temperature ( $T_{leaf}$ ) was also monitored. The CO<sub>2</sub> concentration of the chamber was maintained at 400  $\mu\text{mol/mol}$ , with a 400  $\mu\text{mol/s}$  flow rate, and the PAR was maintained at 1500  $\mu\text{mol/m}^2/\text{s}$  (LI-6400 XT / LI-6800 LED light source). The relative humidity inside the chamber was retained above 50% to prevent the oscillation of the stomata. The LI-COR software calculated Leaf-to-air vapour pressure deficit ( $VPD_{leaf}$ ).

The photosynthetic light, CO<sub>2</sub>, VPD and temperature response ( $A/C_i$ ) curves were derived using the auto program function of the LI 6800 on two randomly selected fully mature leaves and sun-exposed on each of the four instrumented trees.  $A/C_i$  curves were produced on 23 February 2022, 17 July 2022 and 21 July 2022. Light response curves were produced on 19 November 2021, 26 February 2022 and 8 July 2022. The PAR and CO<sub>2</sub> concentrations within the chamber were altered to produce the light and  $A/C_i$  curves. The light response curves measurements were conducted with the CO<sub>2</sub> concentration controlled at 400  $\mu\text{mol/mol}$  and PAR set at 2000, 1500, 1000, 600, 400, 200, 100, 50 and 0  $\mu\text{mol/m}^2/\text{s}$ . The  $A/C_i$  measurements were made with PAR set at 1500  $\mu\text{mol/m}^2/\text{s}$  and CO<sub>2</sub> concentrations set at 400, 300, 200, 150, 100, 50, 0, 400, 600, 700, 1000 and 2000  $\mu\text{mol/mol}$ . The  $T_{leaf}$  was cooled with Peltier coolers and set within 5°C of ambient temperature, and RH was retained above 50%.

Data were logged within two minutes, and measurements were conducted when  $A$  stabilised. The stability factor of  $A$  was set at less than 0.5  $\mu\text{mol/m}^2/\text{s}$  standard deviations and a less than 0.1  $\mu\text{mol/m}^2/\text{s}$  rate of change per minute. The monomolecular function Causton and MP (1990) described for light response curves, and the Sharkey *et al.* (2007) model for CO<sub>2</sub> response curves was used to produce the best curve fit and analysis of the collected data. Additionally, the stomatal limitation ( $l$ ) was calculated from the CO<sub>2</sub> response curves generated (Bernacchi, 2003). The Causton and MP (1990) model was used to calculate mango's light saturation point, approximately 90% of  $A_{max}$  from the light response curves.



Figure 3.11: Infrared gas analyser measuring leaf photosynthesis, transpiration, and stomatal conductance of a mango tree in Malelane.

### 3.3.8. Water Productivity

The evapotranspiration and yield data were used in equations 3.8 and 3.9 to calculate the biophysical water productivity ( $\text{kg}/\text{m}^3$ ) for a high-yielding mature mango orchard as the ratio of yield produced per unit of total water consumed as follows:

$$WP = \frac{\text{yield}}{ET_c} \quad (3.8)$$

$$WP = \frac{\text{yield}}{(R + I)} \quad (3.9)$$

where yield is the total kg per ha harvested,  $ET_c$  is the total evapotranspiration of the orchard in mm,  $R$  is the total seasonal rainfall in mm, and  $I$  is the total seasonal irrigation in mm.

### 3.3.9. Modelling mango orchard water use

Two approaches were used to estimate the water use and crop coefficients for the mango orchard. The first approach involved use of the modified Allen and Pereira (2009) (A & P) approach as detailed in Mobe *et al.* (2021). The second approach involved the use of a dual source  $ET_c$  model proposed by Shuttleworth and Wallace (1985). It was necessary to apply this model given that the eddy covariance  $ET_c$  data were collected over a short period from 03 March to 03 July 2022. Therefore, this model gap filled the missing data for the other months. The Shuttleworth and Wallace model calculates  $ET_c$  as the algebraic sum of evaporation from the orchard floor ( $E_s$ ) and transpiration ( $T_{act}$ ) from the tree canopy layer, i.e.:

$$ET_c = T_c + E_s \quad (3.10)$$

The detailed equations of the model are shown in Shuttleworth and Wallace (1985) and Dzikiti *et al.* (2018), among other publications. The original Shuttleworth and Wallace model assumes a constant stomatal resistance of about 380 s/m, which is a significant source of uncertainty. In this study, as in many others, e.g. Li *et al.* (2002); Dzikiti *et al.* (2018), we adopt a variable stomatal resistance that is parameterised for mango trees according to the approach by Jarvis *et al.* (1976). Using this method, the stomatal conductance ( $g_s$ , in m/s) at a given time can be calculated from the maximum stomatal conductance ( $g_{max}$ , in m/s) moderated by environmental stress factors such that.

$$g_s = g_{max} \times f(T) \times f(VPD) \times f(\theta) \times f(R) \quad (3.11)$$

where  $f(T)$ ,  $f(VPD)$ ,  $f(\theta)$  and  $f(R)$  are empirical dimensionless stress factors for the air temperature (T), vapour pressure deficit of the air (VPD), the soil water content in the root zone ( $\theta$ ), and solar irradiance (R). The stress factors have values between 0 and 1 with zero representing maximum stress and 1.0 no stress.

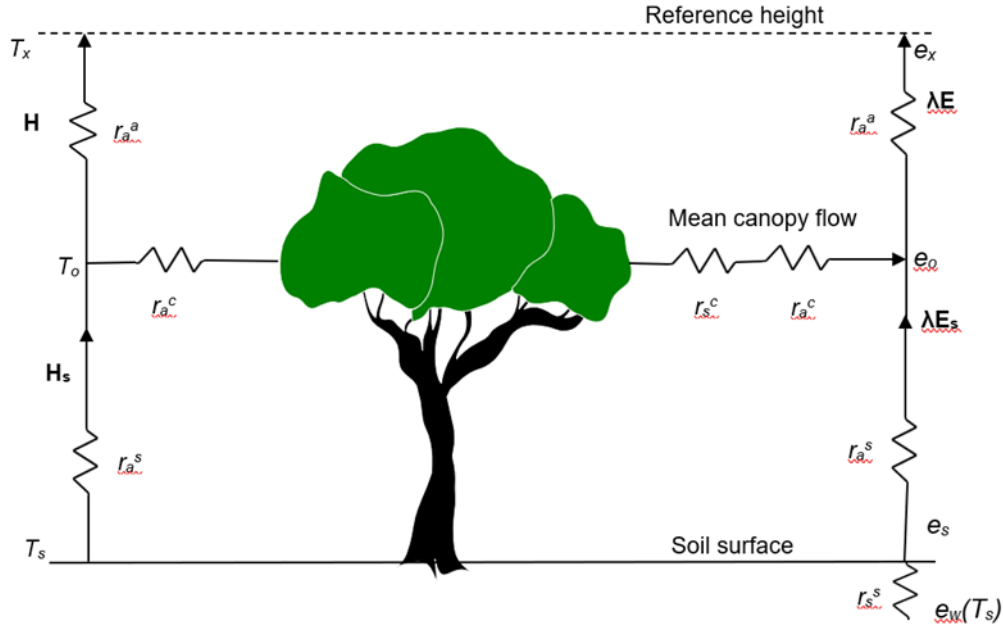


Figure 3.12: Schematic representation of the Shuttleworth and Wallace model (after Shuttleworth and Wallace, 1985).

For the mango orchards, the stress factors were calculated as:

$$f(R) = \frac{R}{R + k_r} \quad (3.12)$$

$$f(T) = \left( \frac{T - T_{\min}}{T_{\text{opt}} - T_{\min}} \right) \times \left( \frac{T_{\max} - T}{T_{\max} - T_{\text{opt}}} \right)^{\left( \frac{T_{\max} - T_{\text{opt}}}{T_{\text{opt}} - T} \right)} \quad (3.13)$$

$$f(VPD) = e^{-k_{vpd} * VPD} \quad (3.14)$$

$$f(\theta) = \begin{cases} 1 & \theta \geq \theta_{FC} \\ \left( \frac{\theta - \theta_{WP}}{\theta_{FC} - \theta_{WP}} \right)^\beta & \theta < \theta_{FC} \\ 0 & \theta \leq \theta_{WP} \end{cases} \quad (3.15)$$

where  $k_r$ ,  $k_{vpd}$ , and  $\beta$  are parameters obtained by model optimization and are defined in Table 3.7. In equation 4.19,  $T_{\max}$  and  $T_{\min}$  are the maximum and minimum temperatures at which the mango stomata close.  $T_{\text{opt}}$  is the optimal temperature for mango trees. In equation 3.15,  $\theta_{FC}$  and  $\theta_{PWP}$  represent the volumetric soil water content at the field capacity and permanent wilting point, respectively. The model was developed using the ModelMaker Software (Cherwell Scientific, UK). Model calibration was done using data from 25 April 2022 to 25 May 2022. These periods were chosen because all the variables, including the eddy covariance ET, were measured in the orchard. Model calibration was done using the Marquardt alternative

procedure in which parameter values that minimised the weighted sum of squared differences between the measured and modelled transpiration and evapotranspiration were selected. These parameters are shown in Table 3.7.

Table 3.7: Parameter values for the dual source evapotranspiration model and optimised parameters for Allen and Pereira Model for a mature mango orchard.

<b>Dual Source Evapotranspiration Model</b>		
<b>Parameter</b>	<b>Value</b>	<b>Description and unit</b>
b1	500	Minimum soil surface resistance (s/m)
b2	-1.1	Curvature factor for soil surface resistance function (-)
$\beta$	0.9	Curvature of the soil water stress factor (-)
$k_r$	232	Parameter for solar radiation stress factor (W/m)
$k_{vpd}$	0.27	Vapour pressure deficit stress factor (kPa)
$r_b$	26.5	Boundary layer resistance (s/m)
$r_{ST}$	335	Minimum stomatal resistance for mango (s/m)
$T_{max}$	45	Maximum air temperature at which stomata close ( $^{\circ}C$ )
$T_{opt}$	26.5	Optimal temperature for growth of mango trees ( $^{\circ}C$ )
$T_{min}$	0	Minimum air temperature at which stomata close ( $^{\circ}C$ )
$\theta_{Fc}$	0.43	Volumetric soil water content at field capacity over entire rootzone ( $m^3/m^3$ )
$\theta_{WP}$	0.13	Volumetric soil water content at wilting point over entire rootzone ( $m^3/m^3$ )
<b>Modified Allen and Pereira Model</b>		
$r_l$	380	Mean stomatal resistance for mango leaves (s/m)
$\alpha$	26	Replacement for the resistance of 100 s/m in equation 35
h	4.3	Average tree height (m)

### **3.4. Results and Discussion**

#### **3.4.1. Climatic Conditions**

The study area at Malelane has a typical summer rainfall regime as shown by most weather variables in Fig. 3.13 for one year from August 2021 to July 2022. The daily radiation intensity was maximum in late spring (September-October) peaking at a about 26 MJ/m<sup>2</sup>/d. The mid-summer (January-February) daily solar radiation were lower reaching a maximum of around 24 MJ/m<sup>2</sup>/d. This trend was a result of the high incidence of cloud cover in summer (Fig. 3.13) and it is expected to lower the water use of the mango trees. The maximum air temperature followed a similar trend to the solar irradiance peaking at around 41 $^{\circ}C$  in October

before dropping to a lower maximum of 33°C in January. Both the daily total solar radiation and maximum air temperatures increased again in late February when the peak of the rain season had passed. As expected, the lowest daily minimum air temperature was reached in winter in June when it reached 7.1 °C. The vapour pressure deficit of the air followed a similar trend to the radiation and temperature with a peak of around 2.5 kPa, although the general maximum values hovered around 2.0 kPa. This is much lower than the values recorded in the drier parts of the country in the northern and Western Cape study where the VPD approached 7.0 kPa. In the peak summer months, the maximum VPD was low hovering between 1.0 and 1.5 kPa likely because of the humid conditions due to the relatively high rainfall received in the area.

The daily wind speeds were generally low during all months averaging less than 1.5 m s<sup>-1</sup> on all occasions. January was the wettest month receiving about 233 mm of rainfall followed by December that received almost 100 mm less (Table 3.8). February was surprisingly very dry receiving only 4.8 mm. This indicates that the site experienced a mid-summer dry spell which is frequently observed in the tropical and subtropical climates in the southern hemisphere (Makarau and Jury, 1997). On the other hand, the monthly reference evapotranspiration, which is a measure of the atmospheric evaporative demand was highest in February reaching about 138 mm, followed by January at 135 mm. It is not clear why the periods of maximum radiation intensity and air temperatures in spring did not have correspondingly high monthly total ETo.

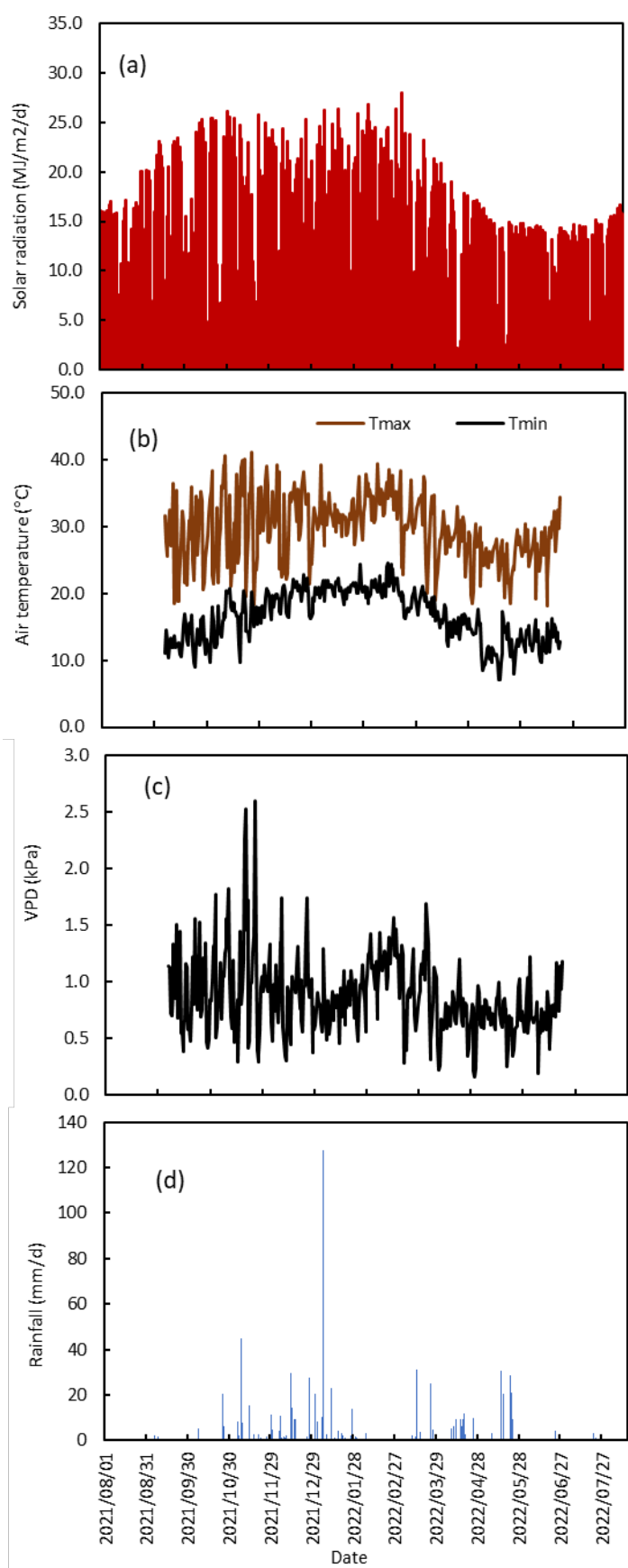


Figure 3.13: Daily weather conditions at Riverside farm in Malelane from September 2021 to August 2022 representing (a) the daily solar radiation, (b) maximum and minimum temperatures, (c) vapour pressure deficit of the air, and (d) rainfall.

The annual total reference evapotranspiration from August 2021 to July 2022 was 1 307 mm which exceeded rainfall which was about 745 mm for the same period. This rainfall amount of a similar order of magnitude with the long-term average for Malelane which is around 700 mm. Because the rain falls during the active fruit growing season, the irrigation water requirements are unlikely to be that high as will be discussed in later sections of this report. So, irrigation essentially supplements rainfall.

Table 3.8: Summary of the monthly weather conditions at Riverside farm from August 2021 to July 2022.

Month	Rs (MJ/m <sup>2</sup> /d)	Tmax (°C)	Tavg (°C)	Tmin (°C)	Rhmax (%)	Rhmin (%)	Uavg (m s <sup>-1</sup> )	Rain (mm)	ETo (mm)
01 August 2021	13.5	36.5	22.8	9.0	100	12	1.5	0.5	102.1
01 September 2021	16.8	40.6	25.1	9.7	100	15	1.2	3.8	114.3
01 October 2021	15.9	41.0	25.3	9.7	100	12	1.3	34.8	125.8
01 November 2021	18.0	39.1	27.3	15.5	100	29	1.1	103.4	127.6
01 December 2021	17.4	39.1	27.7	16.3	100	27	1.0	133.9	128.0
01 January 2022	19.1	35.1	26.7	18.3	100	34	1.1	203.2	134.5
01 February 2022	21.0	39.4	28.9	18.4	100	20	1.2	4.8	137.6
01 March 2022	17.4	38.5	27.4	16.3	100	27	0.9	68.6	121.6
01 April 2022	13.4	37.4	24.8	12.1	100	17	1.2	69.3	90.1
01 May 2022	12.3	33.0	21.9	10.8	100	24	1.1	113.0	76.8
01 June 2022	12.2	28.2	17.6	7.0	100	22	1.3	5.8	71.0
01 July 2022	12.9	30.4	19.1	7.9	100	17	1.2	4.3	77.7
	<b>Total</b>							<b>745.4</b>	<b>1 307.1</b>

### 3.4.2. Rootzone Soil Moisture Dynamics and Canopy Growth

The soil moisture dynamics at different depths in the soil profile corresponded to irrigation and rainfall events (Fig. 3.14 a and b). The soil moisture content declined and had a delayed reaction to watering events (rainfall and irrigation) as the water moved down the soil profile. These effects were more pronounced in the tree row as root water uptake was most evident (Fig. 3.14 a and b). The reduction in soil moisture content in the inter-row was primarily due to evaporation as there were no cover crops. During the season, no water stress was documented in the tree row as evidenced by the soil moisture content data in Fig. 3.14a.

The soil profile beneath the trees received the most water, particularly in the top 20 cm. Here, the volumetric soil water content remained close to field water capacity (Fig. 3.14 a). Rainfall and irrigation rarely infiltrated beyond 500 mm, given that the sensor at 1 000 mm only responded after heavy rainfall on 07 January and 25 August 2022, respectively. Irrigation was

stopped from April to May and reduced from June to July inducing dormancy to promote the initiation of new buds.

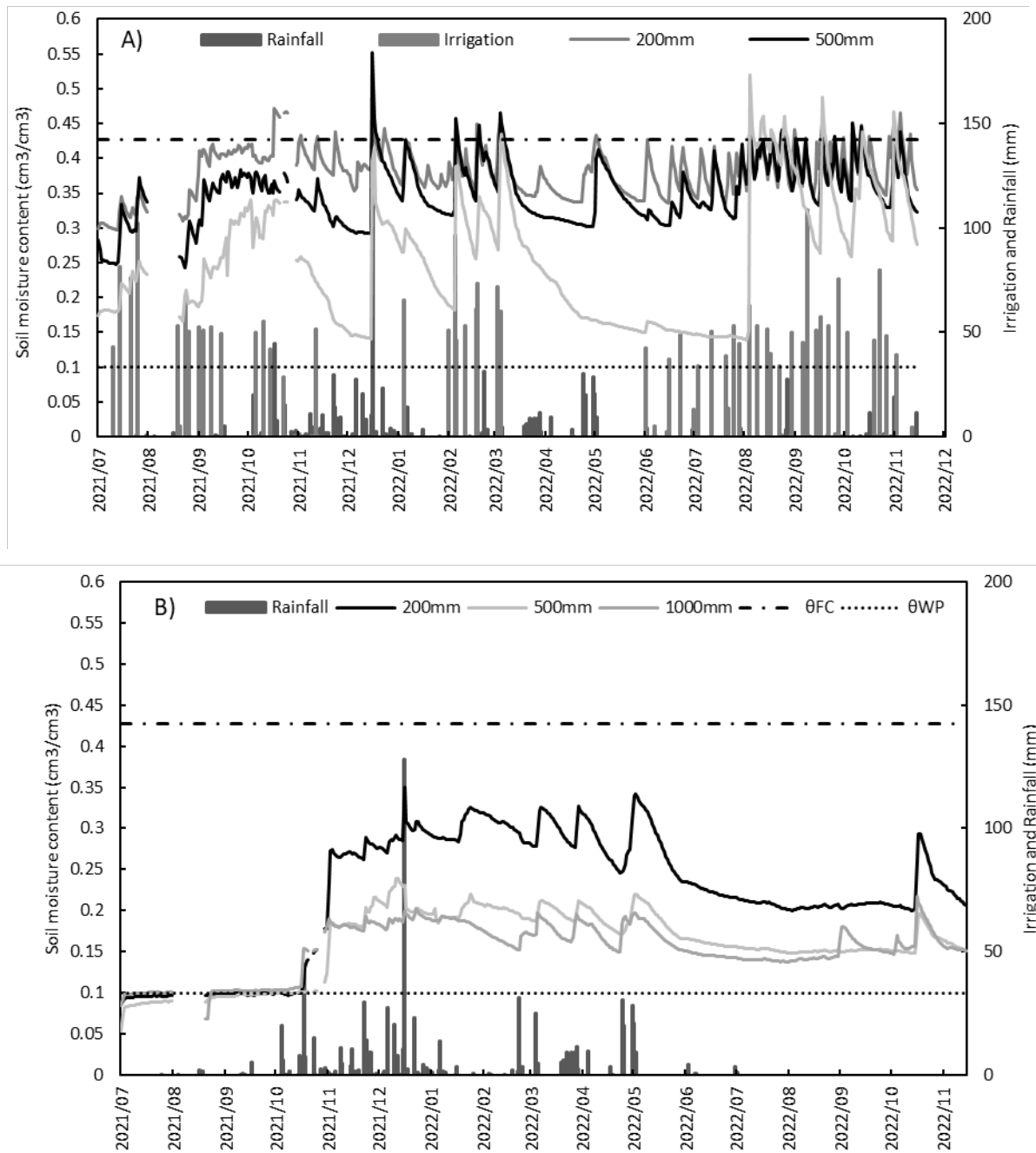


Figure 3.14: The dynamic volumetric soil moisture content in response to irrigation and rainfall events at various depths in a mature full-bearing mango orchard for 2021/22. A) The response of volumetric water content in the tree row reflecting irrigation and rainfall, and B) represents the non-irrigated inter-row area responding to rainfall only. Where 200 mm, 500 mm and 1000 mm is the depth at which the probes were installed in the soil profile.  $\theta_{FC}$  is the field water capacity of the soil and  $\theta_{PVP}$  is the permanent wilting point of the crop.

By comparison with the within-row areas, the soil water content at all depths in between the tree rows remained very low being less than  $0.30 \text{ cm}^3/\text{cm}^3$  (Fig. 3.14 b) except during rain events. Data collection for the between-row region started about four months after the within-row measurements due to equipment malfunctioning. The irrigation frequency was increased to once per week during the winter and spring months due to the absence of rainfall with a total of 108.2 mm and 152.7 mm irrigated in winter and spring and only 84.5 mm irrigated in summer (Fig. 3.14 a).

The LAI of the orchard was measured on six occasions during which the values changed with an average of  $3.3 \text{ m}^2/\text{m}^2$ . The peak LAI of  $3.71 \text{ m}^2/\text{m}^2$  was reached in late December 2021 followed by a drop to  $2.73 \text{ m}^2/\text{m}^2$  in February 2022 due to pruning which had been done in January (Fig. 3.15).

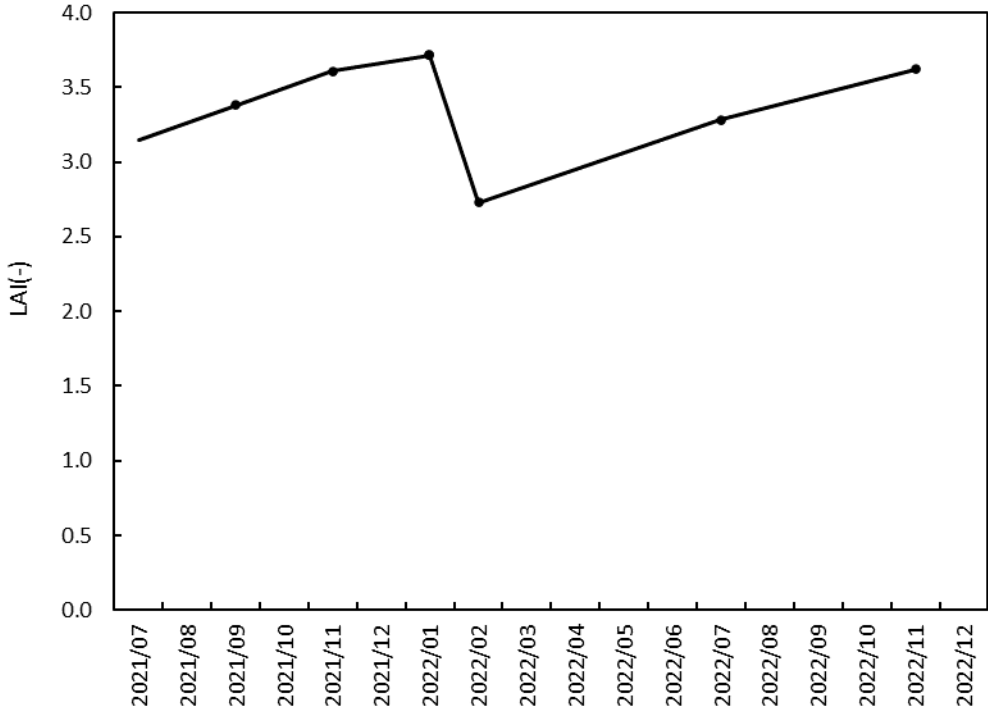


Figure 3.15: Typical seasonal variations in the leaf area index of the mango orchard during the 2021/2022 season. Where I) Indicates when pruning occurred. Measurements were conducted on 06 September 2021, 14 November 2021, 07 February 2022 and 09 July 2022.

### 3.4.3. Stomatal responses to environmental variables

Detailed data were collected on leaf gas exchange to better understand how mango transpiration reacts to changing weather factors. This was thought crucial to comprehend the ecophysiology of this comparatively not-so-widely studied species to ensure accurate model development. However, measurement of the leaf or xylem water potential using the Scholander pressure chamber method was not successful on mango because sap oozed out of the petiole the moment the leaf was excised from the tree. For this reason, tree water status data is not reported in this study. Rather focus was on gas exchange variables, i.e. photosynthesis, leaf transpiration, etc.

The maximum net CO<sub>2</sub> assimilation ( $A_{\max}$ ) peaked at under 6.0  $\mu\text{mol m}^2/\text{s}$  at a temperature between 30 and 35°C. Thereafter, the light-saturated rate of net CO<sub>2</sub> assimilation began to decline slightly. At leaf temperatures above 35°C,  $A_{\max}$  started to taper off only slightly increasing from the 30 to 35°C optimum range (Fig. 3.16 A).  $A_{\max}$  increase in response to rising VPD<sub>leaf</sub> was more prominent and peaked between 2.5 and 3.5 kPa (Fig. 3.16 B), with a rapid decrease in  $A_{\max}$  at VPD<sub>leaf</sub> greater than 3.5 kPa. A similar response was observed between  $g_s$  and VPD<sub>leaf</sub>, with  $g_s$  reaching a maximum between 2.5 and 3.5 kPa, whereafter it declined in a similar manner to that of  $A_{\max}$  in response to increasing VPD<sub>leaf</sub> (Fig. 3.16 C). Under the measured values of  $g_s$ , the relationship between  $A_{\max}$  and  $g_s$  (Fig. 3.16 D) was non-saturating.

The reaction of A to  $C_i$  was linear up to about 400  $\mu\text{mol}/\text{mol}$ , after which the response flattened out as the CO<sub>2</sub>-limited region transitioned into the RuBP-limited region (Fig. 3.16 E). The mean A was roughly three times greater (12.01  $\mu\text{mol m}^2/\text{s}$ ) for  $C_i$  concentrations above 400  $\mu\text{mol}/\text{mol}$  than the mean value of A (A at  $C_i$  when  $C_a=400 \mu\text{mol}/\text{mol}$ ), which was roughly 3.93  $\mu\text{mol}/\text{m}^2/\text{s}$  (Fig. 3.16 E). Based on these response curves, stomatal constraint accounted for roughly 32.7% of all potential photosynthetic limitations. The response of mango leaves to PAR has a sigmoidal curve, with the initial peak of A reached at PAR levels of 400  $\mu\text{mol}/\text{m}^2/\text{s}$  (Fig. 3.16 F). After that, A decreases between 600 and 1400, with an increase at PAR >1 600  $\mu\text{mol}/\text{m}^2/\text{s}$  and a maximum at 2 000  $\mu\text{mol}/\text{m}^2/\text{s}$  (examples of photosynthetic light response curves are given in Fig. 3.16 F). With diurnal PAR values ranging from 50 to 1200  $\mu\text{mol}/\text{m}^2/\text{s}$ , the mean  $A_{\max}$  calculated from light response curves ( $5.14 \pm 2.2 \mu\text{mol}/\text{m}^2/\text{s}$ ) was comparable to the mean seasonal spot measurements of  $A_{\max}$  ( $5.00 \pm 0.35 \mu\text{mol}/\text{m}^2/\text{s}$ ).

This study's seasonal mean  $A_{\max}$  of mangoes was 5.14 mol CO<sub>2</sub>/m<sup>2</sup>/s, which is comparable to González and Blaikie, 2003 results (4.2-9.05  $\mu\text{mol}/\text{m}^2/\text{s}$ ) from spot measurements of leaf gas exchange. Compared to temperate, deciduous fruit and nut crops, including apple, pear, plum, pecan, and almond all have mean  $A_{\max}$  values greater than 15

$\mu\text{mol}/\text{m}^2/\text{s}$ , and mango's net absorption rates were very low (Flore and Lakso, 1989). Furthermore, mangoes' net assimilation rates were also lower than other evergreen subtropical crops such as citrus and macadamia (Syvertsen *et al.*, 2003; Smit *et al.*, 2020). This may be partially explained by the somewhat higher estimated stomatal limits of mangoes (32.7%) than citrus stomatal limitations (23.3%) (Jifon & Syvertsen, 2003) and high sensitivity to high PAR levels above 400  $\mu\text{mol}/\text{m}^2/\text{s}$ . However, several non-stomatal constraints also appear to have an impact on absorption rates.

The orchard photosynthetic potential ( $A_{\text{max}}$ ) and stomatal conductance ( $g_s$ ) are characterised as very low (Table 3.8) with  $A_{\text{max}}$  never exceeding 6  $\mu\text{mol CO}_2/\text{m}^2/\text{s}$  and  $g_s$  fully open under non-stress conditions of 0.1. The  $\text{VPD}_{\text{leaf}}$  during each time period showed lower  $\text{VPD}_{\text{leaf}}$  in the morning and increases in the afternoon with  $\text{VPD}_{\text{leaf}}$  in the mornings of 2.09 kPa and afternoons of 3.25 kPa. The lower  $\text{VPD}_{\text{leaf}}$  readings that were measured on the 27/02/2022 were due to higher relative humidity (RH) and lower solar radiation ( $R_s$ ) during this time (Table 3.9). As expected, the photosynthetic potential was much lower during the 20/07/2022 measurements compared to the 12/11/2021 and 27/02/2022 measurements, this is due to the lower water availability and lower solar radiation during the winter months.

Table 3.9: Mean light-saturated net  $\text{CO}_2$  assimilation rate ( $A_{\text{max}}$ ), stomatal conductance ( $g_s$ ), leaf-to-air vapour pressure deficit ( $\text{VPD}_{\text{leaf}}$ ), leaf temperature ( $T_{\text{leaf}}$ ), relative humidity (RH%) and solar radiation ( $R_s$ ), spot measurements conducted throughout the study period. N is the sample size.

Date	12/11/2021		27/02/2022		20/07/2022		Average	
	AM	PM	AM	PM	AM	PM	AM	PM
$A_{\text{max}}$ ( $\mu\text{mol CO}_2/\text{m}^2/\text{s}$ )	5.84	5.57	3.99	5.10	3.57	3.75	4.47	4.81
$g_s$ ( $\text{mol}/\text{m}^2/\text{s}$ )	0.07	0.05	0.04	0.05	0.03	0.01	0.04	0.04
$R_s$ ( $\mu\text{mol}/\text{m}^2/\text{s}$ )	1720	2080	850	1300	340	450	970	1280
$\text{VPD}_{\text{leaf}}$ (kPa)	2.52	3.67	2.22	2.63	1.54	3.46	2.09	3.25
$T_{\text{leaf}}$ ( $^{\circ}\text{C}$ )	29.82	34.71	29.74	32.61	23.96	34.32	27.84	33.88
RH (%)	35.21	28.78	45.11	42.23	50.69	36.85	43.67	35.95
N	120		138		80			

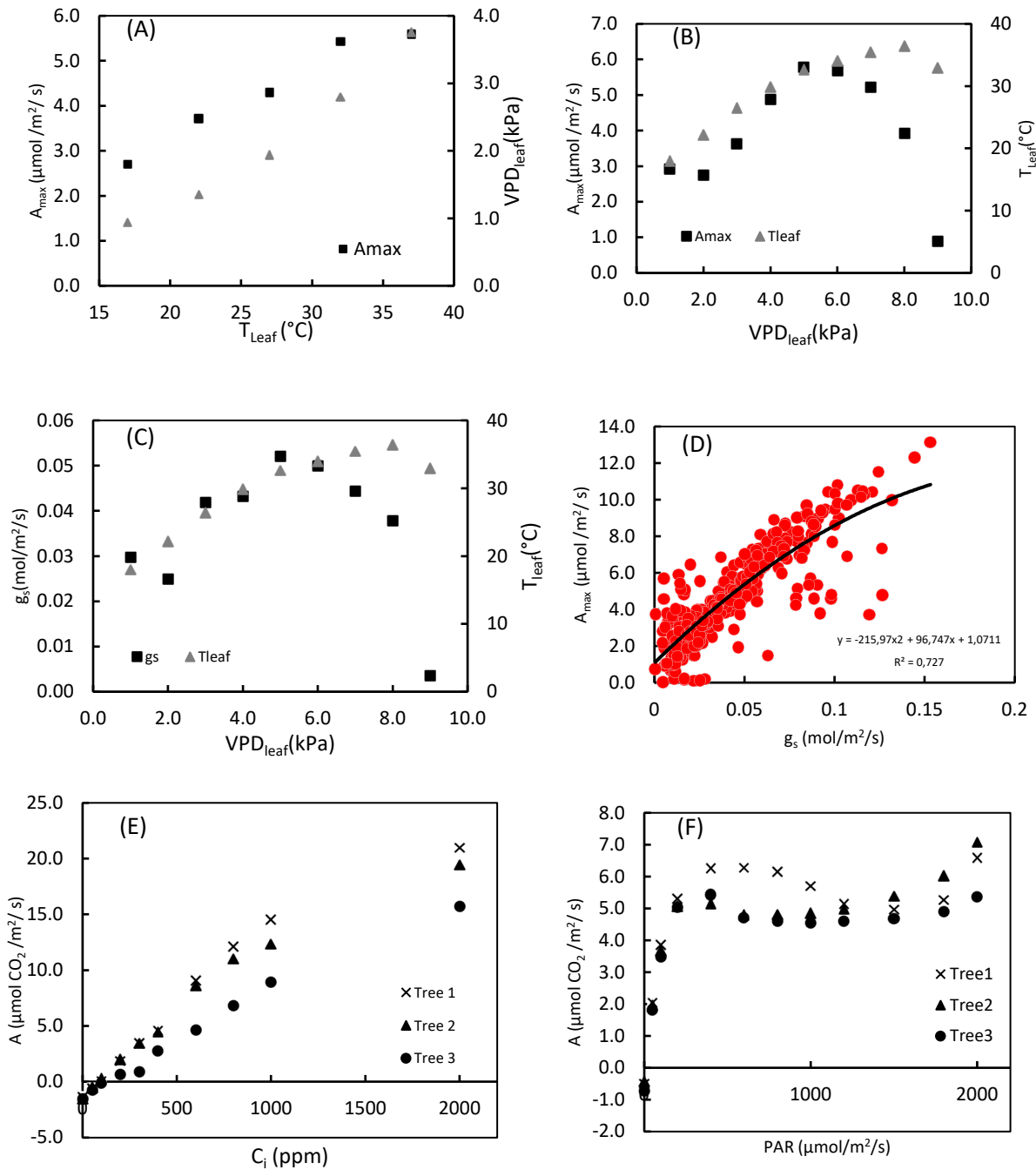


Figure 3.16: Response of  $A_{max}$  to increasing (A)  $T_{\text{leaf}}$  (N= 338) and (B)  $\text{VPD}_{\text{leaf}}$  (N= 338), (C) the response of  $g_s$  to  $\text{VPD}_{\text{leaf}}$  (N= 338) and (D) the response of  $A_{max}$  to  $g_s$  (N= 338). (E) Representative responses of  $A$  to intercellular  $\text{CO}_2$  concentration ( $C_i$ ) showing the method used to calculate stomatal limitations ( $I = (A_{II} - A_I) / A_{II}$ ) as outlined by Long and Bernacchi (2003) of Three experimental trees (N = 99) measured on 2022/02/23 and 2022/07/21. (F) Response of  $A$  to PAR in fully sun-exposed leaves of four trees (N = 126) measured on 2022/02/23 and 2022/07/21. Means followed by the same letter are not significantly different ( $p = 0.05$ ) as analysed using repeated measures ANOVA. Data from figures A-F were pooled data obtained from several measurement campaign.

### 3.4.4. Daily and seasonal trends in measured water use

The seasonal transpiration pattern for a typical mango tree (Fig. 3.17b) closely followed that of the atmospheric evaporative demand (Fig. 3.17a). Both the ETo and daily transpiration (L/tree) reached peaks in late spring declining towards mid-summer due to the high incidence of cloud cover and low atmospheric evaporative demand and rising again in late summer.

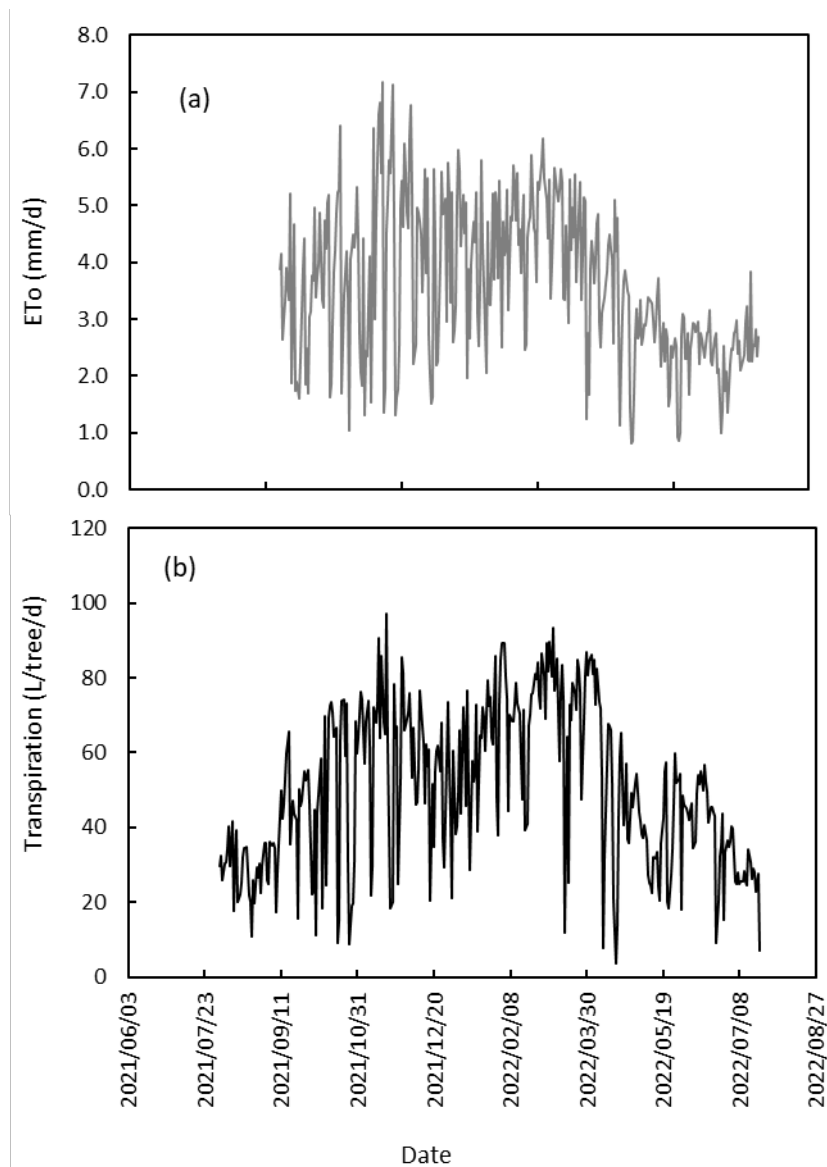


Figure 3.17: (a) Daily reference evapotranspiration; and (b) average daily transpiration of a mango tree from 01 August 2021 to 20 July 2022.

The maximum average daily transpiration of the four instrumented trees peaked at about 97 litres per tree per day on 18 November 2021 (Fig. 3.17b). The mid-summer maximum daily transpiration was lower at 73 litres per tree per day on 28 December 2021. The transpiration then rose again reaching a maximum of about 90 litres per day on 05 March 2022.

The seasonal total water use of the mango orchard was estimated from 01 August 2021 to 31 July 2022 to correspond with the growing season. The total seasonal transpiration of a mature mango tree was about 9 345 L (average of 4 trees). Average daily transpiration over all seasons was about 33.5 L per tree per day from August 2021 to July 2022. The daily transpiration total was strongly driven by climatic factors with the solar radiation showing a strong linear relationship (Fig. 3.18a). The daily total solar radiation explained over 50% of the variation in the measured daily tree transpiration. The daily average VPD on the other hand had a strong curvilinear relationship (Fig. 3.18b) explaining close to 50% of the variation in tree transpiration. Visual inspection of the VPD data suggests that the stomatal closure threshold for mango trees was between 1.0 and 1.50 kPa. Beyond 1.50 kPa, the stomata of the trees began closing.

The reference evapotranspiration, calculated according to the FAO 56 approach combines the effects of the available energy through radiation, and the aerodynamic effects through the VPD and wind speed on the atmospheric evaporative demand. Therefore, it is not surprising that  $E_{To}$  also had a non-linear effect on the daily transpiration (Fig. 3.18c). As expected, increasing soil water deficits (Fig. 3.18d) caused a reduction in the daily total transpiration although the correlation was quite weak compared to the climate drivers. The effect of the atmospheric evaporative demand on the orchard transpiration, and the actual evapotranspiration measured using the eddy covariance system are shown in Fig. 3.19. These data are for the period 03 March to 03 July 2022. The reference evapotranspiration was greater than the other two fluxes although a consistent trend existed between them. An interesting trend can be seen regarding water availability in the orchard either due to rainfall or irrigation and the relationship between evapotranspiration and transpiration. For example, there were dry spells in the orchard with no irrigation or rainfall for the period 29 March to 09 April and again from 02 to 22 June 2022. During these periods, whole orchard  $E_{Tc}$  was accounted for almost entirely by transpiration due to very limited evaporation from the interrow spacing during the dry season. This result also serves to confirm the accuracy of the  $E_{Tc}$  measurements which are expected to be of a similar order of magnitude to the transpiration under dry conditions when orchard floor evaporation was negligible. At other times,  $E_{To} > E_{Tc} > T$ . The fact that  $E_{Tc}$  was lower than  $E_{To}$  implied that the crop coefficient for this mature orchard was less than 1.0.

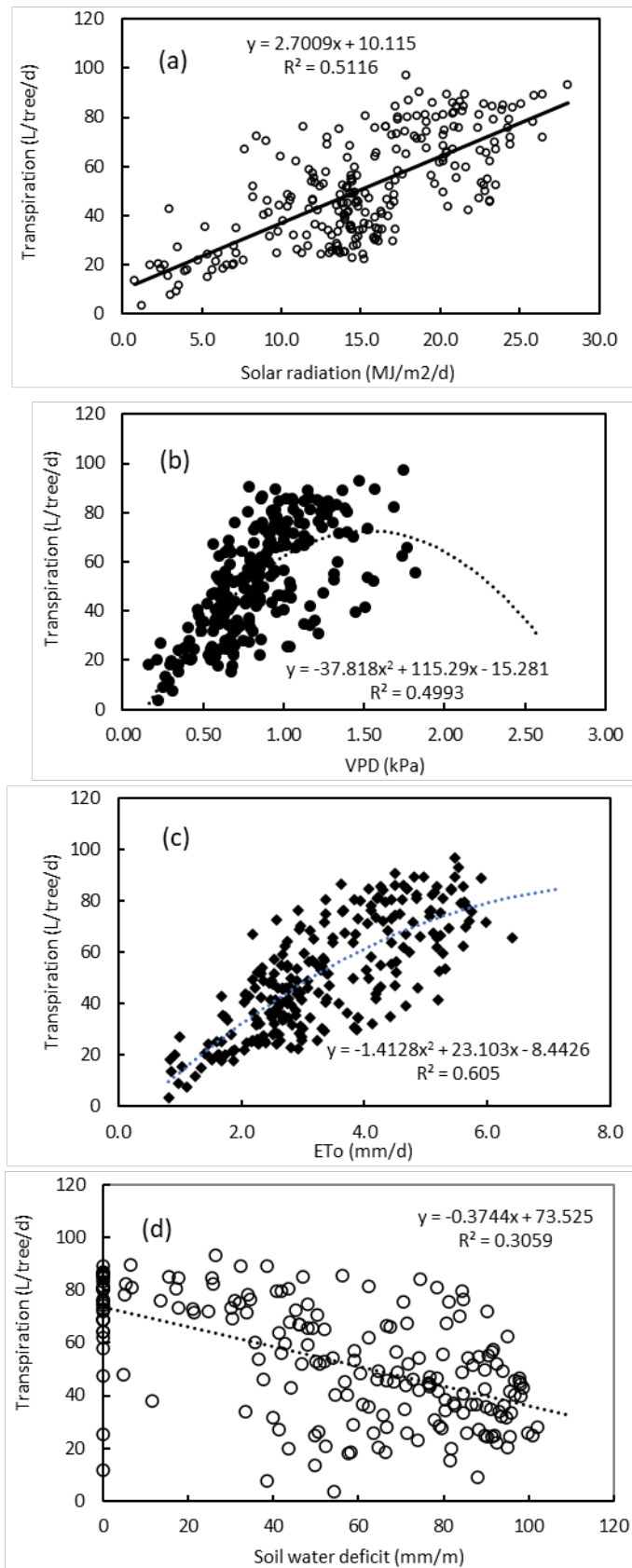


Figure 3.18: Effect of various environmental drivers on transpiration by mango trees which include (a) daily solar radiation, (b) vapour pressure deficit of the air, (c) Eto and (d) soil water deficit.

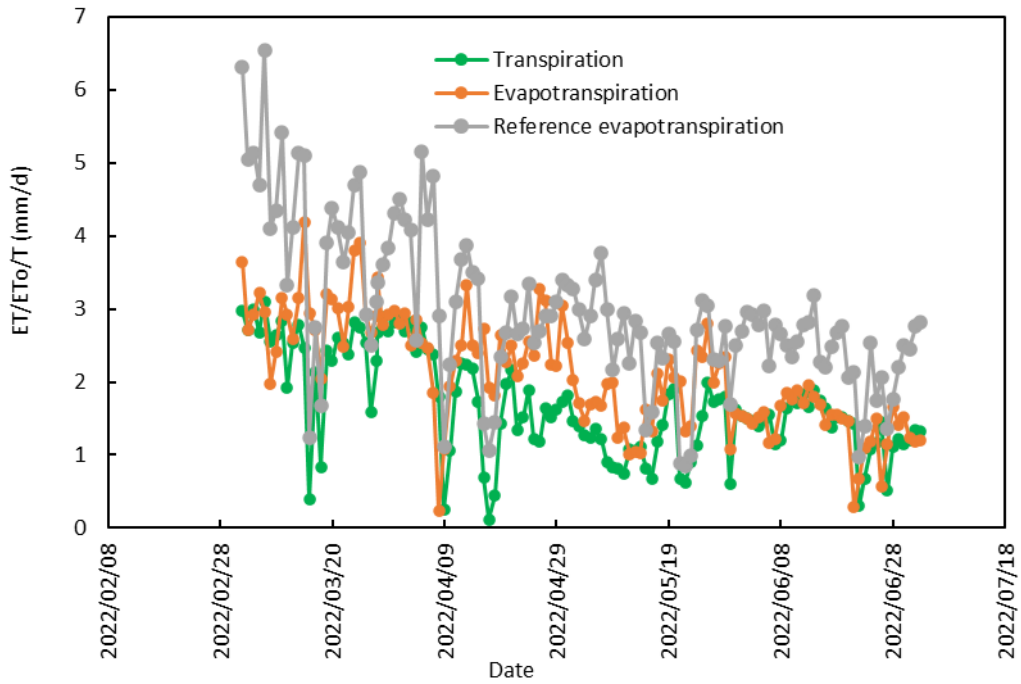


Figure 3.19: Relationship between the whole orchard transpiration, actual evapotranspiration and reference evapotranspiration from March to July 2022.

The atmospheric evaporative demand ( $ETo$ ) explained only about 41% of the changes in the observed evapotranspiration (Fig. 3.20) of the mango orchard. This is in sharp contrast with about 61% for the transpiration shown in Fig. 3.18c. This suggests that the quality of the eddy covariance measured  $ETc$  data was somewhat noisy especially when the soil was dry.

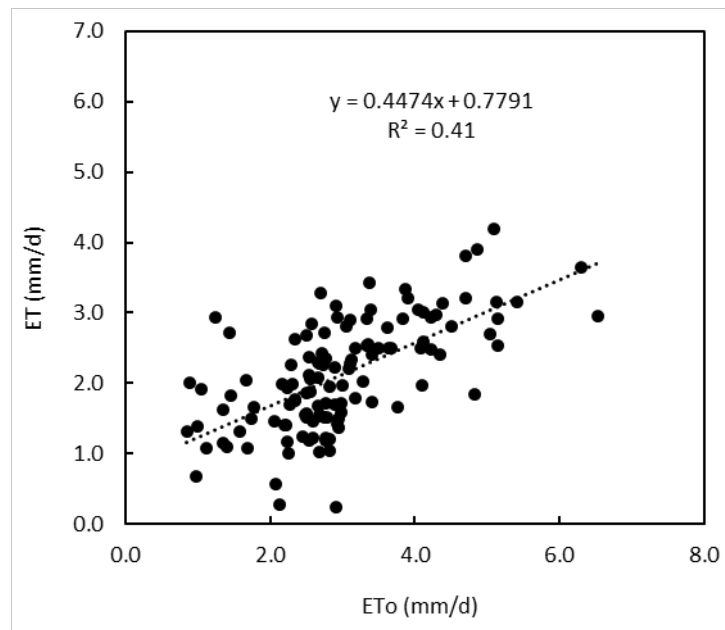


Figure 3.20: Effect of the atmospheric evaporative demand on the actual evapotranspiration of the mango orchard.

This was not surprising given the heterogeneity in the orchard surface due to the wide spacing between the tree rows that exposed large portions of the bare orchard floor. These conditions deviated from the uniform fetch requirements that are essential for the proper operation of most micrometeorological techniques for quantifying  $ET_c$ . The maximum daily  $ET_c$  during the measurement period (April-July 2022) was around 4.2 mm compared to 3.0 mm/d for transpiration.

### 3.4.5. Seasonal trends in modelled water use and crop coefficients for mango orchards

A comparison of the water use estimated by the dual source  $ET_c$  model with the measured values are shown in Fig. 3.21. The data presented is for the period when concurrent transpiration and  $ET_c$  data were collected from 03 March to 03 July 2022. The gaps in  $ET_c$  data in Fig. 3.21b resulted from data loss due to the eddy covariance system malfunction when the batteries ran down. The measured orchard floor evaporation in Fig. 3.21c was calculated as the difference between the measured  $ET_c$  and the measured transpiration. The orchard transpiration component was more accurately modelled by the dual source model than the  $ET_c$  mostly as a result of the greater uncertainty in the orchard floor evaporation simulations (Fig. 3.21c). A statistical comparison of the measured and modelled water use using both the dual source and the modified Allen and Pereira (A&P) approach is shown in Table 3.10. The Nash-Sutcliffe Efficiency (NSE) values for both models are positive suggesting acceptable predictive power for both water use variables. However, comparing all the statistics shown in Table 3.10, it is evident that the modified Allen and Pereira approach had greater accuracy for both the transpiration and evapotranspiration than the dual-source model.

According to Nel (2024), budbreak for 'Tommy Atkins' mangoes in north-easterly South Africa is around early July when temperatures begin to rise. If we designate the first of July as the beginning of the growing season, the typical weekly basal and single crop coefficients are shown in Fig. 3.22. The FAO four-stage crop coefficient curves are shown by the black dotted (Fig. 3.22a) and continuous (Fig. 3.22b) lines and denoted  $K_{cb\text{ FAO}}$  and  $K_{c\text{ FAO}}$ , respectively. To construct the  $K_{cb\text{ FAO}}$  curve (Fig. 3.22a), average  $K_{cb\text{ act}}$  values were calculated for each of the initial, mid and end growth stages. The development and late season trends were obtained by linear interpolation according to Allen *et al.* (1998). The same procedure was followed for the  $K_{c\text{ FAO}}$  curve (Fig. 3.22b) only that average values simulated by the A&P ( $K_{c\text{ A\&P}}$ ) and the dual source model ( $K_{c\text{ mod}}$ ) were used since the measured data did not span the whole year. Seasonal variation in  $K_{cb}$  were small ranging from around 0.45 early in the season (July-August) rising to a peak around 0.53. The measured ( $K_{cb\text{ act}}$ ) and dual source modelled values showed much variation around the four-stage  $K_{cb\text{ FAO}}$  line (Fig. 8a) especially during the periods

when irrigation was withheld from May to end of June. The single crop coefficient curve on the other hand showed clear seasonality (Fig. 8b) and this is attributed to the seasonal changes in evaporation between the tree rows. The crop coefficients predicted by the A&P method closely followed the observed values while the dual-source model-derived values tended to be somewhat lower. During the flowering phase (July), the crop coefficients varied between 0.59 to 0.64 increasing to 0.70 at the fruit set phase (August). During the rest of the growing season (September to January), the  $K_c$  values fluctuated between 0.81 and 0.90 (Fig. 8b).

Applying these crop coefficients to estimate the annual water use showed a superior performance of the modified FAO A&P estimates. The measured cumulative annual transpiration (Fig. 3.23) from January to December 2022 was 677 mm (Table 3.11). The A&P method predicted a cumulative transpiration of 686 mm which was within less than 5% of the measured value while the dual-source model predicted 612 mm which was about 9.6% lower than the measured transpiration. The dual-source model predicted 802 mm (or 8 020 m<sup>3</sup>/ha) annual  $ET_c$  compared to 1 060 mm (or 10 600 m<sup>3</sup>/ha) by the A&P method. According to the dual-source model, the orchard floor evaporative losses accounted for about 24% of the annual orchard water consumption while the A&P method estimated ~ 31% contribution of orchard floor evaporation to the estimated total orchard water consumption.

Table 3.10: Comparison of the daily estimated  $ET_c$  by the modified S&W model and by the FAO Allen and Pereira method for the period 03 March to 03 July 2022.

Variable	Statistic	A&P	SW
Evapotranspiration ( $ET_{act}$ )	R <sup>2</sup>	0.58	0.52
	Slope	0.89	0.81
	NMAE (%)	16.00	25.00
	NRMSE (%)	19.00	23.00
	NSE	0.55	0.51
Transpiration (T)	R <sup>2</sup>	0.74	0.61
	Slope	0.89	0.83
	NMAE (%)	15.00	20.00
	NRMSE (%)	18.00	22.00
	NSE	0.70	0.39

The  $ET_c$  presented in Fig. 3.23 was derived from the Allen and Pereira method. Figure 3.23 also shows that water application (irrigation plus rainfall) closely matched the  $ET_o$ , suggesting that the irrigation was scheduled for the orchard using a  $K_c$  of about 1.0. Our data, however, suggests that the actual orchard crop coefficient ( $K_c$ ) varies throughout the year, and it is generally less than 1.0 (Fig. 3.22).

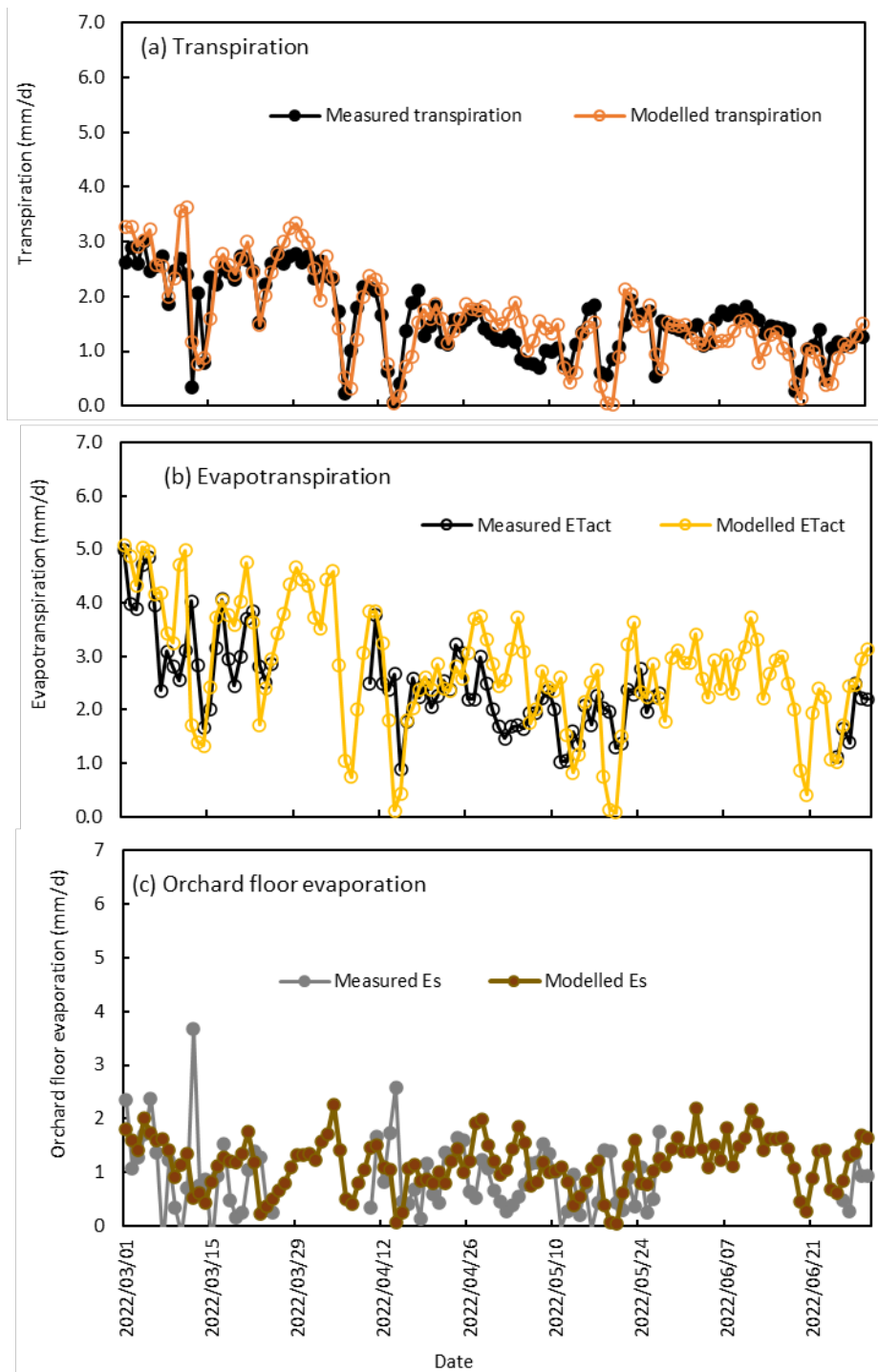


Figure 3.21: Comparison between the measured and dual source (S&W) modelled: (a) orchard transpiration, (b) actual evapotranspiration, and; (c) orchard floor evaporation.

Table 3.11: Summary of the monthly water use, and crop coefficients estimated using the dual-source evapotranspiration model and from the fraction of vegetation cover (A&P) method.

Month	ET model		A & P		K <sub>cb</sub>	ET <sub>c</sub> model		A & P			
	ET <sub>o</sub> (mm)	T (mm)	ET <sub>c</sub> (mm)	E <sub>s</sub> (mm)		ET <sub>c</sub> (mm)	E <sub>s</sub> (mm)	K <sub>c</sub>	K <sub>e</sub>	K <sub>c</sub>	K <sub>e</sub>
Jan-22	133	61	78	11	104	43	0.46	0.57	0.08	0.78	0.32
Feb-22	137	66	74	15	120	54	0.49	0.54	0.11	0.86	0.39
Mar-22	126	76	76	14	108	32	0.61	0.58	0.11	0.86	0.25
Apr-22	92	52	52	10	67	15	0.54	0.52	0.10	0.73	0.16
May-22	77	39	45	8	51	12	0.53	0.53	0.10	0.66	0.16
Jun-22	71	39	38	8	44	5	0.53	0.51	0.11	0.62	0.07
Jul-22	78	29	44	9	50	21	0.38	0.55	0.11	0.64	0.27
Aug-22	103	49	60	12	81	32	0.48	0.58	0.12	0.79	0.31
Sep-22	128	65	73	14	102	37	0.55	0.55	0.10	0.80	0.29
Oct-22	134	75	68	13	109	34	0.58	0.50	0.09	0.81	0.25
Nov-22	137	72	79	13	113	41	0.57	0.56	0.09	0.82	0.30
Dec-22	133	56	66	5	111	55	0.42	0.49	0.09	0.83	0.41
Total	1349	677	802	132	1060	381					

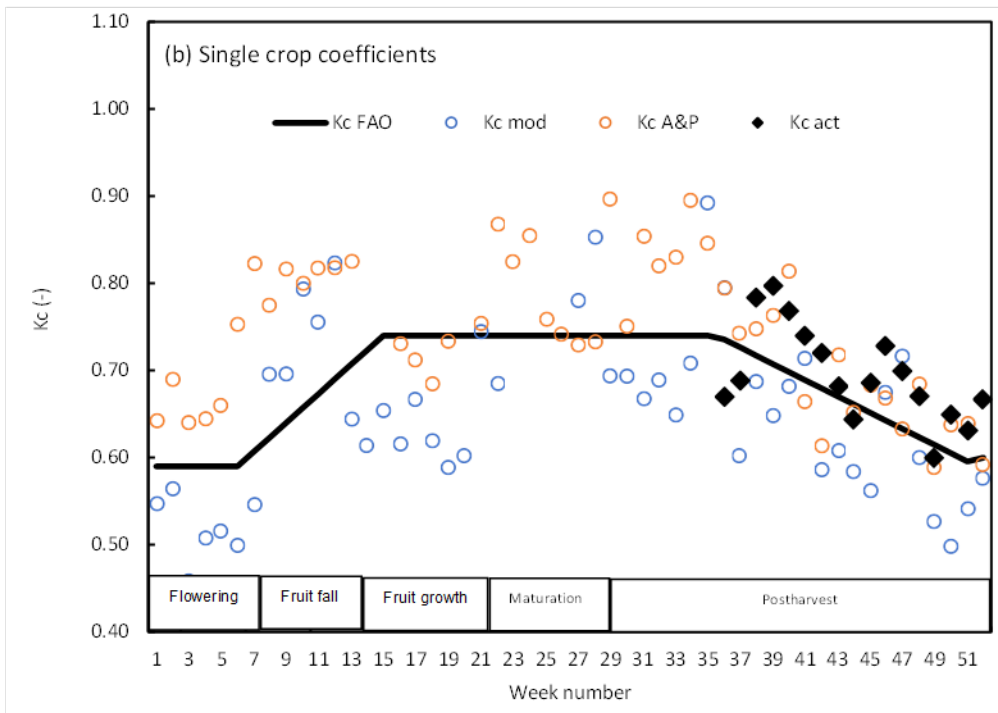
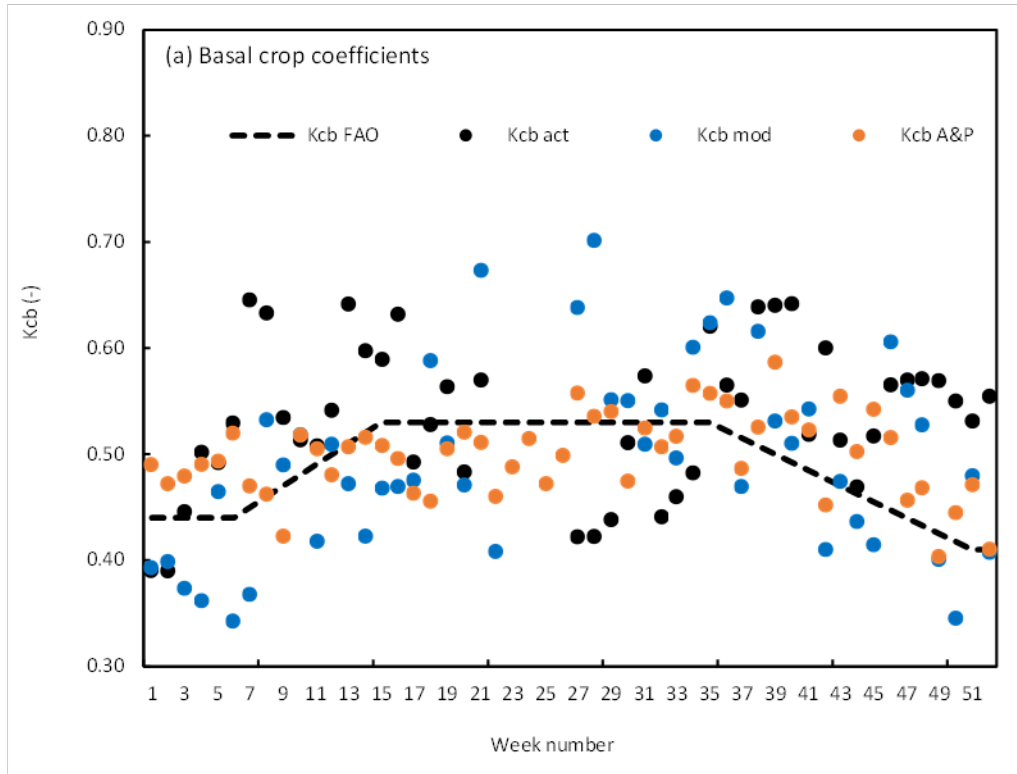


Figure 3.22: Seasonal changes in: (a) the actual and modelled weekly basal crop coefficients, (b) actual and modelled weekly single crop coefficients for the mature mango orchard in comparison with the FAO four stage crop coefficients. Kcb FAO and Kc FAO depict the basal and single crop coefficients from the four stage FAO approach, Kcb A&P, Kc A&P depict the basal and single crop coefficients from the Allen and Pereira method, Kcb mod and Kc mod represents the basal and single crop coefficients modelled by the dual source model.

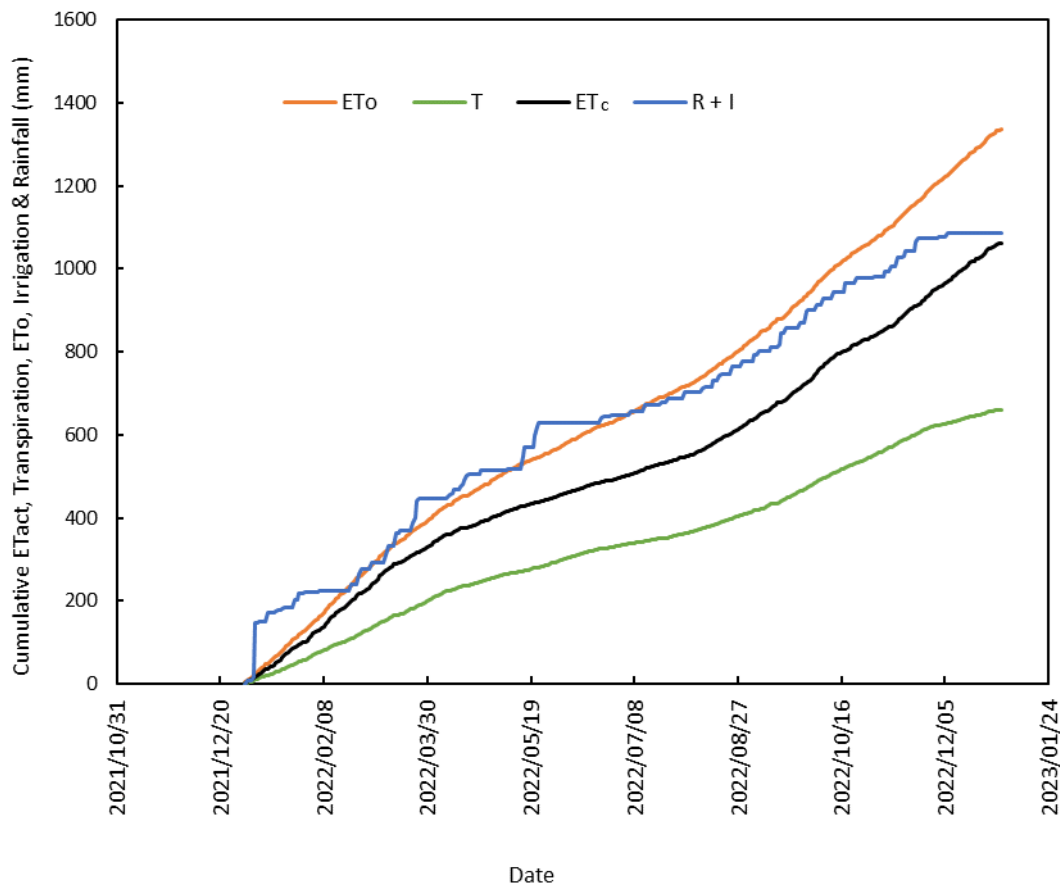


Figure 3.23: Cumulative seasonal fluxes of reference evapotranspiration, modelled evapotranspiration, actual transpiration, and water application (irrigation plus rainfall) from January to December 2022.

### 3.4.6. Discussion

The FAO has developed and tabulated crop coefficients for a range of irrigated crops including mango orchards for ease of access and use by farmers, engineers, consultants, and water resources managers, among others (Allen *et al.*, 1998). However, the data used to develop these crop coefficients were collected under humid temperate conditions (Pereira *et al.*, 2021; Mashabatu *et al.*, 2023). Transferring these values to fields with different growing conditions (climate, soils, management, etc.) has led to uncertainties and this has necessitated numerous studies to derive representative crop coefficients under local conditions (Volschenk *et al.*, 2003; Gush and Taylor., 2014; Girona *et al.*, 2013). Examples of studies that have established crop coefficients for mango orchards include de Azevedo *et al.* (2003) in Brazil, Rodriguez Pleguezuelo *et al.* (2011) and Durán-Zuazo *et al.* (2019) in Spain, and Mohammed *et al.* (2015) in Saudi Arabia, among others. In these studies, orchard water use was quantified using micrometeorological techniques such as the eddy covariance and Bowen ratio methods, soil water balance, and by using lysimeters. These crop coefficients are only applicable to the

specific orchards where they were derived. So, there is a need for robust and accurate methods to transfer them to other orchards which may have different growing conditions.

In this study, we collected detailed data on the water use of a high yielding mango orchard and the associated driving climate and soil data. We used these data to derive crop coefficients for the orchard under subtropical conditions in South Africa. To facilitate their transferability to other orchards, we further used these data to evaluate two independent techniques for estimating crop water use. One method is based on a dual-source evapotranspiration model adopted from Shuttleworth and Wallace (1985). The second method is an extension of the FAO 56 proposed by Allen and Pereira (2009). Orchard evapotranspiration models found in literature vary in complexity, e.g. from the simple big-leaf Penman-Monteith type models implemented in citrus orchards (e.g. Rana *et al.*, 2005) to the more complex multiple source models that recognize the heterogeneous nature of the orchard environment (e.g. Ntshidi *et al.*, 2020; Mobe *et al.*, 2021). Many of these models require large amounts of input data in contrast to the Allen and Pereira (2009) method which was developed primarily to simplify the process of transferring crop coefficients with minimum input data.

The crop coefficients ( $K_c$ ) reported for the 'Tommy Atkins orchard in this study were similar in magnitude and followed the same trends to those observed in other studies. For instance, de Azevedo *et al.* (2003) reported  $K_c$  values that varied through the fruit growing season ranging from 0.45 during flowering and fruit set rising to about 0.93 at fruit maturation. Durán-Zuazo *et al.* (2019) on the other hand recorded a wider range of  $K_c$  values varying from 0.21-0.59 during flowering, (0.57-0.80) during fruit set and 0.31-0.82 during the fruit growth phase. However, these data were collected from an orchard growing on terraces under Mediterranean conditions in Spain which influenced the orchard microclimate and soil water balance conditions.

The measured annual transpiration for the orchard under South African conditions was about 6 770 m<sup>3</sup>/ha and the A&P method gave highly accurate estimates using a constant mean leaf resistance throughout the year. The orchard annual evapotranspiration obtained via the dual source model and the FAO method ranged from 8 000 to just over 10 000 m<sup>3</sup>/ha, respectively. A limitation of the present study is that the annual total evapotranspiration was derived through modelling due to the limited availability of the eddy covariance equipment. However, our water use values are consistent with those reported by Mohammed *et al.* (2015) who obtained annual water consumption rates of 6 527 and 9 790 m<sup>3</sup>/ha/season under drip and full surface irrigation in Saudi Arabia. In another study de Azevedo *et al.* (2003) measured the actual evapotranspiration of a mature mango orchard in Brazil using the Bowen ratio method over a six-month fruit-growing cycle from June to December. They measured an

evapotranspiration total of 555 mm over that period. Again, these water use estimates are in a similar range to those reported in our study which covered a period double that which they reported (i.e. one full year). Estimates of the orchard water use by the dual-source model were somewhat lower than the measured values and had a lower accuracy due to difficulties in accurately calibrating such a model with numerous parameters. On the other hand, limitations of the A&P method are that it does not take water stress into account. Given the possibility of water stress during some stages in the growing season, poor estimates of the A&P method would be expected during these times.

### 3.4.7. Tree water status

Irrigation levels and environmental factors influence tree water status and growth of the fruit and the trees. Tree water status influences the stomatal conductance due to changes in the turgor pressure of guard cells that surround the stomatal aperture (Taiz *et al.*, 2018). The higher the tree water status, the higher the turgor pressure leading to wider stomatal apertures. The stomatal conductance regulates the exchange of water vapour and carbon dioxide across the stomatal pore. High levels of soil water deficit, for example, or excessive atmospheric evaporative demand may lead to stomatal closure which may lower transpiration and photosynthetic rates reducing crop growth and yield. Figure 3.24 shows a typical hourly growth curve for a mango fruit measured in this study.

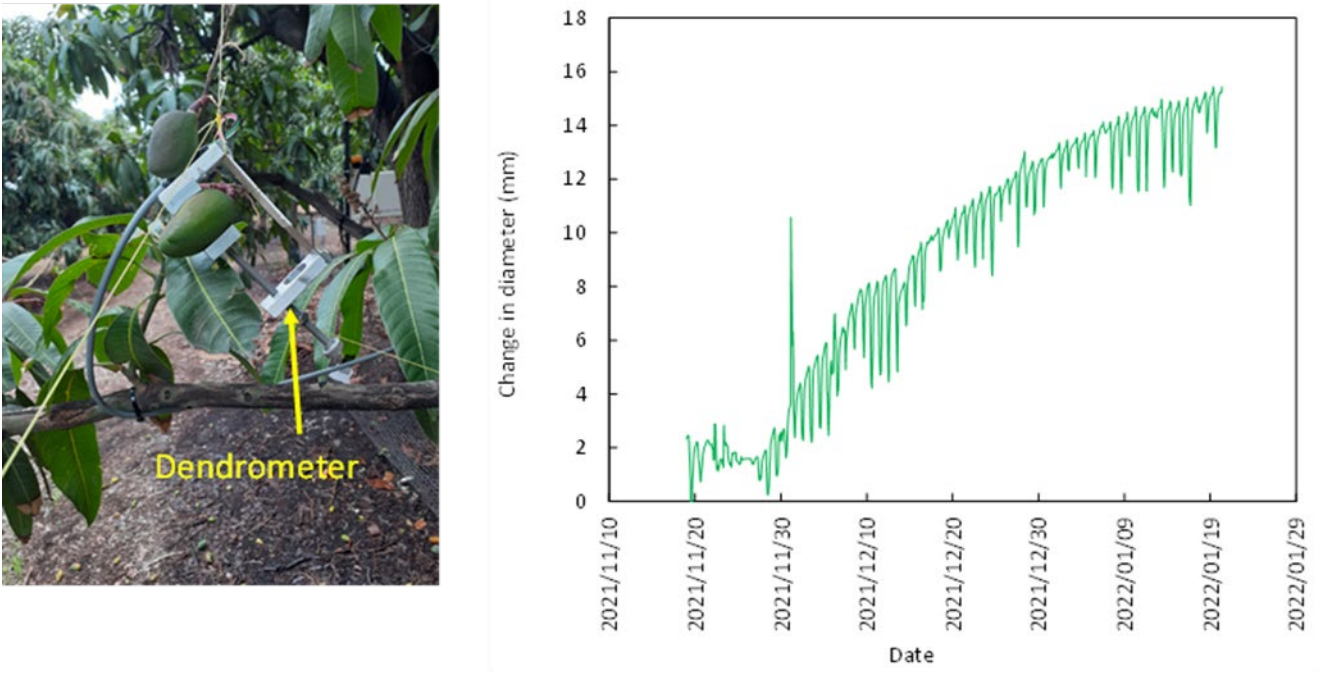


Figure 3.24: (a) Dendrometer measuring hourly growth of the mango. (b) Typical growth curve for a Tommy Atkins mango fruit.

The trend from one day to the next is characterized by shrinking of the fruit at sunrise as water loss via transpiration through the skin of the fruit exceeds water inflows via the xylem. The extent of fruit shrinkage can be used as an indicator of water status of the fruit. Under severe water stress, the fruit is expected to shrink by a larger margin as water loss far exceeds uptake. Therefore, some correlation is expected between the maximum daily shrinkage of the fruit and water deficit in the rootzone of the trees. However, this analysis was not done in the current report due to time constraints. Later in the afternoon, fruit swell as water loss through transpiration becomes less than water inflows driven by a highly negative internal water deficit inside the fruit. In the absence of water stress, the swelling leads to a bigger fruit size the following morning indicating growth. A reduction in the growth rate between consecutive days can also be used as an indicator of tree water status and there are several instances in Fig. 3.25 where stress may have occurred.

Another possible plant-based indicator of water stress is the difference between canopy temperature ( $T_c$ ) and the air temperature ( $T_a$ ). Actively transpiring canopies tend to have low temperatures since evaporation has a cooling effect due to the release of large amounts of energy in the form of the latent heat of vaporization. Figure 3.25a shows a time series of  $T_c - T_a$  against the volumetric soil water content. The results are not convincing that canopy temperature can be used as an indicator of water stress in mango trees. The changes in stem diameter for the mango trees correlated reasonably well with the xylem tension measured using the micro-tensiometer (Fig. 3.25b). But the correlation of both variables with the soil water deficit is not apparent. Detailed trend analysis is required to unravel any correlations between changes in soil water content and the stem diameter variations and changes in xylem tension.

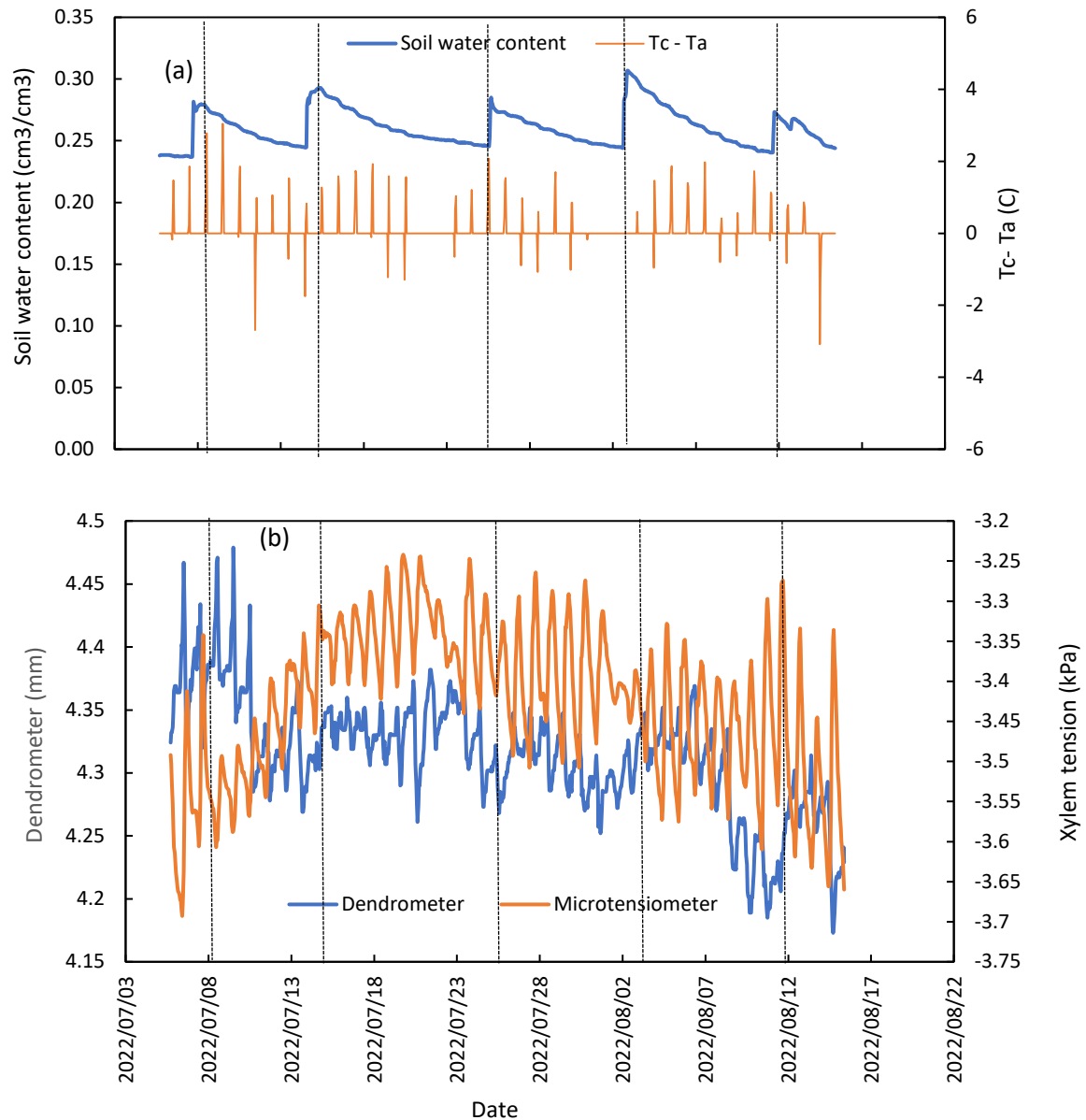


Figure 3.25: (a) Volumetric soil water content and midday canopy-air temperature, and (b) stem diameter variation and micro-tensiometer xylem tension as indicators of water status.

### 3.5. Conclusion

This study provides first quantitative estimates of the water requirements of high performing mango orchards. Results obtained suggest that although mango trees are evergreen species, their water consumption is relatively lower than that of deciduous fruit trees with similar canopy dimensions. The low transpiration rates are supported by corresponding low photosynthesis rates likely because of the lower stomatal conductances than other fruit types. The study orchard was a high-yielding mature mango that produced 44.5 tons/ha of fruit

and a medium-density orchard of 303 trees per ha. The water productivity was about 5.01 kg/m<sup>3</sup> (ETc) and 0.12 kg/m<sup>3</sup> kg/m<sup>3</sup> (under irrigation and rainfall) make this a promising planting density and management practice for mango production in subtropical climates. The present study offers valuable information for improving irrigation management for mango orchards located in the IUWMA.

This study illustrates that evapotranspiration in mango orchards and its partitioning into tree transpiration and orchard floor evaporation can be accurately predicted using the modified Shuttleworth and Wallace model. However, the accuracy appears somewhat lower than estimates from the FAO approach that uses crop coefficients determined from the fraction of vegetation cover and average tree height. The key sources of uncertainty in the dual source model reside with the poor estimates of the orchard floor evaporation given that annual tree transpiration was estimated within 10% of the measured values. The large number of parameters which are difficult to optimise accurately also contributes significantly to the uncertainty. This study also contributes to the growing body of knowledge that supports the use of the Allen and Pereira (2009) approach to estimate accurate crop coefficients. For mango orchards under subtropical conditions in South Africa and possibly other similar environments, a single mean leaf resistance around 380 s/m is sufficient with the reference resistance of 100 s/m replaced with a constant value ( $\alpha = 26$  s/m) to give accurate estimates of both basal and single crop coefficients for mango orchards. The value of  $\alpha$  was obtained by substitution of measured variables into the A&P equations, but we are uncertain if this relationship will hold for mango orchards under different growing conditions than the ones in the study area. Therefore, we recommend further validation of this approach with an independent data set from another mango growing region.

## CHAPTER 4: WATER USE OF MATURE LITCHI ORCHARDS UNDER SUBTROPICAL CONDITIONS

### 4.1. Summary

The Inkomati-Usuthu Water Management Area (IUWMA) in north-east South Africa is a major producer of subtropical fruit. Water resources in this catchment are almost fully allocated. Yet no accurate information currently exists on the water use of major irrigated tree crops such as litchi (*Litchi Chinensis*). This study aimed to quantify the maximum unstressed water use of a full-bearing litchi orchard and to understand the drivers of water use and yield of trees growing under micro-sprinkler irrigation. Actual measurements of tree transpiration and orchard evapotranspiration were done in a 53-year-old commercial litchi orchard over two growing seasons (2021-2023). The trees had huge trunks with thick multiple branches that spread near the base of the stem. Whole tree transpiration was determined as the algebraic sum of transpiration measured from individual branches which were instrumented with the heat ratio method (HRM) of monitoring sap flow. Orchard scale evapotranspiration (ET<sub>c</sub>) was measured over short window periods using the open path eddy covariance method. To explain the observed water use, growth and yield trends, detailed leaf gas exchange data were measured using an infrared gas analyser at selected intervals. To facilitate the scaling up of the results to other litchi orchards, we modified and improved the Allen and Pereira (2009) (A&P) method for deriving crop coefficients from readily available data. The modified A&P method employed a minimum unstressed canopy resistance sub-model derived from a variable stomatal conductance model proposed by Jarvis (1967). The variable leaf conductance was used to replace the constant values in the original A&P method which performed poorly using the litchis data. The measured peak transpiration by an individual tree approached 200 L/d with the two-year average around 125 L/tree/d. However, orchard scale transpiration was quite low peaking at less than 1.3 mm/d due to the low tree density (~70 trees/ha). The stomatal conductance was accurately modelled with the Jarvis-type model ( $R^2 \sim 0.71$  and Nash-Sutcliffe Efficiency of 0.66). The measured annual total transpiration was 335 mm while model simulations gave annual ET<sub>c</sub> of 960 mm 65% of which was lost as orchard floor evaporation. Water productivity of litchis was about 0.85 kg/m<sup>3</sup> of water consumed (ET<sub>c</sub>). If we use a price per kg of litchi to be about R 60, the economic water productivity translates to about R 51/m<sup>3</sup>.

## 4.2. Introduction

Compared to other fruit industries in South Africa, the litchi industry ranks as one of the smallest with an annual production of only 18 000 tons in good years. Litchi orchards are found mostly in the Mpumalanga Province in areas around Malelane and Nelspruit and in the Limpopo Province in the Louis Trichardt, Tzaneen and Levubu areas (DAFF, 2013). These areas have ideal climatic conditions for litchi growth characterized by high summer temperatures (26-32°C max) and low but frost-free winter temperatures. Most of the litchis are consumed as fresh fruit on the domestic market. As little as 1 000 tons is exported mostly to the United Kingdom around the Christmas and new-year period when demand for exotic fruits is high. Litchi originates from the south of China and the trees were imported into South Africa via Mauritius around 1876. The most widely planted litchi cultivars in South Africa are the Mauritius group that include HLH Mauritius, Hazipur, Late Large Red, Muzaffarpur, Rose-Scented and Saharan.

According to DAFF (2013), litchi production in South Africa requires irrigation from flowering in August until the fruit is harvested around December-January, depending on cultivar. Yet water resources in the Inkomati-Usuthu Water Management Area (IUWMA), one of the major production areas in South Africa, are almost fully allocated (3<sup>rd</sup> NWRS, 2022). At present no information currently exists on the water use of litchi orchards in South Africa. This paucity of information compromises water resources management through poor irrigation scheduling, and poor water allocation planning leading to inefficient use of the scarce resource. The overall aim of this study was therefore to quantify the maximum unstressed water use by a mature full-bearing well-managed litchi orchard to close this important information gap. In the next chapters within this report, we use the measured water use data to develop a decision support system that can be used for water allocation planning and to develop irrigation schedules.

Several quantitative techniques are available to estimate the water needs of the litchi trees. Sap flow measurements, for example, enable the estimation of the whole-tree transpiration, hence the tree water use (Allen *et al.*, 2011; Dix & Aubrey, 2021; Zhao *et al.*, 2022). Sap flow measurement techniques in plants are based on thermodynamic, electric, magneto-hydrodynamic, and nuclear magnetic resonance principles. Among the available sap flow measurement techniques, those that use thermodynamic approach are commonly used in the forests and orchards (Čermák *et al.*, 2004). Thermodynamic sap flow measurement techniques are classified into 3 main classes (Kumar *et al.*, 2022) which are namely: (1) heat balance (HB) (Sakuratani, 1981; Sakuratani & Abe, 1985), (2) thermal dissipation (TD)(Granier, 1985, 1987; Hultine *et al.*, 2010; Lundblad & Lindroth, 2002) and (3) heat pulse velocity (HPV)(Forster,

2017; Steppe *et al.*, 2010). Though sap flow measurement in plants is an important tool in determining plant water use, it is impossible to measure the water use of every orchard, thus suitable models are needed to extrapolate measured information to other orchards, as has been successfully achieved in other studies (Dzikiti *et al.*, 2017).

For practical purposes, evapotranspiration (ET<sub>c</sub>) for unstressed orchards is often calculated using the FAO 56 approach in which  $ET_c = K_c \times ET_o$ .  $K_c$  is the crop coefficient which varies with crop growth stages. To facilitate the transferability of coefficients between sites and climatic conditions, Allen & Pereira (2009) derived crop coefficients based on a density coefficient ( $K_d$ ) which is a function of the amount of foliage and the method is referred to as the A&P method (Allen & Pereira, 2009). According to the A&P method,  $K_c$  is computed using the fraction of ground covered by the vegetation, crop height and a stomatal adjustment factor ( $F_r$ ) (Allen & Pereira, 2009; Mobe *et al.*, 2020). The A&P calculated  $K_c$  values were accurate compared to the measured values for various agronomic crops (Pereira *et al.*, 2020). However, for tree crops with different aerodynamic properties to field crops, the A&P method tended to overestimate the crop coefficients (Taylor *et al.*, 2015; Mobe *et al.*, 2020). It was argued that the  $F_r$  in the A&P method was the source of error that caused the overestimation of crop coefficients. Mobe *et al.* (2020) circumvented the problem by introducing a minimum unstressed canopy resistance in  $F_r$  equation and made the A&P method more precise (Mashabatu *et al.*, 2023). This modification by Mobe *et al.* (2020) is applicable when leaf resistance measurements of orchard trees are made so that the minimum unstressed canopy resistance can be computed (Pereira *et al.*, 2020).

Specific objectives of this chapter are therefore to: 1) quantify the maximum unstressed water use (evapotranspiration and its components) by litchi orchards under local conditions; 2) investigate and document the key drivers of water use by litchi orchards, 3) improve a protocol for estimating the crop coefficients for litchi orchards, and; 4) to use the predicted crop coefficients to estimate the dynamics of ET<sub>c</sub> and transpiration over entire seasons. The protocol for estimating the crop coefficients for litchi orchards from readily available data may be used by growers in practice to derive crop coefficients that are appropriate to their specific situations.

## 4.3. Materials and Methods

### 4.3.1 Study Site and Plant Material

Data were collected in a mature litchi orchard (Block L7) at Riverside farm in Malelane (Fig. 4.1). Riverside farm is located about 2.0 km south of the Malelane Gate to the Kruger National Park in Mpumalanga. The block was planted in 1970, so the trees were 51 years when this study commenced in 2021. The cultivar and rootstock were both Mauritius with a spacing of  $13 \times 11$  m giving a tree density of 70 trees per hectare. Total number of trees in the 11.0 ha block was about 943. The trees were irrigated via two micro-sprinklers per tree, each delivering about 50 litres per hour. Irrigation was scheduled according to the DFM capacitance probes installed in the orchard. Their typical irrigation schedule in late spring to early summer comprised 2 to 3 irrigations per week, each irrigation lasting up to 8 hours. Details about the litchi orchard are summarized in Table 4.1.

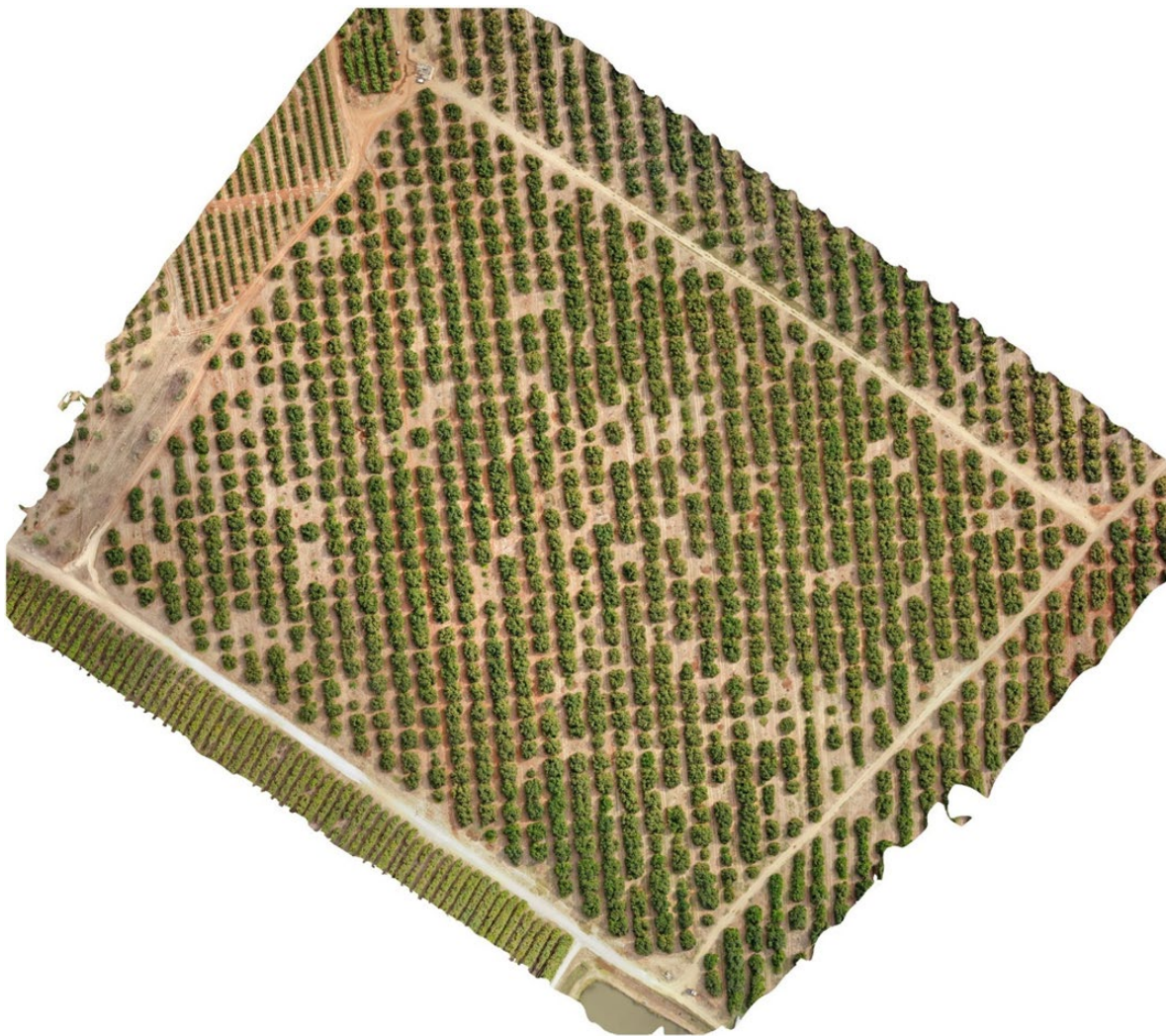


Figure 4.1: Orthomosaic of the litchi orchard created by drone images over the litchi orchard.

Table 4.1: Characteristics of the litchi orchard at Riverside farm.

ORCHARD CHARACTERISTICS	DESCRIPTION
Block name	L7
Cultivar	Mauritius
Rootstock	Mauritius
Planting date	1970
Plant density (no of trees per ha)	70
Tree spacing	11 m x 13 m
Orchard area	13.1 ha
Row orientation	North-South
GPS coordinates	S 25°26'45.49"; E31° 33' 37,21"; 312 m asl
Soil texture	Clayey loam
Irrigation system	Microsprinkler
Irrigation delivery rate	50 L/h
Wetted diameter	1.5 m
Tree dimensions	
- Height	6.0 m
- Canopy width	5.0 m
- LAI (Tree & orchard)	3.14 ± 0.15 & 2.38 ± 0.28
Average yield	1.5 t/ha
Cover crop type and status	Indigenous Vlei Bristle Grass ( <i>Setaria incrasatta</i> )

#### 4.3.2 Soil Water Content and Irrigation Measurements

A two-metre profile pit was dug close to the sap flow instrumented trees using a backhoe loader (Fig. 4.2). This was done to determine the amount of soil water available and to establish the relationship between plant water uptake and soil moisture changes. The CS650 and CS616 sensors were installed horizontally at 30 cm, 60 cm, and 120 cm depths down the profile in both the irrigated zone and the inter row space (see Fig. 4.2). The CS616 sensors measured the volumetric soil water content ( $m^3/m^3$ ) while the CS650 probes measured the volumetric soil water content, electrical conductivity, and soil temperature. The cables of the CS616 and CS650 were labelled for ease of identification, and they were connected to a CR1000 data logger. Irrigation water quantity was monitored using an electronic water flow meter installed on the irrigation line.



Figure 4.2: Soil Moisture probes installed at 30 cm, 60 cm and 120 cm horizontally below the ground in the profile pit.

Soil samples were collected at various depths to determine their physical and chemical properties. The analysis was done at Bemlab in Cape Town and the results are summarized in Table 4.2.

Table 4.2: Typical soil classification analysis for the litchi orchard used in this study. EC = Electrical conductivity; WHC = Water holding capacity.

Crop	Depth (cm)	pH (KCl)	Stone % (v/v)	EC mS/cm	Clay %	Silt %	Sand %	WHC mm/m	Density kg/L
Litchi	0-20	6.15	3	0.462	20	8	72	85	1.3
Litchi	20-80	5.77	3	0.348	27	5	68	74	1.2
Litchi	80-120	5.79	41	0.392	27	8	65	45	1.1
Litchi	120-160	5.40	23	0.408	9	4	87	52	1.1

### 4.3.3 Transpiration Measurements in the Litchi Orchard

Sap flow monitoring on the litchi trees were made using the heat ratio method (see Fig. 4.3). For the complete details of the specific heat ratio method used and the calculation of the overall orchard transpiration refer to Chapter 3. Four trees with different stem sizes were identified and instrumented. Three out of the four selected litchi trees had large stem diameters, and some branched at the base (see Fig. 4.3). In this instance, each branch was considered as a single tree with four probe sets installed as described for the mango trees in Chapter 3. The total volume of sap flow for the whole tree was calculated as the algebraic sum of the sap flow of all the instrumented branches.



Figure 4.3: Heat Ratio Method setup on a litchi tree with multiple stems.

#### 4.3.4 Plant Stress and Radiation Interception Measurements

Leaf area index (LAI:  $\text{m}^2$  of leaf area per  $\text{m}^2$  of ground area) was estimated every 3 months using a canopy analyser (Model LAI2000, Licor, Lincoln, USA). The leaf stomatal conductance ( $g_s$ ) was measured using an infrared gas analyser (IRGA) Model LI-6800 (Li-Cor, Lincoln, Nebraska, USA). Stomatal conductance was measured hourly on tagged, sun-exposed, fully mature leaves on selected clear days (Table 4.3) between sunrise and sunset over the course of the growing season. In all measurements, the IRGA was programmed to collect data at ambient temperature,  $1500 \mu\text{mol m}^{-2} \text{s}^{-1}$  photosynthetically active radiation (PAR) which was provided by the internal red/blue LED lamp and  $400 \mu\text{mol mol}^{-1}$  constant cuvette carbon dioxide ( $\text{CO}_2$ ) concentration which was provided by an external  $\text{CO}_2$  canister connected to the IRGA.

Table 4.3: Specific dates when stomatal conductance measurements were taken on the litchi trees.

Date	Number of Observations	Model Optimization	Model Validation
2022/02/25	8		✓
2022/02/28	11	✓	
2022/11/22	13		✓
2022/11/24	10		✓
2023/07/08	10	✓	
2023/09/30	5		✓



Figure 4.4: Setup of the infrared (IR) thermometer used to continuously measure canopy temperature of litchi trees.

The leaf and stem water potential data were collected using a Scholanda-type pressure chamber on selected days. These data were collected at midday in some cases and

concurrently from with leaf gas exchange from sunrise to sunset according to the schedule in Table 4.3. Canopy temperature was monitored using infrared (IR) thermometers mounted above the tree canopies as shown in Fig. 4.4. These data were collected hourly throughout the study.

#### 4.3.5 Modelling Water Use of Litchi Orchards

##### 4.3.5.1 Modelling Leaf Stomatal Conductance

Most water use models require an accurate representation of the stomatal conductance variable. In this study, the stomatal conductance of the litchi trees was modelled using the Jarvis-type approach (Jarvis, 1976) using data collected at selected intervals during the growing season. According to this method, stomatal conductance can be determined from:

$$g_{ST} = g_{s \max} \times f(R) \times f(T) \times f(VPD) \times f(\theta) \quad (4.1)$$

where  $g_{ST}$  is the modelled stomatal conductance ( $m s^{-1}$ ),  $g_{s \max}$  is the maximum stomatal conductance for litchi ( $ms^{-1}$ ).  $f(R)$ ,  $f(T)$ ,  $f(VPD)$  and  $f(\theta)$  are the solar radiation (R), air temperature (T), vapour pressure deficit of the air (VPD) and volumetric soil water content ( $\theta$ ) stress factors, respectively. These stress factors take values between 0 and 1. The stress factors can be expressed as:

$$f(R) = \frac{R}{R + K_r} \quad (4.2)$$

where  $K_r$  ( $W m^{-2}$ ) describes the curvature of  $f(R)$ .

$$f(T) = \left( \frac{T - T_{\min}}{T_{\text{opt}} - T_{\min}} \right) \times \left( \frac{T_{\max} - T}{T_{\max} - T_{\text{opt}}} \right)^{\left( \frac{T_{\max} - T_{\text{opt}}}{T_{\text{opt}} - T_{\min}} \right)} \quad (4.3)$$

where  $T_{\max}$ ,  $T_{\min}$  and  $T_{\text{opt}}$  are maximum temperature for the complete leaf stomatal closure ( $^{\circ}C$ ), minimum temperature at which stomata close ( $^{\circ}C$ ) and optimum temperature for the growth of the trees ( $^{\circ}C$ ), respectively.

$$f(VPD) = e^{-K_{vpd} \times VPD} \quad (4.4)$$

where  $K_{vpd}$  describes the influence of the VPD stress factor.

$$f(\theta) = \begin{cases} 1 & \theta \geq \theta_{FC} \\ \left( \frac{\theta - \theta_{WP}}{\theta_{FC} - \theta_{WP}} \right)^\beta & \theta_{WP} < \theta < \theta_{FC} \\ 0 & \theta \leq \theta_{WP} \end{cases} \quad (4.5)$$

where  $\beta$  describes the curvature of  $f(\theta)$ .  $\theta_{FC}$  and  $\theta_{WP}$  are volumetric soil water content at field capacity and permanent wilting point in the tree root zone respectively (Dzikiti *et al.*, 2018, 2022; Zhang *et al.*, 1997). The parameters  $K_r$ ,  $T_{opt}$ ,  $K_{vpd}$  and  $\beta$  were derived via model optimization and summarized in Table 4.4. Data used for Jarvis model calibration and validation is shown in Table 4.3.

Table 4.4: Parameter values for the Jarvis model applied to litchi.

Parameter	Description	Value
$\beta$	Describes the curvature of $f(\theta)$ (-)	1.8
$\theta_{FC}$	Volumetric soil water content at field capacity ( $m^3m^{-3}$ )	0.39
$\theta_{WP}$	Volumetric soil water content at permanent wilting point( $m^3m^{-3}$ )	0.18
$G_{s \max}$	Maximum stomatal conductance for litchi ( $mms^{-1}$ )	2.5
$K_{vpd}$	Describes the influence of the VPD stress factor	0.02
$K_r$	Describes the curvature of $f(R)$ (in $Wm^{-2}$ )	1000
$T_{\max}$	Maximum temperature for the complete leaf stomatal closure ( $^{\circ}C$ )	45
$T_{\min}$	Minimum temperature at which stomata close ( $^{\circ}C$ )	0
$T_{opt}$	Optimum temperature for the growth of the trees ( $^{\circ}C$ )	36.5

#### 4.3.5.2 Calculation of Basal Crop Factors ( $K_{cb}$ )

Basal crop coefficients ( $K_{cb}$ ), which represents the transpiration component of evapotranspiration (ET) under well-watered conditions, are calculated by:

$$K_{cb} = \frac{T}{ET_o} \quad (4.6)$$

where,  $T$  is the orchard transpiration, and  $ET_o$  is the reference evapotranspiration for a short grass(Allen *et al.*, 1998). To facilitate the transferability of coefficients between sites and climatic conditions, Allen and Pereira (2009, A&P) defined a density coefficient ( $K_d$ ) which is a function of the amount of foliage. Using this method,  $K_{cb}$  can be expressed in terms of  $K_d$  as:

$$K_{cb} = K_{cb \min} + K_d(K_{cb \text{ full}} - K_{cb \min}) \quad (4.7)$$

where  $K_{cb \text{ full}}$  is the estimated basal crop coefficient under conditions of nearly full cover, that is  $LAI \geq 3.0$ ;  $K_{cb \min}$  is the minimum basal coefficient for bare soil.  $K_d$  can be calculated as a function of mean crop height and the effective vegetation cover:

$$K_d = \min\left(1, M_L f_{c_{\text{eff}}}, f_{c_{\text{eff}}}^{\left(\frac{1}{1+h}\right)}\right) \quad (4.8)$$

where  $h$  is the mean crop height,  $f_{c_{\text{eff}}}$  is the effective vegetation cover and  $M_L$  is a multiplier on  $f_{c_{\text{eff}}}$  describing the effect of canopy density on shading. For mature orchards, a value of 2 is used for  $M_L$  (Mobe *et al.*, 2020). According to the A&P method, a parameter  $F_r$  which is regarded as the  $K_{cb}$  adjustment factor through stomatal control, weather parameters and crop height are used to calculate  $K_{cb_{\text{full}}}$  given by:

$$K_{cb_{\text{full}}} = F_r \left( \min(1.0 + 0.1h, 1.20) + [0.04(u_2 - 2) - 0.004(RH_{\text{min}} - 45)] \left(\frac{h}{3}\right)^{0.3} \right) \quad (4.9)$$

Where  $u_2$  ( $\text{ms}^{-1}$ ) is the mean wind speed measured at 2.0 m height and  $RH_{\text{min}}$  is the minimum relative humidity (%).

The variable mean leaf resistance is calculated using:

$$r_l = \frac{1}{g_{ST}} \quad (4.10)$$

where  $r_l$  ( $\text{s m}^{-1}$ ) is the mean tree leaf resistance and  $g_{ST}$  is the modelled stomatal conductance ( $\text{m s}^{-1}$ ).

In this study, the  $r_l$  in the original A&P  $F_r$  equation was substituted with equation 4.10 to correspond to the variable mean tree leaf resistance throughout the growing season and a standard  $r_l$  of  $100 \text{ s m}^{-1}$  was replaced with a species-specific empirical parameter,  $\alpha$  which represents the minimum unstressed canopy resistance for the litchi tree. The modified  $F_r$  parameter equation took the form:

$$F_r = \frac{\Delta + \gamma(1 + 0.34u_2)}{\Delta + \gamma \left(1 + \frac{0.34u_2}{\alpha g_{ST}}\right)} \quad (4.11)$$

where  $\Delta$  is the slope of the saturation vapour pressure vs temperature curve,  $\gamma$  is the psychrometric constant,  $u_2$  is the mean windspeed at 2 m height,  $\alpha$  is the minimum unstressed canopy resistance (Mashabatu *et al.*, 2023; Mobe *et al.*, 2020) and  $g_{ST}$  is the Jarvis (1976) modelled stomatal conductance. The parameter  $\alpha$  was calculated for the litchi by inverting

equation 11 using measured values of  $K_{cbfull}$  in equation 9 and then solving the A&P equation for  $\alpha$ .

#### 4.3.5.3 Statistical Analysis

The performance of the Jarvis stomatal conductance model and the modelled transpiration was evaluated based on the root mean square error (RMSE), mean absolute error (MAE), the gradient, axis intercept and coefficient of determination ( $R^2$ ) when compared to the measured data. The Nash-Sutcliffe Efficiency (NSE) was used to evaluate the predictive accuracy of the stomatal conductance model (Nash & Sutcliffe, 1970) and this is computed as follows:

$$NSE = 1 - \left[ \frac{\sum_{i=1}^n (Y_i^{obs} - Y_i^{sim})^2}{\sum_{i=1}^n (Y_i^{obs} - Y^{mean})^2} \right] \quad (4.12)$$

Where NSE ranges between  $-\infty$  and 1.0,  $Y_i^{obs}$  is the  $i^{th}$  observation of the stomatal conductance,  $Y_i^{sim}$  is the  $i^{th}$  simulated stomatal conductance,  $Y^{mean}$  is the mean stomatal conductance value and  $n$  is the total number of observations.  $NSE = 1.0$  is regarded as the optimal value and the values that fall between 0 and 1.0 are regarded as acceptable levels of performance (Moriassi *et al.*, 2007). It is important to note that  $NSE \leq 0$  show unacceptable model performance as this indicates that the mean observed value will be a better predictor than the simulated value (Dzikiti *et al.*, 2018).

## 4.4. Results and Discussion

### 4.4.1 Leaf Area Index and Soil Moisture Dynamics

The average monthly orchard leaf area index (LAI) for the trees had a maximum and minimum value of  $3.74 \pm 0.18$  and  $2.40 \pm 0.22$ , respectively (Fig. 4.5). The minimum LAI was observed in December 2022 which coincided with the harvesting and pruning periods.

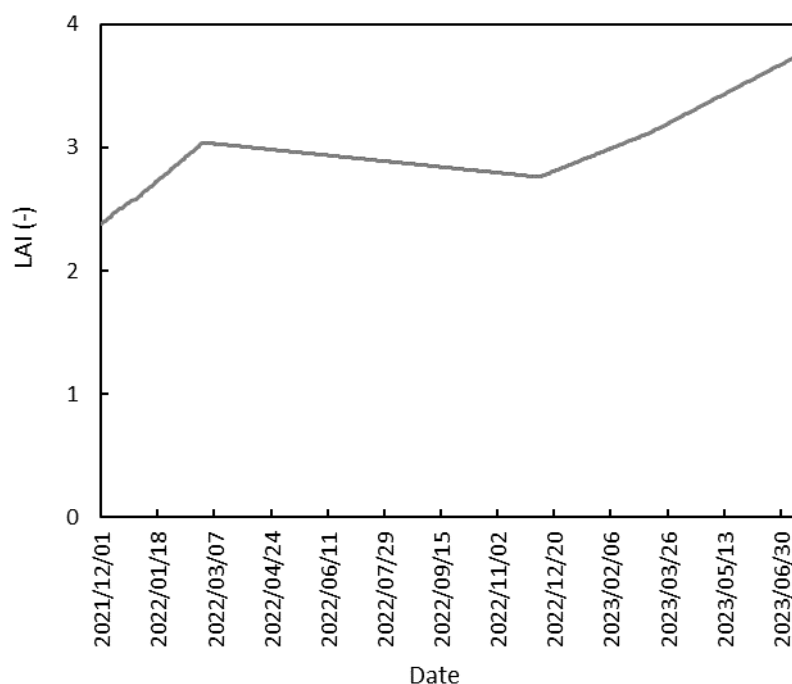


Figure 4.5: Leaf area index of the litchi orchard over the study period.

Although the trees had large canopies, these were spread over a wide area such that the overall LAI was not much higher than that of other tree crops. New flushes were observed in summer after harvest and in spring. Irrigation of the trees continued after harvest presumably to build reserves for new growth in the next season.

The high levels of frequent irrigation are shown in Fig. 4.6 a and b for the within and between row spacings. Within the tree rows the soil water content was maintained close to field capacity at about  $0.40 \text{ cm}^3/\text{cm}^3$  at all depths except the 120 cm depth. Within the tree rows, the soil water content was high at 90 cm and it matched that in the 30 to 60 cm range indicating deep irrigation. But it appeared to be lower at the 120 cm depth where it fluctuated between 0.1 and  $0.2 \text{ cm}^3/\text{cm}^3$ . The soil water content for the shallow probes between the rows (Fig. 4.6b) were relatively high reaching between  $0.36$  and  $0.37 \text{ cm}^3/\text{cm}^3$  because of the larger area wetted by the micro-sprinklers. However, the soil water content at 90 cm depth were similar between and within the tree row spacings. A typical irrigation cycle in this orchard lasted between 8 to 10 hours suggesting that between 400 and 500 litres of water were given per tree during each irrigation event to match the high-water consumption by the trees (see next section). There was a heavy rainfall event around 26 February 2023 which wetted the entire soil profile reaching beyond 120 cm. However, these rainfall data are not included in the figure. Irrigation of the orchard was stopped at the end of March and resumed in July when new flushes emerged.

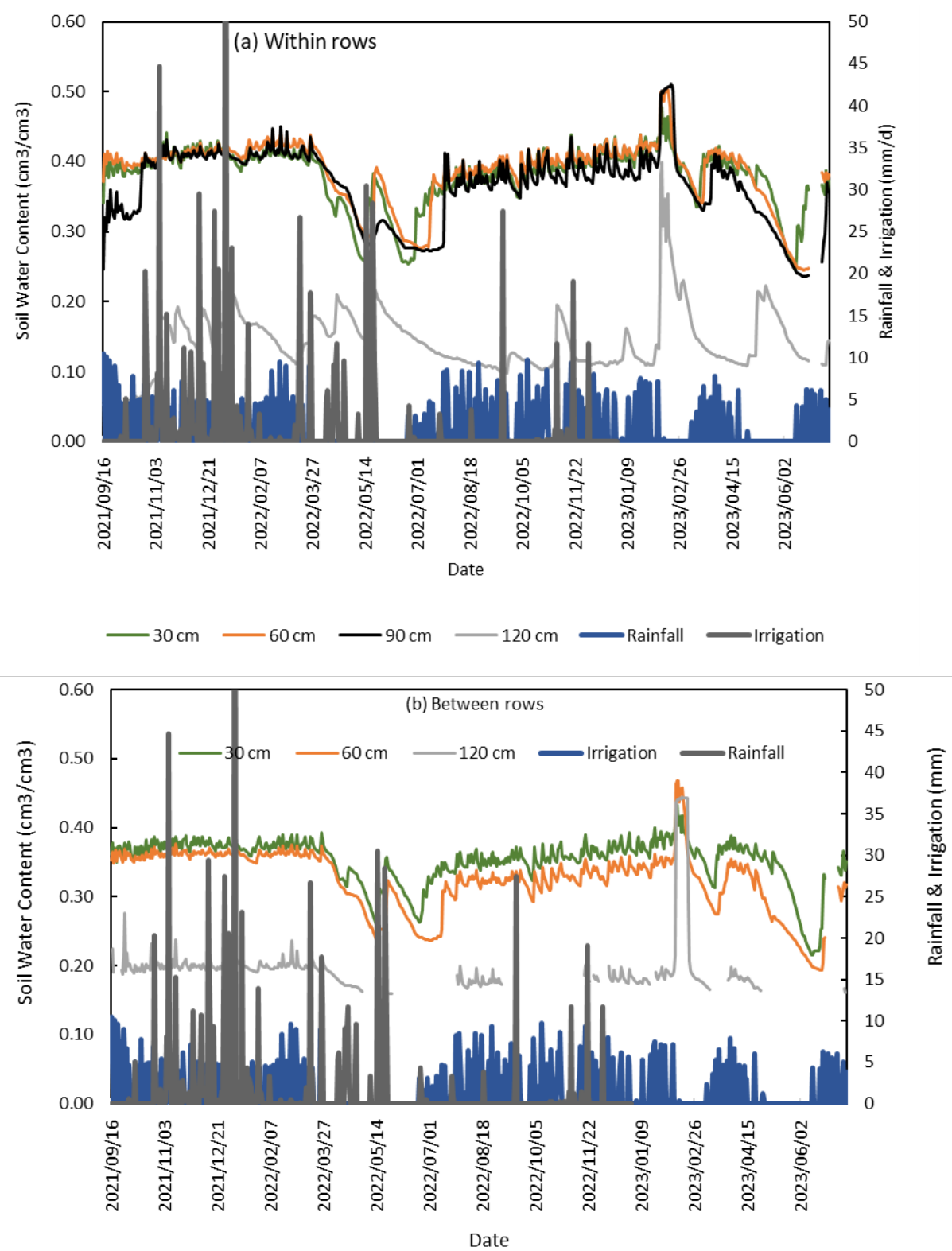


Figure 4.6: Seasonal dynamics in the soil water content in the rootzone of the litchi trees representing (a) the within and (b) between row positions.

#### 4.4.2 Leaf Gas Exchange and Transpiration Dynamics of Litchi Trees

The typical diurnal trends in the stomatal conductance and photosynthesis for a well-watered litchi tree on a clear day are shown in Fig. 4.7. These data show that both the photosynthesis rate and stomatal conductance for litchi are quite low compared to other fruit tree species, e.g. mango reported in Chapter 3. Maximum photosynthesis for litchi was less than  $3.0 \mu\text{mol}/\text{m}^2/\text{s}$  compared to close to  $6.0 \mu\text{mol}/\text{m}^2/\text{s}$  for mango and it is even higher for apples, for example. The low gas exchange rates imply that losses of water via transpiration per unit leaf area are not as high as expected.

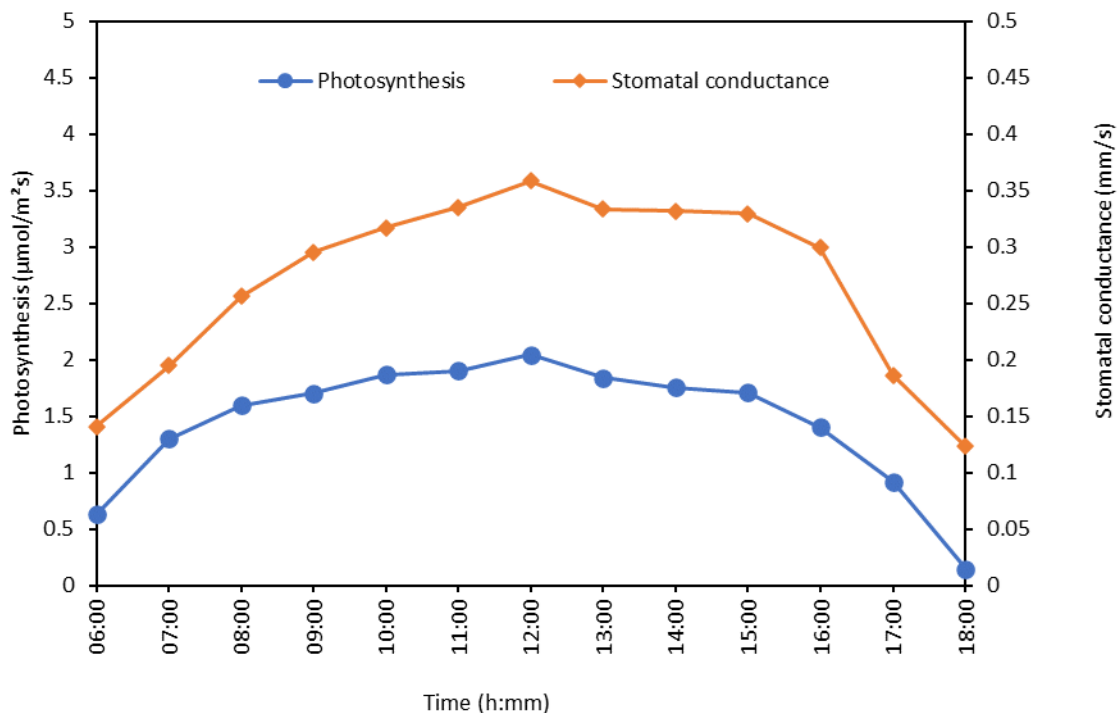


Figure 4.7: Diurnal photosynthesis and stomatal conductance for a litchi tree.

Stomatal regulation for the litchi trees is controlled by the leaf water status as illustrated in Fig. 4.8. Predawn leaf water potential in Fig. 4.8 was higher than  $-0.4 \text{ MPa}$ . At sunrise, the stomata opened leading to water loss via transpiration leading to a steady decline in the leaf xylem water potential. Stomata in plants open in response to light which is the stimulus for stomatal opening. The stomata open in response to the depletion in the internal  $\text{CO}_2$  in guard cells during photosynthesis. Stomata must open to replenish the  $\text{CO}_2$ . The second mechanism is in response to blue light which activates a proton pump that leads to the opening of inward directed  $\text{K}^+$  channels at the guard cell membranes. However, regulation of the stomatal opening for much of the day and indeed the closing stages in late afternoon are thought to be regulated by variations in starch content in the leaves (Taiz *et al.*, 2018). The midday stomatal

conductance also displayed a clear seasonal effect (Fig. 4.9) peaking in the summer months being low during winter.

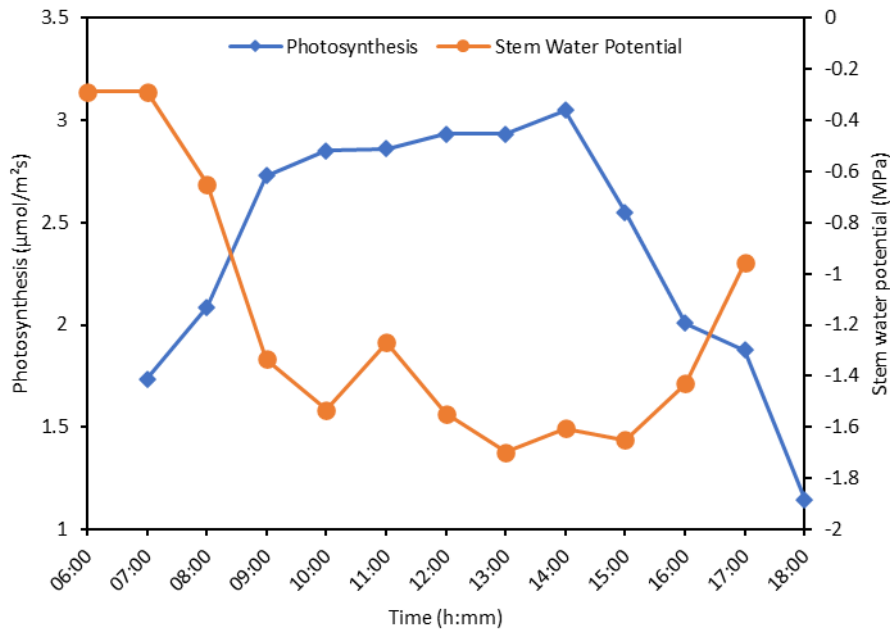


Figure 4.8: Diurnal course of the stem/ xylem water potential and leaf photosynthesis for a litchi tree.

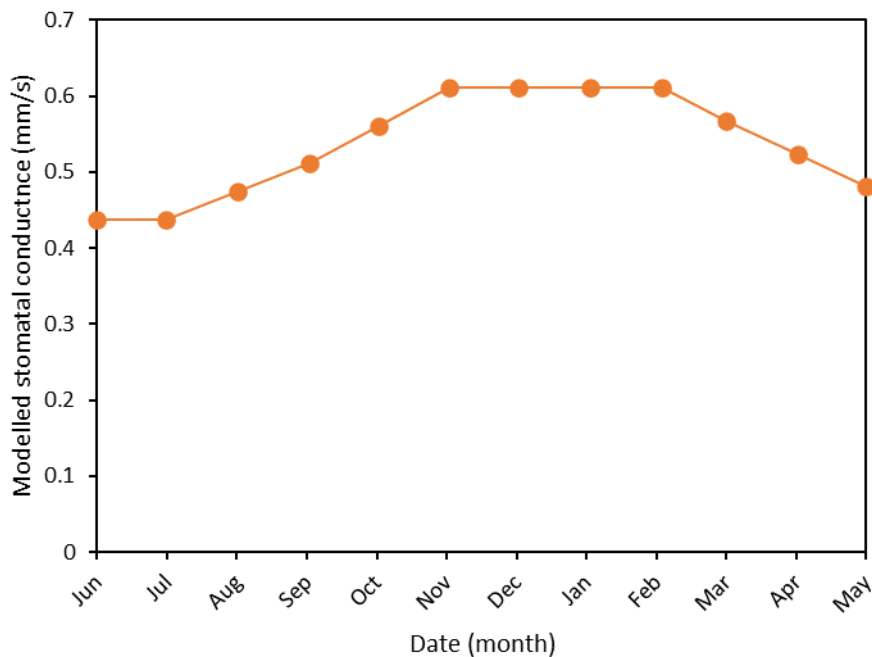


Figure 4.9: Seasonal variation of the measured stomatal conductance for the litchi trees at midday.

The average transpiration rate of the individual litchi trees, expressed in litres per day in relation to the atmospheric evaporative demand are shown in Fig. 4.10. The maximum transpiration peaked at close to 200 litres per tree per day. This is because of the huge leaf surface area even the transpiration per unit area may have been lower as suggested by the gas exchange

measurements. There was a slight decline in peak water use in summer due to the reduced atmospheric evaporative demand because of the increased cloud cover.

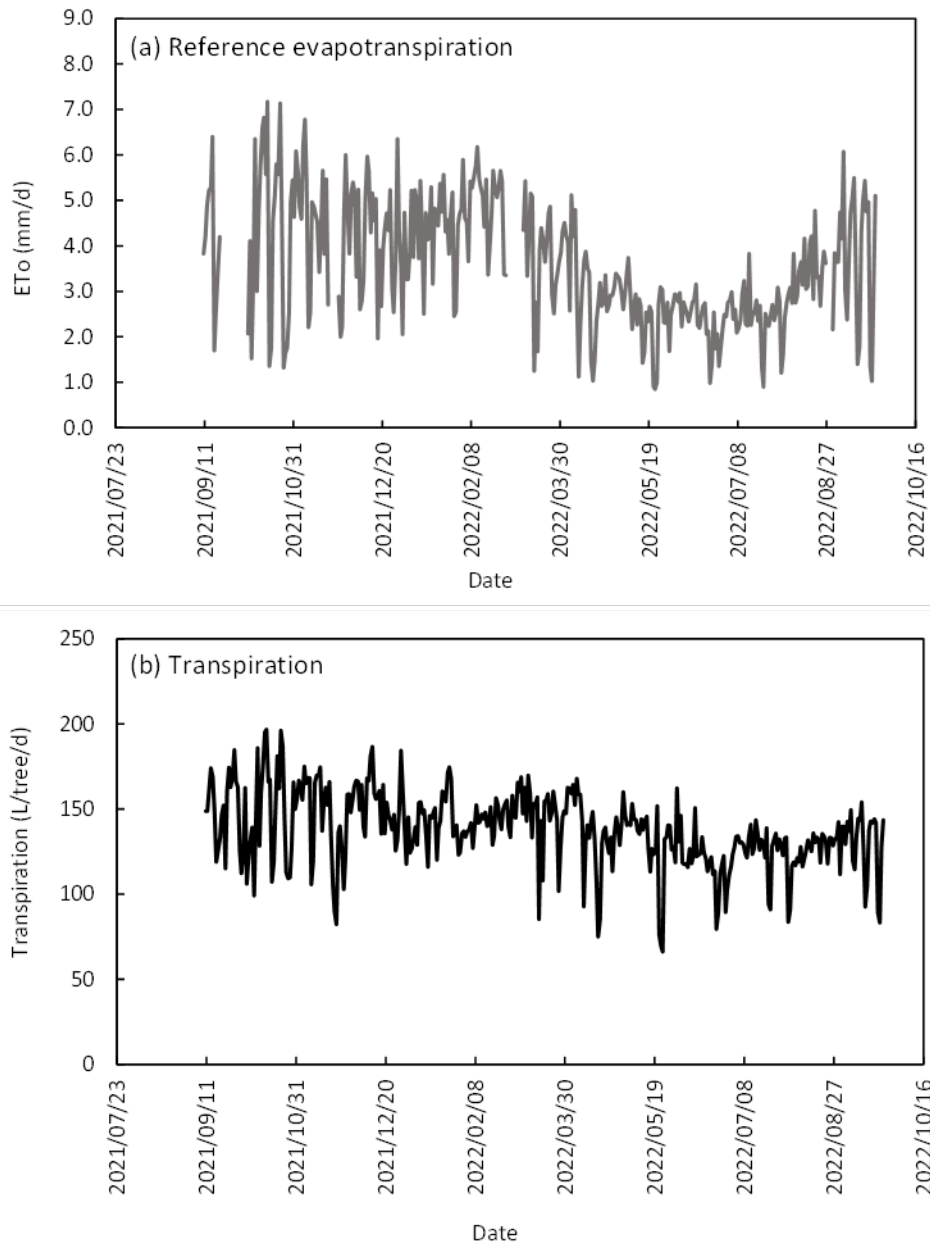


Figure 4.10: Daily (a) reference evapotranspiration and (b) single litchi tree transpiration (in L/d) in Malelane.

A comparison of the seasonal relative magnitude of the reference evapotranspiration and transpiration are shown in Fig. 4.11. Even though the changes in transpiration were small compared to changes in ETo over the course of the season, the drivers of daily transpiration were quite clear as shown in Fig. 4.12.

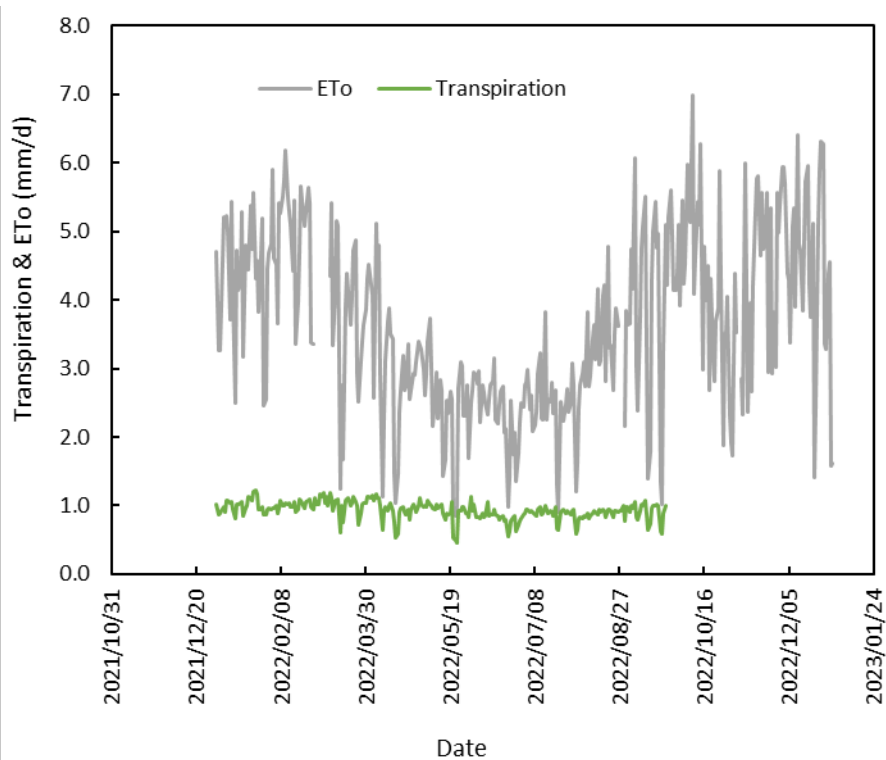


Figure 4.11: Seasonal transpiration dynamics of the mature litchi orchard in comparison with the reference evapotranspiration.

All the key climate variables namely the solar radiation (Fig. 4.12a), vapour pressure deficit of the air (Fig. 4.12b), and the reference evapotranspiration (Fig. 4.12c) had a strong non-linear influence on daily transpiration with  $R^2$  values between 0.58 and 0.69. The strong influence of the climate drivers on tree transpiration suggests that soil water availability was not a limiting factor. This is not surprising given the high irrigation volumes applied to this orchard. Despite the high irrigation levels, there is no evidence of drainage beyond the root zone based on the soil moisture probe data reported earlier. This confirms the high-water requirements of the individual trees.

Even stronger correlations were found between the basal crop coefficient ( $T/ETo$ ) and the solar radiation (Fig. 4.13a) and the VPD (Fig. 4.13b) of 0.81 and 0.67, respectively. These data suggest that at higher solar irradiances or VPD,  $Kcb$  declines because of the increasing  $ETo$ .

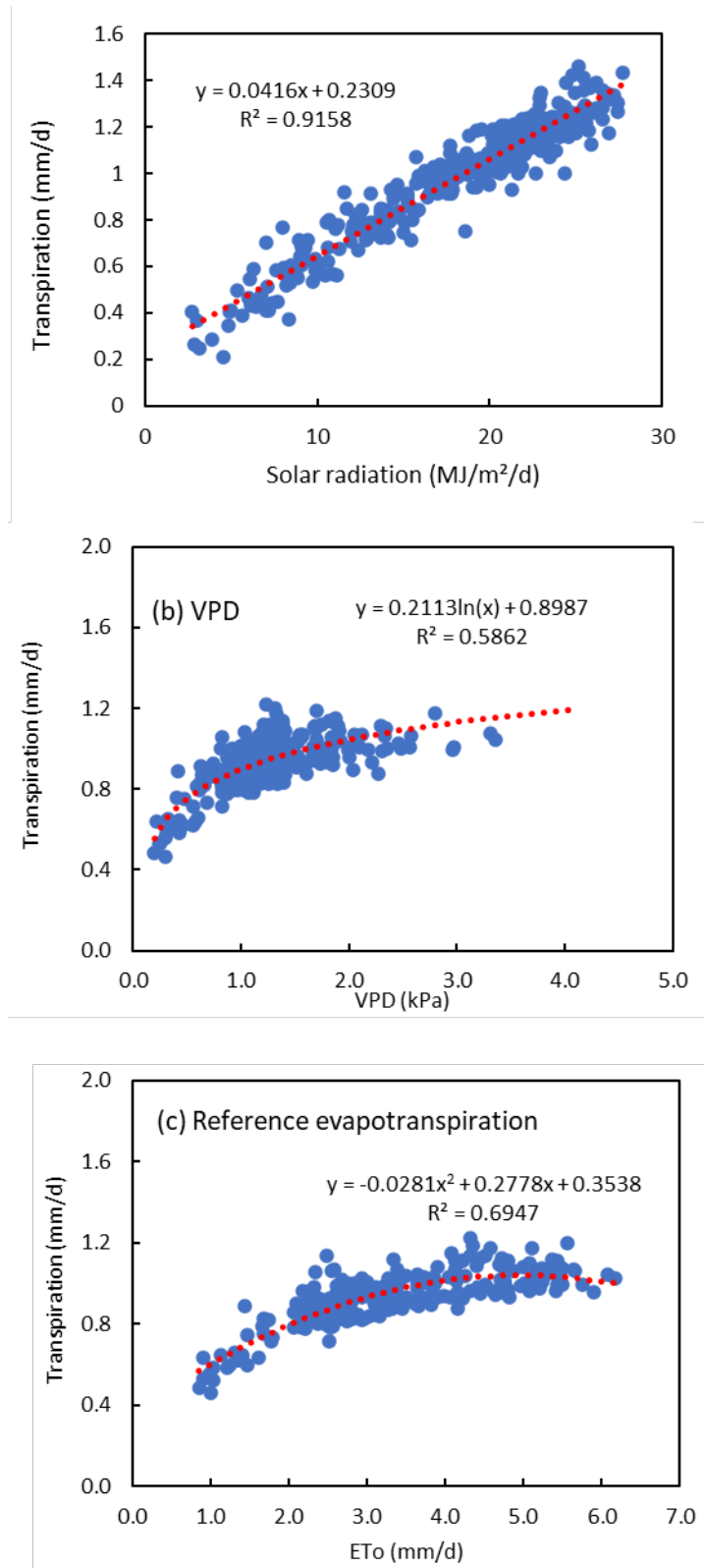


Figure 4.12: Effect of (a) solar radiation, (b) VPD and (c) reference evapotranspiration on the transpiration of a litchi orchard.

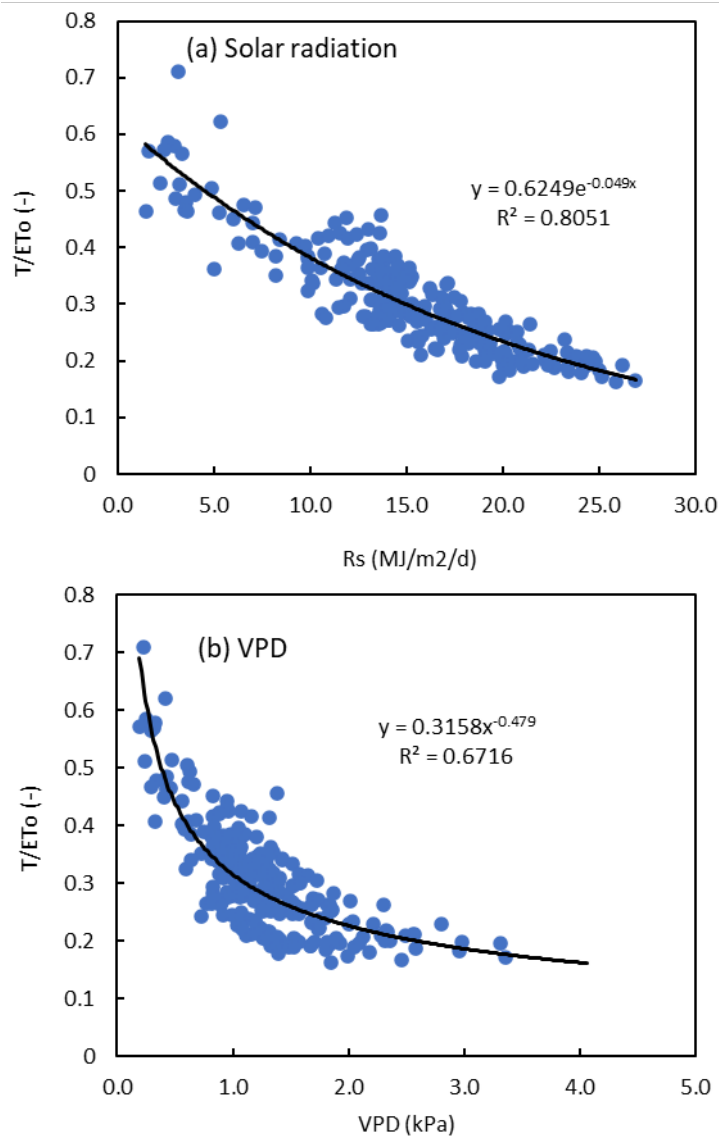


Figure 4.13: Effect of (a) the daily total solar radiation and, (b) VPD on the basal crop coefficient for litchi orchards.

The basal crop coefficient curve for the litchi orchard was rather unexpected as shown in Fig. 4.14. It does not follow the typical 4-stage crop coefficient curve of the FAO (Allen *et al.*, 1998). It appears the basal crop coefficient was higher during the winter season, and it decreased during the warm season when irrigation is most needed. This trend is likely a reflection of the very small fluctuations in the seasonal transpiration dynamics of litchi trees. The resultant Kcb curve is therefore influenced by the falling ETo in winter which leads to higher Kcb values and vice versa.

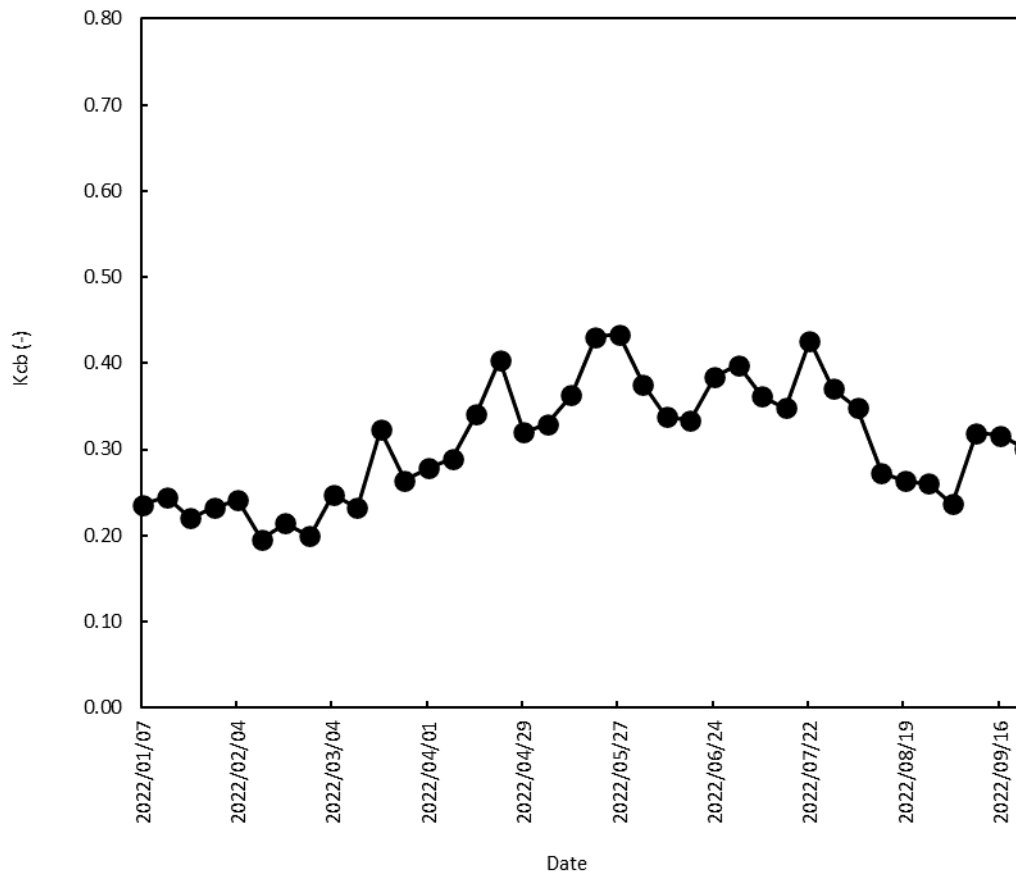


Figure 4.14: Weekly basal crop coefficients for a mature litchi orchard in Malelane.

#### 4.4.3 Litchi Orchard Evapotranspiration

Whole orchard evapotranspiration data were collected from 16-31 July 2022 and again from 20 September to 18 October and lastly from 14 November to 01 December 2022. There were numerous technical issues with the eddy covariance system which resulted in substantial loss of data. Maximum daily ET<sub>c</sub> peaked at about 4.0 mm during the rainy season when the understory vegetation density was greatest. This implies that up to 60% of the ET<sub>c</sub> flux in the litchi orchard emanated between the tree rows during summer and this contribution declined to less than 20% in winter. There was much lower correlation between the orchard ET<sub>c</sub> and the daily solar radiation, VPD or ET<sub>o</sub> with  $R^2 < 0.40$  (Fig. 4.15). We attribute this to the heterogenous nature of the litchi orchard with a large proportion of the ET<sub>c</sub> flux emanating between the tree rows where the vegetation would suffer from water stress during long dry spells. This argument is supported by the data in Fig. 4.15d which showed a somewhat stronger correlation between the orchard ET<sub>c</sub> and soil water content. Soil water content variation appears to be a stronger driver of ET<sub>c</sub> in the litchi orchard.

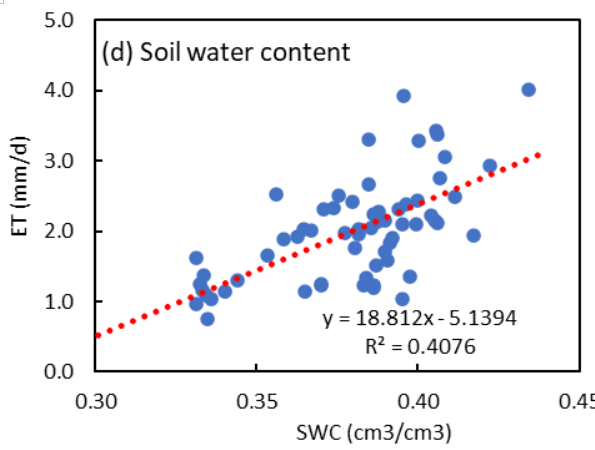
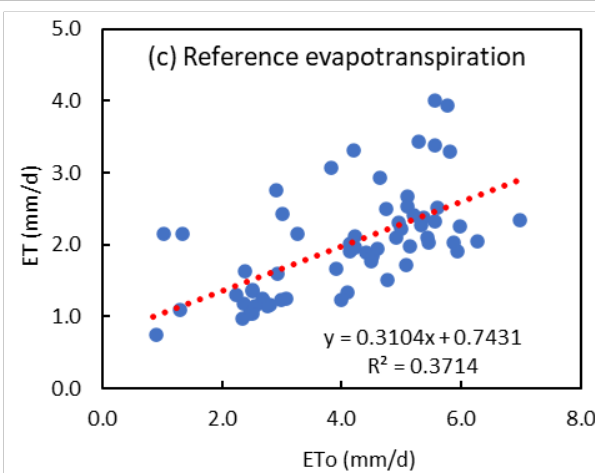
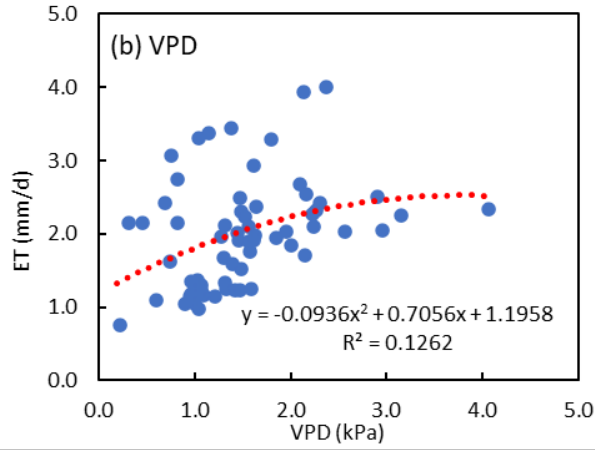
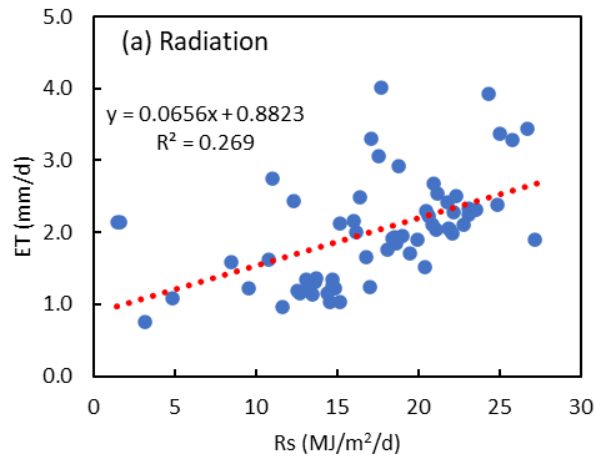


Figure 4.15: Effect of (a) solar radiation, (b) VPD, (c) ETo, and (d) soil water content on ETc.

The monthly summary shown in Table 4.5 suggests that on an annual basis, total transpirational losses for the litchi orchard was about 3 350 m<sup>3</sup>/ha. Total rainfall and irrigation were 558 and 437 mm, respectively. The estimated annual total ETc for the litchi orchard was about 960 mm or 9 600 m<sup>3</sup>/ha/yr with over 65% of the water lost from the orchard floor due to the high irrigation levels and the wide tree spacing.

Table 4.5: Monthly total water use summary for the litchi orchard.

Month	ETo (mm)	Rain (mm)	Irrigation (mm)	T (mm)	ET (mm)
Jan-22	135	203.2	17.6	31	98.6
Feb-22	137	4.8	56.4	28	113.7
Mar-22	113	68.6	47.1	32	81.4
Apr-22	92	69.3	0	28	63.5
May-22	77	113	0	29	53.9
Jun-22	71	5.8	8.3	25	49.7
Jul-22	78	4.3	43.2	28	54.6
Aug-22	99	3.8	64.3	27	69.3
Sep-22	121	31	50.7	27	92.0
Oct-22	135	6	65.8	27	93.2
Nov-22	123	36.8	42.2	25	92.3
Dec-22	140	11.7	41.4	28	98.0
	<b>1321</b>	<b>558.3</b>	<b>437</b>	<b>335</b>	<b>960</b>

#### 4.4.4 Modelling Crop Coefficients and Water Use of a Litchi Orchard

##### 4.4.4.1 Stomatal Conductance

The Jarvis modelled hourly stomatal conductance for selected clear sky days throughout the growing season produced good results when compared to the measured values (Fig. 4.16). The model produced a coefficient of determination,  $R^2 \approx 0.80$ , root mean square error (RMSE),  $\pm 0.14$  mm/s and mean absolute error (MAE)  $\pm 0.12$  mm/s. It also exhibited an acceptable Nash-Sutcliffe Efficiency (NSE) of 0.66 reinforcing its predictive accuracy when compared to the actual stomatal conductance measurements. The results indicate that Jarvis stomatal modelling has a strong potential for modelling litchi trees stomatal conductance throughout the growing season. The hourly modelled stomatal conductance from 1100 hrs to

1400 hrs each day were averaged over the course of each month spanning the growing season (Fig. 4.17). Monthly average stomatal conductance indicated minimum stomatal conductance value of 0.1 mm/s during the winter month of June; it gradually increased to reach a maximum of approximately 0.6 mm/s in the summer in January.

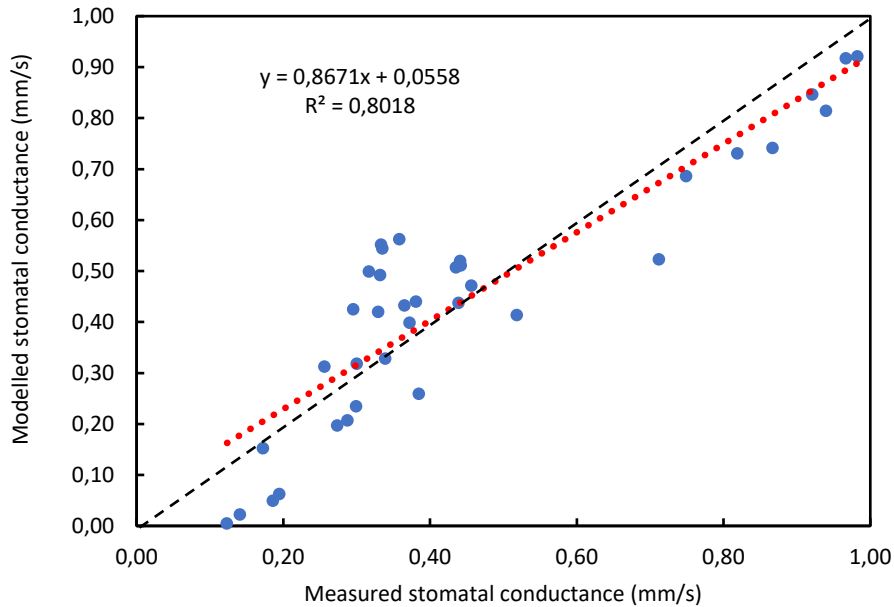


Figure 4.16: Relationship between modelled and measured stomatal conductance for Litchi trees over selected days during the growing season.

The stomatal conductance gradually decreased until it reached a value of about 0.15 mm/s towards the end of the growing season. Reference evapotranspiration was the strong driver of seasonal stomatal conductance with a coefficient of determination,  $R^2 \approx 0.8$  (Fig. 4.18a) followed by the solar radiation (Fig. 4.18b) and then vapour pressure deficit which had the least influence on the monthly stomatal conductance. The results in Fig. 4.18a have potential to help farmers that do not have access to very expensive leaf gas exchange equipment derive crop coefficients from available weather data. Furthermore, the results indicate that a combination of weather variables are responsible for controlling the litchi leaf gas exchange. The maximum monthly average stomatal conductance recorded during the growing season for the litchi was generally lower than other temperate fruit trees, though it is difficult to definitively compare measurements made by instruments of different precision and accuracy (Chang & Lin, 2007; DeJong, 1983; Flore & Lakso, 1989).

#### 4.4.4.2 Estimating the Basal Crop Coefficients ( $K_{cb}$ ) and Orchard Transpiration

The minimum unstressed canopy resistance for the litchi ( $\alpha$ ) 37 s/m was calculated by inverting the modified A&P equation (Equation 4.11).

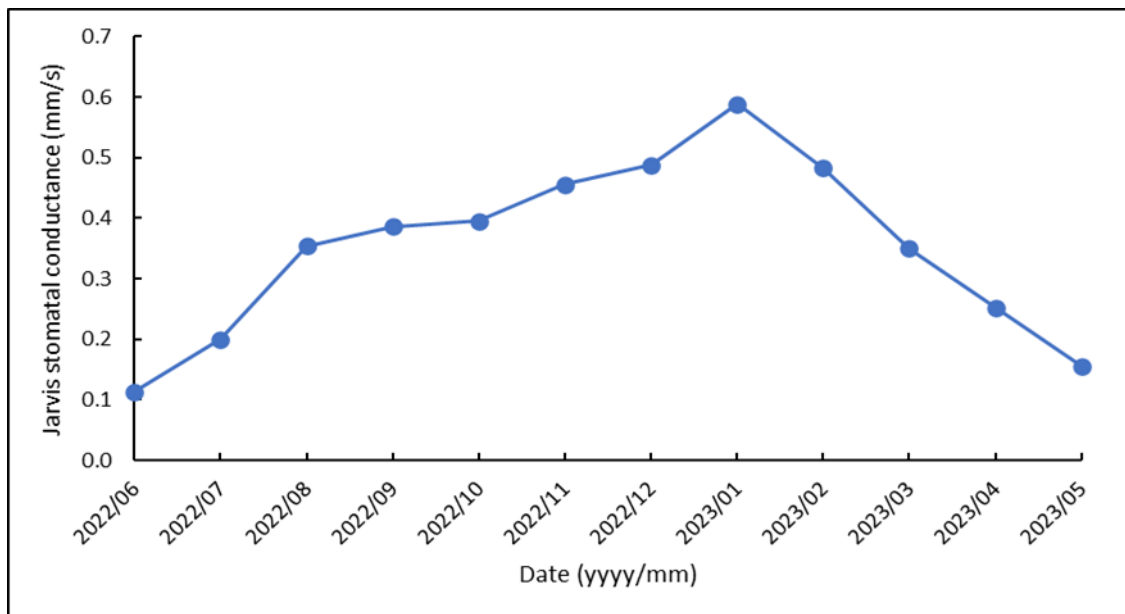


Figure 4.17: Jarvis modelled stomatal conductance monthly averages for the litchi trees over the course of the growing season.

By substituting the parameter  $\alpha$  and the average monthly stomatal conductance, the modified A&P equation produced good basal crop coefficients that closely matched those derived from the orchard transpiration (Table 4.6).

Table 4.6: Measured monthly basal crop coefficient ( $K_{cb\_measured}$ ), modelled monthly basal crop coefficient ( $K_{cb\_modelled}$ ) and minimum unstressed canopy resistance ( $\alpha$ ).

Date	$K_{cb\_measured}$	$K_{cb\_modelled}$	$\alpha$ (s/m)
2022/05	0.12	0.11	37
2022/06	0.11	0.10	37
2022/07	0.13	0.12	37
2022/08	0.15	0.14	37
2022/09	0.12	0.15	37
2022/10	0.12	0.15	37
2022/11	0.13	0.15	37
2022/12	0.10	0.16	37
2023/01	0.10	0.17	37
2023/02	0.11	0.14	37
2023/03	0.13	0.15	37
2023/04	0.19	0.14	37

There was a marked overestimation of basal crop coefficients around the months of December 2022 to January 2023. This was attributed to the heavy floods that occurred in January that caused a lot of spikes in the model data as well as the late orchard harvesting that occurred in December 2022 that caused a huge decrease in the orchard leaf area index and may have affected the model performance.

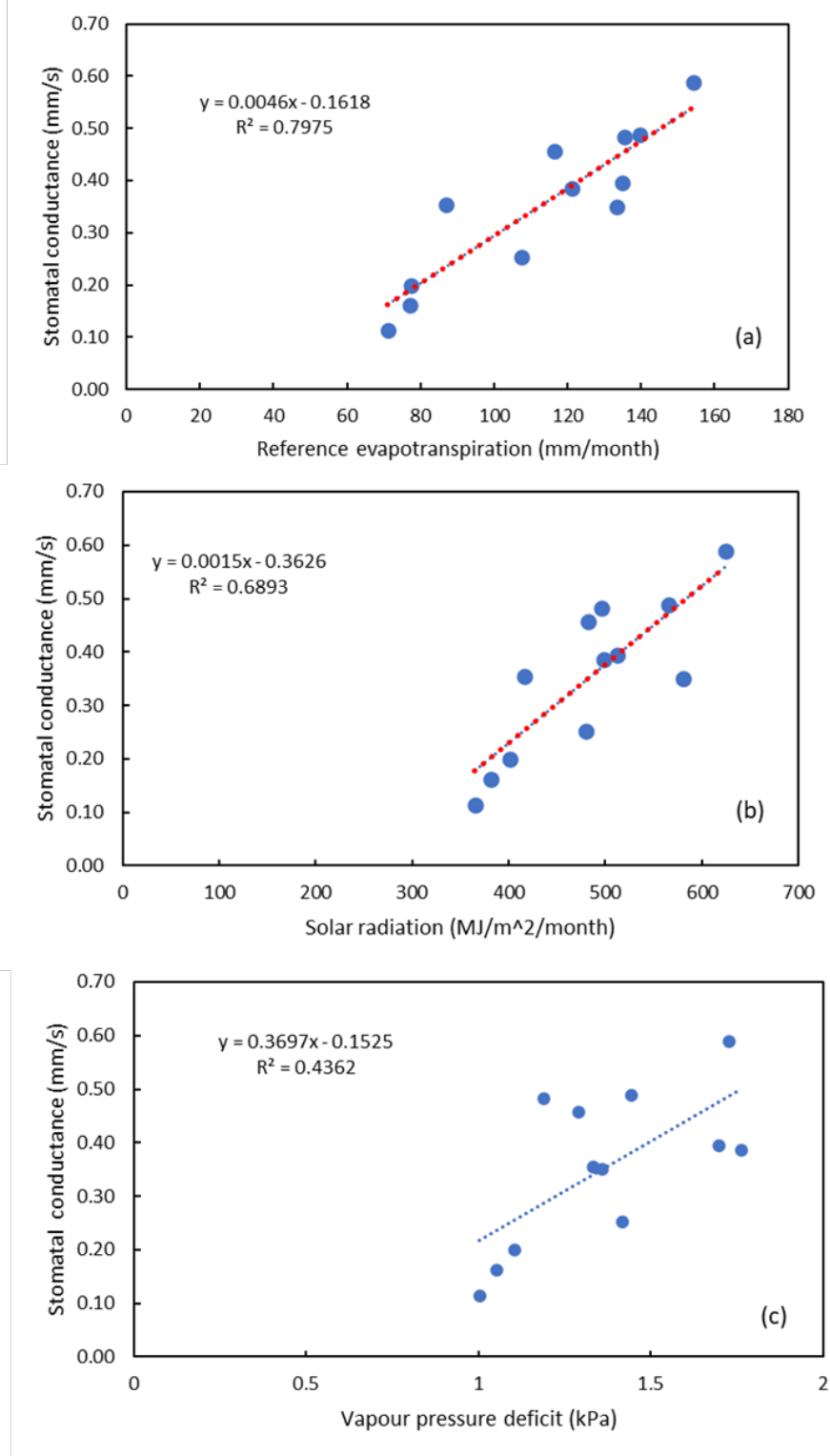


Figure 4.18: Relationship between monthly average stomatal conductance and (a) reference evapotranspiration, (b) solar radiation, (c) vapour pressure deficit of the air.

The transpiration model using the original A&P parameters caused the monthly total transpiration to be grossly overestimated (Fig. 4.19a). This result is consistent with observations from earlier studies by Taylor *et al.* (2015) and Mobe *et al.* (2020) among others. However, the modified A&P method combined with a variable mean leaf resistance modelled using the Jarvis approach has a strong potential to predict litchi orchard transpiration with good accuracy (Fig. 4.19b & c). This is consistent with the observations by Taylor *et al.* (2015), although they proposed a different form of the stomatal resistance sub model.

Using the modified transpiration model as described here as a base, evapotranspiration by the litchi orchard was modelled using the equations detailed in Mobe *et al.* (2020). Typical seasonal variations in the crop coefficients are shown in Fig. 4.20. The modelled peak  $K_c$  was under 1.0 throughout the year and clearly the soil evaporation coefficient dominated the  $K_{cb}$ . This was because of the very low tree density in the orchard and the large exposed surfaces with bare ground. A summary of the monthly crop coefficients is shown in Table 4.7.

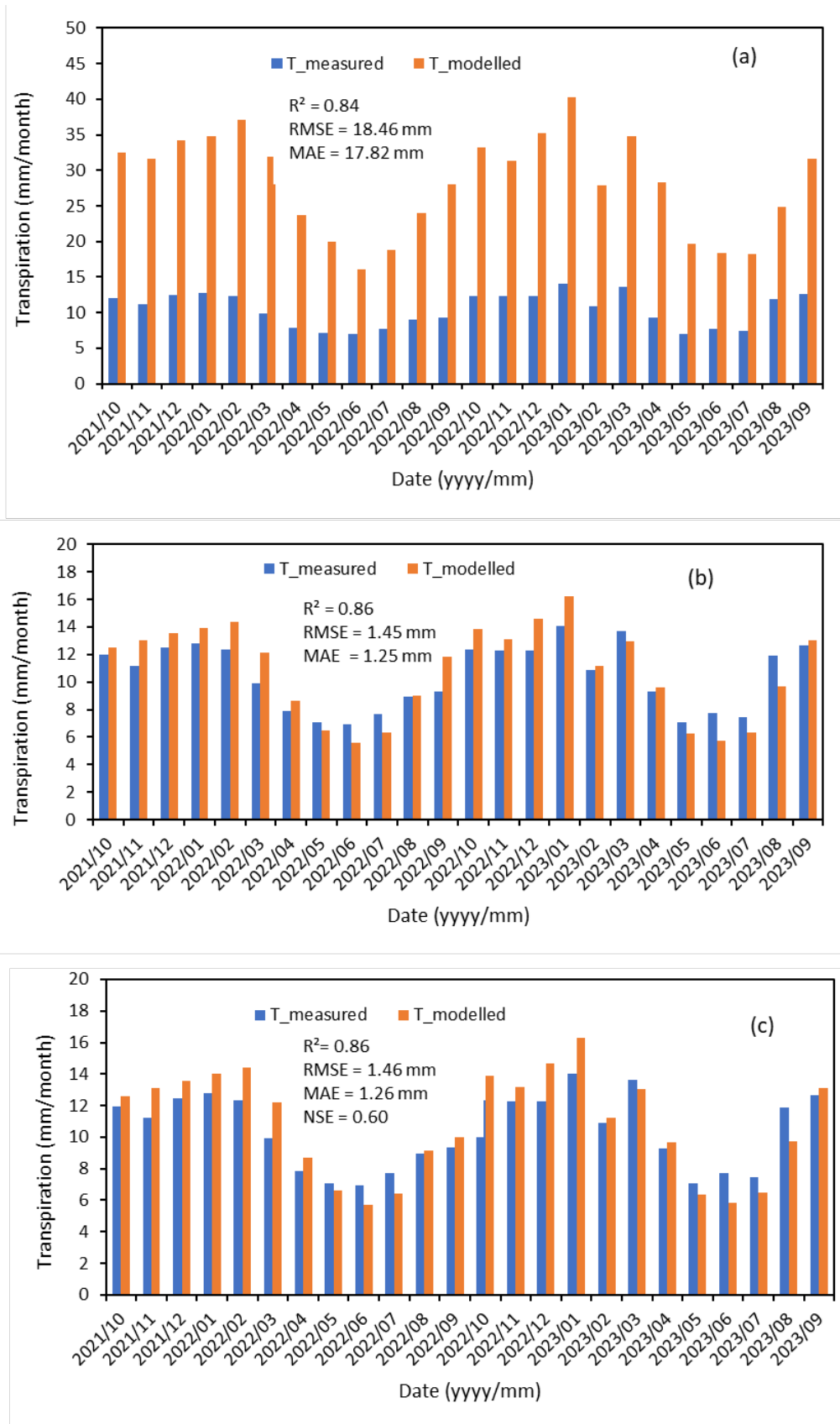


Figure 4.19: Comparison between measured monthly transpiration and modelled tree transpiration using, (a) Allen and Pereira (2009, A&P) method using measured stomatal conductance, (b) Modified Allen and Pereira (2009, A&P) method using Jarvis (1976) derived stomatal conductance and a resistance parameter, (c) Modified Allen and Pereira (2009, A&P) method using measured stomatal conductance and a resistance parameter for the litchi tree.

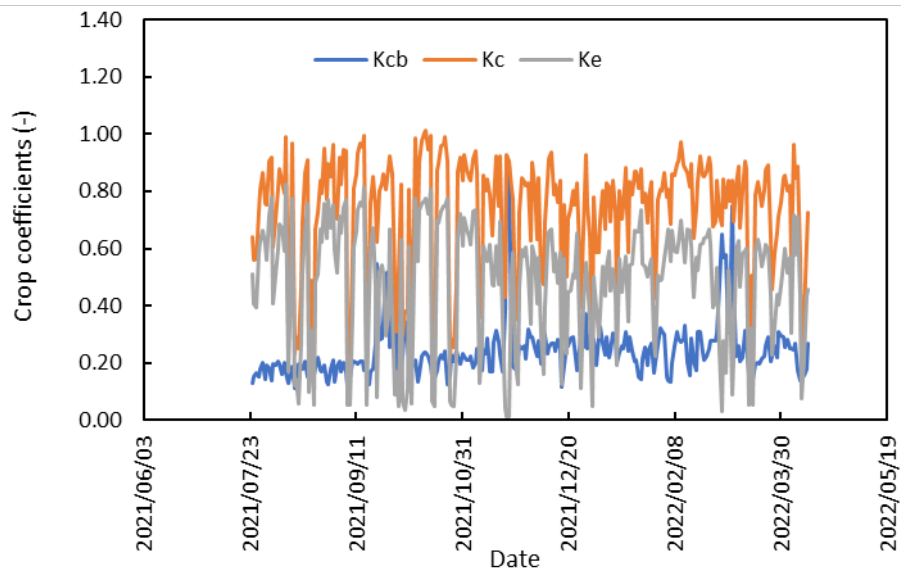


Figure 4.20: Seasonal changes in the crop coefficients for a mature litchi orchard at Malelane, Mpumalanga Province.

Table 4.7: Typical monthly crop coefficients for a mature litchi orchard.

Month	Kc	Kcb	Ke
September	0.76	0.26	0.51
October	0.69	0.20	0.50
November	0.75	0.22	0.53
December	0.70	0.24	0.46
January	0.73	0.22	0.51
February	0.83	0.23	0.60
March	0.72	0.28	0.44
April	0.69	0.20	0.49
May	-	-	-
June	-	-	-
July	-	-	-
August	-	-	-

#### **4.5. Conclusion**

In this chapter we quantified the water use and its partitioning in litchi orchards under micro-sprinkler irrigation. The data shows although transpiration per unit leaf area is relatively low, the overall transpiration by entire trees is quite high because of the very large leaf area. Peak transpiration by whole trees approached 200 litres per day on typical clear days. However, when the transpiration is expressed into equivalent water depth units, the transpiration rates were quite low, with peaks less than 1.3 mm/d because of the very low tree density (~ 70 tree/ha). Annual total transpiration was approximately 3 350 m<sup>3</sup>/ha while total evapotranspiration estimated via modelling approached 960 m<sup>3</sup>/ha. A single litchi tree consumed about 41 717 litres of water per year with an average yield of about 116 kg/tree. The water use efficiency (or Water Productivity) translates to about 0.85 kg/m<sup>3</sup> based on ETc.

## CHAPTER 5: WATER USE OF MATURE GRAPEFRUIT ORCHARDS UNDER SUBTROPICAL CONDITIONS

### 5.1. Summary

Grapefruit (*Citrus x paradisi*) is one of the most widely planted citrus varieties in South Africa mostly for the export market. Major plantings can be found in the Mpumalanga and Limpopo provinces with Star Ruby being the most widely planted cultivar. Previous studies funded by the Water Research Commission and by Citrus Research International have focused on establishing the water requirements of a number of citrus cultivars. But grapefruit had not been studied yet. This study therefore sought to close this information gap to understand where the water use by this species ranks relative to the other citrus species. In this study data were collected on 13-year-old Star Ruby grapefruit in Malelane, Mpumalanga between December 2021 and September 2023. Similar data as in the other species reported earlier were collected. Our results show that, as with other citrus species, grapefruit trees appear to have conservative water use characteristics due to the strict regulation of the stomatal conductance. The maximum stomatal conductance for well-watered trees on a typical clear day did not exceed 1.0 mm/s while peak leaf photosynthesis was lower than 4.0  $\mu\text{mol}/\text{m}^2/\text{s}$ . Daily maximum transpiration expressed over the entire orchard surface was around 2.4 mm/d highlighting not only the low water use rates of this cultivar, but also the low tree density (< 750 trees/ha). The annual total transpiration from January to December 2022 was 437 mm compared to a modelled annual evapotranspiration of about 1069 mm. Larger than necessary irrigation amounting to 997 mm was applied during the same period that received about 558 mm of rainfall. Therefore, there is a high probability that during 2022, this orchard was massively over-irrigated. The crop coefficients fluctuated between 0.70 and 0.91 for this specific orchard. The average yield per tree was about 79 kg while each tree consumed about 3 499 litres of water per year. The water productivity for grapefruit was about 3.52 kg/m<sup>3</sup> based on annual ET<sub>c</sub> estimates.

## 5.2. Materials and Methods

### 5.2.1 Plant material

This grapefruit (*Citrus x paradisi*) orchard (Block E11 at Riverside farm, Malelane) was 13 years old at the start of the trial in 2021, planted in 2009. The cultivar was Star Ruby on C35/5×5B rootstock. Star Ruby is the most widely planted early season grapefruit variety in South Africa accounting for at least 84 percent of the production followed by the Marsh variety at 13 percent. In terms of the production area, about 81 percent of the grapefruit in South Africa is produced in the Limpopo and Mpumalanga Provinces. While past research has quantified the water use of citrus orchards (Gush and Taylor. 2014; Varmeter and Taylor. 2018), no studies have been done on grapefruit. Some of these studies have shown substantial cultivar effects on the water use characteristics with some cultivars using more water than others (Steppe *et al.*, 2006; Dzikiti *et al.*, 2007; Dzikiti *et al.*, 2011).

Table 5.1: Characteristics of the grapefruit orchard at Riverside Farm.

ORCHARD CHARACTERISTICS	DESCRIPTION
Block name	E11
Cultivar	Star Ruby
Rootstock	C35/5 x 5B
Planting date	2009
Plant density (no of trees per ha)	476
Tree spacing	7 m x 3 m
Orchard area	6.25 ha
Row orientation	North-South
GPS coordinates	S25°25'21.58"; E31° 36' 24,15"; 274 m asl
Soil texture	Clayey loam
Irrigation system	Microsprinkler
Irrigation delivery rate	50 L/h
Wetted diameter	1.5 m
Tree dimensions	
- Height	3.5 m
- Canopy width	3.0 m
- LAI (Tree & orchard)	3.78 ± 0.15 & 2.60 ± 0.28
Average yield	40 t/ha
Cover crop type and status	Indigenous Vlei Bristle Grass ( <i>Setaria incrasatta</i> )

About 60% of the grapefruit produced in the country is exported to Japan and the remainder to various other markets including Russia, Europe, UK, the East and the Middle East. Trees in this orchard were planted on a flat slope and were surrounded by windbreaks (Fig. 5.1). Orchard size was approximately 6.25 hectares, and the trees were planted with a 7 m x 3 m spacing giving a tree density of 476 trees per hectare. Average tree height was approx. 3.5 m maintained by regular pruning after harvest each year while the mean canopy diameter was about 3.0 m. Irrigation was via a microsprinkler system delivering about 50 L/tree. The orchard was previously under drip irrigation which was converted to micro about two years before the study commenced.



Figure 5.1: Location of the ‘grapefruit’ orchard at Riverside farm.

### **5.2.2 Soil Water Content, Growth, and Water Use Measurements**

Soils in the grapefruit orchard were the dark-red clayey loam soils with a high stone content (data not shown). Soil samples were collected at different depths in the range 0 to 120 cm and taken to a commercial lab at CRI for analysis. The volumetric soil water content in the

root zone was measured in a similar fashion to that described for the mango and litchi orchards, respectively. Weather data were also obtained from the weather station located on the farm as described earlier. Canopy temperature and radiation interception were measured. As with the other orchards, the heat ratio method of monitoring sap flow was used to measure the transpiration rates of the grapefruit trees as illustrated in Fig. 5.2. Four trees with different stem sizes were identified and instrumented. Details of the trees and probe installation depths are summarized in Table 5.2. Transpiration data collection commenced in November 2021.



Figure 5.2: Illustration of the setup for the monitoring transpiration using the heat ratio method (HRM) sap flow technique.

Table 5.2: Summary of heat pulse sap flow monitoring equipment installed in the citrus orchard at Riverside farm.

Location	No of trees	Equipment	Stem diameters	No. of probe sets	Installation date	Installation depth
Riverside farm	4	1× CR1000 data logger 1× multiplex 16× heaters 32× thermocouples 1× security box 5× battery		Tree #1: 4 probes Tree #2: 4 probes Tree #3: 4 probes Tree #4: 4 probes	10 Sep 2021	Tree #1: 10; 20; 30; 40 mm Tree #2: 10; 20; 30; 40 mm Tree #3: 10; 20; 30; 40 mm Tree #4: 10; 20; 30; 40 mm

The eddy covariance system (Fig. 5.3) was deployed in the grapefruit orchard in November 2022. The system ran until February 2023, although there are many gaps in the data due to equipment failure.



Figure 5.3: Eddy covariance system measuring evapotranspiration in the grapefruit orchard.

### 5.2.3 Leaf Gas Exchange and Plant Water Status

Leaf gas exchange (net CO<sub>2</sub> assimilation rate [A], stomatal conductance [gs], transpiration rate [E] and intercellular CO<sub>2</sub> concentration [ci]) were measured using an infra-red gas analyser (IRGA) Model LI-6800 (Li-Cor, Lincoln, Nebraska, USA). Sensors inside the cuvette monitored the leaf surface temperature and the leaf-to-air vapour pressure deficit (VPD<sub>leaf</sub>) was calculated. Photosynthetic water use efficiency [WUE] was derived from A and gs values. Spot measurements were taken in the morning (09h30-12h00) and afternoon (14h00-15h30) on two fully mature sun exposed leaves in the outer canopy. The conditions were ambient temperature; saturating photosynthetically active radiation (PAR) (1500 μmol m<sup>-2</sup> s<sup>-1</sup>) provided by the internal red/blue LED lamp; constant cuvette CO<sub>2</sub> concentration (390 μmol mol<sup>-1</sup>) provided by an external CO<sub>2</sub> canister.

Tree water stress was quantified by measuring the stem (or xylem) water potential using a Scholander pressure chamber (Model: 615, PMS Instrument Company. Albany. OR. USA) employing the enclosed leaf method.



Figure 5.4: Measuring the leaf gas exchange with the Li 6800 in a mature grapefruit orchard.

Leaves were enclosed in the morning using zip-lock silver reflective stem water potential bags (prune bags) (PMS Instrument Company. Albany, OR, USA) for the leaf water potential to equilibrate with the true xylem water potential. Selected leaves were mature, fully expanded leaves located inside the canopies close to the stem. Measurements were then taken at midday (12h00-14h00) on two leaves per tree.

### 5.3. Results and Discussion

#### 5.3.1 Seasonal Tree Growth

The observed LAI trend for the grapefruit orchard is shown in Fig. 5.5 from December 2021 to June 2023. As with the litchi and mango orchards, respectively, the trees were pruned soon after harvest in March/ April. This was done by removing excessive growth and opening the canopy to maximize light interception. The LAI of the trees was between 2.8 and 3.5 on average. For some unknown reason, the trees were not pruned in 2022 leading to a peak LAI of approaching 5.0.

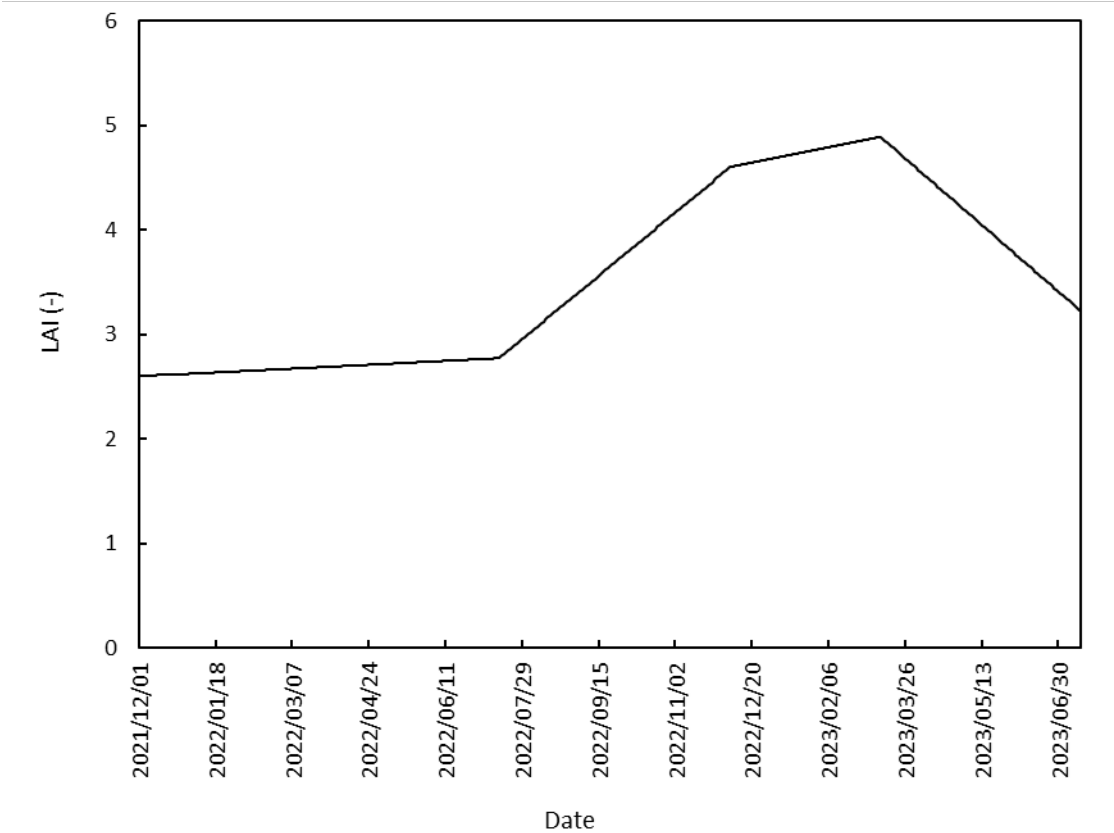


Figure 5.5: Leaf area index for the grapefruit orchard in Malelane from December 2021 to June 2023.

### 5.3.2 Soil Water Content, Irrigation, and Leaf Gas Exchange

The soil moisture dynamics in the grapefruit orchard were similar to those in the litchi (Fig. 5.6). However, soils in the grapefruit orchard were heavier, so the field capacity was at a higher volumetric soil water content around  $0.45 \text{ cm}^3/\text{cm}^3$ . The soil moisture probes stopped working in the period September to December 2022 due to technical issues and this explains the gap in the data in Fig. 5.6. As expected, the soil water content was relatively low in between the tree rows (Fig. 5.6b) than within the rows (Fig. 5.6a). Increases in the soil water content were strongly correlated with rainfall or irrigation events.

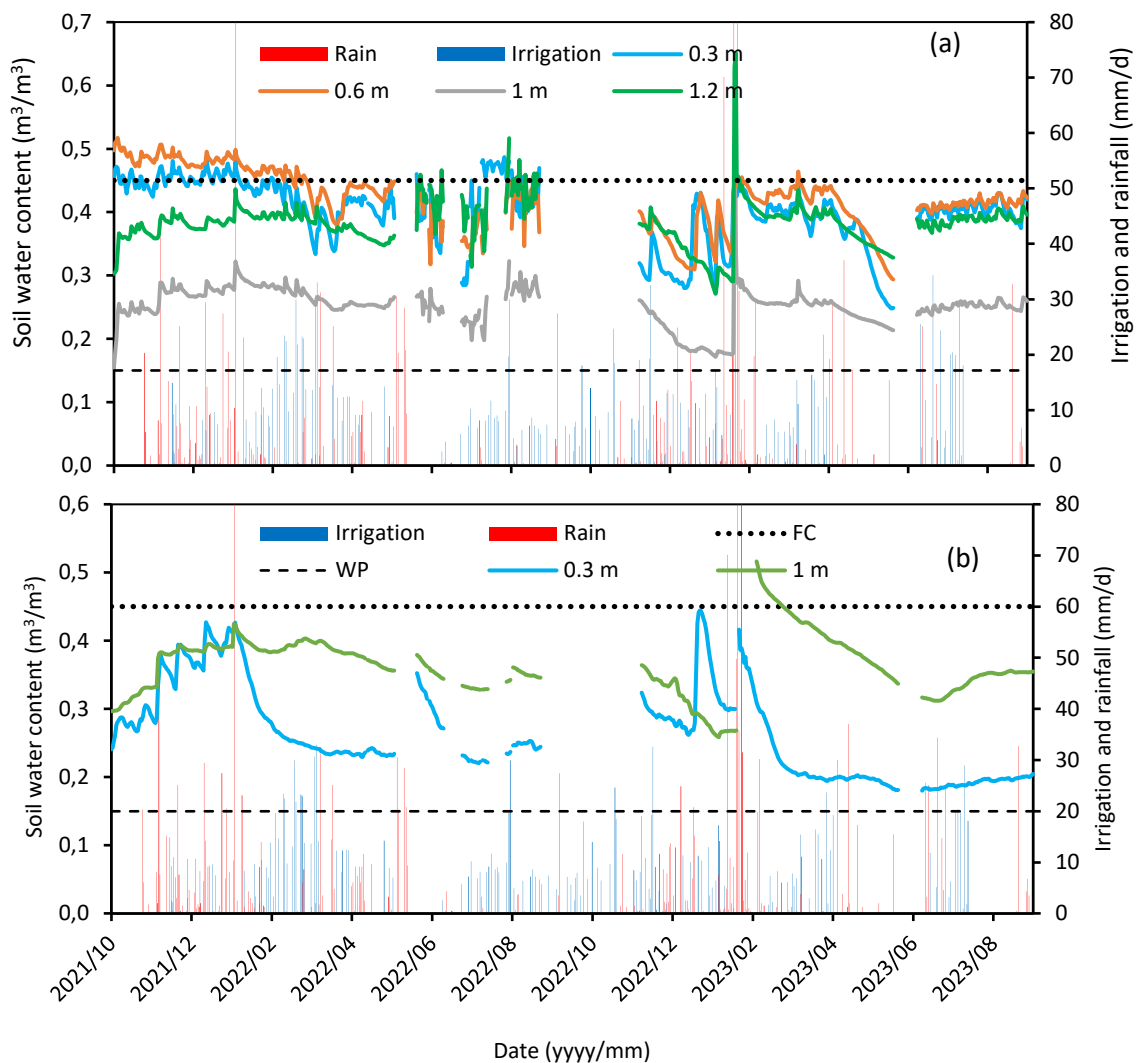


Figure 5.6: Measured soil water content in the root zone of the grapefruit orchard, (a) within tree row and (b) between tree rows for the period October 2021 to October 2023.

The typical diurnal cycle in the leaf photosynthesis and stomatal conductance for a grapefruit tree are shown in Fig. 5.7 for a clear day in Mpumalanga. A clear diurnal trend was evident but with a low peak stomatal conductance at less than  $1.0 \text{ mm/s}$ , characteristic of citrus trees as reported in Steppe *et al.* (2006) and Dzikiti *et al.* (2007). This low stomatal

conductance significantly reduces leaf gas exchange (photosynthesis and transpiration) as shown by the photosynthesis data in Fig. 5.7. Photosynthesis for the grapefruit trees peaked at only  $3.4 \mu\text{mol}/\text{m}^2/\text{s}$ , which is significantly lower than that of other fruit trees notably apple ( $> 12 \mu\text{mol}/\text{m}^2/\text{s}$ ).

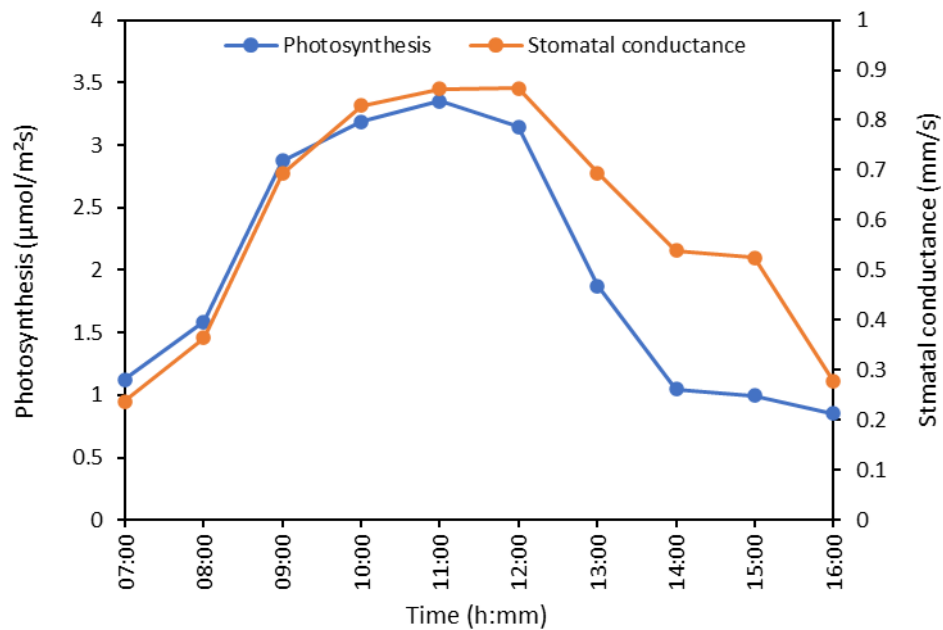


Figure 5.7: Diurnal variation of the measured photosynthesis rate and stomatal conductance for the grapefruit tree on a sunny day.

The relationship between the leaf water status and the stomatal conductance for grapefruit trees is illustrated in Fig. 5.8. The stem water potential varied from around  $-0.4 \text{ MPa}$  at predawn to about  $-1.65 \text{ MPa}$  after midday. We are not aware of the stem water potential stress threshold for grapefruit, but for apples it is around  $-1.60 \text{ MPa}$ . Therefore, it is probable that the grapefruit may have experienced some mild stress during the time of measurement. Generally, the xylem water potential was in anti-phase with the stomatal conductance suggesting that stomata opened at high xylem water potentials and closed as the water potential declined.

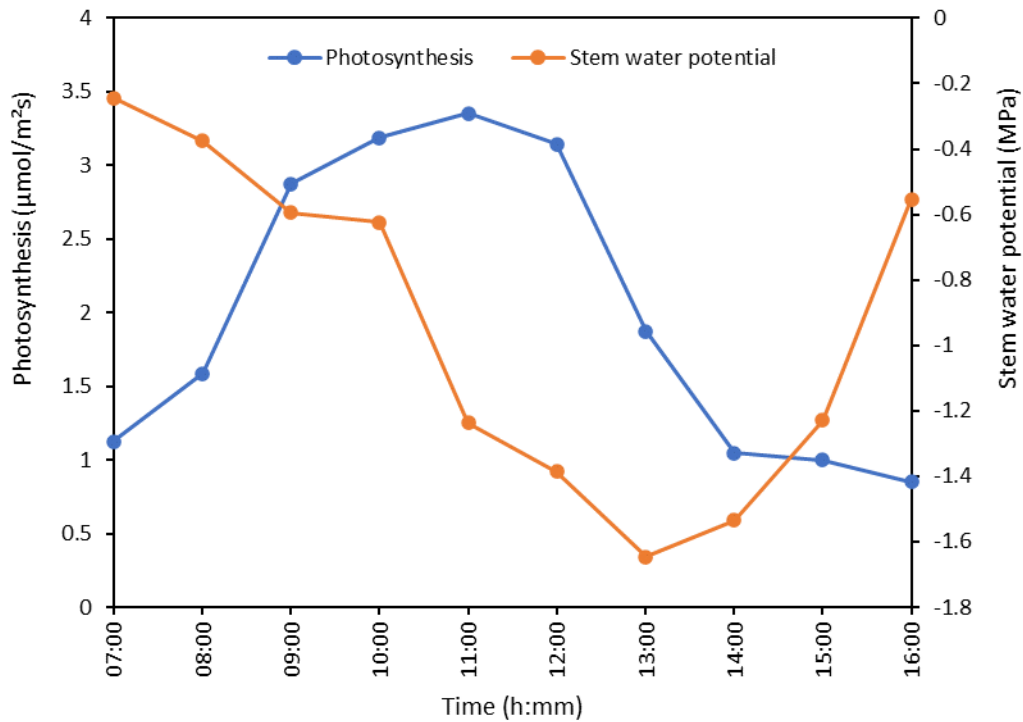


Figure 5.8: Diurnal variation of the measured photosynthesis rate and stem water potential for the grapefruit tree on a sunny day.

### 5.3.3 Water Use of Grapefruit Orchards and its Drivers

The time series of daily total transpiration expressed in equivalent water depth units from December 2021 to June 2023 is shown in Fig. 5.9. Even if the maximum daily transpiration per tree was fairly high ( $> 20$  L/tree/d), the area averaged water use was low because of the low tree density. The maximum daily transpiration recorded during the entire study period peaked at around 2.4 mm/d in summer while the lowest recorded value was around 0.1 mm/d on a rainy day in winter. The long term daily average transpiration of the grapefruit trees was around 1.2 mm/d. The annual total measured transpiration from January to December 2022 was around 437 mm translating to about 4 370 m<sup>3</sup>/ha/yr. Over the same period the annual total ETo was about 1331 mm, but irrigation levels were much higher than in the other orchards at 997 mm/yr (Table 5.3).

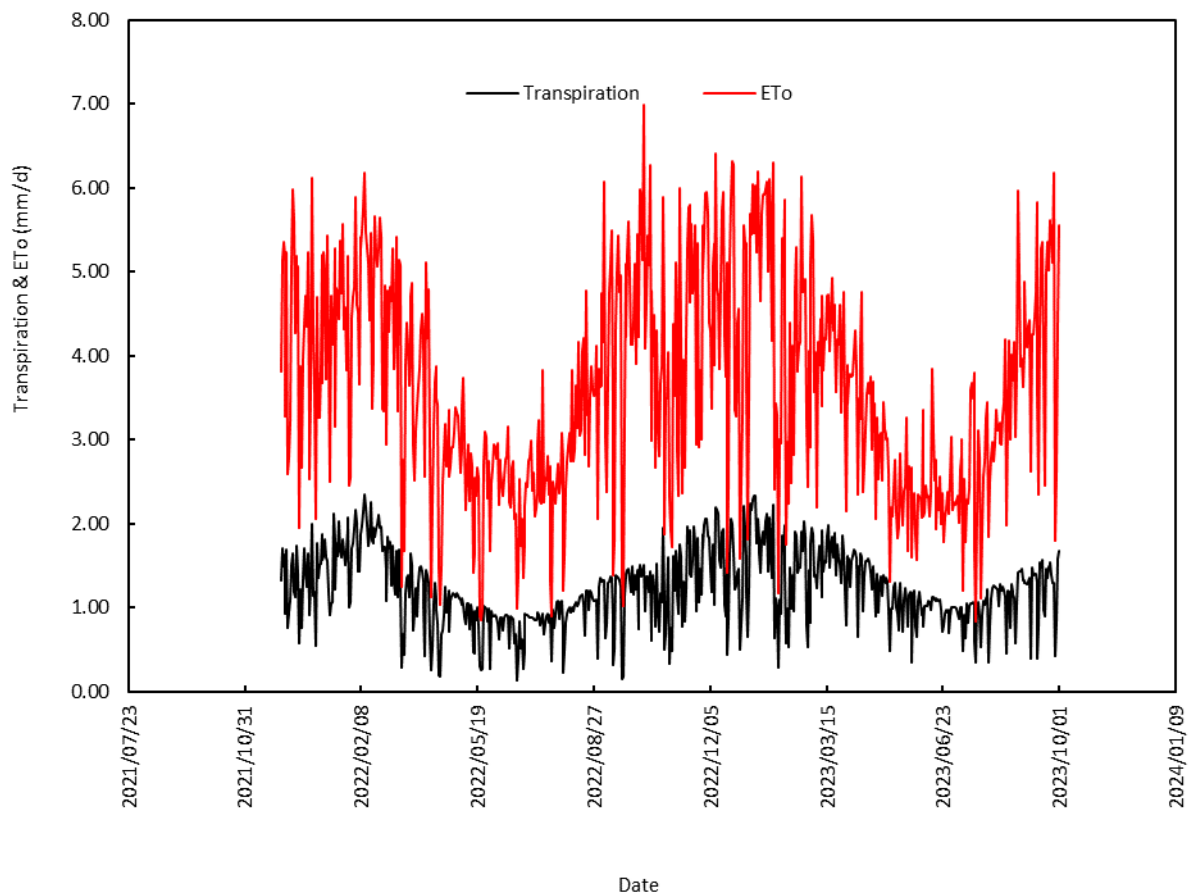


Figure 5.9: Measured grapefruit transpiration and reference evapotranspiration from December 2021 to September 2023.

There was a strong linear relationship between the daily solar radiation and the daily total transpiration (Fig. 5.10a) with an  $R^2$  of 0.79. Increasing radiation levels led to higher transpiration rates for the grapefruit trees. As with other fruit tree species, the air's VPD had a curvilinear relationship with the measured transpiration (Fig. 5.10b) with an  $R^2$  of 0.47. The relationship appeared linear up to about 1.5 kPa, beyond which the stomatal began to close. The relationship with ETo showed the combined effects of both the radiation and the VPD being slightly curvilinear (Fig. 5.10c) with an  $R^2$  around 0.73. Soil water deficit did not affect the transpiration rates at all (Fig. 5.10d) with an  $R^2$  of 0.04. This is not surprising given that the orchard was generally over irrigated as will be detailed in the next sections.

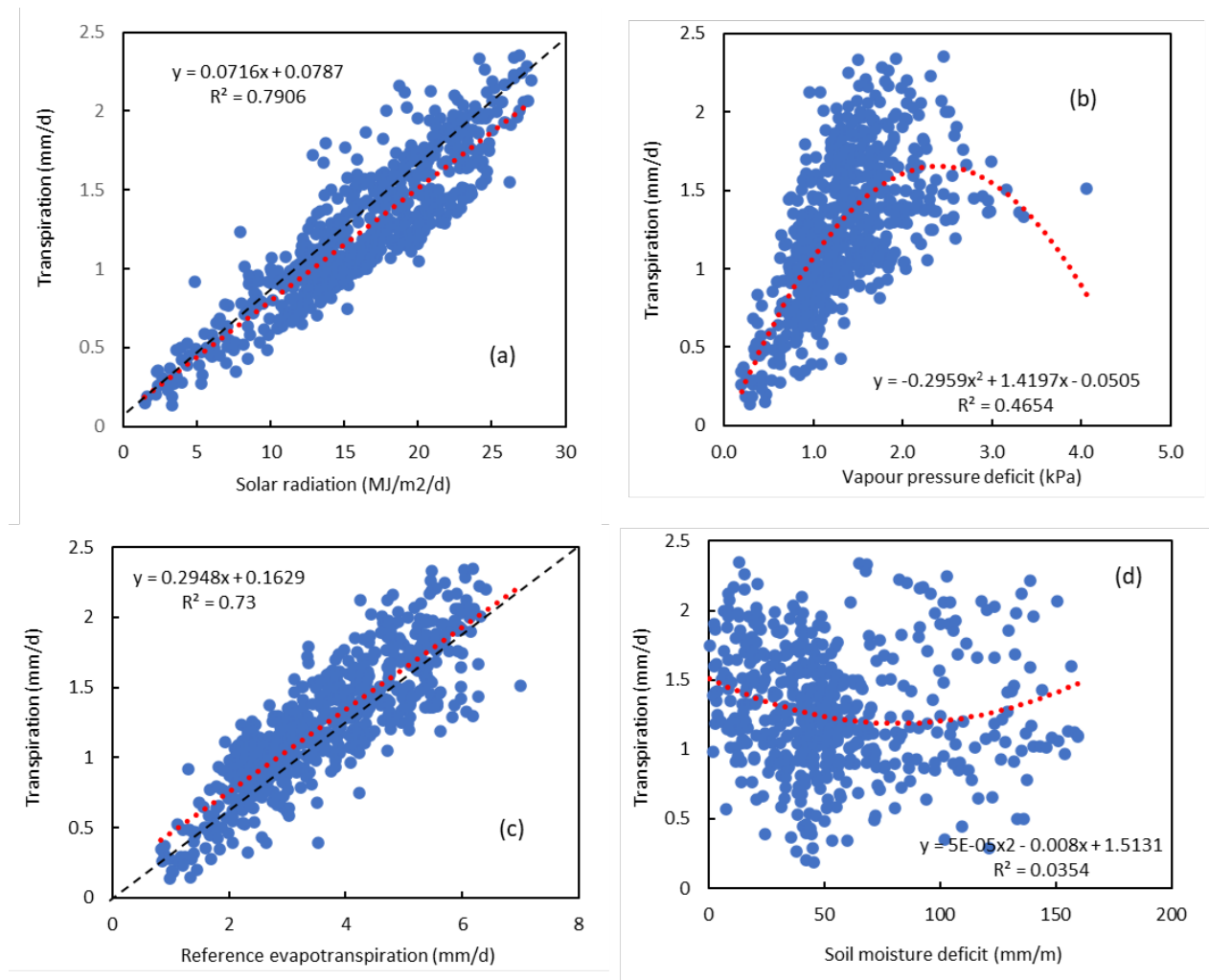


Figure 5.10: Effect of various environmental drivers on transpiration by grapefruit trees which include, 2(a) solar radiation, 2(b) vapour pressure deficit, 2(c) reference evapotranspiration, and 2(d) soil moisture deficit for the period November 2021 to September 2023.

The modified Allen and Pereira method was used to simulate the crop coefficients and hence the transpiration and evapotranspiration as detailed in the previous chapters. The other  $\alpha$  parameter that gave the best fit between the measured and modelled transpiration for grapefruit was around 37 s/m. Figure 5.11 shows a comparison of the monthly basal crop coefficients from December 2021 to September 2023. Both measured and modelled  $K_{cb}$  were in the range 0.27 and 0.44 indicating relatively low transpiration rates by the grapefruit trees.

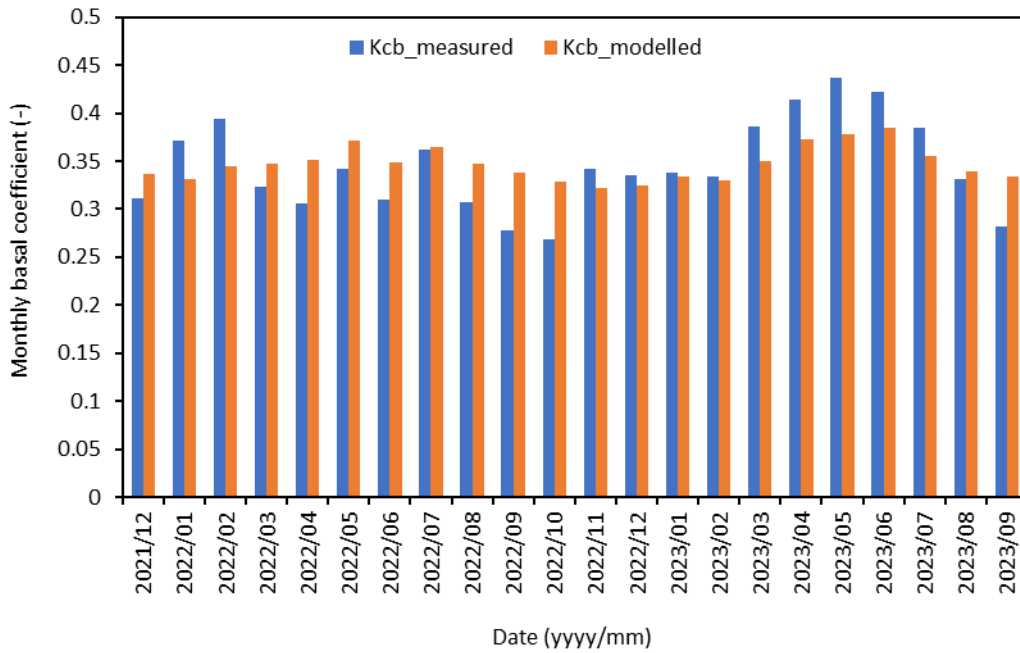


Figure 5.11: Measured monthly basal coefficient and modelled basal coefficients for the grapefruit tree using a modified Allen and Pereira (2009, A&P) method which includes measured stomatal conductance.

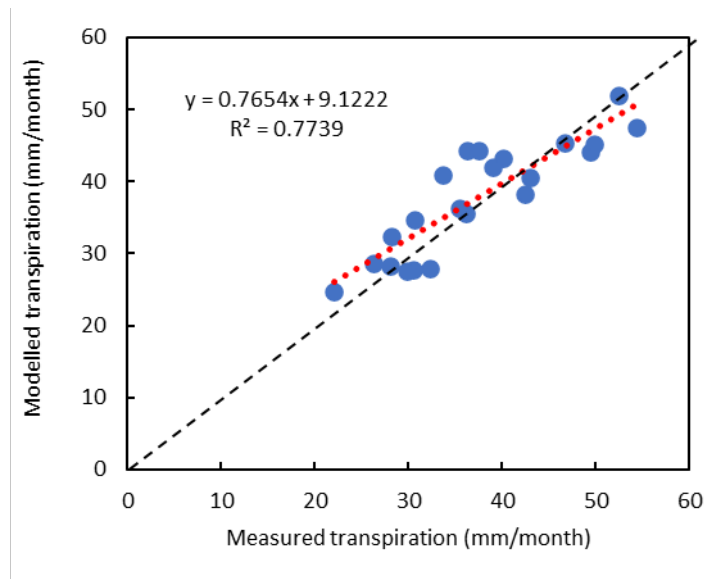


Figure 5.12: Relationship between measured monthly transpiration and modelled transpiration for the grapefruit using the modified Allen and Pereira (2009, A&P) method which includes measured stomatal conductance and a minimum leaf resistance of 200 s/m.

Converting the Kcb into monthly transpiration yielded Fig. 5.12 when comparing the measured and modelled transpiration values. The dotted line depicts a 1:1 line. The seasonal variation in the monthly measured and modelled values are shown in Fig. 5.13 together with the relevant statistics that include the RMSE, MAE and the NSE.

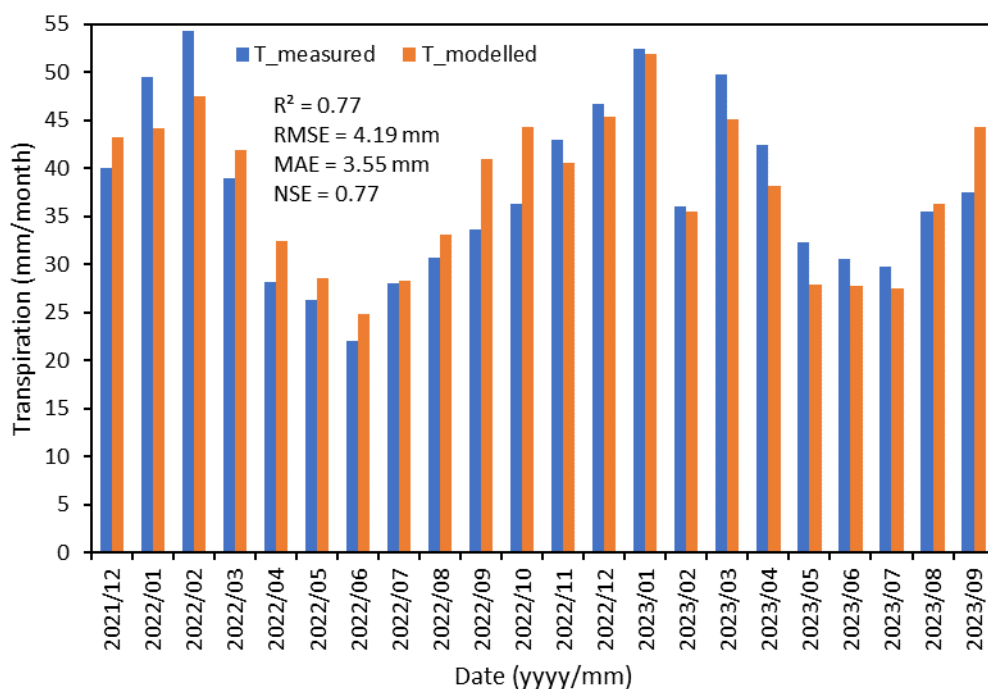


Figure 5.13: Comparison between measured monthly transpiration and modelled transpiration for the grapefruit using the modified Allen and Pereira (2009, A&P) method which includes measured stomatal conductance and a minimum leaf resistance of 1000 s/m.

Less than 20 days of ET<sub>c</sub> data were measured in the grapefruit orchard due to technical issues with the eddy covariance system. For this reason the seasonal ET<sub>c</sub> data presented in Fig. 5.14 was derived from the modified A&P model. The blue open circles indicate the position of the measured data which were quite close to the modelled values. It is apparent from Fig. 5.14 that orchard ET<sub>c</sub> exceeded the measured transpiration by about two orders of magnitude. This outcome is not surprising given the wide spacing between the trees (~ 700 tree/ha) and the massive amount of irrigation which contributed towards substantial orchard floor evaporation. On average, about 59% of water loss from the grapefruit orchard emanated from the orchard floor. There are opportunities to optimize the irrigation, e.g. by implementing a more accurate irrigation schedule and by reducing evaporative losses, e.g. by mulching.

The monthly crop coefficients for the grapefruit orchard varied between 0.70 and 0.91 as detailed in Table 5.3. The current data shows that the soil evaporation coefficient was quite substantial and ways should be explored to reduce it.

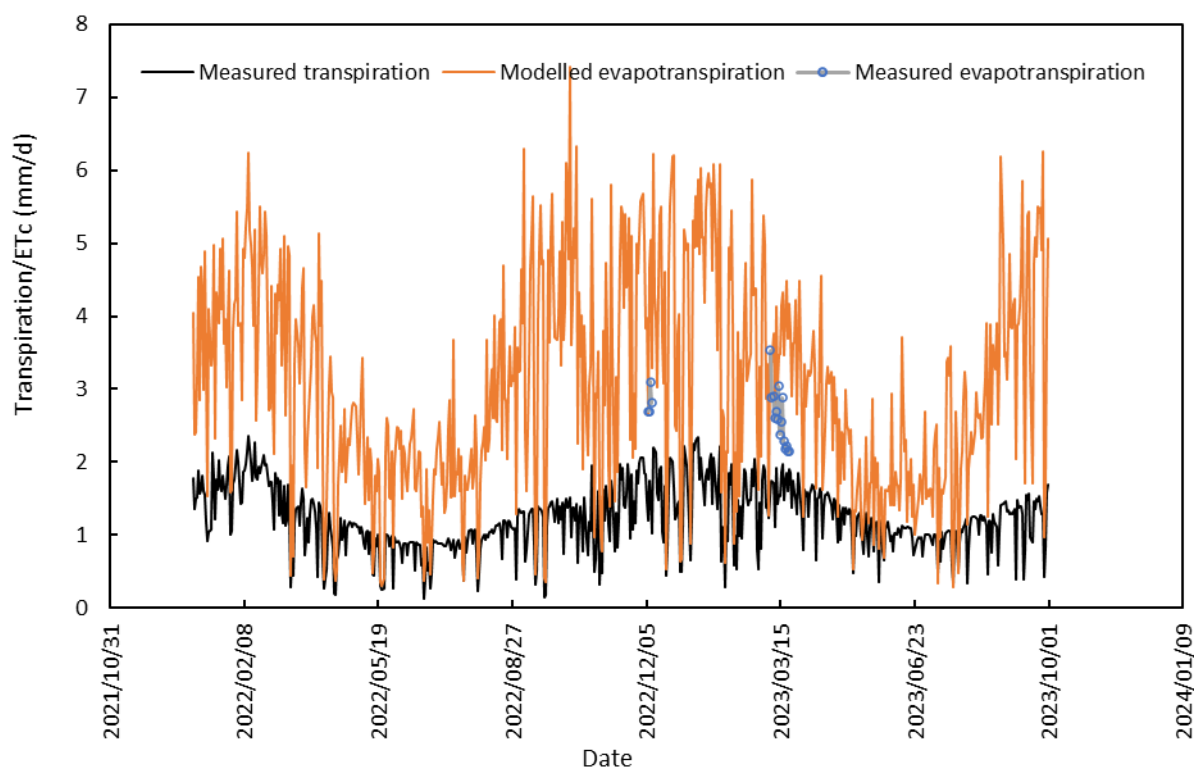


Figure 5.14: Seasonal dynamics in the measured transpiration and modelled ETc for the grapefruit orchard. The blue circles depict the measured ETc.

Table 5.3: Monthly crop coefficients for the grapefruit orchard

	Kc	Kcb	Ke
October	0.82	0.40	0.41
November	0.80	0.34	0.46
December	0.82	0.38	0.44
January	0.83	0.36	0.46
February	0.90	0.38	0.52
March	0.83	0.36	0.46
April	0.74	0.33	0.41
May	0.70	0.32	0.37
June	0.71	0.27	0.44
July	0.81	0.28	0.53
August	0.86	0.38	0.48
September	0.91	0.41	0.50

A summary of the orchard water balance from January to December 2022 showed that a massive amount of irrigation amounting to 997 mm was applied while transpiration was less than half the amount. Total evaporative losses amounted to 1 069 mm/yr or 10 690 m<sup>3</sup>/ha/yr while water inputs amounted to 1 555 mm/yr. There is very high possibility that this orchard was over-irrigated and this is clearly visualized in Fig. 5.15.

Table 5.4: Monthly summary of the water use data from the grapefruit orchard in Malelane.

Date	ETo (mm/mth)	T_measured (mm/mth)	Irrigation (mm/mth)	Rain (mm/mth)	ET
2022/01/31	133.2	49.4	41.1	203.2	108.8
2022/02/28	138.0	54.3	208.4	4.8	113.8
2022/03/31	120.7	39.0	155.0	68.6	108.5
2022/04/30	92.2	28.2	53.2	69.3	76.2
2022/05/31	77.0	26.3	31.0	113	57.2
2022/06/30	71.1	22.0	2.6	5.8	49.4
2022/07/31	77.5	28.1	67.2	4.3	54.7
2022/08/31	100.0	30.7	117.4	3.8	80.8
2022/09/30	121.1	33.7	44.6	31	96.9
2022/10/31	134.9	36.2	84.8	6	110.2
2022/11/30	125.9	43.0	78.0	36.8	101.0
2022/12/31	139.6	46.8	113.9	11.7	111.6
<b>Total</b>	<b>1331.2</b>	<b>437.7</b>	<b>997.3</b>	<b>558.3</b>	<b>1069.2</b>

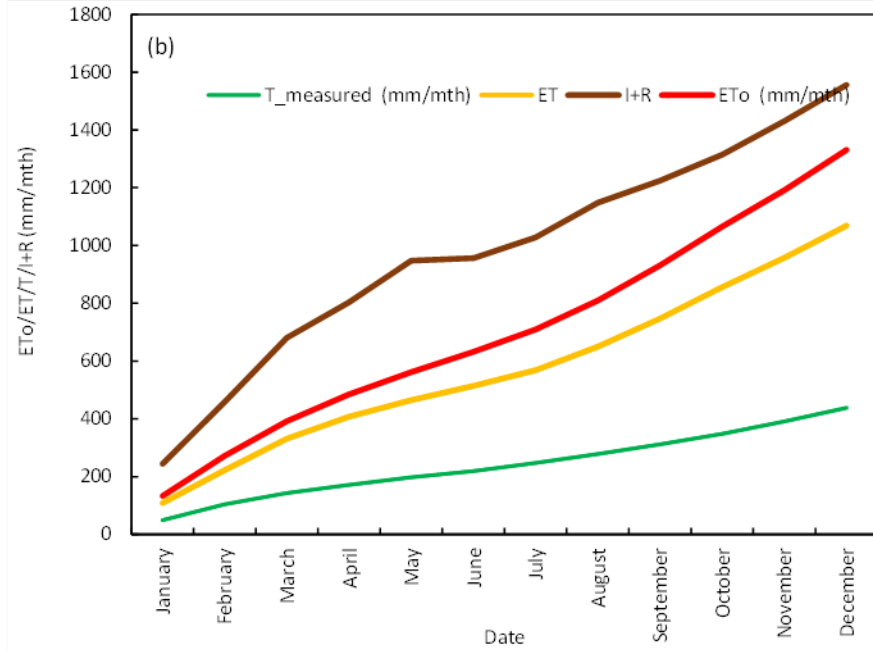
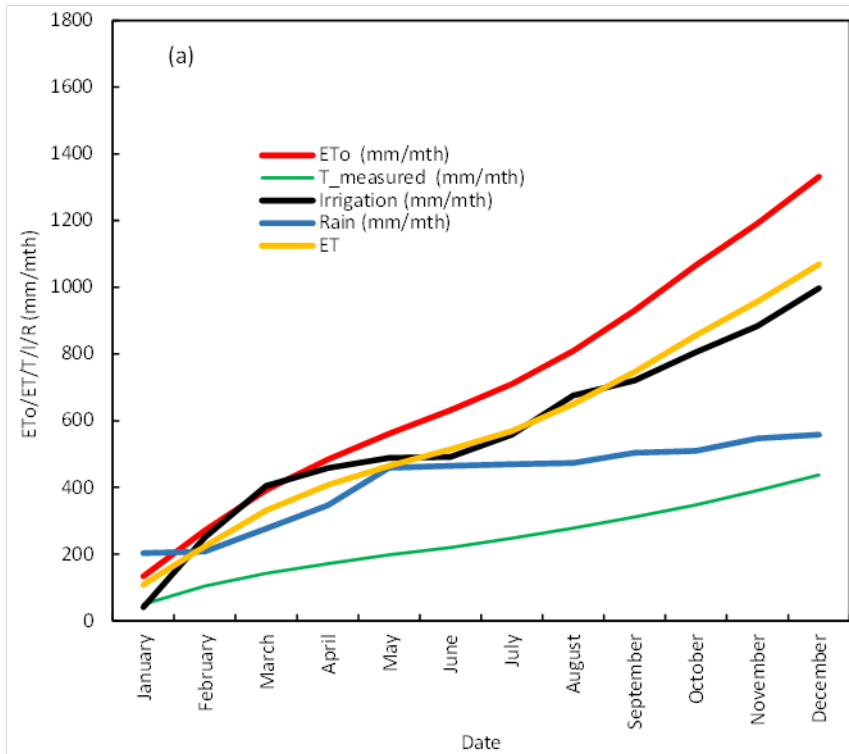


Figure 5.15: Water balance of the grapefruit orchard from January to December 2022 (a) with irrigation and rainfall presented separately, and (b) with irrigation and rainfall combined.

## 5.4. Conclusions

In this chapter we report on the water use characteristics of grapefruit growing in a commercial orchard under subtropical conditions in Mpumalanga over two growing seasons. These data show that, as with other citrus cultivars, grapefruit have low water use rates as a result of tight stomatal regulation of gas exchange. Both photosynthesis and stomatal conductance were low suggesting a strict stomatal control of gas exchange. Trees in the orchard were sparsely planted and this contributed to a low orchard scale transpiration which amounted to about 4 370 m<sup>3</sup>/ha/yr for 2022. The wide-open spaces between trees and the high irrigation levels led to a substantially high orchard ET<sub>c</sub> amounting to about 10 690 m<sup>3</sup>/ha/yr. However, most of this evaporation (up to 59%) emanated from the orchard floor which is a really high value. Yield from the orchard during the 2022 season was about 38 t/ha. Annual total transpiration of an individual tree was about 3 499 L. The water productivity of the grapefruit in the study orchard was about 3.52 kg/m<sup>3</sup> of water evapotranspired. Assuming a retail price per kilogram of about R 25 for grapefruit, the economic water productivity translates to about R 88 / m<sup>3</sup>.

## CHAPTER 6: WATER USE OF A BANANA ORCHARD UNDER SUBTROPICAL CONDITIONS

### 6.1. Summary

An experiment was conducted to quantify the water use of a banana orchard using the surface renewal (SR) and thermal dissipation probe (TDP) methods. The SR method was used to estimate evapotranspiration ( $ET_c$ ) from sensible and latent heat fluxes while whole plant transpiration was measured using TDPs. The SR method was calibrated against the eddy covariance system and the calibration factor subsequently used to correct independent SR measurements for  $ET_c$  estimation. Two-time lags ( $r = 0.4$  and  $r = 0.8$  s) were used in the datalogger for SR measurements. SR estimates of sensible heat flux varied with thermocouple placement height and time lag. The  $ET_c$  derived from SR ( $ETSR_r = 0.4$  and  $ETSR_r = 0.8$ , respectively) were compared to the  $ET_c$  calculated using the crop coefficient method ( $ETK_c$ ). The SR method overestimated  $ETK_c$  with a normalised root mean square error ( $NRMSE$ ) of 22.2% and a normalised mean absolute error ( $NMAE$ ) of 15.1% for  $ETSR_r = 0.4$ . The corresponding error measures for  $ETSR_r = 0.8$  were 20.3 and 13.7%. The  $ET$  estimated using surface renewal was closer to the  $ET$  obtained from the crop coefficient method when a time lag of 0.8 s was used for SR measurements. Using a suitable time lag enables surface renewal to be used as an alternative to the crop coefficient method for estimating banana evapotranspiration at field level in areas where crop coefficients are not available. To determine banana transpiration, TDPs were installed in the corm of the banana plant to measure sap flow. Measurements from 1 TDP were in phase with measurements of photosynthetically active radiation (PAR). The other 3 TDPs produced sap flow measurements which were out of phase with PAR. Results from the 3 TDPs were not expected indicating some technical problems with the data.

### 6.2. Introduction

The Mpumalanga Province, located in the north-eastern part of South Africa, is a key banana producing area. Mpumalanga has a sub-tropical climate with most of the rain falling in summer, during the months of October to March (Simpson *et al.*, 2019). Therefore, irrigation is critical during the banana growth periods in the dry months (April to September). About 46% of the surface water in Mpumalanga is channelled towards irrigation (Simpson *et al.*, 2019). According to the Second National Water Resources Strategy of South Africa (NWRS2, 2013), the available surface water resources in Mpumalanga and some catchments are already fully allocated. Therefore, there is a need for information and tools to improve water saving and

water use estimates in these catchments. At present, no accurate quantitative information exists in South Africa on the water use of banana. While tools are available for research, they are not usually available for use at farm level because of the high cost and the need for expertise to operate them. As a result, farmers use rough estimates of water use to schedule their irrigations often leading to chronic over-irrigation and wastage of the scarce water resources due to poor irrigation scheduling (Dzikiti *et al.*, 2018; Volschenk *et al.*, 2003). Crop evapotranspiration (*ET*) is believed to be the major consumptive water use in cropped fields (Minacapilli *et al.*, 2016; Wagle *et al.*, 2017; Yavuz *et al.*, 2015). Thus, determining crop *ET* may provide good estimates of the amount of water consumed by the crop. Various methods of determining *ET* exist; however, their utility at farm level is limited by a variety of factors including data requirements, accuracy, cost as well as the scale of measurement. Traditional micrometeorological methods such as the eddy covariance and Bowen ratio have been used to determine banana water use (e.g. Dicken *et al.*, 2013a, b; Tanny *et al.*, 2006; Tanny *et al.*, 2018), however, these methods have been mainly applied in screenhouses and not much is known on banana water use in open fields. The newer micrometeorological surface renewal method has also been used to estimate banana water use in a screenhouse (Mekhmandarov *et al.*, 2015). The study of Mekhmandarov *et al.* (2015) showed that the SR system can be used routinely by farmers for irrigation management. Findings of many other studies also suggest that the SR method can be used successfully at farm level (e.g. Gray *et al.*, 2021; Haymann *et al.*, 2019; Holwerda *et al.*, 2021; Masanganise *et al.*, 2022; Suvočarev *et al.*, 2019; Suvočarev *et al.*, 2014; Tosoni *et al.*, 2021; Xiong *et al.*, 2022). The SR method is believed to be less costly while the SR system is considered simpler to operate compared to traditional micrometeorological methods, hence it is more attractive for use at farm level. The SR method has not yet been used for determining water use of banana in South Africa and the current study offers further investigation of the applicability of the method. Measurements of crop transpiration are also important for irrigation management as they are often used for partitioning *ET* into beneficial and nonbeneficial crop water use. At the late-season growth stage, banana transpiration is difficult to measure for example using lysimeters because of the size of the crop at that stage. The soil water balance method has been shown to be problematic in estimating whole-plant water use of banana due to uncertainties in quantifying drainage (Turner, 1987). Other methods of measuring tree transpiration, based on sap flow, which have been widely used in woody trees include the stem heat balance method, (Grime and Sinclair, 1999; Hoelscher *et al.*, 2018; Langensiepen *et al.*, 2014), the heat pulse method (Dragoni *et al.*, 2005; Dzikiti *et al.*, 2018; Edwards and Warwick, 1984; Mobe *et al.*, 2020; Ntshidi *et al.*, 2021; Poblete-Echeverría *et al.*, 2012; Tfwala *et al.*, 2018) and the thermal dissipation probe (TDP) method (Ford *et al.*, 2004; Granier, 1987; Liu *et al.*, 2008a, b; Lu *et al.*, 2004; Lu *et al.*, 2002; Ntshidi *et al.*, 2021). The banana tree has a pseudostem, hence the movement of water in banana is different from that in woody trees due to the absence of a stem which contains

the xylem (Liu *et al.*, 2008b). This makes some common methods inappropriate for measuring banana sap flow. The base of the banana tree has a rounded and harder structure called the corm inside which is a central cylinder into which water flows from the roots. Xylem vessels originate from the central cylinder and spread out to the pseudostem (Liu *et al.*, 2008b). Lu *et al.* (2002) measured banana sap flow in the central cylinder using thermal dissipation probes and concluded that the method was reliable. The current study is the first to use the TDP method for determining transpiration of banana in South Africa, therefore, the aim of the current study was to test the utility of the surface renewal and the thermal dissipation probe methods in determining banana water use at farm level in an open field.

### **6.3. Materials and Methods**

#### **6.3.1 Description of the study site and plant material**

Field experiments were conducted from 31 May to 4 July (35 days) in a banana orchard at the Welgelegen Farm in Komatipoort, South Africa. The geographic location of the site is 25°30'32.8" S, 31°56'38.7" E, 1515 m a.s.l. The climate is classified as sub-tropical with dry, cool winters and warm, rainy summers. Based on the climatic data recorded at the Komati-SASRI (South African Sugarcane Research Institute) weather station from June 2012 to June 2022, the annual average of daily total rainfall for the site was 564.4 mm, Monthly averages of maximum and minimum air temperatures were 30.3 and 15.0°C, respectively with a long term mean of 22.7°C. The daily average grass reference evapotranspiration (FAO56 standard) was 3.8 mm d<sup>-1</sup>. The soil at the site is classified as the Hutton form (Soil Classification Working Group, 1991). The orchard was Block 703B which was planted to William Cavendish bananas on 2 September 2021. Typically, the growing season for bananas in the area extends from August to July. Orchard size was approximately 3.82 ha, and the crop was planted with a 3 m x 1.5 m spacing giving a planting density of 2222 trees per hectare. Average crop height at the time of equipment installation was approximately 4.5 m while the mean canopy diameter was about 1.8 m. Welgelegen is a commercial farming environment and the farm management was responsible for all cultural practices.

#### **6.3.2 Data collection**

##### **6.3.2.1 Orchard microclimate**

Weather data (air temperature, relative humidity, rainfall, wind speed and solar radiation) were recorded at a weather station which is located within 4 km of the trial site. The

weather station is maintained by the South African Sugarcane Research Institute (SASRI). The radiation intercepted by the canopy is critical for driving water use and other physiological processes. In the current study, the intercepted Photosynthetically Active Radiation (PAR) was measured using line quantum sensors (Model SQ110-apogee, Campbell Scientific, USA). One sensor was installed above and the other below the canopy about 1.50 m from the soil surface. These line sensors were installed on a flux tower, 6 m tall and supported on horizontal levelling fixtures aligned in a north-south orientation.

### 6.3.2.2 Eddy covariance and surface renewal measurements

Eddy covariance (EC) measurements were used to quantify the energy balance of the orchard as well as to calibrate the surface renewal (SR) method. An open path eddy covariance system was used to provide direct measurements of sensible heat flux  $H = H_{EC}$  ( $W m^{-2}$ ) required to calibrate SR. Sensors for both EC and SR systems were installed on the same flux tower, 6 m tall. For the EC system, a three-dimensional sonic anemometer (Campbell Scientific, Logan, Utah, USA) was installed at 5.40 m above the soil surface and used to measure high frequency air temperature. Measurements of air temperature were used to derive half-hourly means of  $H_{EC}$ . Water vapour concentration was measured using an infrared gas analyser (Model: LI-7500A, LI-COR Biosciences, USA). Raw data were collected at a frequency of 10 Hz and stored in a Campbell CR1000 datalogger. To determine other energy balance components, net radiation  $R_n$  ( $W m^{-2}$ ) was measured using a four-component net radiometer (Model: Kipp & Zonen, The Netherlands) which was installed at the height of the tower. The net radiometer was maintained at the same height throughout the sampling period. Soil heat flux  $G_{plate}$  ( $W m^{-2}$ ) was measured using two Hukseflux soil heat flux plates (HFP01-15, Delft, The Netherlands) buried horizontally at a depth of 0.080 m below the soil surface. Two pairs of Campbell TCAV-L averaging soil thermocouple probes were installed above the soil heat flux plates and below the surface at depths of 0.02 and 0.06 m to measure soil temperature. Soil water content was measured using two Campbell CS616 water content reflectometers installed horizontally in the neighbourhood of the soil heat flux plates and the averaging soil thermocouple probes. Measurements were averaged every thirty minutes and stored in the CR1000 datalogger. Soil heat storage  $G_{stored}$  ( $W m^{-2}$ ) above the heat flux plates was calculated from soil temperature and soil water content using

$$G_{stored} = \rho_{soil} c_{soil} \frac{\Delta z_{soil} \overline{\Delta T}_{soil}}{\Delta t} \quad (6.1)$$

where,  $\rho_{soil}$  is the bulk density of dry soil ( $\text{kg m}^{-3}$ ),  $c_{soil}$  the specific heat capacity of soil ( $\text{J kg}^{-1}\text{C}^{-1}$ ),  $\overline{\Delta T}_{soil}$  the change in the average soil temperature ( $^{\circ}\text{C}$ ) between the depth of 0.02 and 0.06 m measured over the time interval  $\Delta t$  (s) and  $\Delta z_{soil}$  the soil depth (m). The volumetric heat capacity of the soil was calculated using

$$\rho_{soil} c_{soil} = \rho_{soil} c_{dsoil} + \rho_w \theta_v c_w \quad (6.2)$$

where  $c_{dsoil}$  is the specific heat capacity of dry soil ( $840 \text{ J kg}^{-1}\text{C}^{-1}$ ),  $\rho_w$  the density of water ( $1000 \text{ kg m}^{-3}$ ),  $\theta_v$  the soil water content ( $\text{m}^3 \text{ m}^{-3}$ ),  $c_w$  the specific heat capacity of water ( $4200 \text{ J kg}^{-1}\text{C}^{-1}$ ). The total soil heat flux  $G$  ( $\text{W m}^{-2}$ ) was calculated as

$$G = G_{plate} + G_{stored} \quad (6.3)$$

The SR method (called SR1) proposed by Paw U and Brunet (1991) and Paw U *et al.* (1995) is an indirect method for estimating turbulent fluxes above an evaporating surface and it requires calibration. The method uses a fine-wire thermocouple (TC) to measure high frequency air temperature above the surface. Fluctuations in air temperature data reveal ramp-like structures which are analysed to determine the sensible heat flux  $H = H_{SR}$  ( $\text{W m}^{-2}$ ) above the surface. The sensible heat flux is calculated from the mean values of the amplitude and period of the ramps over a given time interval, typically 30 min. The theory and details of the SR method are documented by Paw and Brunet (1991) and Paw *et al.* (1995). In the current study, two type-E fine-wire Campbell (TCs) of diameter  $76 \mu\text{m}$  were used. The TCs were installed at different heights above the banana canopy. Each TC was installed on an arm extending from the flux tower and pointing in the main wind direction. The upper TC (TC1) was installed at 5.65 m above the soil surface while the lower TC (TC2) was at 5.15 m. Two different heights were used to observe the effect of air temperature measurement height on the calibration factor, hence on the estimates of sensible heat flux. Both TCs were connected to a separate Campbell CR1000 datalogger. Measurements of air temperature were made at a frequency of 10 Hz and lagged by time lags  $r = 0.4$  and  $r = 0.8$  s. The average canopy height was 4.50 m during the study period. The SR method was calibrated by taking simultaneous measurements of  $H_{EC}$  and plotting a regression line of  $H_{SR}$  (x-axis) versus  $H_{EC}$  (y-axis) and calculating the slope which is equal to the calibration factor  $\alpha$ .

### 6.3.2.3 Transpiration measurements

Individual plant transpiration was measured using thermal dissipation probes (TDP), also called Granier probes. The TDP consists of two steel needles, a heated and a non-heated (reference) needle. Each needle contains a type-T thermocouple (copper-constantan). Constant heat is supplied to the heated needle and a temperature gradient is established between the two needles. Both needles were inserted in the sapwood, which is located in the central cylinder, in the corm part of the banana plant. To install the TDPs, the topsoil was removed to a depth good enough to reach the corm. A metal template with two precisely drilled holes was used to mark the positions where the two needles were installed on the corm. A drill was then used to make holes 40 mm apart, with one hole vertically below the other. The heated needle was inserted in the upper hole while the reference needle in the lower hole. Half eggs were used to support the needles and to keep them in place. An aluminium reflective jacket was used to shield the sensors. The difference between the temperature of the heated needle and that of the reference needle was measured as a voltage difference. The heated probe measures the sapwood heat dissipation, which increases with sap flow while the reference probe measures the ambient temperature of the sap. When the sap velocity is minimum, the temperature difference between the two needles is maximum. Four plants with different corm sizes were instrumented. All the probes were connected to a Campbell CR1000 data logger. The sap flow data were collected at hourly intervals throughout the study period. The circumference of the corm was measured using a standard tape measure for each tree at the time of installation.

### 6.3.2.4 Irrigation

Irrigation volume was monitored using an electronic water flow meter (Model: ARAD Multi-Jet Water Meter, Germiston, South Africa) with a pulse rate of 10 L pulse<sup>-1</sup> installed on the irrigation line. The flow meter cable was connected to the same Campbell CR1000 data logger. The irrigation data were logged every hour throughout the study period. The amount of irrigation received by each plant was calculated as the volume of water that passes through the flow meter divided by the number of plants downstream of the flow meter.

### 6.3.2.5 Evapotranspiration

Evapotranspiration from a crop field is driven by the available energy ( $R_n - G$ ) and can be represented by the shortened surface energy balance equation:

$$R_n - G = H + LE \quad (6.4)$$

where  $LE$  ( $W\ m^{-2}$ ) is the energy equivalent of evapotranspiration. The actual daily evapotranspiration ( $ET$ ) from the banana orchard was quantified using the surface renewal (SR) method and the Food and Agriculture Organisation (FAO) crop coefficient ( $K_c$ ) approach. The SR method uses the energy balance equation (Eq. 4) to estimate  $ET$ . Therefore, in addition to  $H$ , other components of the energy balance namely  $R_n$  and  $G$  are also required. Soil heat flux plates were not available to measure  $G$ . Values of  $G$  were modelled following the procedure of Seguin and ITIER (1983) which has also been used in several studies (e.g. Anderson *et al.*, 1997; Liu, 2022; Miralles *et al.*, 2011; Norman *et al.*, 2003; Norman *et al.*, 1995). Using the values of  $H$ ,  $R_n$  and  $G$ , it is possible to determine the latent heat flux ( $LE$ ) as a residual of the shortened energy balance equation. Half-hourly SR-derived  $ET$  ( $ETSR_r = 0.4$  and  $ETSR_r = 0.8$ ) was calculated from  $LE$  by dividing  $LE$  by the latent heat of vaporisation of water using measurements from TC2 for both time lags. The half-hourly values of  $ETSR_r = 0.4$  and  $ETSR_r = 0.8$  were integrated to daily. The FAO crop coefficient approach was used to calculate daily  $ET$  ( $ET = ETK_c$ ) as the product of daily grass reference evapotranspiration ( $ET_o$ ) and late-season crop coefficient of banana, i.e. ( $ETK_c = K_c \times ET_o$ ) which was corrected for  $ET_o$  using the method of Guerra *et al.* (2014).

### 6.3.2.6 Data processing

Raw SR data were averaged in the datalogger every 30 min. Temperature measurements from SR were used to determine the second, third and fifth order air temperature structure functions ( $S^n(r)$ ) calculated as (Van Atta, 1977):

$$S^n(r) = \frac{1}{m-j} \sum_{i=1+j}^m (T_i - T_{i-j})^n \quad (6.5)$$

Where  $n$  is the order of the function,  $m$  the number of data points over 30 minutes measured at a frequency  $f$  (10 Hz in the current study),  $j$  the number of sample lags between data points corresponding to a time lag ( $r = j/f$ ) and  $T_i$  the air temperature sample at time  $i$ . The Van Atta (1977) structure function assumes that  $r$  should be much less than the ramp period  $\tau$  (s). The mean ramp amplitude  $a$  ( $^{\circ}C$ ) over 30 min was determined by solving for real roots the depressed third order equation:

$$a^3 + pa + q = 0 \quad (6.6)$$

using an iterative method (Savage, 2010, 2017), where

$$p = 10S^2(r) - \frac{S^5(r)}{S^3(r)} \quad (6.7)$$

$$q = 10S^3(r) \quad (6.8)$$

and  $\tau$  was calculated using

$$\tau = -\frac{a^3 r}{S^3(r)} \quad (6.9)$$

Half-hourly mean values of sensible heat flux  $H_{SR}$  were estimated as (Paw *et al.*, 1995):

$$H_{SR} = \rho_a c_p \alpha z \frac{a}{\tau} \quad (6.10)$$

where  $\rho_a$  is the density of air ( $\text{kg m}^{-3}$ ),  $c_p$  the specific heat capacity of air at constant pressure ( $\text{J kg}^{-1} \text{K}^{-1}$ ),  $z$  (m) the height of air temperature measurement and  $\alpha$  the calibration factor. Raw data for transpiration were processed using Baseline (version 4) (Oishi *et al.*, 2016). Baseline is a software for processing sap flux data from thermal dissipation probes (Granier 1985, 1987). The software provides a graphical user interface which is used for automatic and manual data cleaning, visualisations and estimating sap flux from raw TDP measurements. Details on software algorithms are documented in Oishi *et al.* (2016). Input data (day of year, time of day, photosynthetically active radiation and temperature difference between the heated and nonheated probe) were loaded into Baseline. The software does not calculate the sap flux density, instead it outputs a dimensionless sap flow index ( $K$ ) defined as (Granier, 1985):

$$K = \frac{dT_{max} - dT}{dT} \quad (6.11)$$

Where  $dT$  is the temperature difference between the heated and nonheated probe and  $dT_{max}$  the maximum temperature difference at zero flux. Hourly mean values of sap flux density  $F_h$  ( $\text{kg cm}^{-2} \text{h}^{-1}$ ) were calculated using the relationship (Granier, 1985, 1987):

$$F_h = 0.04284K^{1.231} \quad (6.12)$$

The total sap flow  $F$  ( $\text{L h}^{-1}$ ) was calculated by multiplying  $F_h$  by the total sapwood area calculated following Liu *et al.* (2008b) and dividing by the density of water.

### 6.3.2.7 Statistical analysis

The orchard energy balance was assessed using the slope, intercept and coefficient of determination ( $R^2$ ). A slope of 1 and an intercept of 0 indicate a perfect match between the consumed and available energy flux. The values of  $R^2$  lie in the range  $0 \leq R^2 \leq 1$  with values of  $R^2$  close to 1 indicating good agreement between the data being compared (Adeboye *et al.*, 2017a). The statistical indicators for evaluating the SR method for estimating sensible heat flux were the slope ( $= \alpha$ ) and  $R^2$ . A value of  $\alpha = 1$  indicates a perfect agreement between  $H_{SR}$  and  $H_{EC}$ . When  $\alpha < 1$ , the SR method overestimated  $H$  compared to EC while  $\alpha > 1$  shows that the SR method underestimated  $H$  compared to EC. The FAO crop coefficient approach was used as the benchmark for comparing  $ETKc$  with  $ETSR$ . The accuracy of SR in estimating  $ET$  was evaluated using two statistical indicators: the normalised root mean square error ( $NRMSE$ ) and the normalised mean absolute error ( $NMAE$ ). The indicators are calculated using:

$$NRMSE = \frac{1}{\bar{Q}} \sqrt{\frac{\sum_{i=1}^n (P_i - Q_i)^2}{n}} \times 100 \quad (6.13)$$

$$NMAE = \frac{\sum_{i=1}^n |P_i - Q_i|}{n\bar{Q}} \times 100 \quad (6.14)$$

where  $P_i$  are the values of  $ETKc$ ,  $Q_i$  are the values of  $ETSR_r = 0.4$  or  $ETSR_r = 0.8$ ,  $\bar{Q}$  are the mean values of  $ETSR_r = 0.4$  or  $ETSR_r = 0.8$  and  $n$  is the number of data points. The target value for  $NRMSE$  is 0% and  $NRMSE$  values close to 0% indicate a good agreement between  $ETKc$  and  $ETSR_r = 0.4$  or  $ETSR_r = 0.8$ . According to Jamieson *et al.* (1991),  $NRMSE$  values are excellent if smaller than 10%, good if between 10 and 20%, fair if between 20 and 30% and poor if greater than 30%. Values of  $NMAE$  that are less than 15% are considered low while values in the range 20-35% are considered high (Alessandrini and Sperati, 2017). The relationship between SR-derived  $ET$  or sap flow with  $ET_o$ , VPD and  $R_s$  were assessed using  $R^2$ .

## 6.4. Results

### 6.4.1 Microclimate

The climatic conditions during the study period are summarised in Table 6.1. The total amount of rainfall received was 11.3 mm from 5 rainfall events, with each event recording less than 7 mm per day. The Welgelegen Farm is located in a summer rainfall area. During winter, the region is predominantly dry, making irrigation a critical source of soil moisture for the growth

of bananas. The maximum and minimum air temperatures were 32.1 and 0.3°C recorded on 4 July and 17 June respectively with an average of 16.2°C. The total grass reference evapotranspiration which was calculated using the method of Allen *et al.* (1998) was 63.1 mm. The daily maximum solar radiation peaked at 15 MJ m<sup>-2</sup> day<sup>-1</sup> during the study period.

Table 6.1: Summary of daily rainfall (Rain); maximum (Tmax), minimum (Tmin) air temperature; solar radiation (Rs); grass reference evapotranspiration (ET<sub>o</sub>); maximum (RHmax), minimum (RHmin) relative humidity and wind speed (U) at the farm recorded from 31 May to 4 July 2022.

DATE	Rain (mm)	Tmax (°C)	Tmin (°C)	Rs (MJ m <sup>-2</sup> day <sup>-1</sup> )	ET <sub>o</sub> (mm day <sup>-1</sup> )	RHmax (%)	RHmin (%)	U (m s <sup>-1</sup> )
31-May	0.0	28.0	9.9	13.4	2.5	95.0	28.0	1.0
01-Jun	0.0	24.8	6.0	15.0	2.1	96.0	26.0	0.6
02-Jun	0.0	25.5	3.5	14.8	1.6	98.0	27.0	0.2
03-Jun	0.0	24.9	4.6	14.6	1.7	97.0	44.0	0.3
04-Jun	0.0	25.9	6.5	14.6	1.9	98.0	45.0	0.5
05-Jun	0.3	25.8	8.8	12.2	2.2	98.0	45.0	1.1
06-Jun	0.0	24.6	8.4	10.2	1.8	96.0	42.0	0.8
07-Jun	0.0	26.3	4.4	14.1	1.6	98.0	39.0	0.2
08-Jun	0.1	25.8	4.7	14.4	1.6	98.0	42.0	0.2
09-Jun	0.0	24.1	6.4	14.0	1.7	98.0	43.0	0.4
10-Jun	0.0	25.6	6.0	9.8	1.7	98.0	47.0	0.7
11-Jun	0.0	26.2	9.2	13.9	1.7	98.0	43.0	0.3
12-Jun	0.0	25.9	5.7	14.4	2.0	97.0	36.0	0.6
13-Jun	0.0	27.0	3.6	11.4	1.8	96.0	33.0	0.5
14-Jun	0.0	27.2	3.1	11.2	2.2	96.0	31.0	0.9
15-Jun	0.0	24.8	8.4	6.1	1.7	94.0	28.0	0.8
16-Jun	0.0	22.2	4.2	11.2	1.4	98.0	32.0	0.4
17-Jun	0.0	22.9	0.3	11.0	1.7	97.0	39.0	0.7
18-Jun	0.0	26.4	3.8	10.9	1.8	97.0	38.0	0.7
19-Jun	0.0	27.7	6.0	10.9	2.0	96.0	47.0	0.9
20-Jun	0.0	25.2	12.9	6.5	1.4	96.0	50.0	0.6
21-Jun	0.0	15.4	13.9	11.2	1.7	95.0	92.0	1.2
22-Jun	6.3	13.9	13.4	3.1	0.8	99.0	99.0	0.7
23-Jun	0.0	24.0	11.3	14.9	1.9	100.0	52.0	0.6
24-Jun	0.0	18.6	18.2	12.7	2.5	79.0	68.0	1.9
25-Jun	0.0	15.2	11.6	9.1	1.7	88.0	84.0	1.2
26-Jun	0.0	11.4	8.6	8.8	1.2	95.0	92.0	0.6
27-Jun	2.3	14.8	13.0	6.1	1.0	98.0	93.0	0.3
28-Jun	2.3	14.3	11.0	9.3	1.3	96.0	94.0	0.6
29-Jun	0.0	14.1	8.2	13.8	1.3	95.0	83.0	0.2
30-Jun	0.0	10.9	7.4	14.1	1.4	96.0	93.0	0.6
01-Jul	0.0	24.6	5.0	14.2	1.9	90.0	41.0	0.7
02-Jul	0.0	21.0	10.7	13.8	1.6	95.0	67.0	0.3

DATE	Rain (mm)	Tmax (°C)	Tmin (°C)	Rs (MJ m <sup>-2</sup> day <sup>-1</sup> )	<i>ET<sub>o</sub></i> (mm day <sup>-1</sup> )	RHmax (%)	RHmin (%)	U (m s <sup>-1</sup> )
03-Jul	0.0	10.9	10.6	13.9	1.6	95.0	94.0	0.8
04-Jul	0.0	32.1	8.5	14.0	2.3	87.0	23.0	0.6

### 6.4.2 Energy balance for the banana orchard

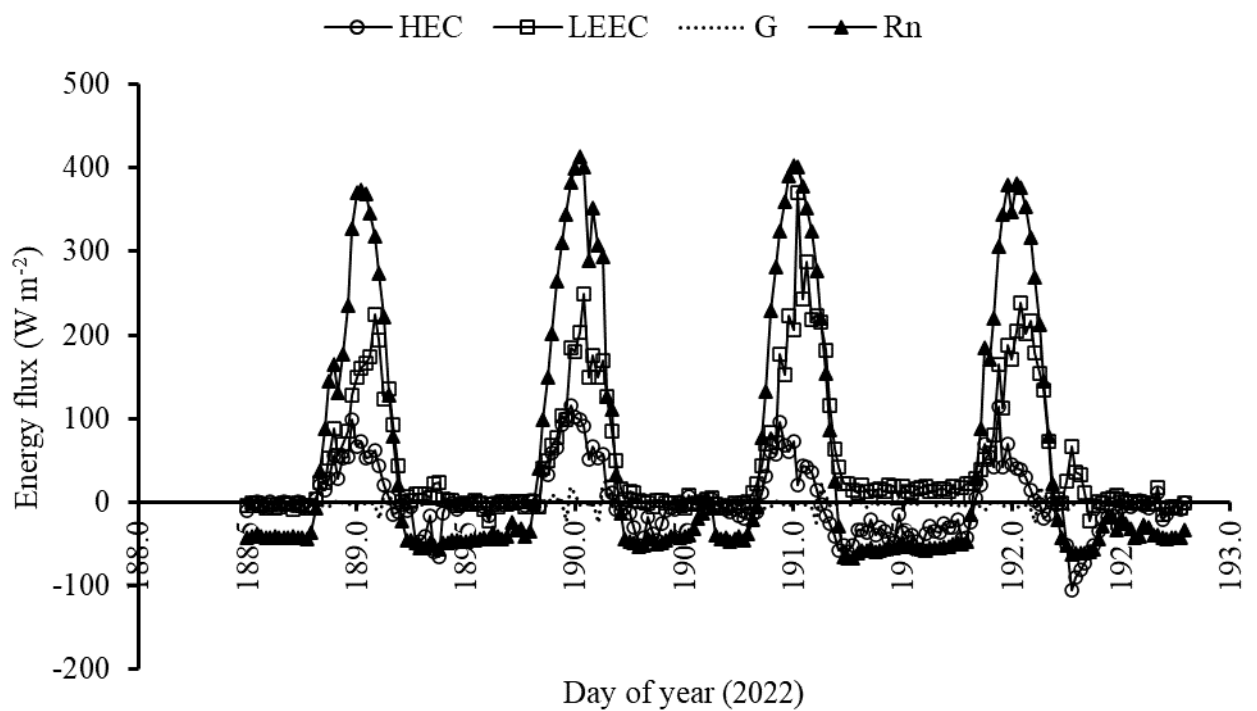


Figure 6.1: Diurnal variations of half-hourly sensible heat flux ( $H_{EC}$ ), latent heat flux ( $LE_{EC}$ ), net radiation ( $R_n$ ) and soil heat flux ( $G$ ).

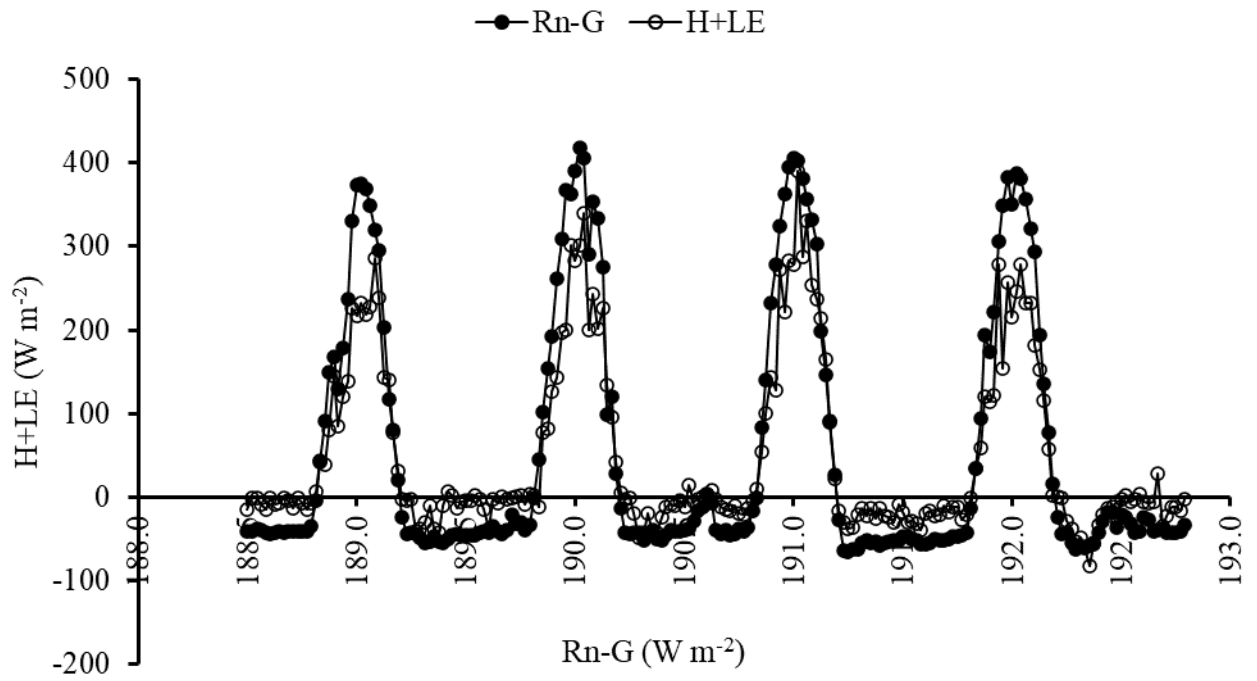


Figure 6.2: Diurnal variations of half-hourly values of the consumed energy flux ( $H + LE$ ) and the available energy flux ( $R_n - G$ ) derived from EC measurements of  $H$  and  $LE$ .

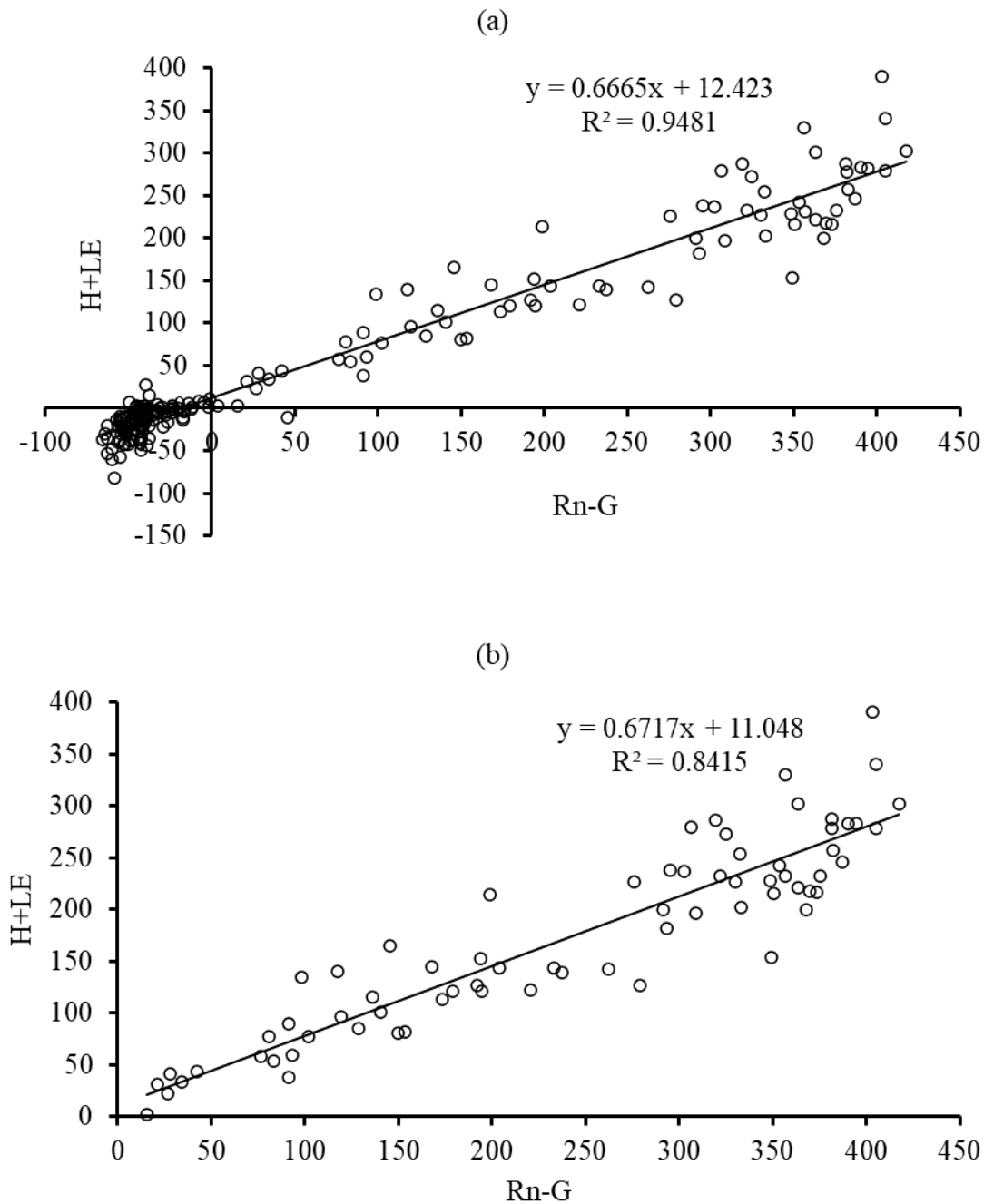
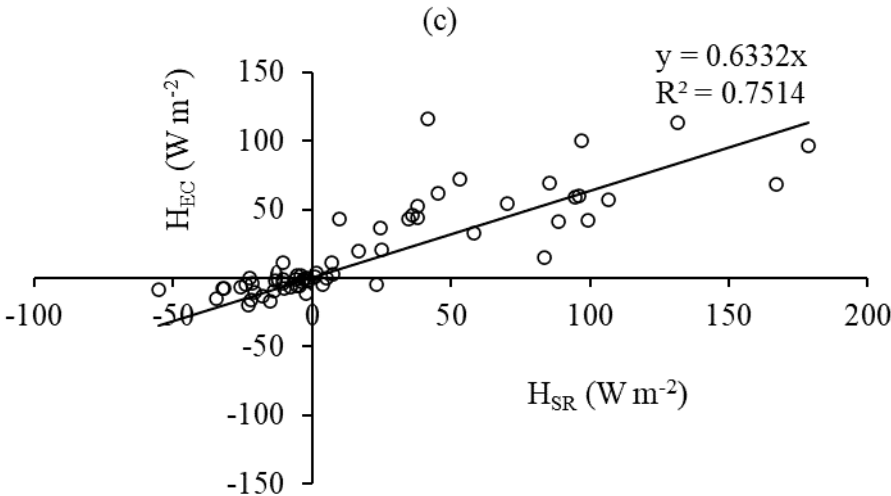
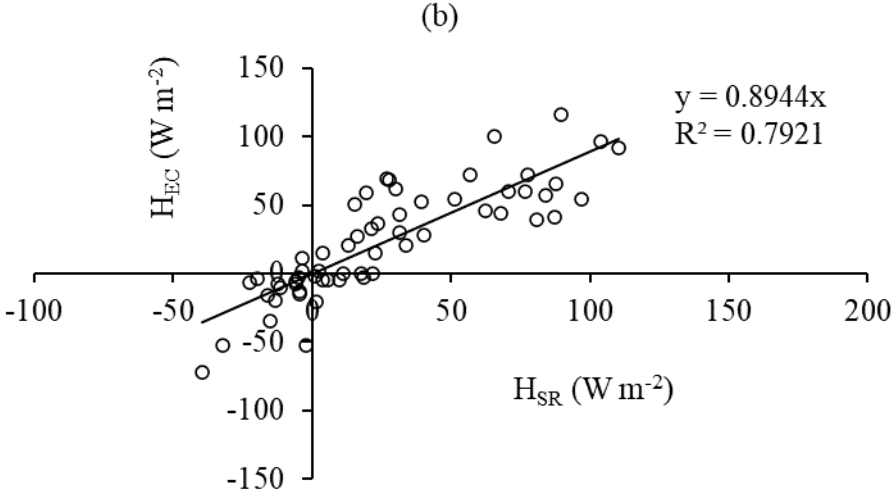
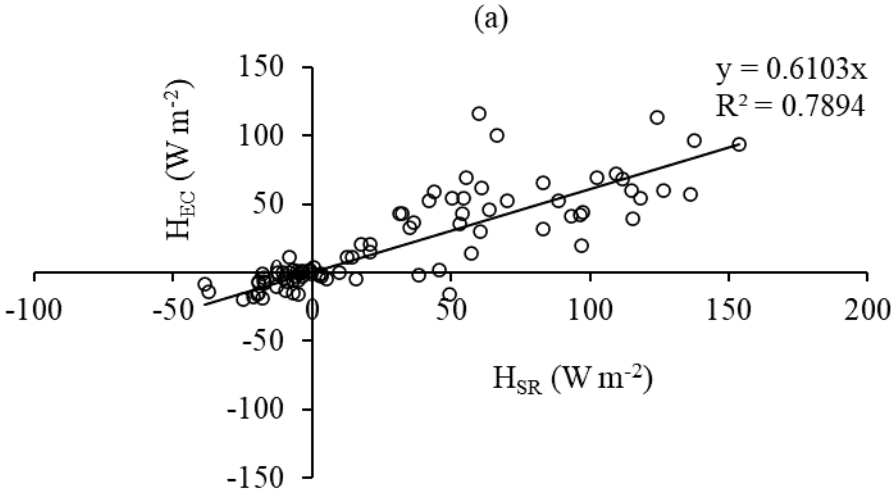


Figure 6.3: Energy balance closure for the banana orchard based on EC measurements of  $H$  and  $LE$  using (a) data for stable and unstable conditions and (b) data for unstable conditions only.

Diurnal half-hourly fluxes of  $H$  and  $LE$  measured by the covariance system are shown in Fig. 6.1 together with measured fluxes of  $R_n$  and  $G$ . Fig. 6.2 shows the diurnal variations of half-hourly values of the consumed energy flux ( $H + LE$ ) against the available energy flux ( $R_n - G$ ) during 4 days. A good agreement between  $H + LE$  and  $R_n - G$  was found; however, consumed energy flux was lower than the available energy flux. A plot of half-hourly values of  $H + LE$  against  $R_n - G$  is shown in Fig. 6.3. Such a scatter plot is commonly used for verifying eddy covariance measurements. Using data for both stable and unstable conditions, a straight

line fitted to the data points had a slope of 0.667, an intercept of 12.42 W m<sup>-2</sup> and the R<sup>2</sup> value was 0.948. (Fig. 6.3a). Using data for unstable conditions only, the slope, intercept and R<sup>2</sup> values were 0.672, 11.05 W m<sup>-2</sup> and 0.842 (Fig. 6.3b). According to Wilson *et al.* (2002) open canopies produce closure slopes in the range 0.55-0.99. We found a good energy balance closure for the banana orchard with slopes in the range of reported values and relatively small values of intercept which shows that the fluxes were valid. The high value of R<sup>2</sup> indicates a strong correlation between the consumed and available energy fluxes. Using data for unstable conditions only slightly increased the slope and slightly decreased the intercept.

6.4.3 Calibration of surface renewal



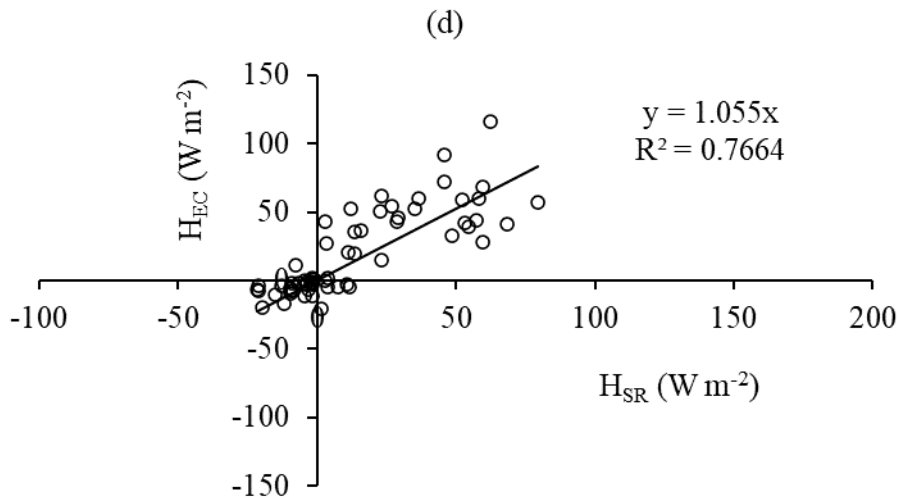


Figure 6.4: Regression lines for calibrating surface renewal using eddy covariance. The lines were generated using SR measurements from (a) TC1 and a time lag of 0.4 s; (b) TC1 and a time lag of 0.8 s; (c) TC2 and a time lag of 0.4 s and (d) TC2 and a time lag of 0.8 s. The slope of each line is the  $\alpha$  value.

Using a time lag of 0.4 s, the slope for the measurement height of 5.65 m was 0.610 and the  $R^2$  value was 0.789 (Fig. 6.4a). For a time lag of 0.8 s at the same measurement height, the corresponding values were 0.894 and 0.792 (Fig. 6.4b). At 5.15 m, the slope was 0.633 and the  $R^2$  value was 0.751 using a time lag of 0.4s (Fig. 6.4c). Using a time lag of 0.8 s at the same measurement height, the slope and  $R^2$  values were 1.055 and 0.766 respectively (Fig. 6.4d). For the same measurement height, the slope increased with increase in time lag. For the same time lag, the slope decreased with increase in measurement height.

#### 6.4.4 Sensible and latent heat fluxes derived from measurements of surface renewal

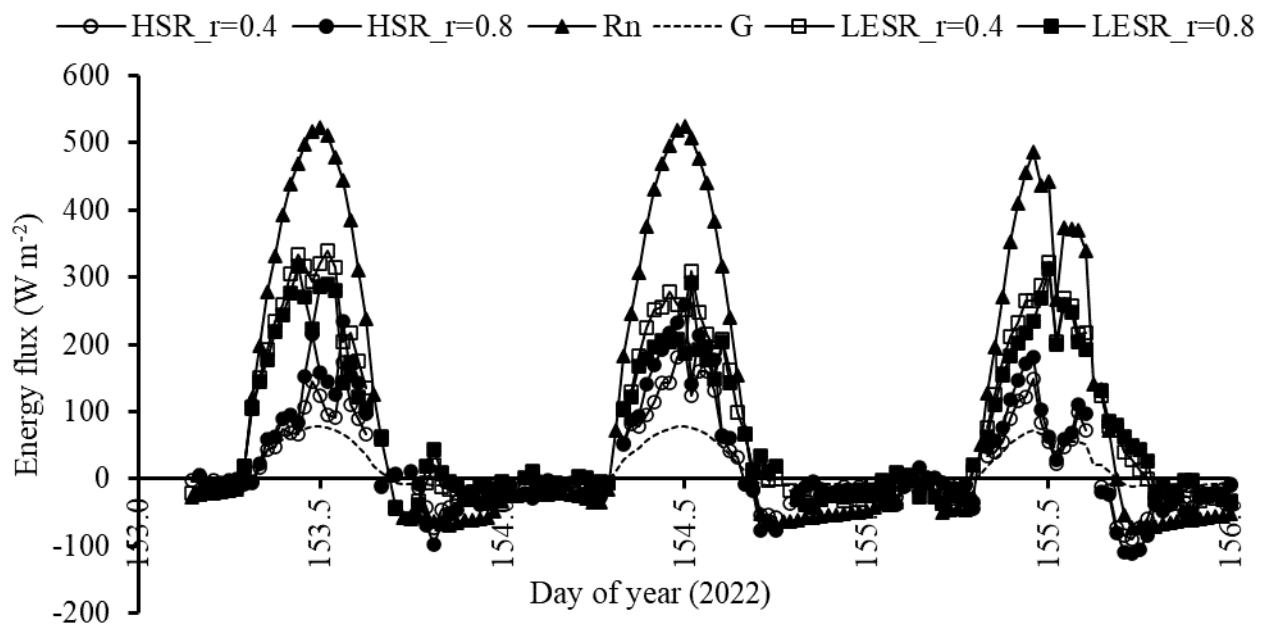


Figure 6.5: Diurnal variations of half-hourly sensible heat flux estimated using a time lag of 0.4 s ( $HSR_r = 0.4$ ), sensible heat flux estimated using a time lag of 0.8 s ( $HSR_r = 0.8$ ), net radiation ( $R_n$ ), soil heat flux ( $G$ ), latent heat flux estimated using a time lag of 0.4 s ( $LESR_r = 0.4$ ) and latent heat flux estimated using a time lag of 0.8 s ( $LESR_r = 0.8$ ).

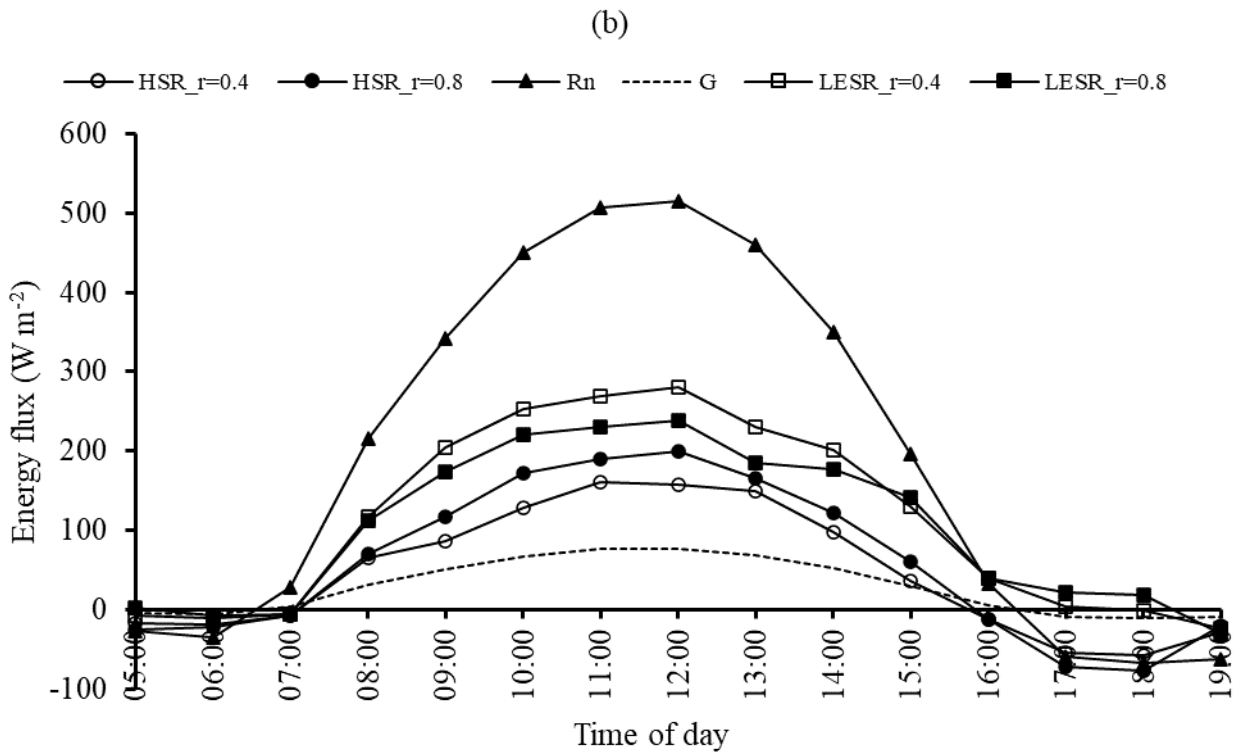
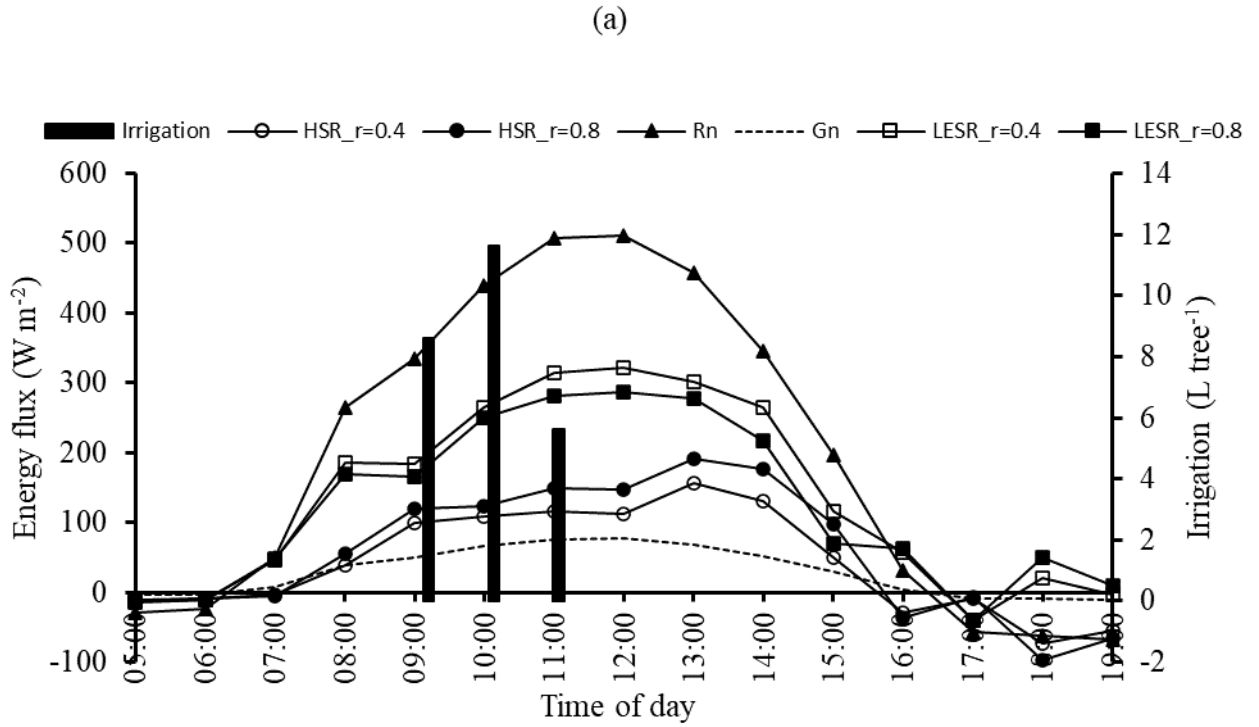


Figure 6.6: Diurnal variations of hourly sensible heat flux estimated using a time lag of 0.4 s ( $HSR_r = 0.4$ ), sensible heat flux estimated using a time lag of 0.8 s ( $HSR_r = 0.8$ ), net radiation ( $R_n$ ), soil heat flux ( $G$ ), latent heat flux estimated using a time lag of 0.4 s ( $LESR_r = 0.4$ ), latent heat flux estimated using a time lag of 0.8 s ( $LESR_r = 0.8$ ) on a day (a) with irrigation and (b) without irrigation.

Diurnal variations of half-hourly sensible heat flux ( $HSR$ ) and latent heat flux ( $LESR$ ) estimated using surface renewal are shown in Fig. 6.5. The diurnal variation of all fluxes was similar to that of  $R_n$ . Fig. 6.6a presents the diurnal trends of hourly  $HSR$ ,  $LESR$ ,  $R_n$  and  $G$  on a typical clear day (DOY 153) with irrigation applied to the orchard. All fluxes followed the diurnal pattern of  $R_n$  which peaked at  $510.9 \text{ W m}^{-2}$ . Both  $HSR_r = 0.4$  and  $HSR_r = 0.8$  were lower than  $LESR_r = 0.4$  and  $LESR_r = 0.8$  respectively. The maximum value of  $HSR_r = 0.4$  was  $156.4 \text{ W m}^{-2}$  while that of  $HSR_r = 0.8$  was  $191.6 \text{ W m}^{-2}$  respectively. Correspondingly,  $LESR_r = 0.4$  and  $LESR_r = 0.8$  peaked at  $321.6$  and  $286.9 \text{ W m}^{-2}$  respectively. The fluctuations of  $G$  were in the range  $-10.0$  and  $76.6 \text{ W m}^{-2}$ . The irrigation event lasted for 3 hours and the total amount of irrigation applied was  $25.8 \text{ L}$ . The variation of the fluxes on a typical clear day (DOY 155) with no irrigation applied is shown in Fig. 6.6b. All the energy fluxes responded to  $R_n$ , following its trend. On this day, the maximum value of  $R_n$  was  $515.5 \text{ W m}^{-2}$ .  $HSR_r = 0.4$  peaked at  $161.5 \text{ W m}^{-2}$  while  $HSR_r = 0.8$  had a maximum value of  $199.6 \text{ W m}^{-2}$ . The corresponding values of  $LESR_r = 0.4$  and  $LESR_r = 0.8$  were  $280.0$  and  $238.6 \text{ W m}^{-2}$ . Fluxes of  $G$  were relatively higher, with a peak value of  $77.3 \text{ W m}^{-2}$ . The  $HSR$  fluxes were lower on DOY 153 compared to the fluxes obtained on DOY 155. Fluxes of  $LESR$  were higher on DOY 153 than the fluxes measured on DOY 155.

#### 6.4.5 Evapotranspiration estimates

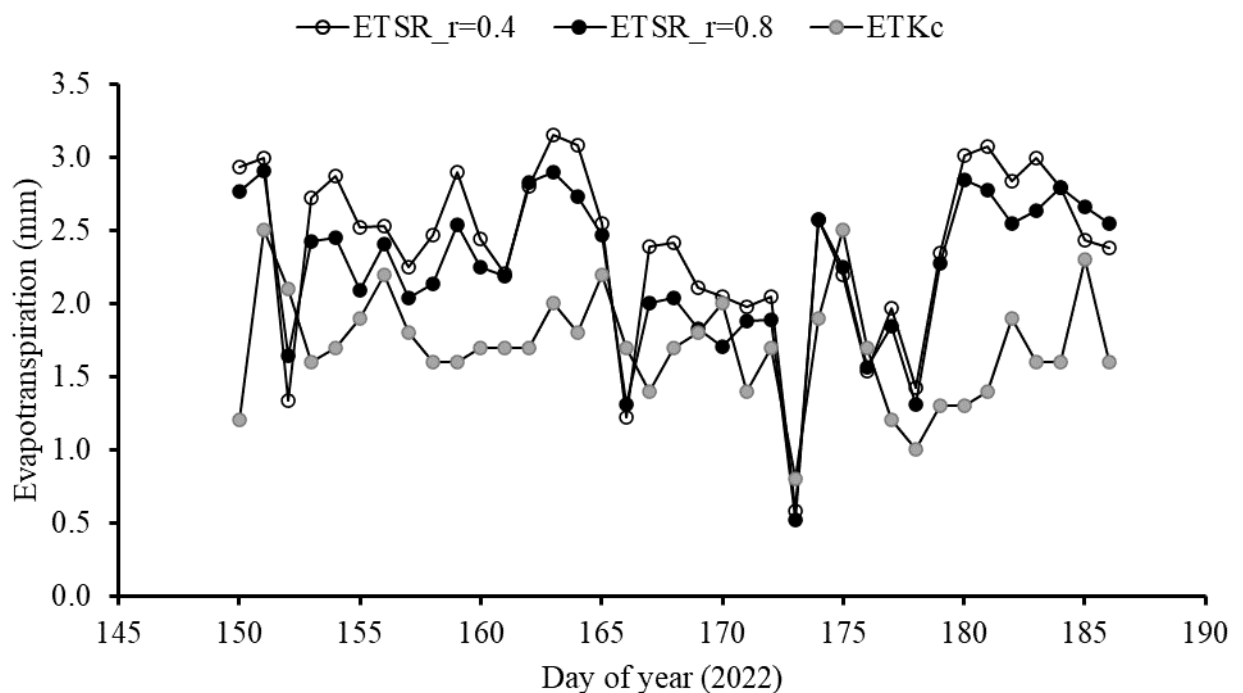


Figure 6.7: Diurnal variations of actual evapotranspiration derived from surface renewal using a time lag of  $0.4 \text{ s}$  ( $ETSR_r = 0.4$ ), using a time lag of  $0.8 \text{ s}$  ( $ETSR_r = 0.8$ ) and daily evapotranspiration derived from the crop coefficient method ( $ETKc$ ).

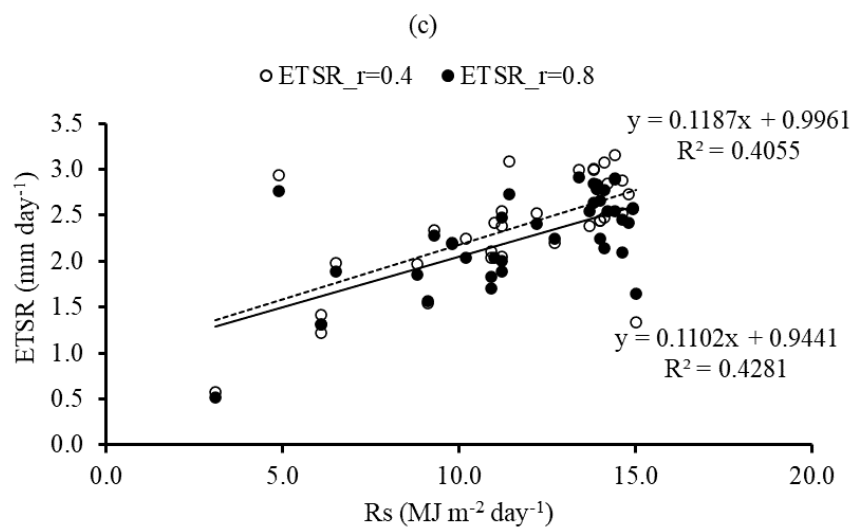
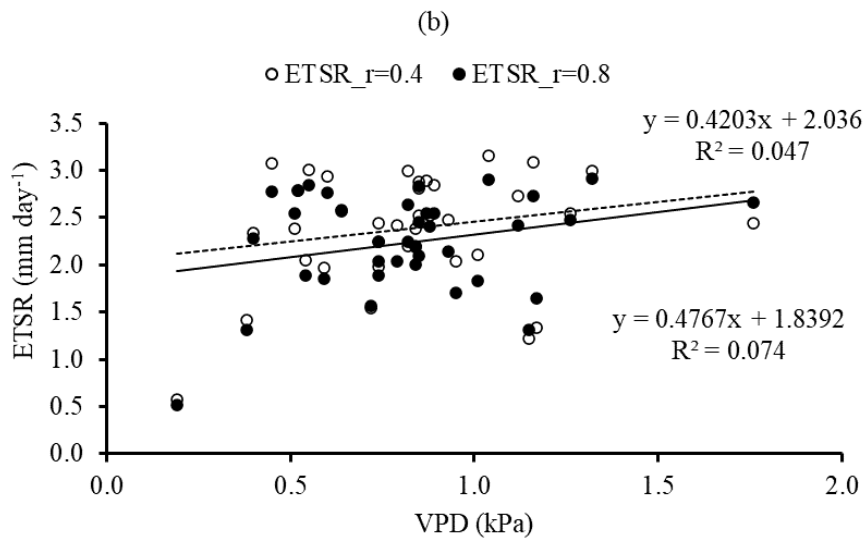
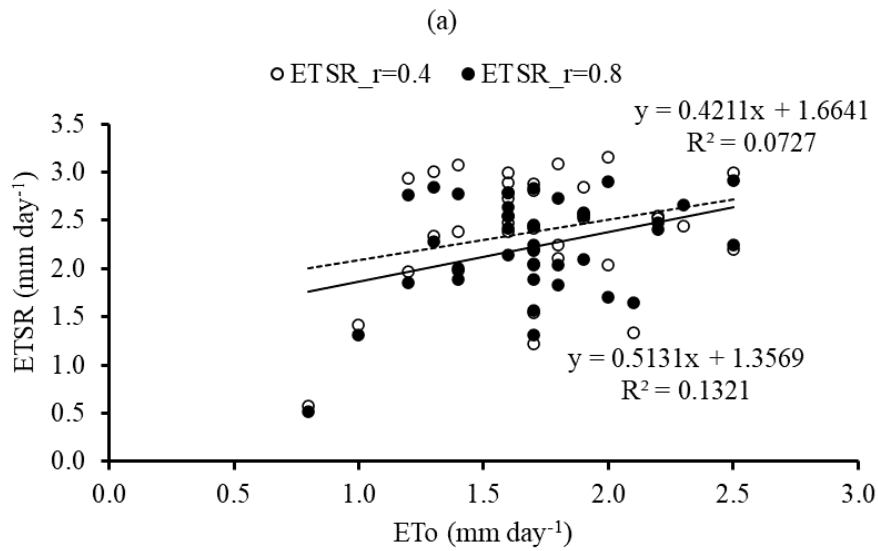
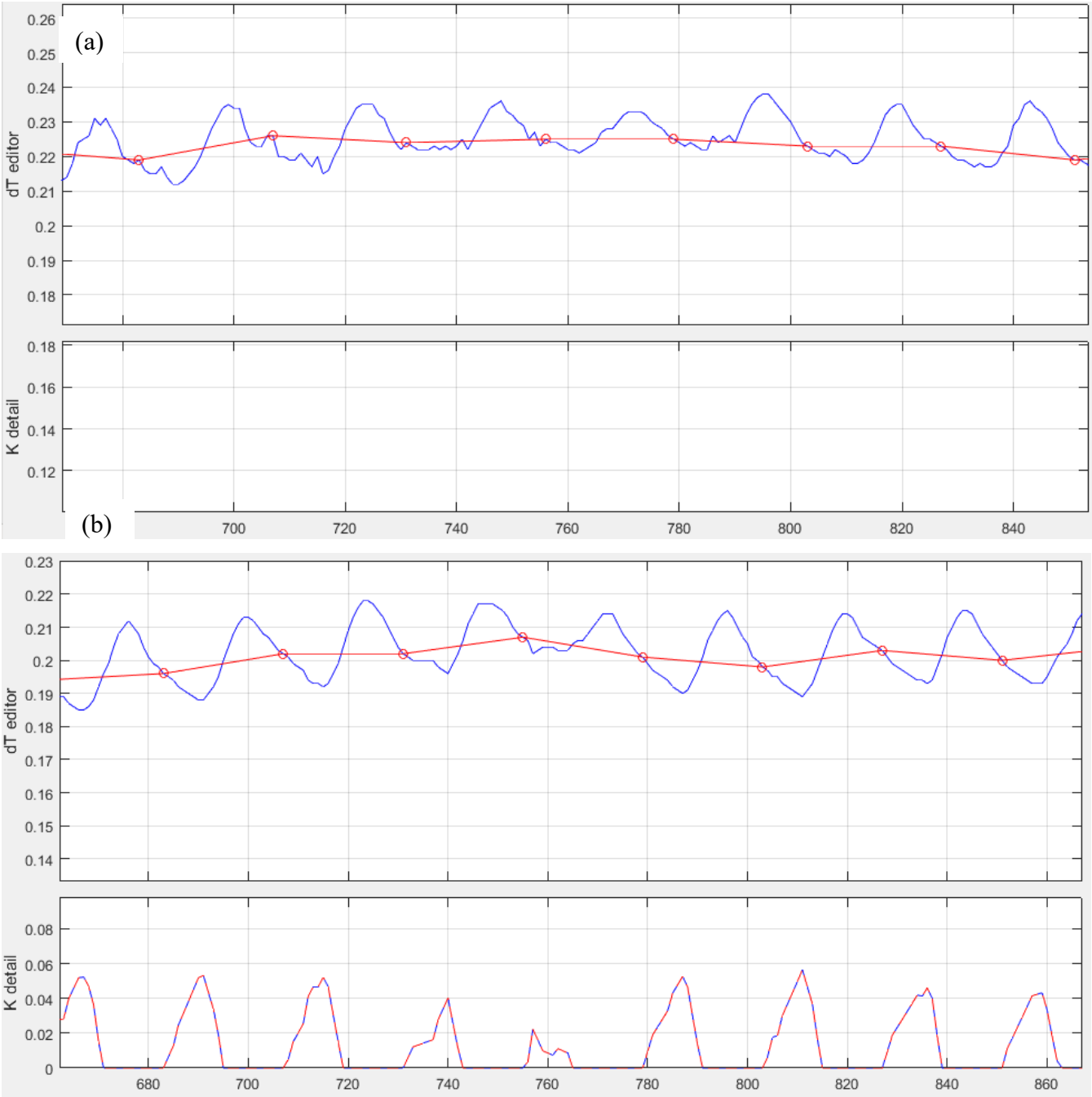


Figure 6.8: Dependence of actual evapotranspiration derived from surface renewal (*ETS<sub>R</sub>*) on (a) reference evapotranspiration (*E<sub>T0</sub>*); (b) vapour pressure deficit (*VPD*) and (c) solar radiation (*Rs*).

The  $ET$  derived from SR ( $ETSR_r = 0.4$  and  $ETSR_r = 0.8$  respectively) were compared to the  $ET$  calculated using the crop coefficient method ( $ETKc$ ). The diurnal patterns of  $ETSR_r = 0.4$  and  $ETSR_r = 0.8$  were in phase with each other, however, both patterns were out of phase with that of  $ETKc$  for much of the time (Fig. 6.7).  $ETSR_r = 0.4$  fluctuated with a maximum value of  $3.2 \text{ mm day}^{-1}$  and a minimum value of  $0.6 \text{ mm day}^{-1}$ . The corresponding values for  $ETSR_r = 0.8$  were  $2.9$  and  $0.5 \text{ mm day}^{-1}$  while the corresponding values for  $ETKc$  were  $2.5$  and  $0.8 \text{ mm day}^{-1}$ . For the study period, the sums of  $ETSR_r = 0.4$ ,  $ETSR_r = 0.8$  and  $ETKc$  were  $88.1$ ,  $82.6$  and  $63.1 \text{ mm}$  respectively. The SR method overestimated  $ETKc$  with a normalised root mean square error ( $NRMSE$ ) of  $22.2\%$  and a normalised mean absolute error ( $NMAE$ ) of  $15.1\%$  for  $ETSR_r = 0.4$ . The corresponding error measures for  $ETSR_r = 0.8$  were  $20.3$  and  $13.7\%$ . Although  $ETSR_r = 0.4$  and  $ETSR_r = 0.8$  did not match  $ETKc$  for much of the time, it is interesting to note that the trends for low  $ET$  rates were similar for  $ETSR$  and  $ETKc$  (Fig. 6.7). The correlation between  $ETSR$  and  $ET_o$ , VPD and  $R_s$  produced  $R^2$  values in the range  $0.05$ - $0.43$  for the two time lags used for surface renewal (Fig. 6.8). The  $R^2$  values were higher for the time lag of  $0.8$  compared to  $0.4 \text{ s}$  across all the drivers of evapotranspiration. The correlation was highest between  $ETSR$  and  $R_s$  and lowest between  $ETSR$  and VPD.

### 6.4.6 Transpiration measurements



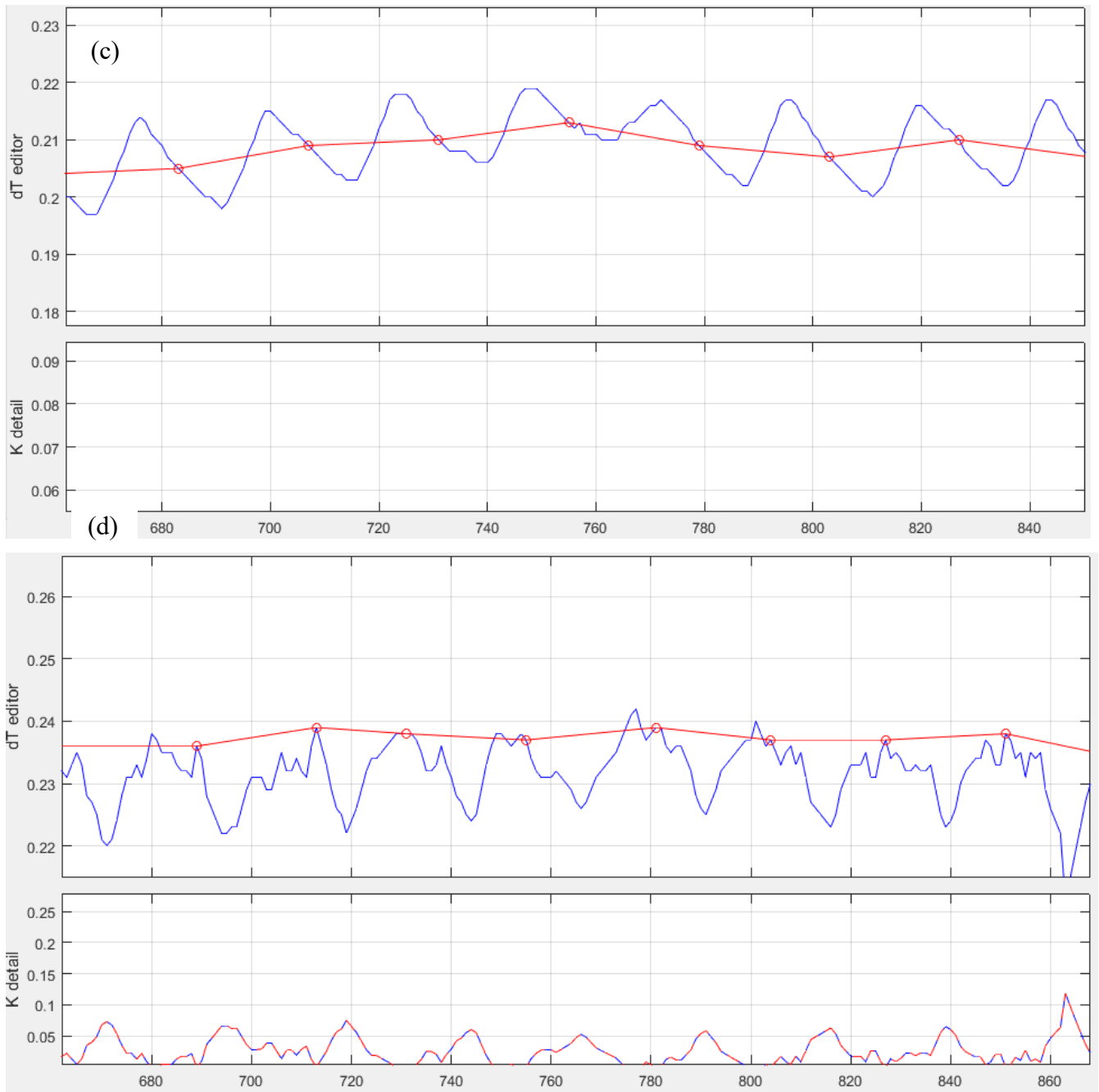


Figure 6.9: An example of Baseline user interface window showing (a; b; c) abnormal trend of  $dT_{max}$  values and (d) normal trend of  $dT_{max}$  values.

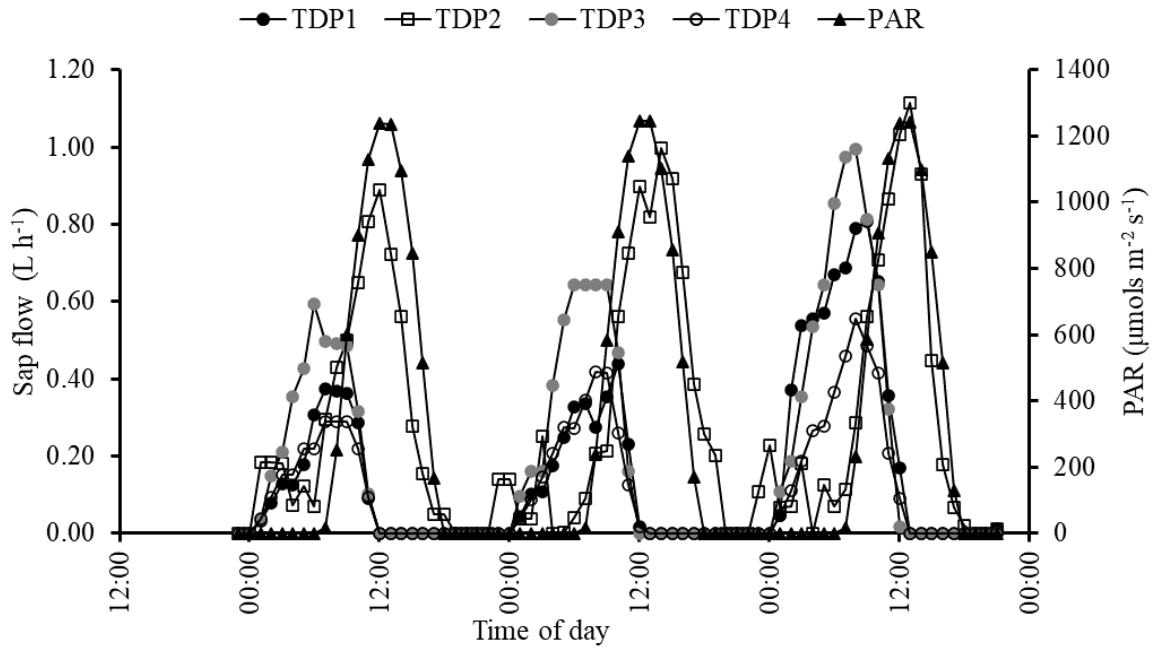


Figure 6.10: Diurnal variations of hourly sap flow ( $F$ ) determined by four TDPs and the photosynthetically active radiation (PAR) during 3 consecutive days.

The trends of  $dT_{max}$  values generated automatically in Baseline 4 for TDP 1, 3 and 4 are shown in Fig. 6.9. The locus of points for the  $dT_{max}$  values shown in Fig. 6.9a, b and c does not indicate that these values are indeed maximum but possibly average. This variation is not expected. Fig. 6.9d shows the trends of  $dT_{max}$  values for TDP 2. For this TDP, the locus of points for  $dT_{max}$  indicates that the values are maximum which agrees with theory (Oishi *et al.*, 2016). The variations of sap flow ( $F$ ) determined by TDPs 1, 3 and 4 were consistently out of phase with variations of PAR (Fig. 6.10), which is not expected. Generally, the values of  $F$  peaked between 08h00 and 10h00 for these sensors. The values of  $F$  were highest for TDP 3 and lowest for TDP 1. Conversely, for TDP 2 (Fig. 6.10), the variations of  $F$  were in phase with variations of PAR which is expected. The values of  $F$  peaked between 12h00 and 13h00 in agreement with peak values of PAR.

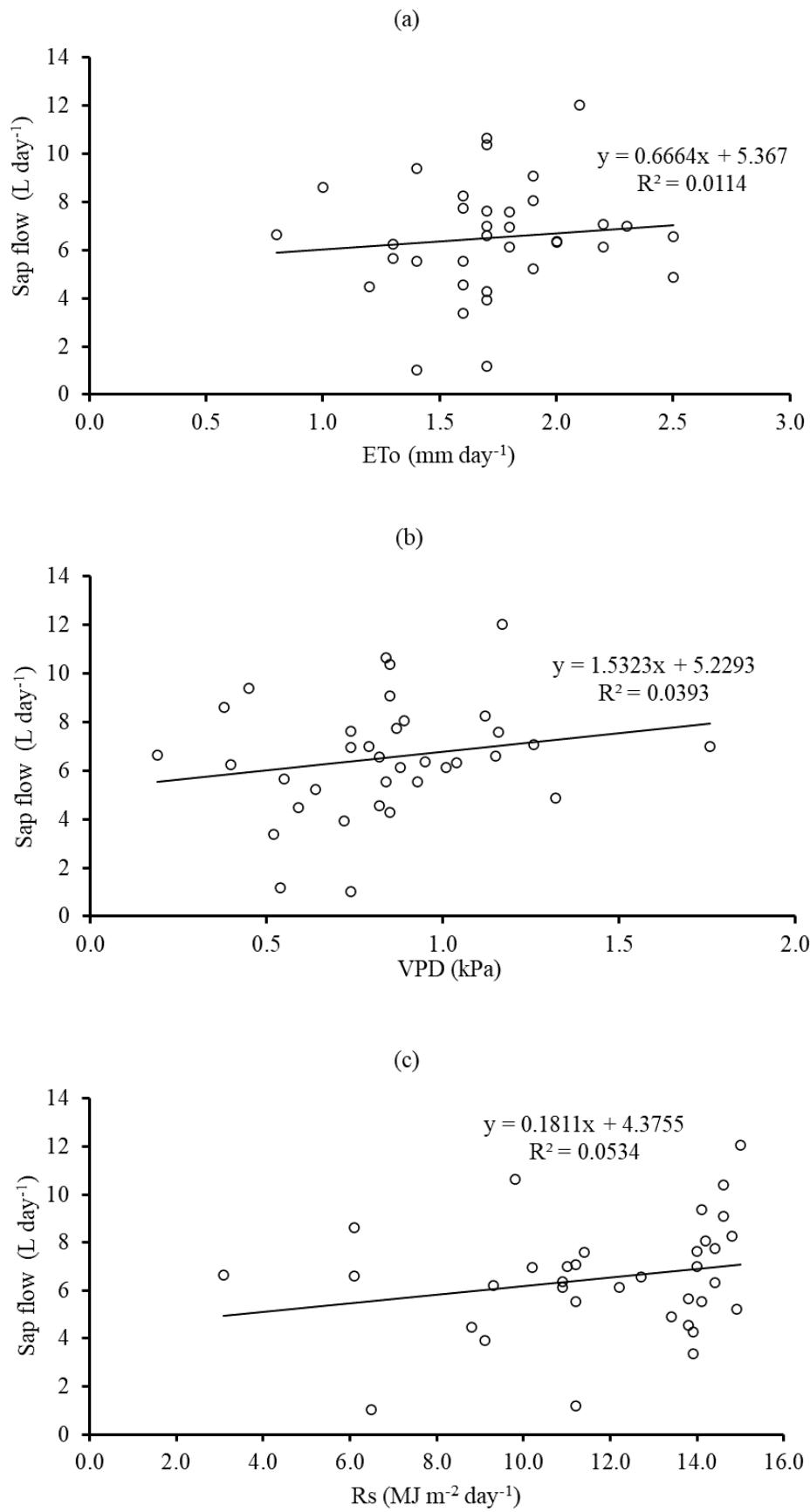


Figure 6.11: Relationship between sap flow ( $F$ ) and (a) reference evapotranspiration ( $ET_o$ ); (b) vapour pressure deficit (VPD) and (c) solar radiation ( $R_s$ ).

The correlation between  $ET_o$ , VPD,  $R_s$  and  $F$  yielded  $R^2$  values ranging from 0.01 to 0.05 which are relatively weak (Fig. 6.11).

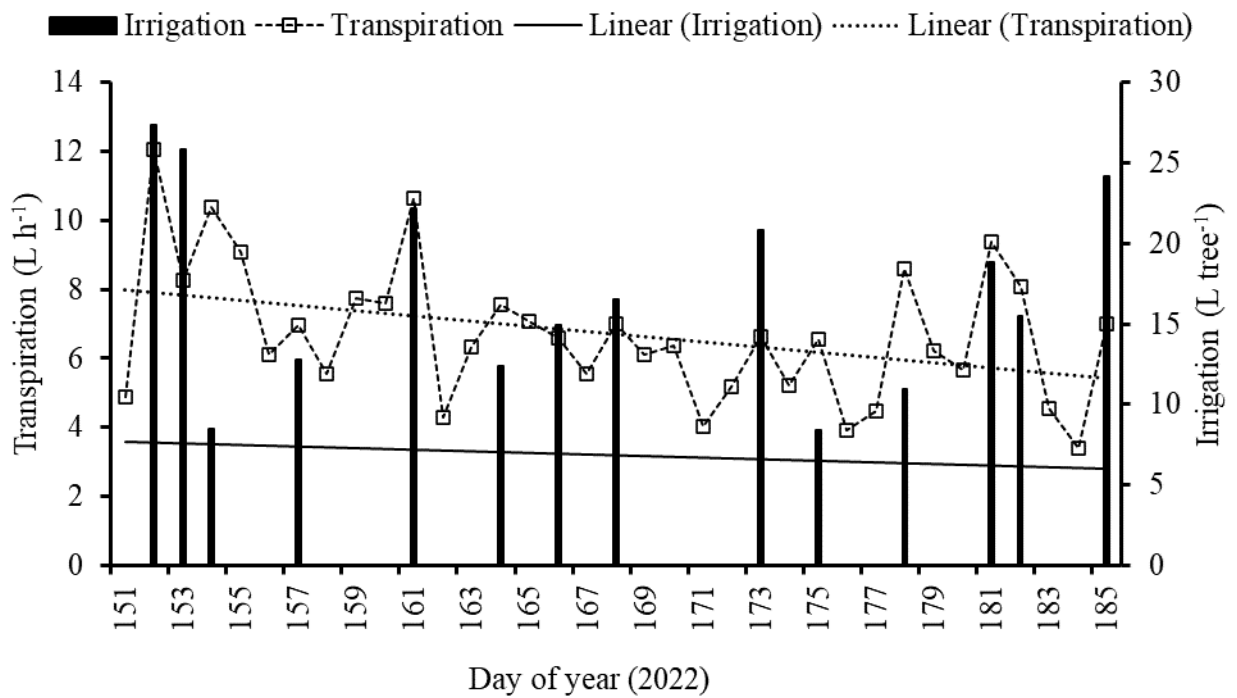


Figure 6.12: Time series for daily transpiration and irrigation during the study period.

Daily transpiration fluctuated on a decreasing trend as shown in Fig. 6.12. During the study period, 14 irrigation events were observed with a total amount of 239.2 L tree<sup>-1</sup> applied to the orchard. The average daily irrigation application rate remained almost constant.

## 6.5. Discussion

A perfect match between consumed and available energy fluxes would yield a slope of unity; however, the banana orchard was heterogeneous, hence the slope of unity was difficult to obtain. In addition, eddy covariance measurements are prone to errors and these would result in the deviation of the slope from unity. Energy balance closure is believed to vary with factors such as friction velocity, stability conditions as well as canopy height (Tanny *et al.*, 2018). We investigated the effect of stability on the energy balance closure for the banana orchard. When data for stable conditions only were used, the slope of the regression line increased by about 0.75% while the intercept decreased by about 11.0% indicating an improvement in the energy balance closure. These findings show that stability had an effect on the energy balance closure for the banana orchard. The results suggest that eddy covariance measurements are more reliable when measurements are taken during unstable compared to stable conditions. Our findings are similar to those of Franssen *et al.* (2010).

The variation of  $\alpha$  with measurement height suggests that there exists a single measurement height at which to install a fine-wire thermocouple above the banana canopy. The variation of  $\alpha$  with time lag also points to the need to establish the sensitivity of SR measurements to time lag. Therefore the height and time lag can be optimised to obtain reliable SR measurements of high frequency air temperature in the banana orchard. Mengistu and Savage (2010) reviewed various studies which calibrated SR using eddy covariance and reported  $\alpha$  values in the range 0.2-1.88 for various agricultural surfaces. Therefore, the  $\alpha$  values found in the current study are in the range of those reported in the literature. Mekhmandarov *et al.* (2015) calibrated the SR method using EC for measurements taken over a banana canopy and found  $\alpha$  values greater than 0.5 for unstable conditions. Additionally, the  $\alpha$  values found by Mekhmandarov *et al.* (2015) increased with increase in time lag and decreased with increase in measurement height which supports our findings. The structure function of Van Atta (1977) requires that the time lag should be substantially less than the ramp period. According to Snyder *et al.* (1996), at lower measurement height (e.g. 5.15 m in the current study), wind shear is greater than that at the higher height (e.g. 5.65 m in the current study) and the ramp period is smaller at the lower height than at the higher height. Therefore, more accurate estimates of sensible heat flux are anticipated at a smaller time lag. At the higher measurement height (5.65 m), wind shear is smaller compared to that at 5.15 m. The ramp period is larger at the higher height thus it is expected that sensible heat flux estimates are more accurate at a larger time lag. The dependence of  $\alpha$  on measurement height that we found for measurements taken above the banana canopy aligns to the previous findings (e.g. Rosa, 2012; Spano *et al.*, 1997). The traditional EC system is usually unaffordable by farmers because of its cost. Additionally, the complexity of EC data acquisition and processing as well as the delicacy of EC sensors and the need for expertise to operate the system limit its application at farm level. An alternative means of determining sensible heat flux at farm level can be provided by the SR method once it is calibrated.

The wetting event of DOY 153 (Fig. 6.6a) would result in the available energy being consumed mainly as latent heat. Therefore, it is expected that during or soon after the event, latent heat flux is higher than sensible heat flux. Conversely, DOY 155 was drier (Fig. 6.6b) than DOY 153 and the available energy would be expected to weight towards sensible heat flux. However, on DOY 155, *LESR* remained higher than *HSR* probably because soil moisture was still available in the deeper soil layers from the previous irrigation event and this soil moisture would be removed by evapotranspiration. Therefore, *LESR* remained higher. Similar findings were also confirmed by Adeboye *et al.* (2017b) for *ET* measurements over a soybean canopy. The response of fluxes shown in Fig. 6.6 helps the farmer to decide on whether or not to irrigate the orchard at a given time.

The SR method overestimated  $ET$  compared to the crop coefficient method. One of the limitations of the SR method is that the calculation of  $LE$  as a residual of the energy balance equation relies on forcing energy balance closure, i.e. it assumes that the slope of  $H + LE$  against  $R_n - G$  is unity which does not always hold. For example, in the current study, although by using eddy covariance measurements, the energy balance closure was good, the slope of  $H + LE$  against  $R_n - G$  was smaller than unity. Therefore is expected that SR-derived  $ET$  would deviate from the expected. The iterative method (Savage, 2010, 2017) for calculating the ramp amplitude and period of high frequency air temperature measurements which are required for determining  $H$  using SR did not determine all  $H$  in the current study, which is problematic. According to Rosa (2012), missing  $H$  values result from the failure of air temperature structure functions to satisfy certain conditions. When half-hourly values of  $H$  are summed to daily values, then  $H$  is underestimated. Since the SR method uses the energy balance equation to calculate  $LE$ , the  $LE$  would be overestimated and consequently  $ET$  would be overestimated. Missing  $H$  values from SR measurements and the overestimation of  $ET$  found in the current study were also reported recently by Masanganise *et al.* (2022) who conducted SR measurements over a soybean canopy. Despite these shortcomings, the SR method produced reasonable estimates of water use of banana and the estimates can be improved by gap filling for missing half-hourly  $H$  values. The SR method can be adopted by farmers for day to day water management. Although crop coefficients are relatively easy to use to calculate banana water use, they are site specific (Allen *et al.*, 1998) and therefore they are not available in some locations, making it difficult for the farmer to use them. The use of published crop coefficients is also limited by the need to correct them for example for humidity, crop height and wind speed (Allen *et al.*, 1998) and  $ET_0$  (Guerra *et al.*, 2014). Therefore, the SR method provides an alternative means of determining banana water use in regions where the crop coefficient method cannot be used and especially in regions with low  $ET$  rates. The correlations in Fig. 6.8 were relatively low, however this does not necessarily indicate that  $ET_0$ , VPD and  $R_s$  are weak drivers of  $ET$ . The correlations could probably be attributed to the values of  $ET$  derived from SR.

Fig. 6.9a, b and c shows  $dT_{max}$  points that likely do not represent the points where zero sap flow occurs while the likelihood of zero sap flow occurrence is shown in Fig. 6.9d. A farmer can easily use the graphical interface of Baseline to do quick checks on TDP output data and also on the sensors for defects or proper installation. The variations of  $F$  in Fig.6.10 for TDPs 1, 3 and 4 are not expected based on the variation of PAR. The variations for TDPs 1, 3 and 4 suggest that tree transpiration was maximum 2 to 4 hours before midday which is highly unlikely. We are not aware of the causes of these observations. However, we speculate that this could be caused by the development of a thermal gradient between the reference and heated probe which is not driven by the heating element (Goulden and Field, 1994; Oishi, Personal communication). Towards the end of the growing season, as in the current study,

sap flow is relatively low and the diurnal variation in  $dT$  is also relatively low. As a result, the signal-to-noise ratio is low, hence the corm would have a greater effect on the  $dT$  signal than it would when sap flow is high (A.C. Oishi, Personal communication). The variation of  $F$  across all the four TDPs suggest that there exist a region within the corm which is ideal for installing the sensors for sap flow measurement. This region is likely to be the one in which TDP 2 was installed. Lu *et al.* (2002) measured sap flow in the central cylinder of a banana crop using TDPs and reported that there was negligible spatial variation of sap flow across the sap conducting region which contradicts our findings. The variation observed in our study may have resulted from circumferential variation on different trees which was also found by Lu (2000). However, it is usually too technical and expensive for a farmer to conduct detailed physiological examination of the corm in order to locate the ideal region. Instead, an array of relatively inexpensive sensors (TDPs) can be used in several positions of the corm and the output data compared to PAR. The correlations between  $ET_o$ , VPD,  $R_s$  and  $F$  shown in Fig. 6.11 show that the relationship between meteorological factors and sap flow may not be used to determine banana transpiration from meteorological measurements in the current study. The trend shown in Fig. 6.12 for transpiration is expected. Usually, the rate of transpiration decreases as trees use less water towards the end of the growing period. The information in Fig. 6.12 helps the farmer to adjust the amount of irrigation water applied to the trees.

## 6.6. Conclusions

The current study tested the utility of the surface renewal and thermal dissipation probe methods for estimating water use of banana in an open field at farm level. We established that thermocouple placement height and time lag affect the sensible heat flux estimated using the surface renewal method. Of the two time lags tested in the estimation of evapotranspiration, the longer time lag produced evapotranspiration estimates which were more in agreement with evapotranspiration determined using the crop coefficient method. A range of placement height and time lag can be tested to obtain an optimized combination for obtaining more reliable estimates of evapotranspiration. When a suitable time lag is used, surface renewal can be used successfully as an alternative to the crop coefficient method for estimating banana evapotranspiration at farm level in areas where crop coefficients are not available. We also established that thermal dissipation probes can be used to obtain estimates of sap flow in banana crops; however, the accuracy of the method depends among other factors on locating the exact position of the sapwood area in the central cylinder of the corm part of the plant. To increase the probability of capturing sap flow in the sap conducting region, the current study can be improved by using more than one thermal dissipation probe per plant and increasing the number of trees sampled. Testing thermal dissipation probes which are less sensitive to thermal gradient is likely to improve the reliability of sap flow outputs found in the current study.

## CHAPTER 7: WATER USE OF A SUGARCANE PLANTATION UNDER SUBTROPICAL CONDITIONS

### 7.1. Summary

Several studies have been done in South Africa to quantify the water use of sugarcane (*Saccharum officinarum*) plantations. There is a unanimous agreement that these are high water consuming crops. What is less known however, is how the water use varies by growing region, soil types, management, irrigation system, and by cultivar, among other variables. Given that sugarcane constitutes the largest irrigated area in Mpumalanga (up to 25% according to Table 2.1) the terms of reference of this project specifically required us to include this crop. However, due to time constraints related to the late start of the project due to the Covid pandemic, there was limited time for detailed field data collection. In this study we quantified evapotranspiration in a cane field at Riverside Farm in Malelane from October 2023 to February 2024. The evapotranspiration was measured using the surface renewal (SR) method that was calibrated using the open path eddy covariance method to derive the adjustment factor. The crop coefficient curve was derived for the four months. Thereafter the monthly crop coefficient trend was estimated from start of the growing season around August to the projected harvest period around June/July 2024. We subsequently derived the monthly total reference evapotranspiration for Malelane for the past five years using weather data provided by the ARC for Malelane. The monthly total evapotranspiration over a typical sugarcane growth cycle was then derived as the product of the crop coefficient and the reference evapotranspiration. According to our data, the  $K_c$  values varied from 0.35 in July peaking at around 1.1 in January. Monthly total evapotranspiration varied from about 27 mm in July reaching about 160 mm in January when canopy cover is at its maximum. The estimated seasonal total evapotranspiration is about 1266 mm translating to about 12 660 m<sup>3</sup>/ha/year. This figure is consistent with estimates obtained by other researchers in South Africa. Compared with irrigated subtropical crops grown in the IUWMA, the annual water consumption of sugarcane exceeds appears to be the highest likely because of the high density of plantings of plant types that exhibit an anisohydric response to water demand. If the plants have access to large amounts of water, they will use it. How the massive water consumption is converted to yield is probably covered in other studies.

## 7.2. Introduction

In South Africa most sugarcane plantations are found in low lying areas of Mpumalanga, along the KwaZulu-Natal coastal regions, up to northern Pondoland in the Eastern Cape Province. A substantial proportion of the crop is grown under rainfed conditions mostly by small scale farmers while only about 30% is grown under irrigation mostly on large commercial farms (Olivier and Singels, 2015). Sugarcane grows well under tropical conditions, but in South Africa and elsewhere, most production regions are under subtropical conditions. It grows in areas with average temperatures ranging from 20 to 35°C mostly on deep well drained soils. It also requires regions with high relative humidities (80-85%) which is thought to favour cane elongation and long day lengths. Because of its high-water requirements, the crop thrives in regions with high annual rainfall varying from 1100 to 1300 mm during the period of active vegetative growth.

The water use of irrigated cane in South Africa has been estimated in different regions using different methods. For example, Oliver and Singels (2015) estimated the annual evapotranspiration for a cane crop in Komatipoort varying between 1340 and 1700 mm over the growing season using the soil water balance approach. Jarman *et al.* (2014) used remote sensing techniques and obtained area averaged evapotranspiration for sugarcane of around 1092 mm/season in the Malelane-Komatipoort areas. They used the SEBAL remote sensing product that uses the Landsat imagery with a spatial resolution of about 1 km x 1 km. A desktop study by Bezuidenhout *et al.* (2005) estimated average industry-wide evapotranspiration for sugarcane at about 598 mm per year. So, there are large variations in the water consumption rates of sugarcane depending to a large extent on the method that is used to estimate the water use rates. In this study we use the surface renewal method calibrated against the eddy covariance method to estimate the seasonal total water use of drip irrigated cane in Malelane. Gokool *et al.* (2016) used the same methods on cane, but unfortunately they do not report on the monthly or seasonal total water consumption. We hope that our study closes this information gap. In addition we will build in sugarcane into the DSS developed in this study when we get the yield data for the 2023/2024 season thereby adding another tool to the IUWMA toolbox to estimate the water use and water use efficiency of sugarcane in the catchment.

### 7.3. Materials and Methods

#### 7.3.1 Study Site and Plant Material

Data were collected in a young sugarcane field (Block 6) at Riverside farm in Malelane, Mpumalanga, South Africa (Fig. 7.1). The field measured 8.31 hectares in size and was planted with the N53 cultivar with a planting density of 18 tons of seedcane per hectare. The block was planted with a row spacing of 1.9 m x 0.45 m giving a plant density of 5 294 plants per hectare. The field was irrigated via drip irrigation and irrigation was scheduled according to the DFM soil capacitance probes installed at several positions throughout the field. Data collection commenced on 10 October 2023 when the sugarcane was approximately 80 cm high (Fig. 7.1) and ended around first week of February 2024 when the plants were just over two metres tall.



Figure 7.1: Sugarcane field at Riverside farm, Malelane.

### 7.3.2 Soil water content and irrigation measurements

A one-metre profile pit was dug within the root zone of the plants using a backhoe loader (Fig. 7.2). This was done to determine the amount of soil available water. Two CS616 sensors (Campbell Scientific Inc., Utah, USA) were installed horizontally at 30 and 60 cm depths, respectively down the profile in the irrigated zone. The cables of the CS616 sensors were carefully labelled for ease of identification.



Figure 7.2: Soil Moisture probes installed at 30 and 60 cm horizontally below the ground in the profile pit.

The irrigation amount was measured using an electronic water flow meter (ARAD Multi-Jet Meter, Germiston, South Africa) with a resolution of 10 L/pulse that was installed on the irrigation line. All the sensors were connected to a CR1000 datalogger (Campbell Scientific Inc., UT, USA) which was programmed to store hourly data.

### 7.3.3 Actual Evapotranspiration

The actual evapotranspiration from the sugarcane field was quantified using the surface renewal method. A 6 m tall flux tower was mounted at the centre of the sugarcane field and a four-component net radiometer (CNR4, Kipp & Zonen, Netherlands) was mounted facing northwards on the top of the tower, extended above the sugarcane crop to measure the field net radiation. Two type-E fine-wire thermocouples (Campbell Scientific Inc.) were mounted on arms which extended from the tower at heights of 4.1 m and 5.1 m above the sugarcane canopy, facing in the direction of prevailing wind. This was done to measure high frequency air temperature above the sugarcane canopy at different heights and time lags, thereby deriving sensible heat flux for the field. Measurement of the air temperature using the two fine-wire thermocouples were made at a frequency of 10 Hz and time lags of 0.4 s and 0.8 s, respectively. All the sensors were connected to the CR1000 data logger (Campbell Scientific Inc.) which was programmed to store half-hourly measurements. Open path eddy covariance system was used to calibrate the surface renewal method output. The open path eddy covariance system was used to make direct measurements of the sensible heat flux in the sugarcane field. An IRGASON (Campbell Scientific Inc.) comprising of both a three-dimensional sonic anemometer and an infrared gas analyser was mounted for three days on the flux tower at the same height as the lowest thermocouple, pointing in the direction of the prevailing wind. The surface renewal method was calibrated by plotting a regression line of the surface renewal sensible heat flux output against the open path eddy covariance sensible heat flux output. The slope of the graph was used as the calibration factor for the surface renewal sensible heat flux. Data for the first two days from the open path eddy covariance system was used for calibration and the data for the third day was used for validation. The actual evapotranspiration was calculated using the energy balance equation:

$$ET = \frac{R_n - G - H}{\lambda} \quad (7.1)$$

where  $ET$  is the actual evapotranspiration,  $R_n$  is the net radiation,  $H$  is the sensible heat flux,  $\lambda$  is the latent heat of vaporization and  $G$  is the soil heat flux taken as  $0.1 \times R_n$  in this study.

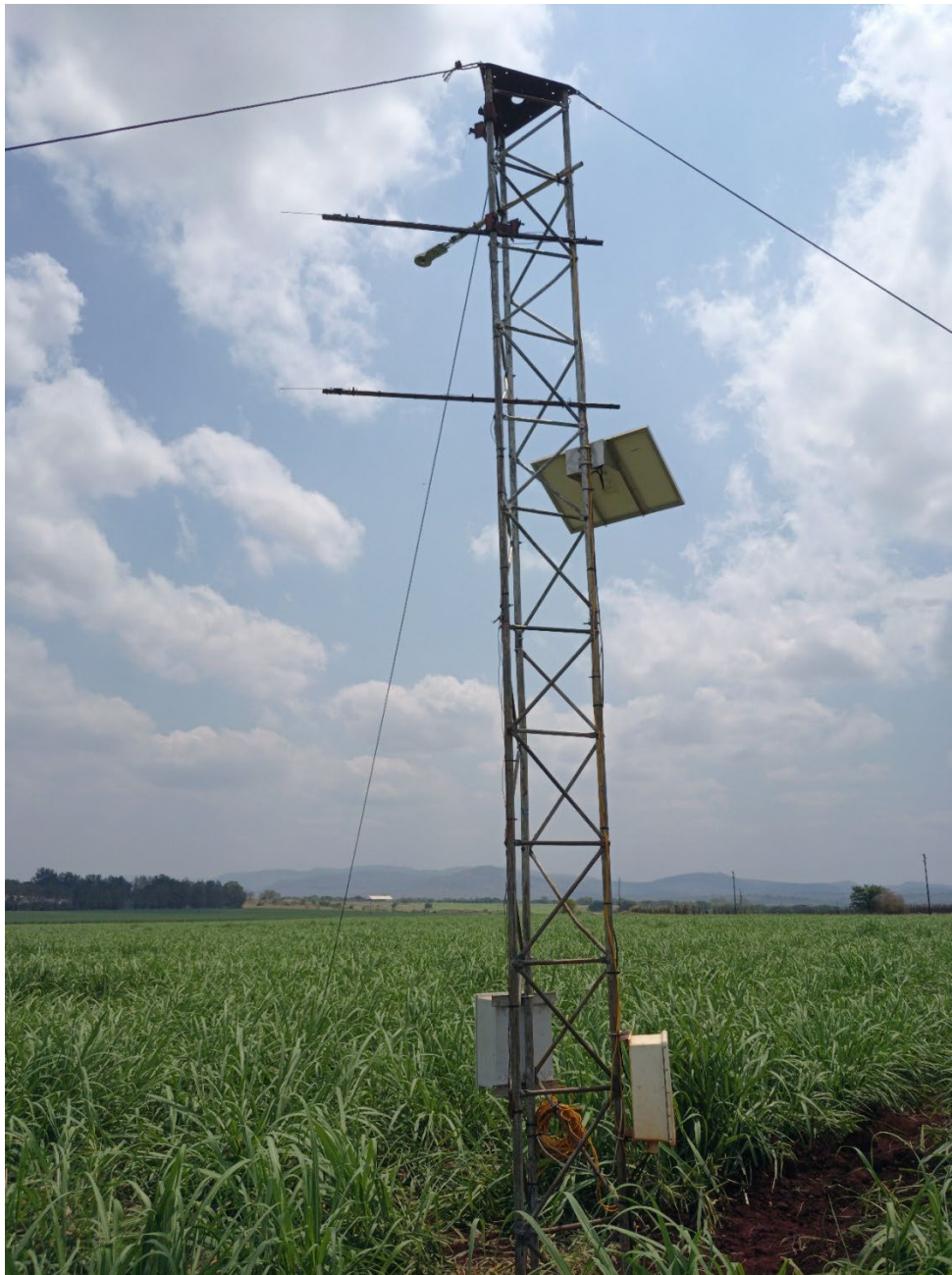


Figure 7.3: Surface renewal setup for measuring the sugarcane field evapotranspiration.



Figure 7.4: Calibration of the surface renewal method using the open path eddy covariance system.

### 7.3.4 Modelling sugarcane plantation water use

Two approaches were used to estimate the water use and crop coefficients for the sugar plantation. The first approach involved the use of single crop coefficient ( $K_c$ ) approach as detailed in Allen *et al.* (1998). In this approach, actual evapotranspiration data was measured over a period of 4 months starting from October 2023 to February 2024, due to time constraints. The single crop coefficient was determined using the following equation,

$$K_c = \frac{ET_c}{ET_o} \quad (7.2)$$

Where  $K_c$  is the crop coefficient,  $ET_c$  is the crop evapotranspiration and  $ET_o$  is the reference crop evapotranspiration. A complete seasonal  $K_c$  data were created by extrapolating the measured monthly  $K_c$  values by considering different growth stages of the crop. The second approach involved the use of Priestley-Taylor (1972) model. In this model, the crop evapotranspiration was calculated using the equation,

$$ET_c = \alpha \left[ \frac{\Delta}{\Delta + \gamma} \right] \left[ \frac{R_n - G}{\lambda} \right] \quad (7.3)$$

Where  $ET_c$  is the crop evapotranspiration,  $\alpha$  is the Priestley-Taylor parameter taken as 1.26 in this study for freely evaporating surfaces,  $\Delta$  is the slope of saturated vapour pressure,  $\gamma$  is the psychrometric constant,  $\lambda$  is the latent heat of vaporization,  $R_n$  is the net radiation and  $G$  is the soil heat flux taken as  $0.1 \times R_n$  in this study.

## 7.4. Results and Discussion

### 7.4.1 Soil Moisture Dynamics

Volumetric soil moisture content and irrigation in the sugarcane plantation were measured from October 2023 to February 2024 (Fig. 7.5). There was not much difference in volumetric soil moisture content measured at depths of 30 cm and 60 cm from 14 October 2023 to 9 December 2023 when the total irrigation applied in the field was approximately below 30 mm per irrigation event. A major change in volumetric soil moisture content was observed on 10 December 2023 when the total irrigation reached 68 mm. This indicated that drip irrigation does not contribute to deep percolation when water is applied in smaller quantities unless the irrigation events are prolonged. On 24 January 2024, volumetric soil moisture content at 30 cm depth dropped below the volumetric soil moisture content measured at 60 cm depth. This can be attributed to the fact that sugarcane do not have a deep rooting system where most of its roots are concentrated in the 30 cm depth soil profile and during this time

irrigation events were reduced in the plantation. As a result, a combination of plant water uptake and soil evaporation was significant in the 30 cm compared to the 60 cm depth soil profile. Hence the 30 cm depth indicated less soil moisture content as compared to the 60 cm depth.

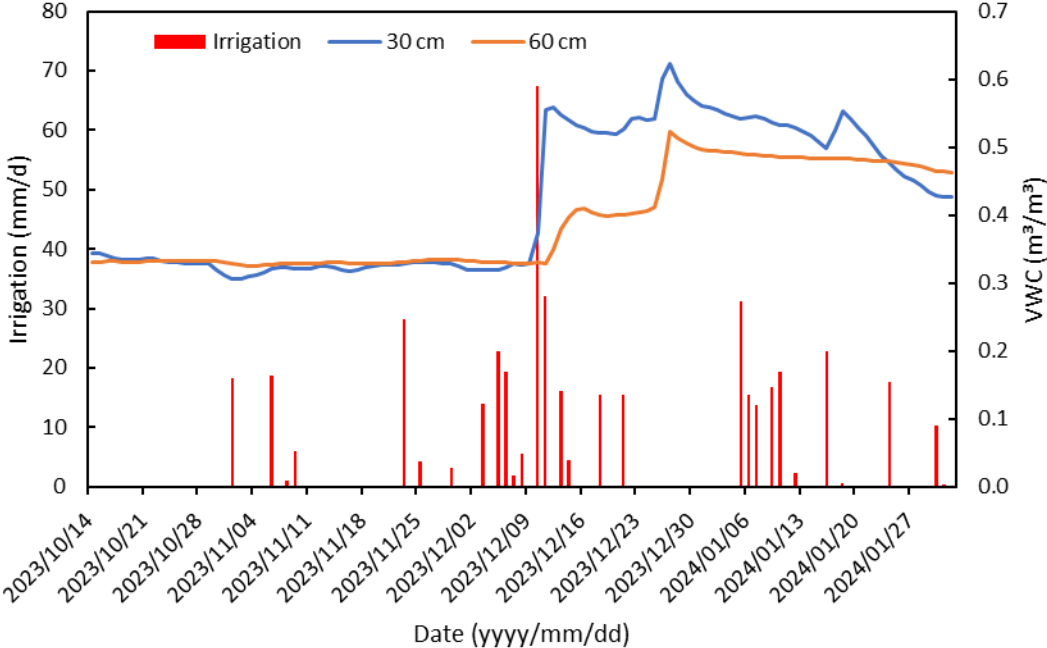


Figure 7.5: Measured volumetric soil moisture content and irrigation in the sugarcane plantation.

**7.4.2 Climatic drivers of evapotranspiration**

Solar radiation was the strong driver of evapotranspiration (Fig. 7.6a), explaining at least 90% of the daily sugarcane plantation evapotranspiration. This was followed by reference evapotranspiration which had a coefficient of determination of approximately 0.84 (Fig. 7.6c) and then vapour pressure deficit (VPD) of the air (Fig. 7.6b) which had a 0.73 coefficient of determination. Sugarcane plantation evapotranspiration increased linearly with solar radiation. On the other hand, the combined effect of solar radiation, vapour pressure deficit and windspeed on the plantation evapotranspiration in the form of reference evapotranspiration also exhibited a linear relationship. The vapour pressure deficit reflected a second order polynomial relationship (Fig. 7.6b) with evapotranspiration, furthermore evapotranspiration diminished as the VPD increased. Evapotranspiration in the plantation was mainly due to the sugarcane transpiration and soil evaporation since the field did not have any understorey vegetation. The plantation was irrigated via drip irrigation, hence soil wetted radius due to irrigation was minimized which led to less evaporation and hence the sugarcane transpiration had a greater contribution towards evapotranspiration as compared to soil evaporation. The

observed reduction in evapotranspiration as VPD increased can be attributed to the stomata closure of the sugarcane at high VPD levels, leading to a reduction in the rate of transpiration. The effect of the climatic driving factors on the sugarcane plantation under drip irrigation indicated that the available energy was the main driver of plantation water use.

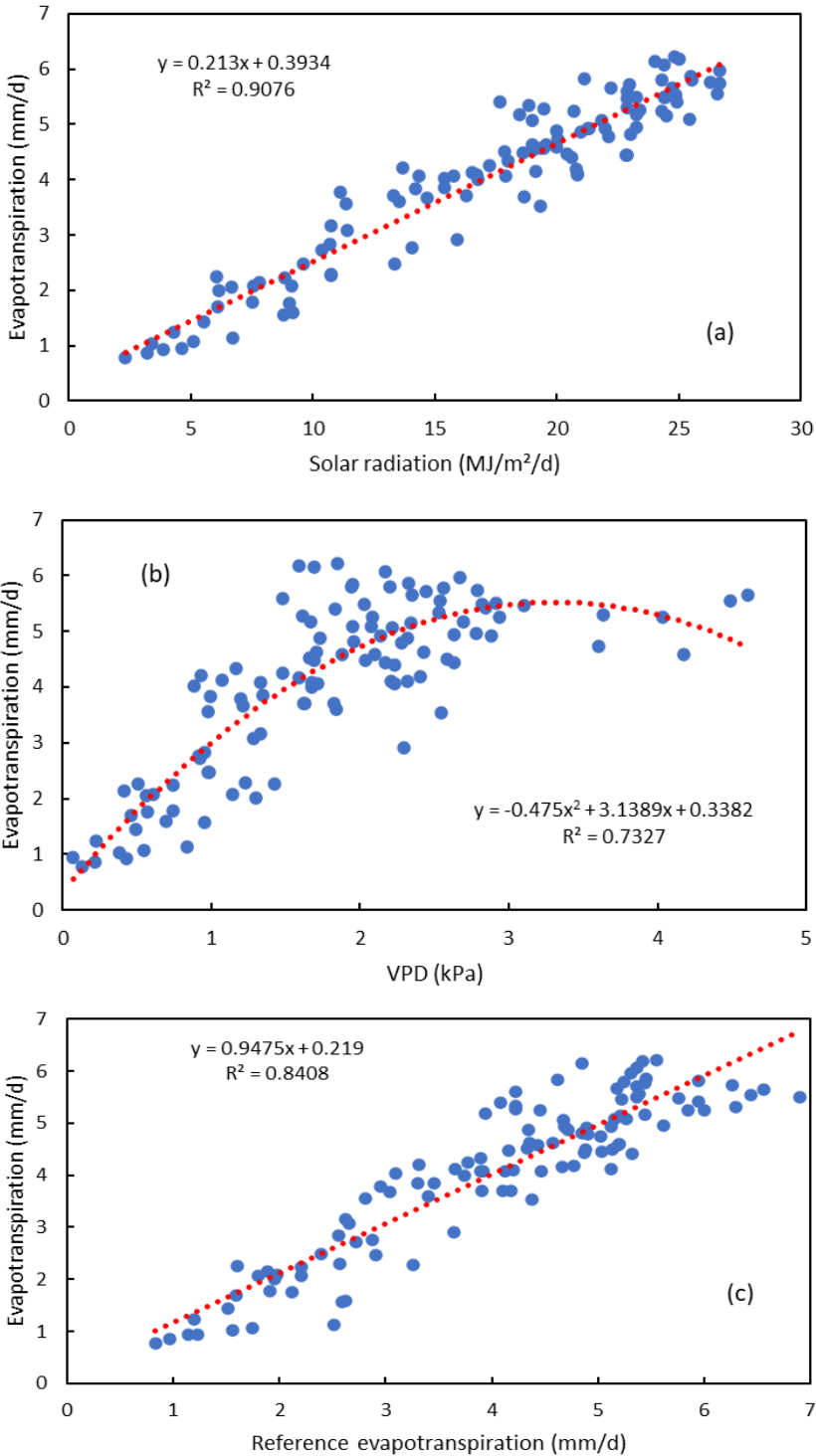


Figure 7.6: Climate drivers of sugarcane plantation evapotranspiration showing, (a) solar radiation, (b) vapour pressure deficit and (c) reference evapotranspiration.

### 7.4.3 Calibration and validation of SR method

The first lower type-E fine-wire thermocouple (TC1) at time lag of 0.8 seconds produced best output for the sensible heat flux. The surface renewal sensible heat flux was calibrated using 2 day measured data from the open path eddy covariance system producing a 0.308 calibration factor. The calibrated data for surface renewal sensible heat flux was further validated using an independent one day's data from the open path eddy covariance system. Results of a regression between calibrated surface renewal sensible heat flux and the open path eddy covariance sensible heat flux produced good results with a coefficient of determination of 0.87 (Fig. 7.7).

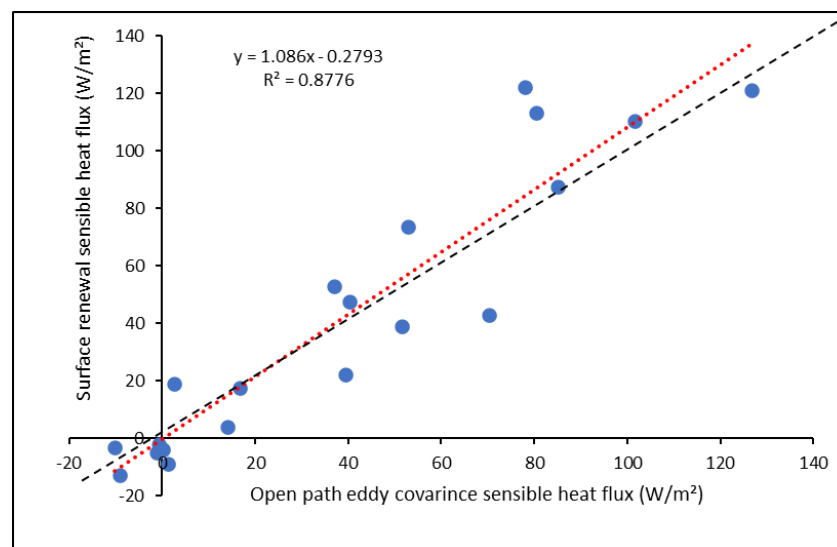


Figure 7.7: Validation of the surface renewal sensible heat flux calibration.

### 7.4.4 Sugarcane plantation crop coefficients and modelled evapotranspiration

A comparison of the evapotranspiration estimated by the Priestley-Taylor model with the Surface Renewal measured evapotranspiration are shown in Figure 7.8. Results indicated that the Priestley-Taylor model slightly overestimated the evapotranspiration on some days but the regression between measured and modelled evapotranspiration produced a 0.98 coefficient of determination. This indicates that the Priestly-Taylor model has a huge potential for modelling evapotranspiration of high planting density fields such as sugarcane plantations.

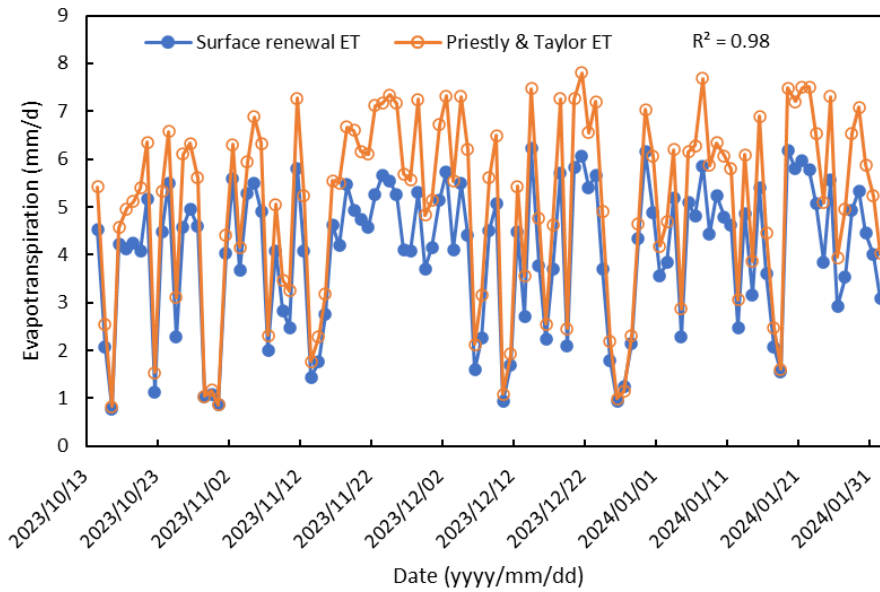


Figure 7.8: Comparison between measured evapotranspiration using surface renewal method and modelled evapotranspiration using Priestley-Taylor model.

The measured and extrapolated monthly sugarcane crop coefficients are shown in Fig. 7.9. The minimum and maximum monthly extrapolated  $K_c$  values were 0.35 and 1.12 respectively. The monthly evapotranspiration totals were calculated using a combination of derived crop coefficients and measured evapotranspiration totals as shown in Figure 7.10. Month of January produced the greatest evapotranspiration total of 160 mm and least evapotranspiration was in July. This is because the months of January and July falls under summer and winter seasons, respectively in the Malelane region. In the summer season solar radiation totals are higher than those observed in the winter season and since solar radiation is one of the main drivers of evapotranspiration in the sugarcane plantations, this will be accompanied by high evapotranspiration levels in summer months as compared to the winter months.

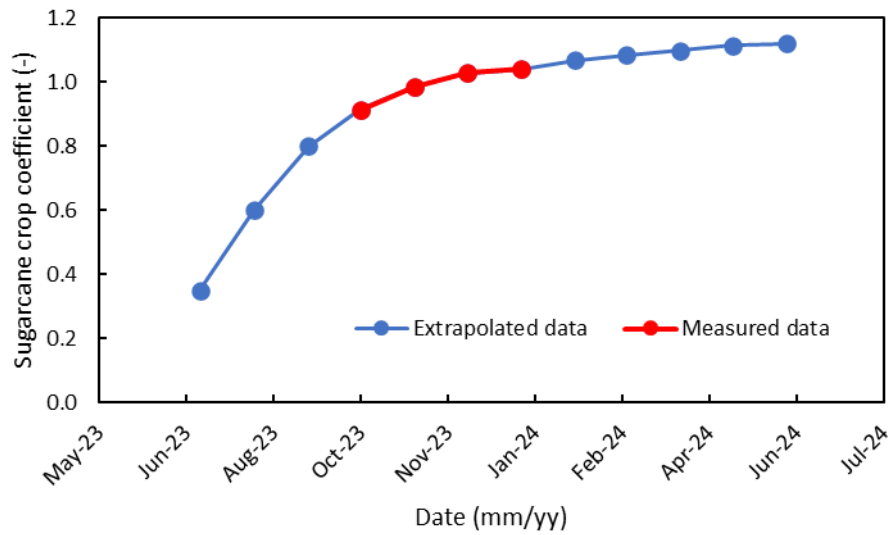


Figure 7.9: Monthly sugarcane crop coefficients.

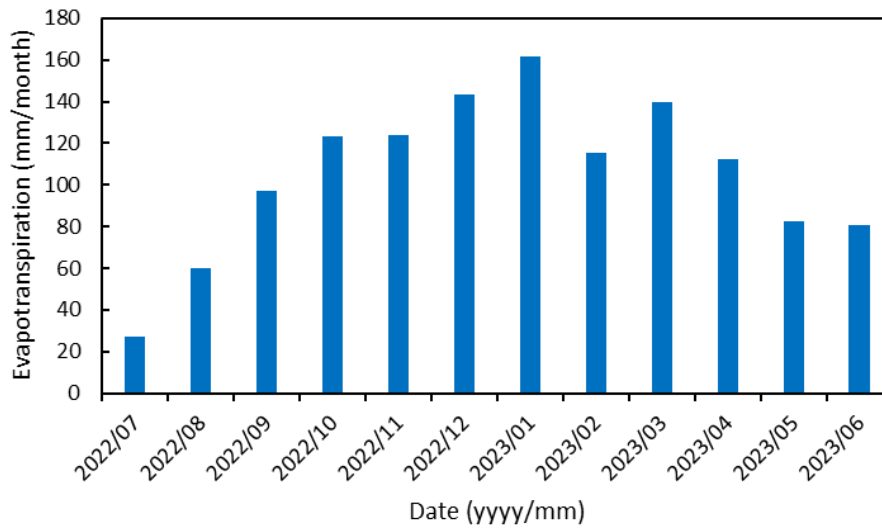


Figure 7.10: Modelled monthly total evapotranspiration.

A summary of the monthly crop coefficients, reference evapotranspiration and evapotranspiration for sugarcane plantation are shown in Table 7.1.

Table 7.1: Typical monthly crop coefficients, reference evapotranspiration and evapotranspiration for sugarcane plantation in Malelane, Mpumalanga

Date	ET <sub>o</sub>	K <sub>c</sub>	ET
	(mm/month)	(-)	(mm/month)
2022/07	77.5	0.35	27.1
2022/08	100.0	0.60	60.0
2022/09	121.1	0.80	96.9
2022/10	134.9	0.91	123.1
2022/11	125.9	0.99	124.1
2022/12	139.6	1.03	143.3
2023/01	155.3	1.04	161.4
2023/02	108.0	1.07	115.2
2023/03	129.2	1.08	139.8
2023/04	102.3	1.10	112.3
2023/05	74.0	1.11	82.4
2023/06	72.3	1.12	80.9
<b>Total</b>	1340.1		1266.6

## 7.5. Conclusion

As stated earlier, numerous studies have been conducted to quantify the water use-yield relationships for sugarcane in South Africa. Different estimates of the water use have been obtained depending on the quantification method used. Area averaged data using desktop and remote sensing methods estimated annual water use in the range 600 to 1100 mm but including both irrigated and rain-fed fields. Individual field-based measurements on the other hand using either the soil water balance or the micrometeorological techniques led to much higher seasonal evapotranspiration of irrigated cane exceeding 1200 mm/ season. Clearly there is need for more studies covering entire seasons to come up with more credible water use estimates for cane than those that are currently available.

## **CHAPTER 8: DEVELOPMENT AND TESTING OF A DECISION SUPPORT SYSTEM FOR WATER USE AND WATER USE EFFICIENCY OF IRRIGATED TREE CROPS**

### **8.1. Summary**

In this chapter we present the decision support system (DSS), the science behind it, and the functions of the system. The primary goal of developing the DSS was to come up with a tool that can be used by catchment managers, farmers, irrigation boards, etc. to estimate the amount of water required to irrigate crops at a given location in the catchment. Given the need for good quality long-term weather data to drive the algorithms behind the DSS, we used the 50-year climate data record by Schulze *et al.* for all the quaternary catchments within IUWMA. The farmer inputs information such as the crop type, soil type, fractional vegetation cover, vegetation height, irrigation system, cover crop status, etc. Based on the user inputs, the DSS first calculates the crop coefficients for the orchards. The crop coefficients are then used to calculate the monthly ET<sub>c</sub> and crop transpiration averaged over 50 years. The water use calculations follow the internationally acclaimed FAO 56 approach. Monthly irrigation requirements are calculated from the ET<sub>c</sub> and rainfall data. The expected maximum yield is also calculated using the water use-yield functions for each crop type according to Stewart's model. The water use efficiency (or water productivity) is calculated as the ratio of the estimated yield to the water consumed. The DSS is available as a web-based tool given that it is difficult to display the farm boundaries on a smartphone APP-type platform.

### **8.2 Scientific basis behind the DSS**

Crop water use and yield are influenced by environmental conditions principally the climate and the available soil water. Management practices such as pruning, fruit thinning (to control crop load), mulching, etc. also play a role. Given that climatic conditions vary from year to year, the Decision Support System (DSS) developed in this study (see Fig. 8.1) used daily averages of a long-term (50 yr. daily) data set to estimate crop water requirements. The DSS follows the widely used FAO 56 approach (Allen *et al.*, 1998) wherein crop evapotranspiration (ET<sub>c</sub>) is estimated as the product of the reference evapotranspiration (ET<sub>o</sub>) and a crop coefficient (K<sub>c</sub>). For row crops such as orchards, it is preferable to split K<sub>c</sub> into a basal (K<sub>cb</sub>) and a soil evaporation (K<sub>e</sub>) coefficient. The product of ET<sub>o</sub> and K<sub>cb</sub> gives the unstressed transpiration while K<sub>e</sub> times ET<sub>o</sub> gives an estimate of the soil evaporation.

Inaccurate crop coefficients are a source of uncertainty in the FAO approach. The tabulated FAO crop coefficients were derived using data from temperate subhumid locations, and they cannot be readily transferred to other growing regions. In an extension of the FAO 56, and to attempt to resolve the transferability issue Allen and Pereira (2009) developed an approach to calculate the crop coefficients using readily available data. This is the approach that we followed in the DSS. Details of how this methodology has been adapted for fruit tree crops are published in Mobe *et al.* (2020) and Mashabatu *et al.* (2023). Crop yield ( $Y_a$ ) is estimated in the DSS using Stewart's model wherein the maximum yield ( $Y_m$ ) is reduced by a transpiration deficit via a water-yield response function ( $K_y$ ) such that:

$$1 - \frac{Y_a}{Y_m} = K_y \left(1 - \frac{T_c}{T_m}\right) \quad (8.1)$$

where  $T_c$  is the observed actual annual total transpiration,  $T_m$  is the maximum unstressed transpiration. The water use efficiency (WUE) is then calculated as the ratio of the yield to the annual total transpiration. The DSS calculates the monthly irrigation requirement as the difference between the monthly  $ET_c$  and effective rainfall.

The outputs from the DSS are therefore monthly means over 50 years for: 1) crop transpiration ( $m^3/ha$ ), 2) evapotranspiration ( $m^3/ha$ ), and; 3) irrigation requirements ( $m^3/ha$ ). An estimate of crop yield (in tons/ha) is calculated at the end of the year. Water use efficiency is then calculated as the ratio of the yield to the annual transpiration.

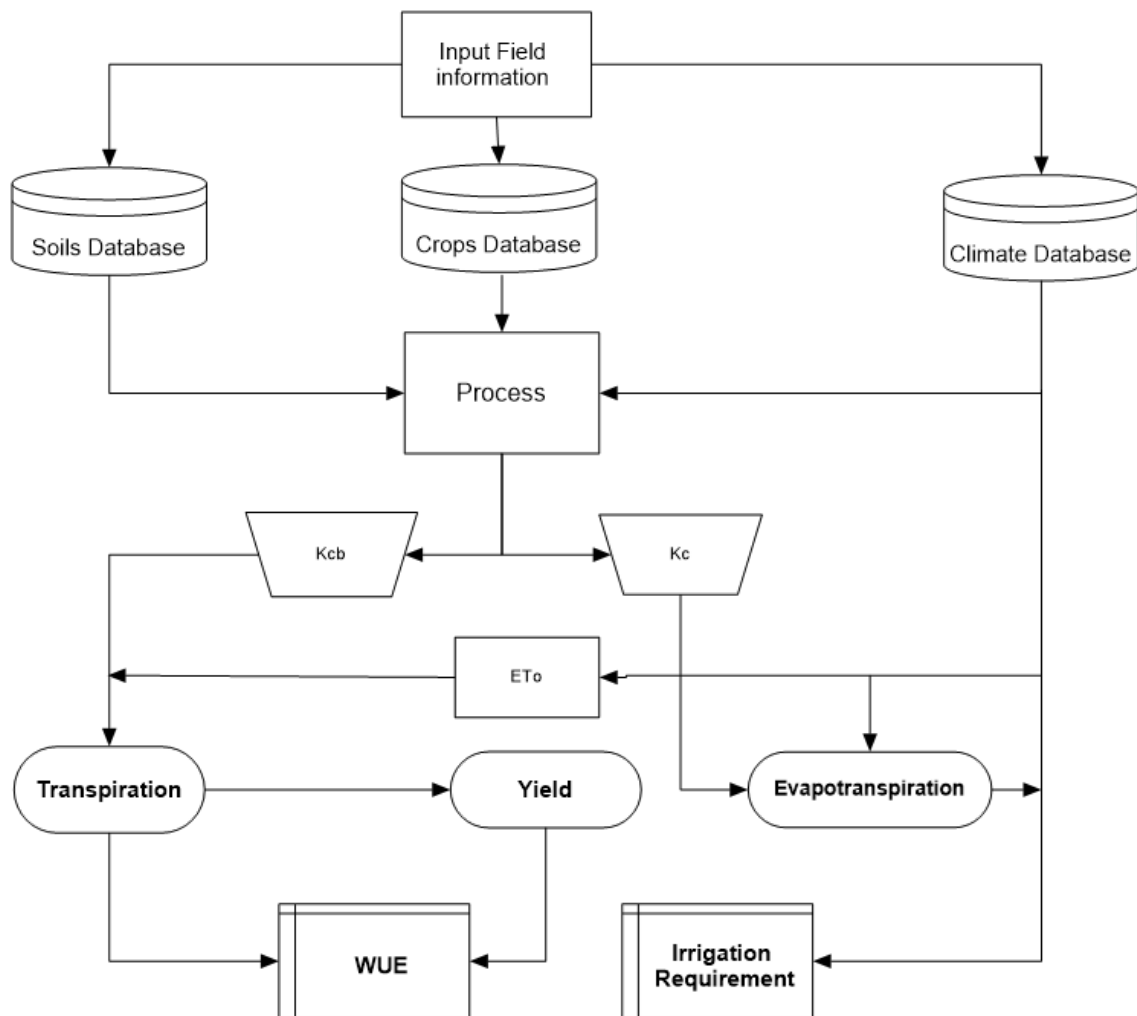


Figure 8.1: Schematic representation of the DSS for water use and water use efficiency of selected subtropical crops.

### 8.3 Description of the DSS

At the heart of the DSS are three databases for soil properties, crop parameters, and the 50-year daily climate record (Fig. 8.1). The DSS has been developed in the form of a web-based tool which can also be accessed on a smartphone with internet connectivity. It is accessible via the following link.

<https://map-crop-factors-smrvo-qfvmr.mongodbstitch.com/>

User inputs are:

- 1) field location (coordinates or dragging and drop marker)
- 2) crop type,
- 3) average vegetation height,
- 4) fractional vegetation cover,
- 5) soil type,
- 6) irrigation system, and;
- 7) status of the understorey vegetation (dense, medium or bare ground).

Currently, the DSS has the following crops: mango, litchi, macadamia, grapefruit, and citrus. The area bounded in red in Fig. 8.2 is the IUWMA area of interest. The height and fractional cover inputs are entered for the initial, mid, and late season stages of crop development according to the FAO 56 four stage crop coefficient approach (Allen *et al.*, 1998). For tree crops, the height is usually constant for all the three stages. The fractional vegetation cover takes values between 0 and 1.0 estimated at noon from the canopy area relative to the area allocated to the tree (see Allen and Pereira, 2009). These numbers vary by small amounts for the fully grown evergreen subtropical tree crops.

When the user enters the field coordinates, the DSS links them to the nearest quaternary catchment (QC) within the IUWMA. The relevant input data (e.g. climate, soils) are extracted from the databases related to that QC. The location of the field is shown by the blue marker in Fig. 8.2. The marker can be moved to the right field by dragging and dropping it or by entering the coordinates of the field if these are known. To assist with orienting the user, we have included the farm boundaries. The user can click the “Load boundaries” tab to show the boundaries and navigate to the right location.

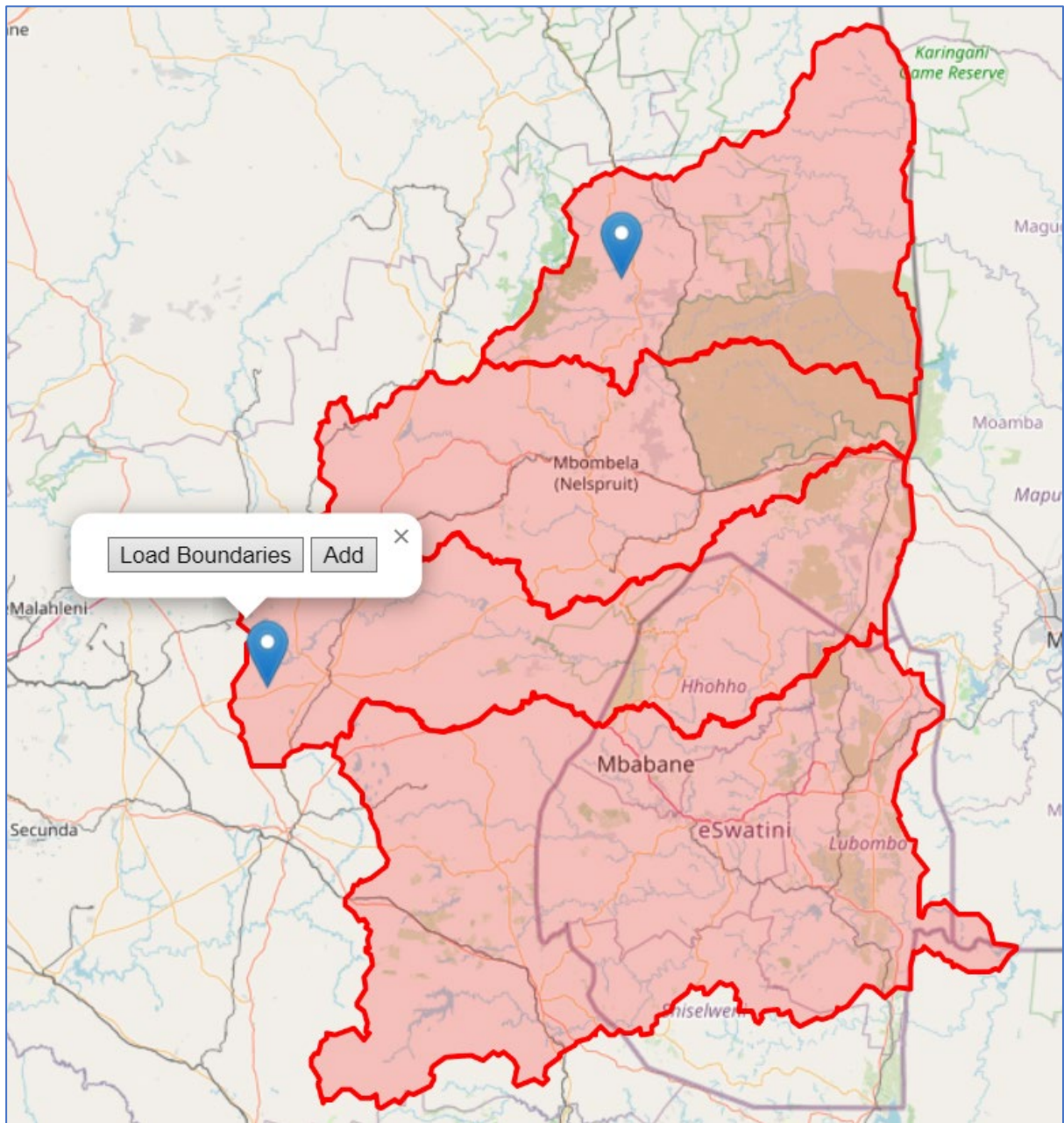


Figure 8.2: Landing page of the DSS. Area bounded in red is the IUWMA.

Because of the large number of farms (Fig. 8.3a), it is necessary to zoom out (Fig. 8.3b) to see the boundaries of individual farms clearly. Next, to enter the rest of the inputs press the “ADD” button and a form such as the one shown in Fig. 8.3 will pop up. Populate the form in line with your field and crop conditions. The required inputs are simple and can be obtained without high level technical competence of the user.

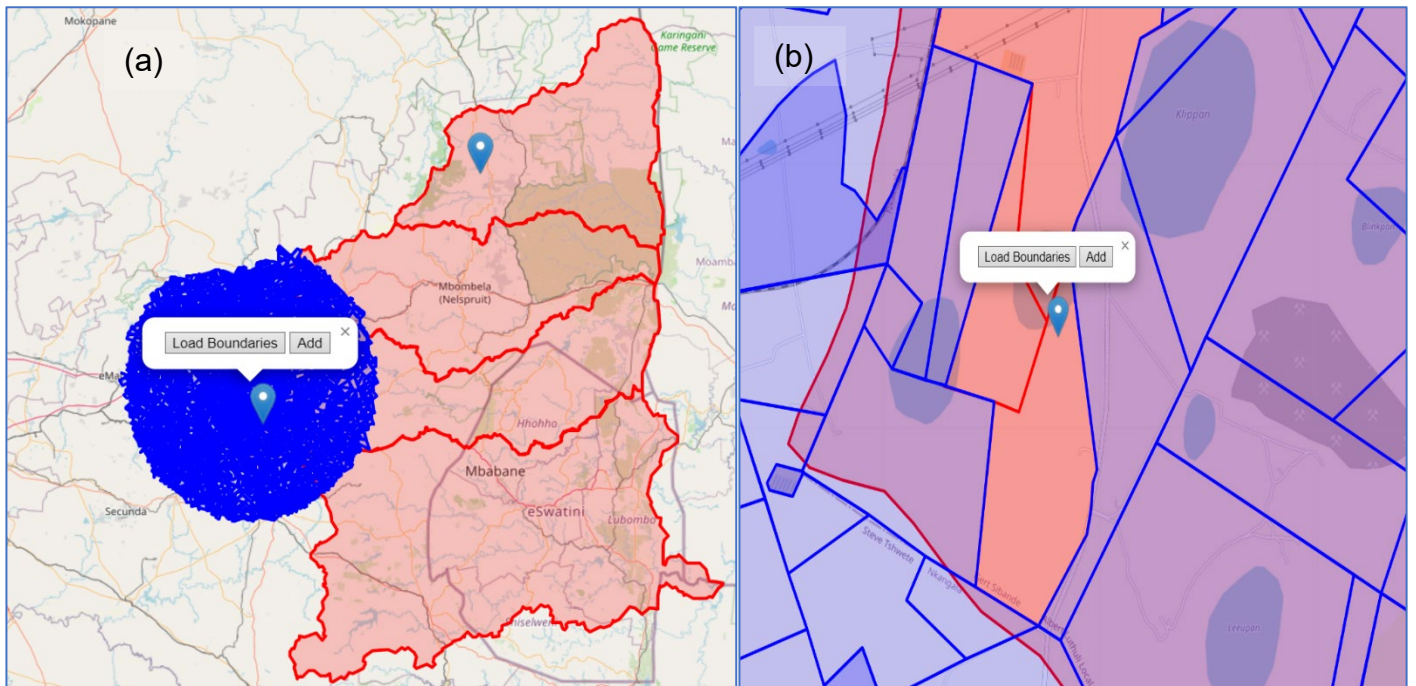


Figure 8.3: Location of interest (a) on the landing page, and; (b) after zooming to the site of interest. The blue lines depict farm boundaries.

Figure 8.4 is an example of a litchi orchard at Dube farm. Average tree height is about 6.0 m and it remains the same over all three growth stages. The fractional vegetation cover was 0.80 at the initial, rising to 0.85 at the mid-season, dropping to 0.80 after harvest when pruning was done. The soil type is loamy and the orchard is irrigated via a micro-sprinkler system. There is a well-maintained understorey vegetation cover, so the option “medium” is chosen. The trees are mature and have a “large canopy”. There are various options under each tab allowing the user to enter information that is specific to their field, here we have only described an example.

### Add new Place ✕

**Farm/Plaas**

**Latitude**

**Longitude**

**Crop Type**

**Plant Height**

**Init**

**Mid**

**Late**

**Fractional Cover**

**Init**

**Mid**

**Late**

**Soil Type**

**Irrigation method**

**Active Ground Cover**

**Canopy**

Figure 8.4: Input form to be populated.

## 8.4 Outputs from the DSS

Once the form is populated, press “SUBMIT” to process the data. Once completed, press the blue marker again, and chose “VIEW OUTPUTS” to see the outputs. The OUTPUTS are available in Tabular and Graphical formats. Table 8.1 (a) shows an example of the outputs in the form of monthly total water use and irrigation requirements estimates. Table 8.1 (b) shows an example of the cumulative fluxes over a typical growing season which is equal to one year. The same information is displayed in graphical form in Figs 8.5 to 8.7.

Table 8.1: Typical outputs of water use and yield variables for a litchi orchard at IUWMA.

(a)

### MONTHLY WATER USE ESTIMATES

Month	Kc	Kcb	Eto	T	ET	Rain	IR
			mm	mm	mm	mm	mm
July	0.36	0.28	44.5	12.3	16.1	58.6	-42.5
August	0.54	0.28	62.8	17.4	34.4	62.0	-27.5
September	0.68	0.28	87.1	24.0	59.7	63.0	-3.3
October	0.74	0.27	110.5	29.9	82.0	61.1	20.9
November	0.76	0.27	127.9	34.2	97.6	62.6	35.0
December	0.77	0.27	139.6	37.3	107.2	64.0	43.2
January	0.77	0.27	131.6	35.2	100.8	60.7	40.0
February	0.75	0.27	110.4	29.7	83.2	58.2	25.0
March	0.71	0.27	96.5	26.4	68.8	60.5	8.3
April	0.61	0.28	71.9	19.9	44.1	62.0	-18.0
May	0.42	0.28	53.3	14.7	22.8	63.2	-40.4
June	0.34	0.28	42.3	11.7	14.2	61.5	-47.2
Total water use (m3/ha/yr.)				2927	7309	737	-7
Yield (tons/ha)					3.24		
WUE (kg/m3)					1.11		

Catchment: usuthu

Monthly Water Use | Cumulative Water Use

Table | Graph

(b)

### CUMULATIVE WATER USE ESTIMATES (mm)

Month	ET	T	Rain	IR
			mm	mm
July	16.11	12.32	58.6	-42.5
August	50.53	29.68	120.6	-70.0
September	110.20	53.67	183.5	-73.3
October	192.24	83.57	244.6	-52.4
November	289.81	117.81	307.2	-17.4
December	397.04	155.09	371.3	25.8
January	497.82	190.29	432.0	65.8
February	580.98	220.01	490.2	90.8
March	649.78	246.39	550.7	99.1
April	693.85	266.26	612.7	81.1
May	716.63	280.98	675.9	40.7
June	730.87	292.68	737.4	-6.5
Total Rainfall				

### Keys

- Kc - crop coefficient
- Kcb - basal crop coefficient
- ETo - short grass reference evapotranspiration

Catchment: usuthu

Monthly Water Use   Cumulative Water Use

Table   Graph

### MONTHLY WATER USE ESTIMATES

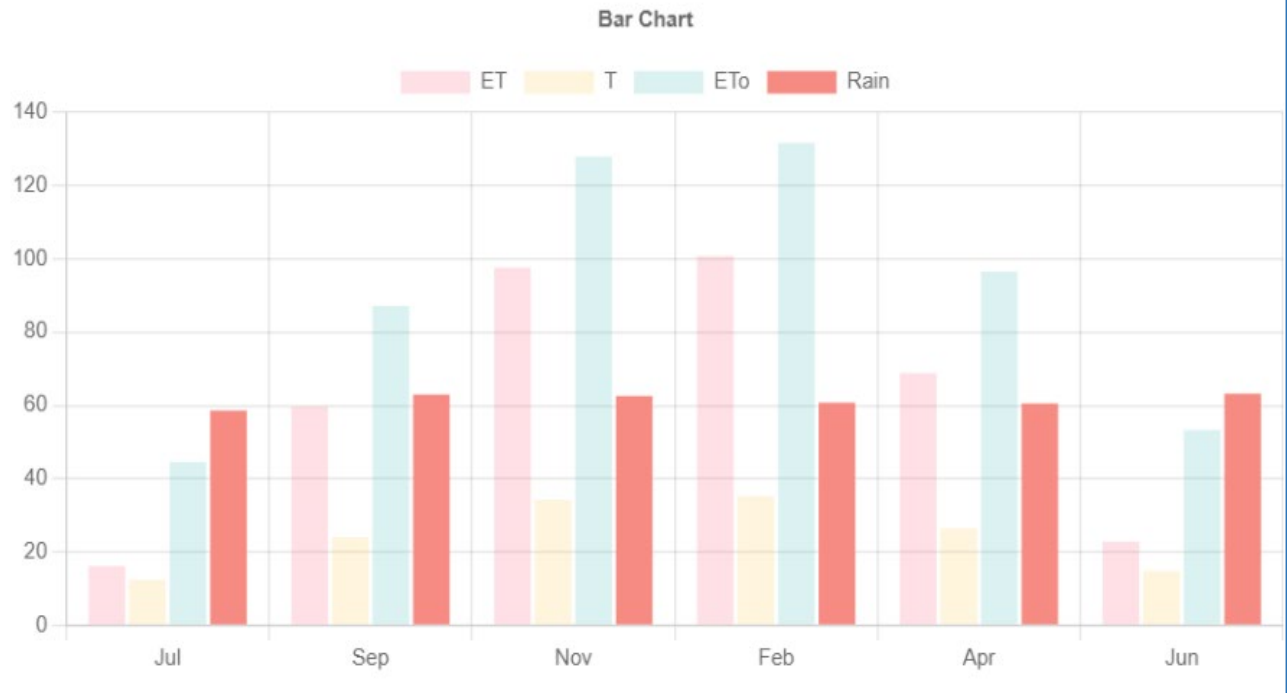


Figure 8.5: Long-term monthly total water use and rainfall for a litchi orchard.

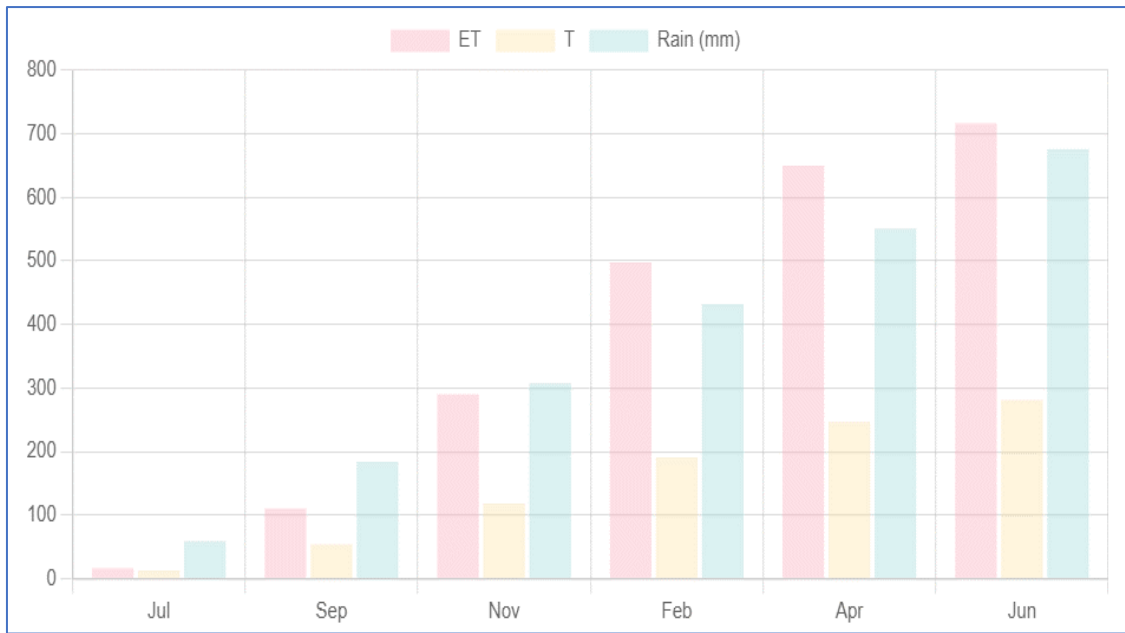


Figure 8.6: Cumulative total water use by a litchi orchard and rainfall

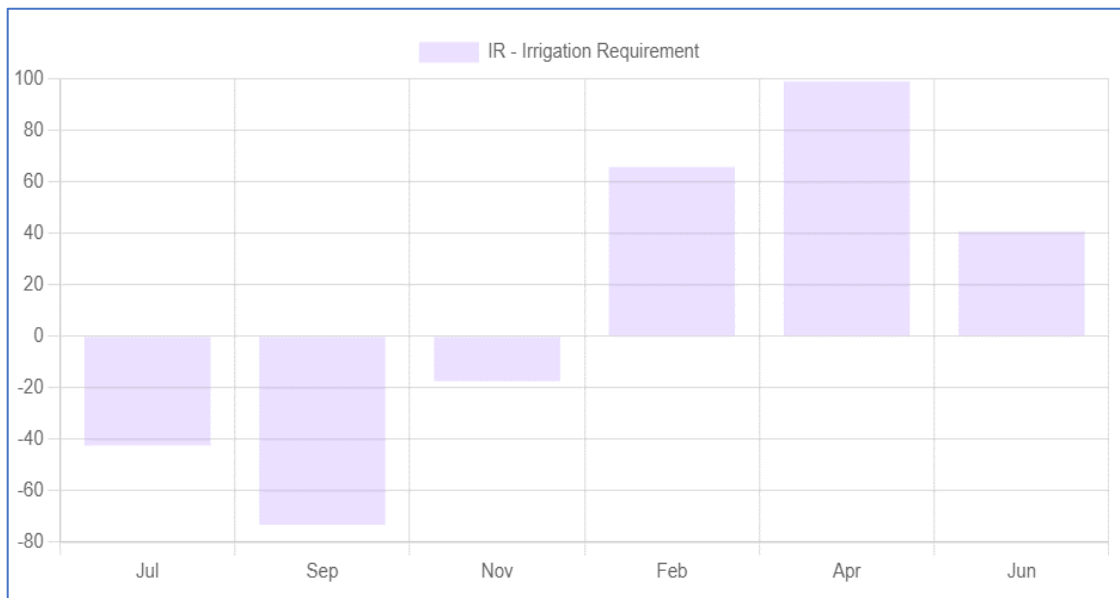


Figure 8.7: Two monthly irrigation requirement for a litchi orchard.

## CHAPTER 9: CONCLUSIONS AND RECOMMENDATIONS

### 9.1. Conclusions

The availability of adequate water will be a major factor influencing profitability of various industries in the coming years, not only because of the rising competition for the resource, but also because of the threat posed by climate variability and change. Therefore, there is need for accurate tools and decisions support systems to improve the management of water so that every drop is made to count. Over the years, the Water Research Commission (WRC) and its industry partners have initiated and funded research on the water use of irrigated crops. A detailed update on progress with irrigation research on WRC funded studies in South Africa was published by Annandale *et al.* (2011) although another update is due given the volume of work that has been done in this field in recent years. The outputs from the earlier studies range from complex physically-based models such as the SWB, PUTU, BEWAB, SAPWAT, to simple crop coefficients. Practical utilization of most of the tools however remains low due to a range of factors. These include complexity, accuracy, representativeness outputs, the availability of low cost and cheap alternatives such as soil moisture probes, weather data, etc.

SAPWAT on the other hand has achieved relatively greater success and uptake due to its simplicity being based on the internationally acclaimed FAO 56 guidelines. Consequently, it has undergone several updates in recent years, and it still remains as a useful tool for irrigation decision-making within South Africa and beyond. Other irrigation management tools that have come onboard in recent years is the Western Cape Department of Agriculture's (WCDoA) remote sensing based FRUITLOOK product. FRUITLOOK provides spatial information on water use, yield, fractional vegetation cover, leaf area index, evaporation deficit, etc. It has proved to be a useful diagnostic tool for irrigation uniformity and for optimizing water allocation in general. Currently it is being fully subsidized by the WCDoA and questions remain over its viability in the long run when growers are expected to pay for the service.

This study had two main aims. The first was to expand the current database of actual measured water use for irrigated crops. Focus was on establishing the maximum unstressed water use for irrigated crops that had not been studied before and to establish relationships with yield. So, we focused on mango, litchi, grapefruit, banana, and sugarcane for which little or no information currently exists. We provided quantitative information on the actual water use, its partitioning between beneficial (transpiration) and non-beneficial water use (orchard floor evaporation) thereby providing insights on potential water saving options. Overall, the tree species reported in this study, i.e. mango, litchi, and grapefruit have conservative transpiration

rates, compared for example to their deciduous counterparts, e.g. apples, pears, pecans (Volschenk, 2003; Gush and Taylor, 2014; Dzikiti *et al.*, 2018). Other studies have reported on the high-water use rates of irrigated sugarcane and banana crops. We confirm this in the current study.

Weather data are widely used for irrigation scheduling following the FAO 56 approach. However, a lack of accurate crop coefficients is a factor that limits the accuracy of this approach mostly because the FAO tabulated values were obtained from temperate subhumid climates. These often-required local calibration to avoid substantial errors in water management decision making. An important novelty in this study was that we fine-tuned an approach for calculating the crop coefficients of tree crops using readily available data in a methodology that has been published in two recent papers by the research team in international peer reviewed journals (Mobe *et al.*, 2020; Mashabatu *et al.*, 2023). We have applied this methodology to the subtropical tree crops reported in this study, i.e. mango, litchi, grapefruit, citrus, and macadamia nuts.

The second goal of this study was to use the water use and environmental data collected in previous studies in IUWMA to develop a decision support tool. This is an important departure from the previous projects whose main mandate was to determine the crop water use without detailing how the information could be used beyond the life of the project. In this study we developed a decision support system that has potential applications in: i) water allocation planning, ii) irrigation scheduling, and iii) as a teaching tool to demonstrate the effect of canopy cover, soil type, wetted soil area, cover crop management, etc. on orchard water use. Building up on the success of platforms like SAPWAT, focus in our DSS was on developing an accurate, but simple tool that requires few readily available inputs. The core of our DSS is the FAO 56 approach, but with the crop coefficients derived from readily available inputs such as the average vegetation height, fractional vegetation cover, soil type, wetted soil fraction, etc.

We also recognise the spatial variability in growing conditions across the IUWMA due to the wide range in topography and the year-to-year variations in climatic conditions. To account for these in the DSS, we divided the entire study area into small water management units (quaternary catchments). We subsequently placed a weather station (50 years of daily data) at the centroid of each quaternary catchment (QC) according to the approach by Schulze *et al.* (1997). Within the DSS when the user inputs their site coordinates, the system links them to the nearest quaternary catchment and uses that QC's data to calculate the monthly weather variables averaged over the 50-year period. The weather data is then used to calculate the long-term monthly average reference evapotranspiration, which is subsequently used to derive

ETc or T using the FAO 56 approach. Other outputs from the DSS include crop coefficients, which allow it to be used for irrigation scheduling if the user enters the current conditions of their field. The DSS also calculates the irrigation requirements from the difference in ETc and the effective rainfall and the potential yield from some water use-yield response functions for the different crops. The ratio of the yield to the ETc gives an indication of the water use efficiency which is yet another output.

The major advantages of the DSS developed in this study is its simplicity and flexibility allowing the user to input easy to get parameters that are relevant to their fields. Farm boundaries are also included that allow the user to identify their specific farm. The DSS is on an online platform that allows the user to access the tool from any location if they have internet connectivity.

## **9.2 Recommendations**

Recommendations from this study are as follows:

- 1) The improved protocol for deriving crop coefficients of irrigated tree crops still needs to be tested widely in a range of crops and growing conditions;
- 2) The DSS itself also needs to be validated even with current environmental, water use and yield data;
- 3) More irrigated crops should be included in the DSS, e.g. avocados, pecans, vegetables, etc.;
- 4) The DSS can potentially generate spatial information if a remote sensing functionality is built into the system;
- 5) There is need for training of potential users (i.e. farmers, catchment managers, irrigators, etc.) on how to use the DSS.

## REFERENCES

- ADAMS, JB., SABOL, DE., KAPOS, V., FILHO, RA., ROBERTS, DA., SMITH, MO., GILLESPIE, AR., 1995. Classification of Multispectral Images Based on Fractions of Endmembers: Application to Land-Cover Change in the Brazilian Amazon. *Remote Sensing of Environment*. 52. 137-154.
- ADEBOYE, O.B., SCHULTZ, B., ADEKALU, K.O., PRASAD. K.,2016. Impact of water stress on radiation interception and radiation use efficiency of soybeans (*Glycine max L. Merr.*) in Nigeria. *Brazilian Journal of Science and Technology*. 3(1). pp.1-21.
- ADETORO, AA., SINGELS, A., PARASKEVOPOULOS, AL., OWUSU-SEKYERE, E., JORDAAN, H., ORIMOLOYE, IR., 2020. Alleviating water shortages by decreasing water footprint in sugarcane production: The impacts of different soil mulching and irrigation systems in South Africa. *Groundwater for Sustainable Development* .11 (2020) 100464.
- ALAM, S.M., NAQVI, S.S.M., ANSARI, R.A.Z.I.U.D.D.I.N., 1999. Impact of soil pH on nutrient uptake by crop plants. *Handbook of plant and crop stress*. 2. pp.51-60.
- ALLEN, RG., PEREIRA, LS., RAES, D., SMITH, M., 1998. Crop evapotranspiration. FAO Irrigation and Drainage Paper 56. *Food and Agriculture Organization (FAO)*. Rome. Italy.
- ALLEN, RG., TASUMI, M., TREZZA, R., 2007. Satellite-based energy balance for mapping evapotranspiration with internalized calibration (METRIC) – Model. *Journal of Irrigation and Drainage Engineering*. 133(4). 380-394.
- ANDERSON, MC., NORMAN, JM., MECIKALSKI, JR., OTKIN, JA., KUSTAS, W P., 2007. A climatological study of evapotranspiration and moisture stress across the continental United States based on thermal remote sensing: Model formulation. *Journal of Geophysical Research: Atmospheres*. 112 (D10).
- ARC., 2008. Banana production. ARC-Institute for Tropical and Sub-tropical Crops. Mbombela.
- BARTLETT, R.J., RIEGO, D.C., 1972. Toxicity of hydroxy aluminium in relation to pH and phosphorus. *Soil Science*. 114(3). pp.194-200.
- BASTIAANSEN, WG., MENENTI, M., FEDDES, R., HOLTSLAG, A., 1998. A remote sensing surface energy balance algorithm for land (SEBAL) Formulation. *Journal of Hydrology*. 212. 198-212.
- BASTIDAS-OBANDO, E., BASTIAANSEN, W.G.M., JARMAIN, C., 2017. Estimation of transpiration fluxes from rainfed and irrigated sugarcane in South Africa using a canopy resistance and crop coefficient model. *Agricultural Water Management* 181. 94-107.

- BASTIAANSEN, W.G.M., NOORDMAN, E.J.M., PELGRUM, H., DAVIDS, G., THORESON, B.P. AND ALLEN, R.G., 2005. SEBAL model with remotely sensed data to improve water-resources management under actual field conditions. *Journal of irrigation and drainage engineering*, 131(1), pp.85-93.
- BEGEMANN, G.J., 2014. The South African litchi industry – an overview. *Acta Horticulturae* 1029: 35-39
- BLONGUIST Jr., J.M., NORMAN, J.M., and BUGBEE, B., 2009. Automated measurement of canopy stomatal conductance based on infrared temperature. *Agricultural and forest Meteorology*. 149(12). pp.2183-2197.
- BOTHA, A., 2019. Mango irrigation challenges. *Subtrop. Journal*. 25 : 30
- BURGESS, S.S.O, ADAMS, MA., TURNER, NC., BEVERLY, CR., ONG, CK., KHAN, AAH., BLEBY, TM., 2001. An improved heat pulse method to measure low and reverse rates of sap flow in woody plants. *Tree Physiol*. 21. 589-598.
- CANCELA, JJ., ALLEN, RG., 2010. Prediction of crop coefficients from fraction of ground cover and height. Background and validation using ground and remote sensing data. *Agricultural Water Management*. 241. <https://doi.org/10.1016/j.agwat.2020.106197>.
- CAO, X., WANG, Y., WU, P., ZHAO, X., 2015. Water productivity evaluation for grain crops in irrigated regions of China. *Ecological Indicators* 55.107-117.
- CHAVEZ, JS., HOWELL, TA., MAREK, TH., NEW, LL., 2007. Evapotranspiration Mapping Using METRIC™ for a Region with Highly Advection Conditions. *ASABE Annual International Meeting. Minneapolis. Minnesota. USA. 17-20 June 2007*.
- CARR, MKV., 2013. The water relations and irrigation requirements of macadamia (macadamia spp.): a review. *Journal of Experimental Agriculture*. 49. 74-90. Cambridge University Press 2012 doi:10.1017/S0014479712000804.
- DAFF., 2003. Cultivating sub-tropical crops. Directorate Agricultural Information Services. *Department of Agriculture. Forestry and Fisheries. Pretoria*.
- DAFF., 2011. A profile of the South African banana market value chain. *Department of Agriculture. Forestry and Fisheries. Pretoria*.
- DAFF., 2019. Abstract of Agricultural Statistics 2019. *Department of Agriculture. Forestry and Fisheries. Pretoria*.
- DWA., 2012. Business Case for the Inkomati-Usuthu Catchment Management Agency. V1.2 submitted as Final Draft. *Department of Water Affairs. Pretoria*.

De VILLIERS, E.A, JOUBERT, P.H., eds.. 2008. The cultivation of mango. *ARC-Institute for Tropical and Subtropical Crops*.

DZIKITI, S., SCHACHTSCHNEIDER, K., NAIKEN, V., GUSH, M., LE MAITRE, D., 2013. Comparison of water-use by alien invasive pine trees growing in riparian and non-riparian zones in the Western Cape Province, South Africa. *For. Ecol. Manage.* 293, 92-102. <https://doi.org/10.1016/j.foreco.2013.01.003>

DZIKITI S. GUSH MB., LE MAITRE DC., MAHERRY A., RAMOELO A., JOVANOVIC NZ. 2016. Quantifying potential water savings from clearing invasive alien *Eucalyptus camaldulensis* using *in situ* and high resolution remote sensing data in the Berg River Catchment, Western Cape, South Africa. *Forest Ecology and Management Journal.* 361, 69-80.

DZIKITI, S. T., VOLSCHENK, S.J.E, MIDGLEY, E., LÖTZE, N.J, TAYLOR, M.B., GUSH, Z., NTSHIDI., S.F, ZIREBWA, Q., DOKO., M., SCHMEISSER., C., JARMAIN., W.J, STEYN., H.H., PIENAAR., 2018a. Estimating the water requirements of high yielding and young crop orchards in the winter rainfall areas of South Africa using a dual source evapotranspiration model. *Agricultural Water Management.* 208. 152-162.

DZIKITI, S., VOLSCHENK, T., MIDGLEY, S., GUSH, M., TAYLOR, N., LÖTZE, E., ZIREBWA, S., NTSHIDI, Z., MOBE, NT., SCHMEISSER, M., DOKO, Q., 2018b. Quantifying water use and water productivity of high performing crop orchards of different canopy sizes. *WRC Report No. TT 751/18. Pretoria: Water Research Commission.*

DZIKITI, S., STEPPE, K., LEMEUR, R., MILFORD, JR., 2007. Whole-tree level water balance and its implications on stomatal oscillations of young orange trees under natural climatic conditions. *Journal of Experimental Botany.* 58. 1893-1901.

FAO., 2020a. Banana. *Accessed on 15 December 2020.* <http://www.fao.org/land-water/databases-and-software/crop-information/banana/en/>.

FAO., 2020b. Sugarcane. *Accessed on 15 December 2020.* <http://www.fao.org/land-water/databases-and-software/crop-information/sugarcane/en/>.

FARES, A., DOGAN, A., ABBAS, F., PARSONS, L., OBREZA, T., MORGAN, K., 2008. Water balance components in a mature citrus orchard. *Soil Science Society of America Journal* 72 578-585.

FINNEMORE, HJ., 2000. A perspective on the South African mango industry (past and future). *Acta Horticulturae.* 509: 39-50

GAO, L., WANG, X., JOHNSON, BA., TIAN, Q., WANG, Y., VERRELST, J., MU, X., XINGFA, GU, X., 2020. Remote sensing algorithms for estimation of fractional vegetation cover using pure vegetation index values: A review. *ISPRS Journal of Photogrammetry and Remote Sensing*. 159. 364-377. <https://doi.org/10.1016/j.isprsjprs.2019.11.018>.

GARCÍA, PETILLO, M., CASTEL, J., 2007. Water balance and crop coefficient estimation of a citrus orchard in Uruguay. *Spanish Journal of Agricultural Research* 5 232-243.

GLENN, EP., NEALE, CM., HUNSAKER, DJ., NAGLER, PL., 2011. Vegetation index based crop coefficients to estimate evapotranspiration by remote sensing in agricultural and natural ecosystems. *Hydrological Processes*. 25(26). 4050-4062.

GONTIA, NK., TIWARI, KN., 2010. Estimation of crop coefficient and evapotranspiration of wheat (*Triticum aestivum*) in an irrigation command using remote sensing and GIS. *Water resources management*. 24(7). 1399-1414.

GUSH, M., DZIKITI, S., VAN DER LAAN, M., STEYN, M., MANAMATHELA, S., PIENAAR, H., 2019. Field quantification of the water footprint of an crop orchard. and extrapolation to watershed scale within a winter rainfall Mediterranean climate zone. *Agric. For. Meteorol.* 271. 135-147. <https://doi.org/10.1016/j.agrformet.2019.02.042>

GUSH, MB., TAYLOR, NJ., 2014. The water use of selected fruit tree orchards (Volume 2): Technical report on measurements and modelling. *WRC report No. 1770/2/14*. 1-285.

GRISMER, ME., 2000. Long-term evapotranspiration in a coastal citrus/avocado orchard. *Journal of irrigation and drainage engineering*. 120: 1-9.

GUZINSKI, G., NIETO, H., 2019. Evaluating the feasibility of using Sentinel-2 and Sentinel-3 satellites for high-resolution evapotranspiration estimations. *Remote Sensing of Environment*. 221. 157-172. <https://doi.org/10.1016/j.rse.2018.11.019>.

IBRAIMO., N.A., TAYLOR, N.J., GHEZEHEI, S., GUSH, M.B, ANNANDALE, J.G., 2014. Water use of macadamia orchards. In: Gush. M.B. and Taylor. N.J. (Eds). 2014. The water use of selected fruit tree orchards (Volume 2): *Technical report on measurements and modelling*. *Water Research Commission. Pretoria. RSA*. WRC Report 1770/2/14. Section 6.

IUWMA., 2018. Inkomati-Usuthu Catchment Management Agency Annual Performance Plan. *Final draft for 2018/19 financial year*. IUWMA. Mbombela.

JARMAIN, C., EVERSON, CS., SAVAGE, MJ., MENGISTU, M., CLULOW, AD., 2009. Refining Tools For Evaporation Monitoring In Support Of Water Resources. *WRC Report*.

JONES, M.R., SINGELS, A., 2018. Refining the Canegro model for improved simulation of climate change impacts on sugarcane. *Eur. J. Agron.* 100, 76-86.

KALRA, YP., 1998. Handbook of reference methods for plant analysis. *CRC Press. London.* 287pp.

LAGERWALL, G., undated. Bananas in KwaZulu-Natal. *Department of Agriculture and Rural Development. Province of KwaZulu-Natal.* Pietermaritzburg.

LARY, DJ., ALAVI, AH., GANDOMI, AH., WALKER, AL., 2016. Machine learning in geosciences and remote sensing. *Geoscience Frontiers.* 7. 3-10.

<http://dx.doi.org/10.1016/j.gsf.2015.07.003>

LE MAITRE, D.C., VERSFELD, D.B., CHAPMAN, R.A., 2000. Impact of invading alien plants on surface water resources in South Africa: A preliminary assessment.

LEVIN, AG., PERES, M., NOY, M., LOVE, C., GAL, Y., NAOR, A., 2018. The response of field-grown mango (cv. Keitt) trees to regulated deficit irrigation at three phenological stages. *Irrigation Science.* 36:25-35.

LI, H., ZHENG, L., LEI, Y., LI, C., LIU, Z., ZHANG, S., 2008. Estimation of water consumption and crop water productivity of winter wheat in North China Plain using remote sensing technology. *Agricultural Water Management.* 95. 1271-1278. <https://doi.org/10.1016/j.agwat.2008.05.003>

LUND, Z.F., 1959. Available water-holding capacity of alluvial soils in Louisiana. *Soil Science Society of America Journal.* 23(1). pp.1-3.

MAPONYA, P., MPANDELI, S., ODUNIY, S., 2013. Climate Change Awareness in Mpumalanga Province. South Africa. *Journal of Agricultural Science.* Vol. 5. No. 10; 2013

MASELLI, F., CHIESI, M., ANGELI, L., FIBBI, L., RAPI, B., ROMANI, M., SABATINI, F., BATTISTA, P., 2020. An improved NDVI-based method to predict actual evapotranspiration of irrigated grasses and crops. *Agricultural Water Management.* 233. 106077. <https://doi.org/10.1016/j.agwat.2020.106077>.

McBRIDE, M.B., 1994. *Environmental Chemistry Of Soil* (Vol. 141580. p. 5263). Obtenido de Recuperado de: [https://d1wqtxts1xzle7.cloudfront.net/35536696/Environmental\\_soil](https://d1wqtxts1xzle7.cloudfront.net/35536696/Environmental_soil).

MAZAHERI, M.R., MAHMOODABADI, M., 2012. Study on infiltration rate based on primary particle size distribution data in arid and semiarid region soils. *Arabian Journal of Geosciences.* 5(5). pp.1039-1046.

MIDGLEY, SJE., DZIKITI, S., GUSH, MB., NTSHIDI, Z., MOBE, NT., 2020. Water use productivity of high performing crop orchards in the winter rainfall area of South Africa. *Acta Horticulturae.*

MOBE, NT., S, DZIKITI, T, VOLSCHENK, ZIBERWA, SF, Z, NTSHIDI, SJE, MIDGLEY, WJ, STEYN, E, LÖTZE, S, MPANDELI, D, MAZVIMAVI, 2020a. Using sap flow data to assess

variations in water use and water status of crop orchards of varying age groups in the Western Cape Province of South Africa. *Water SA*

MOBE, NT., S., DZIKITI, SF, ZIREBWA, SJE, MIDGLEY, W, VON LOEPER, D, MAZVIMAVI, Z, NTSHIDI, NZ, JOVANOVIC, 2020b. Estimating crop coefficients for crop orchards with varying canopy cover using measured data from twelve orchards in the Western Cape Province. South Africa. *Agricultural Water Management Journal*.

MOSTERT, PG., 2014. Irrigation of litchis in South Africa – an overview. *Acta Horticulturae* 1029: 177-182.

MUCHENA, L., DZIKITI, S., LOTZE, E., MIDGLEY, SJE., 2020. Using sap flow sensors to study the influence of rootstock and mid-summer water deficit on transpiration of crop trees in South Africa. *Acta Horticulturae*.

NTSHIDI, Z., DZIKITI, S., D, MAZVIMAVI, NT, MOBE., 2020. Contribution of understory vegetation to evapotranspiration partitioning in crop orchards under Mediterranean climatic conditions in South Africa. *Agricultural Water Management journal*.

OLIVIER, F., SINGELS, A., 2003. Water use efficiency of irrigated sugarcane as affected by row spacing and variety. *Proc S Afr Sug Technol Association*.

OLIVIER F, SINGELS A. 2015. Increasing water use efficiency of irrigated sugarcane production in South Africa through better agronomic practices

OLNESS, A., ARCHER, D., 2005. Effect of organic carbon on available water in soil. *Soil Science*. 170(2). pp.99.

PAÇO, T., PAREDES, P., PEREIRA, L., SILVESTRE, J., SANTOS, F., 2019. Crop coefficients and transpiration of a super intensive arbequina olive orchard using the dual kc approach and the kcb computation with the fraction of ground cover and height. *Water*. 11. 383. <https://doi.org/10.3390/w11020383>.

PANIGRAHI, N., THOMPSON, A.J., ZUBELZU, S., KNOX, J.W., 2021. Identifying opportunities to improve management of water stress in banana production. *Scientia Horticulturae*. 276 (2021) 109735.

PEREIRA, LS., PAREDES, P., MELTON, F., JOHNSON, L., WANG, T., LOPEZ-URREA, R., REYES-GONZÁLEZ, A., KJAERGAARD, J., TROOIJEN, T., HAY, C., AHIABLAME, L., 2017. Estimation of crop Evapotranspiration Using Satellite Remote Sensing-Based Vegetation Index. *Advances in Meteorology*. 2018. <https://doi.org/10.1155/2018/4525021>.

QUEENSLAND GOVERNMENT, 2004. Sub-tropical banana information kit. *Department of Agriculture and Fisheries*. Accessed on 14 December 2020. [http://era.daf.qld.gov.au/id/eprint/1966/1/1\\_subtrop-banana.pdf](http://era.daf.qld.gov.au/id/eprint/1966/1/1_subtrop-banana.pdf).

RAWLS, W.J., PACHEPSKY, Y.A., RITCHIE, J.C., SOBECKI, T.M., BLOODWORTH, H., 2003. Effect of soil organic carbon on soil water retention. *Geoderma*. 116(1-2). pp.61-76.

RUIQI Ren, Gang Liu, Minmin Wen, Robert Horton, Baoguo Li, Bingcheng Si. 2017.

The effects of probe misalignment on sap flux density measurements and in situ probe spacing correction methods, *Agricultural and Forest Meteorology*, Volume 232, 2017, Pages 176-185

ROBINSON, J.C., ALBERTS, A.J., 1989. Seasonal variations in the crop water use coefficient of banana (cultivar "Williams") in the subtropics. *Scientia Horticulturae* .40(3). 215-225.

ROGERS, K.H., LUTON, R., 2016. Building an adaptive and stakeholder-centred catchment management agency in the inkomati/usuthu river catchment.

SASA., 2020. South African Sugar Industry Directory 2019/2020. Accessed on 14 December 2020. [https://sasa.org.za/custom\\_content/downloads/SASA-ID-2019-20.pdf](https://sasa.org.za/custom_content/downloads/SASA-ID-2019-20.pdf).

SENAY, G.B., BUDDE, M., VERDIN, J.P., MELESSE, A.M., 2007. A coupled remote sensing and simplified surface energy balance approach to estimate actual evapotranspiration from irrigated fields. *Sensors*. 7(6). 979-1000.

SETTLE, J.J., DRAKE, N.A., 1993. Linear mixing and the estimation of ground cover proportions. *International Journal of Remote Sensing*. 14. 6. 1159-1177. <https://DOI:10.1080/01431169308904402>

SIBULALI, A., 2018. Analysing the competitive performance of the South African sub-tropical fruit industry. *Thesis (MCom)--Stellenbosch University*. <http://hdl.handle.net/10019.1/104958>

SINGELS, A., PARASKEVOPOULOS, A.L., MASHABELA, M.L., 2019. Farm level decision support for sugarcane irrigation management during drought. *Agricultural Water Management*. 222. 274-285.

SIMPSON, G.B., BADENHORST, J., JEWITT, G.P., BERCHNER, M., DAVIES, E., 2019. Competition for Land: The Water-Energy-Food Nexus and Coal Mining in Mpumalanga Province. South Africa. *Frontiers in Environmental Science*. doi: 10.3389/fenvs.2019.00086

SMITH, D.M., ALLEN, S.J., 1996. Measurement of sap flow in plant stems. *Journal of Experimental Botany*. 47: 1833-1844.

SMITH, R.M., BROWNING, D.R., 1948. Soil moisture tension and pore space relations for several soils in the range of the "field capacity". *Soil Science Society of America Journal*. 12(C). pp.17-21.

STATISTICS SOUTH AFRICA, 2020a. Census of commercial agriculture. 2017. Financial and production statistics. Report No. 11-02-01 (2017). *Statistics South Africa*. Pretoria.

STATISTICS SOUTH AFRICA, 2020B. Census of commercial agriculture. 2017. Mpumalanga: Financial. production and related statistics. Report No. 11-02-09 (2017). *Statistics South Africa*. Pretoria.

STATISTICS SOUTH AFRICA, 2020C. Census of commercial agriculture. 2017. *Fact sheets. Version 2: published 17 April 2020*. [http://www.statssa.gov.za/?page\\_id=1854&PPN=Report-11-02-01&SCH=7902](http://www.statssa.gov.za/?page_id=1854&PPN=Report-11-02-01&SCH=7902)

STEPPE, K., DE PAUW, DJW., DOODY, TM., TESKEY, RO., 2010. A comparison of sap flux density using thermal dissipation. heat pulse velocity and heat field deformation methods. *Agricultural and Forest Meteorology*. 150: 1046-1056.

STEPPE, K., DZIKITI, S., LEMEUR, R., MILFORD, JR., 2006. Stomatal oscillations in orange trees under natural climatic conditions. *Annals of Botany* .92. 831-835.

SU, Z., 2002. The Surface Energy Balance System (SEBS) for estimation of turbulent heat fluxes. *Hydrology and Earth System Sciences Discussions*. 6(1). 85-100.

SUBTROP BULLETIN, 2020. *Volume 6 Special census edition – December 2020*

SWANSON, RH., WHITFIELD, DWA., 1981. A numerical analysis of heat pulse velocity and theory. *J. Exp. Bot* .32. 221-239.

TAYLOR NJ., MAZHAWU E., CLULOW A., MIDGLEY SJE., ROETS N., SMIT T., ANNANDALE JG. 2021a. Water use of avocado orchards, Volume 1. WRC report.

TAYLOR NJ., SMIT T., A SMIT., CLULOW A., MIDGLEY SJE., DLAMINI K., ANNANDALE JG. 2021b. Water use of macadamia orchards, Volume 2. WRC report.

TAYLOR, NJ., MAHOHOMA, W., VAHRMEIJER, JT., GUSH, MB., ALLEN, RG., ANNANDALE, JG., 2015. Crop coefficient approaches based on fixed estimates of leaf resistance are not appropriate for estimating water use of citrus. *Irrig. Sci*. 33. 153-166. <https://doi.org/10.1007/s00271-014-0455-z>.

THE NON-AFFILIATED SOIL ANALYSES WORK COMMITTEE, 1990. Handbook of standard soil testing methods for advisory purposes. *Soil Sci. Soc. S.A.*. P.O. Box 30030. Sunnyside. Pretoria.

VAHRMEIJER, TJ., TAYLOR, NJ., 2018. Quantifying citrus water use and water stress at orchard level. *WRC TT no 772/2/18*.

VAN DER LAAN, M., VAN ANTWERPEN, R., BRISTOW, KL., 2012. River water quality in the northern sugarcane-producing regions of South Africa and implications for irrigation: A scoping study. *Water SA* .38. 87-96.

- VOLSCHENK, T., 2017. Evapotranspiration and crop coefficients of Golden Delicious/M793 crop trees in the Koue Bokkeveld. *Agric. Water Manag.* 194. 184-191. <https://doi.org/10.1016/j.agwat.2017.09.002>
- WANG, Y., HUANG, Q., LIU., C., DING, Y., LIU, L., TIAN, Y., WU, X., Li, H., AWASTHI, MK, ZHAO, Z., 2020. Mulching practices alter soil microbial functional diversity and benefit to soil quality in orchards on the Loess Plateau. *Journal of Environmental Management.* 271. p.110985.
- WRC, 2017. The South African Mine Water Atlas. WRC Project No. K5/2234//3. *Water Research Commission of South Africa. Pretoria.* [www.wrc.org.za](http://www.wrc.org.za).
- XIAO, Z., WANG, T., LIANG, S., SUN, R., 2016. Estimating the Fractional Vegetation Cover from GLASS Leaf Area Index Product. *Remote Sensing.* 8. 337. 2-19. <https://doi:10.3390/rs8040337>.
- YANG, J., WEISBERG, PJ., BRISTOW, NA., 2012. Landsat remote sensing approaches for monitoring long-term tree cover dynamics in semi-arid woodlands: Comparison of vegetation indices and spectral mixture analysis. *Remote Sensing of Environment.* 119. 62-71. <https://doi:10.1016/j.rse.2011.12.004>.
- YUE, J., TIAN, Q., 2020. Estimating fractional cover of crop, crop residue, and soil in cropland using broadband remote sensing data and machine learning. *International Journal of Applied Earth Observation and Geoinformation* .89. <https://doi.org/10.1016/j.jag.2020.102089>.

## APPENDICES

### Appendix 1. Capacity Building

The following researchers have been trained under this project:

- 1) Mr George Nel was registered for an MSc Agriculture (Horticultural Science) at Stellenbosch University. He completed his thesis entitled;

*Establishing the water requirements and crop coefficients of a mature mango orchard under subtropical conditions*

He graduated in March 2024.

- 2) Mr Prince Dangare is registered for a PhD Science (agriculture) at Stellenbosch University. He is in the second from last year of his study and hopes to submit his thesis in 2025.

Thesis title:

*Development and testing of a decision support system for estimating water use and water use efficiency of irrigated tree crops.*

- 3) Dr Joseph Masanganise did a two-and half-year postdoctoral fellowship on the project. His work was mostly on quantifying the water use of banana orchards.

## Appendix 2. Summary of crop growth stages used in the DSS.

Crop type	Stage name	Length (days)	Budbreak date
Avocado	Ini	30	
	Dev	60	
	Mid	215	15-Aug
	Late	60	
Banana	Ini	120	
	Dev	60	
	Mid	180	15-Aug
	Late	5	
Citrus	Ini	60	
	Dev	90	
	Mid	120	15-Aug
	Late	95	
Litchi	Ini	30	
	Dev	60	15-Aug
	Mid	120	
	Late	150	
Macadamia	Ini	45	
	Dev	30	15-Aug
	Mid	260	
	Late	30	
Mango	Ini	45	
	Dev	60	15-Aug
	Mid	90	
	Late	165	
Pecans	Ini	20	
	Dev	30	15-Aug
	Mid	90	
	Late	120	
Pomegranate	Ini	20	
	Dev	60	15-Aug
	Mid	70	
	Late	30	
Plum	Ini	20	
	Dev	70	15-Jul
	Mid	120	
	Late	60	

### Appendix 3. Typical soil water characteristics for different soils (FAO 56).

Soil type (USDA soil texture classification)	Soil water characteristics			Evaporation parameters		
	$\theta_{FC}$ $m^3 m^{-3}$	$\theta_{WP}$ $m^3 m^{-3}$	$(\theta_{FC}-\theta_{WP})$ $m^3 m^{-3}$	Amount of water that can be depleted by evaporation		
				Stage 1 REW (mm)	Stages 1 and 2 TEW <sup>a</sup> ( $Z_e=0.10$ m) (mm)	Stages 1 and 2 TEW <sup>a</sup> ( $Z_e=0.15$ m) (mm)
Sand	0.07–0.17	0.02–0.07	0.05–0.11	2–7	6–12	9–13
Loamy sand	0.11–0.19	0.03–0.10	0.06–0.12	4–8	9–14	13–21
Sandy loam	0.18–0.28	0.06–0.16	0.11–0.15	6–10	15–20	22–30
Loam	0.20–0.30	0.07–0.17	0.13–0.18	8–10	16–22	24–33
Silt loam	0.22–0.36	0.09–0.21	0.13–0.19	8–11	18–25	27–37
Silt	0.28–0.36	0.12–0.22	0.16–0.20	8–11	22–26	33–39
Silt clay loam	0.30–0.37	0.17–0.24	0.13–0.18	8–11	22–27	33–40
Silty clay	0.30–0.42	0.17–0.29	0.13–0.19	8–12	22–28	33–42
Clay	0.32–0.40	0.20–0.24	0.12–0.20	8–12	22–29	33–43

Note: USDA=United States Department of Agriculture; REW=readily evaporated water; and TEW=totally evaporated water.

<sup>a</sup>TEW=( $\theta_{FC}-0.5\theta_{WP}$ ) $Z_e$ .